Statistical Inference with High-Frequency Financial Data: New Perspectives from Alternative Observation Schemes

Shifan Yu

Department of Accounting and Finance

Lancaster University

Submitted in fullfilment of the requirements for the degree of

Doctor of Philosophy in Finance

July 2024

Abstract

This thesis is a compilation of three main studies with the common theme: statistical inference with high-frequency financial data under alternative observation or sampling schemes. The increasing availability of high-frequency financial data has motivated the development of new statistical inference tools, such as (i) advanced volatility estimators with better robustness in the presence of local extreme phenomena in intraday asset prices, and (ii) techniques for identifying these unusual extreme events, which contribute to a comprehensive understanding of their impact on financial markets. The investigation on both topics in this thesis adopts an innovative perspective by exploring potential enhancements from utilizing high-frequency financial data under alternative observation schemes, which stands in contrast to traditional methods that rely on equidistantly sampled transaction price records.

In Chapter 2, we introduce a novel nonparametric high-frequency jump test for discretely observed Itô semimartingales. Based on observations sampled recursively at first exit times from a symmetric double barrier, our method distinguishes between threshold exceedances caused by the Brownian component and jumps, which enables the construction of a feasible, noise-robust statistical test. Simulation results demonstrate superior finite-sample performance of our test compared to classical methods. An empirical analysis of NYSE-traded stocks provides clear statistical evidence for jumps, with the results highly robust to spurious detections.

In Chapter 3, we develop a new nonparametric estimator of integrated variance that utilizes intraday candlestick information, comprised of the high, low, open, and close prices within short time intervals. The range-return-difference volatility (RRDV) estimator is robust to short-lived extreme return persistence hardly attributable to the diffusion component, such as gradual jumps and flash crashes. By modeling such sharp but continuous price movements following some recent theoretical advances, we demonstrate that RRDV can provide consistent estimates with variances about four times smaller than those obtained with the differenced-

return volatility (DV) estimator. Monte Carlo simulations and empirical applications further validate the practical reliability of our proposed estimator with some finite-sample refinements.

In Chapter 4, we introduce an innovative semiparametric framework for duration-based volatility estimation. We filter out daily volatility dynamics from intraday price durations by employing a nonparametrically predicted threshold that dynamically adapts to the volatility of each day. This enables the application of parametric models to price durations collected over various days, which greatly enhances the flexibility of model estimation and facilitates the construction of more accurate volatility estimators. Simulation results demonstrate superior finite-sample performance of our duration-based estimators for both spot and integrated volatility compared to some established methods. An empirical application based on intraday data for the SPDR S&P 500 ETF highlights the improved forecasting accuracy of our integrated volatility estimator within a standard daily volatility forecasting framework. Furthermore, an intraday analysis based on our spot volatility estimator reveals an immediate and substantial impact of FOMC news announcements on market volatility.

Declaration

I hereby declare that except where specific reference is made to the work of others, the contents of this dissertation are original and have not been submitted in whole or in part for consideration for any other degree or qualification in this, or any other university. This dissertation is my own work and contains nothing which is the outcome of work done in collaboration with others, except as specified in the text and Acknowledgements.

Shifan Yu

July 2024

Acknowledgements

Completing this Ph.D. thesis has been a challenging but definitely rewarding journey. I owe my deepest gratitude to numerous individuals and organizations who have supported me every step of the way. This thesis would not have been possible without their help and support.

First and foremost, I would like to express my deepest gratitude to my Ph.D. supervisors, Prof. Ingmar Nolte and Prof. Sandra Nolte at Lancaster University, and Dr. Yifan Li at the University of Manchester. Thank you for introducing me to the world of financial econometrics and for your unwavering support since we first met seven years ago. I am incredibly grateful for the opportunity to collaborate with and learn from all of you. You are always available for in-depth discussions on research projects and to help me navigating the obstacles of the revision process for our papers. I have greatly benefited from your career advice and support, which has inspired me to pursue an academic career in financial econometrics.

I would like to extend my sincere appreciation to my Ph.D. viva examiners, Dr. Manh Pham (Lancaster University) and Prof. Roberto Renò (ESSEC Business School), for reviewing my thesis. I greatly appreciate your time, availability, and the insightful comments and feedback.

I am grateful to the North West Social Science Doctoral Training Partnership (NWSSDTP) of the Economic and Social Research Council (ESRC) for the Advanced Quantitative Methods Ph.D. Scholarship.[1] I am also thankful to the Department of Accounting and Finance and the Centre for Financial Econometrics, Asset Markets and Macroeconomic Policy (EMP) at Lancaster University Management School (LUMS) for providing comprehensive academic training, organizing stimulating academic events, and generously supporting my travel and visits. I thank all the academic and administrative staffs at Lancaster University, especially our Head of Department, Prof. Sandra Nolte, the EMP director, Prof. Ingmar Nolte, and the

[1]The thesis is funded by a four-year ESRC NWSSDTP studentship on "Jump robust volatility estimation and jump tests using renewal processes" (Ref. 2203142), with additional Advanced Quantitative Methods enhanced stipend, the Overseas Institutional Visits (OIV) scholarship, and the COVID-19 Phase 3 studentship extension.

program director of Ph.D. in Finance, Dr. Chelsea Yao.

I would like to thank Prof. Kim Christensen, Dr. Seok Young Hong, Dr. Aleksey Kolokolov, Prof. Olga Kolokolova, Dr. Manh Pham, Prof. Roberto Renò for their invaluable advice on both my research and career development. I deeply appreciate the time and expertise you have generously shared with me, and I am truly fortunate to have had the opportunity to learn from each of you. Specifically, I would like to express my gratitude to Prof. Kim Christensen for agreeing to be my host and advising me during my research visit at Aarhus University. It was a wonderful experience to have the opportunity to learn from your extensive knowledge and expertise in financial econometrics during our regular discussions.

Finally, I extend my heartfelt gratitude to my family and friends. While there are too many names to mention individually, the past five years have certainly been a remarkable experience and one of the most joyful episodes of my life, thanks to their continuous support and encouragement. I am profoundly fortunate to have all of you as a constant source of strength and inspiration in my life.

Contents

List of Figures xiii

List of Tables xv

1 Introduction 1

1.1 Overview . . . 1

1.2 Thesis Outline . . . 2

2 Testing for Jumps in a Discretely Observed Price Process with Endogenous Sampling Times 5

2.1 Introduction . . . 5

2.2 Setting and Assumptions . . . 8

2.2.1 Observation Scheme . . . 9

2.2.2 Price Duration Sampling . . . 12

2.3 Main Results . . . 16

2.3.1 Test Statistic . . . 16

2.3.2 Noise Mitigation . . . 18

2.4 Monte Carlo Simulations . . . 22

2.4.1 Simulation Design . . . 22

2.4.2 Test Performance in the Absence of Market Microstructure Noise . . . 25

2.4.3 Test Performance in the Presence of Market Microstructure Noise . . . 27

2.5 Empirical Analysis . . . 31

2.6 Conclusions . . . 33

3 Realized Candlestick Wicks **35**

3.1 Introduction . . . 35

3.2 Volatility Estimation Based on Range-Return Differences . . . 39

3.2.1 Range-Return-Difference Volatility (RRDV) Estimator . . . 39

3.2.2 Limit Theorems for Continuous Itô Semimartingales . . . 40

3.2.3 Jumps . . . 42

3.3 Extreme Return Persistence . . . 44

3.3.1 Drift Burst Model . . . 44

3.3.2 Persistent Noise Model . . . 46

3.4 Finite-Sample Refinements . . . 48

3.4.1 Finite-Sample Bias I: Discretization Errors . . . 48

3.4.2 Finite-Sample Bias II: V-Shapes . . . 52

3.5 Monte Carlo Simulations . . . 53

3.5.1 Simulation Design . . . 53

3.5.2 Asymptotic Unbiasedness . . . 55

3.5.3 Finite-Sample Performance . . . 57

3.6 Empirical Analysis . . . 58

3.6.1 Data . . . 60

3.6.2 Heterogeneous Autoregressive (HAR) Model . . . 60

3.6.3 Empirical Results . . . 62

3.7 Conclusions . . . 65

4 Decoupling Interday and Intraday Volatility Dynamics with Price Durations **67**

4.1 Introduction . . . 67

4.2 Econometric Framework . . . 70

4.2.1 Spot and Integrated Volatility Estimation with Price Durations . . . 72

4.2.2 A Semiparametric Model for Daily and Intraday Volatility Dynamics . . . 77

4.3 Simulation Results . . . 80

4.3.1 Simulation Design . . . 80

4.3.2 Model Estimation . . . 81

4.3.3 Spot Volatility Estimation . . . 82

4.3.4 Integrated Variance Estimation . . . 85
4.4 Empirical Analysis . . . 87
4.4.1 Overview . . . 88
4.4.2 Daily Volatility Forecasting . . . 90
4.4.3 Intraday Volatility Dynamics Around FOMC Announcements . . . 93
4.5 Conclusions . . . 94

References **97**

Appendix A Appendix to Chapter 2 **111**
A.1 Proofs . . . 111
A.1.1 Proof of Theorems 2.1 and 2.2 . . . 111
A.1.2 Proof of Proposition 2.1 . . . 122
A.2 Supplementary Results . . . 126
A.2.1 Parameter Choices for Other Tests . . . 126
A.2.2 Simulation Results with Other Noise Specifications . . . 126
A.2.3 Supplementary Empirical Results . . . 133

Appendix B Appendix to Chapter 3 **135**
B.1 Normalized High, Low, and Close . . . 135
B.2 Proofs . . . 141
B.2.1 Proof of Theorem 3.1 . . . 141
B.2.2 Proof of Theorem 3.2 . . . 144
B.2.3 Proof of Corollary 3.1 . . . 146
B.2.4 Proof of Proposition 3.1 . . . 147
B.2.5 Proof of Proposition 3.2 . . . 149
B.2.6 Proof of Proposition 3.3 . . . 151
B.2.7 Proof of Proposition 3.4 . . . 151
B.2.8 Proof of Corollary 3.2 . . . 155
B.3 Supplementary Materials . . . 155
B.3.1 Simulation Scheme . . . 155
B.3.2 Discretized Factors . . . 155

B.3.3 Monte Carlo Bias Results of Other Estimators 157
B.3.4 Monte Carlo RMSE Results of Other Estimators 157
B.3.5 Monte Carlo RMSE Results with Market Microstructure Noise 161

Appendix C Appendix to Chapter 4 **163**
C.1 Proofs 163
C.1.1 Proof of Proposition 4.1 163
C.1.2 Proof of Proposition 4.2 164
C.1.3 Proof of Corollary 4.1 166

List of Figures

2.1 Examples of price duration sampling 13
2.2 Rejection rates under two different sampling schemes 14
2.3 Some market activity variables of simulated price observations 25
2.4 Comparison of simulated latent prices and noise-contaminated prices 25
2.5 Finite-sample distributions of the standardized test statistic 26
2.6 Finite-sample distributions of the standardized test statistic in the presence of noise 27
2.7 Testing results for selected NYSE stocks 33

3.1 Examples of one-minute intraday candlestick charts for the simulated second-by-second log-prices from different DGPs 37
3.2 Comparison of approximated and simulated values of $\Lambda_{2,N}$ and Θ_N 50
3.3 5-minute candlesticks around a simulated V-shaped flash crash. 52
3.4 Examples of simulated price paths with extreme return persistence 55
3.5 Histograms and QQ plots of studentized estimation errors of one-second RRDV 57

4.1 Intraday variation of returns and annualized RVs of a simulated Heston process 81
4.2 Annualized spot volatility estimates over equidistant intervals 83
4.3 Comparisons of 5-minute spot volatility estimates when there exist jumps . . . 86
4.4 Correlograms of log-durations obtained with a fixed threshold and the predicted daily thresholds 88
4.5 Intraday seasonality for the conditional mean and variance of durations 90
4.6 Annualized spot volatility estimates on FOMC and non-FOMC days 95

List of Tables

2.1 Finite-sample size and power of the standardized test statistic 26
2.2 Finite-sample size and power in the presence of market microstructure noise . . 28
2.3 Finite-sample size and power of other tests 29
2.4 Finite-sample size and power of other noise-robust tests 30
2.5 Descriptive statistics of daily trades on selected NYSE stocks 32
2.6 Empirical rejection rates for selected NYSE stocks 32
2.7 Adjusted empirical rejection rates for selected NYSE stocks 34

3.1 Monte Carlo bias results of the RRDV estimator 56
3.2 Monte Carlo RMSE results of different IV estimators 59
3.3 Daily out-of-sample 5-minute HAR volatility forecasts 63
3.4 MSEs on days with/without discontinuities and episodic extreme return persistence 64

4.1 Parameter estimates of the log-ACD-GARCH model 82
4.2 Monte Carlo results for spot volatility estimation 85
4.3 Monte Carlo results for IV estimation 87
4.4 Parameter estimates of the log-ACD-GARCH model 89
4.5 Daily out-of-sample HAR volatility forecasts 93
4.6 Diebold-Mariano p-values for duration-based volatility forecasts 94

A.1 Finite-sample size and power under Gaussian noise 127
A.2 Finite-sample size and power of other tests under Gaussian noise 128
A.3 Finite-sample size and power of other noise-robust tests under Gaussian noise . 128
A.4 Finite-sample size and power under autocorrelated Gaussian noise 129

A.5 Finite-sample size and power of other tests under autocorrelated Gaussian noise 130
A.6 Finite-sample size and power of other noise-robust tests under autocorrelated Gaussian noise 130
A.7 Finite-sample size and power under t-distributed noise 131
A.8 Finite-sample size and power of other tests under t-distributed noise 132
A.9 Finite-sample size and power of other noise-robust tests under t-distributed noise 132
A.10 Empirical rejection rates of other tests for selected NYSE stocks 133
A.11 Adjusted empirical rejection rates of other tests for selected NYSE stocks . . . 134

B.1 Analytical values of $\lambda_{p,r} = \mathbb{E}[\omega^p |c|^r]$ 142
B.2 Bias factor $M_{p,r}$ for discrete moment $\lambda_{p,r,N}$ 154
B.3 Polynomial regression results for discrete factors 156
B.4 Simulated values for discrete factors 156
B.5 Monte Carlo bias results: Truncated realized volatility (TRV) 157
B.6 Monte Carlo bias results: Differenced-return volatility (DV) 158
B.7 Monte Carlo bias results: Generalized differenced-return volatility (DV_{1-3}) . . 159
B.8 Monte Carlo RMSE results of other estimators 160
B.9 Monte Carlo RMSE results with market microstructure noise 162

Chapter 1

Introduction

1.1 Overview

The advent of high-frequency intraday data for various financial assets and instruments, starting in the early 2000s, sparked the development of both theoretical innovations and empirical insights related to the enhanced measurement, modeling, forecasting, and pricing of time-varying financial market volatility (Bollerslev, 2022). Based on the idea that the distance between price observations over fixed time intervals shrinks towards zero, the volatility measures constructed from high-frequency data rationalize the econometric analyses of volatility within the continuous-time Itô semimartingale framework, with theoretical statistical properties under so-called "infill asymptotics". Since the realized volatility (RV) estimator of Andersen and Bollerslev (1998), the increasing data availability has motivated significant advancements in the field of high-frequency financial econometrics over the past two decades (Aït-Sahalia and Jacod, 2014). However, as highlighted by recent empirical findings in the literature, the persistent occurrence of deviations from the theoretical models in real-world high-frequency data raises new challenges for traditional techniques to extract relevant economic information for practitioners. The primary aim of current research in this field is to address the following research questions: How can the traditional econometric methods for high-frequency financial data be enhanced to mitigate the impact of both well-known and newly discovered data characteristics? How can the accuracy of extreme event identification be improved to extract useful economic information?

This thesis revolves around the development of new statistical inference tools with high-frequency financial data under some alternative observation or sampling schemes. Chapter 2

develops a novel high-frequency jump test based on intraday price observations recursively sampled at first exit times. Chapter 3 introduces a new volatility estimator constructed from high-frequency candlesticks, which are more accessible to general investors than the tick-level Trade and Quote (TAQ) data. Finally, Chapter 4 proposes an adaptive endogenous sampling scheme, which decomposes daily volatility dynamics from intraday durations obtained across multiple days, and thus enhance the flexibility of parametric duration-based volatility estimation.

1.2 Thesis Outline

The three main chapters of this thesis are self-contained research articles that can be read independently from each other. The outline for the thesis is as follows.

Chapter 2: Testing for Jumps in a Discretely Observed Price Process with Endogenous Sampling Times

There exists a consensus in the financial literature that modeling asset price dynamics requires the specification of different components. In addition to the stochastic volatility component which accommodates the persisitence of volatility, extreme price shifts or "jumps" serve as an explanation for abnormal large variations that play an important role in the tail behavior of return distributions. Over the past two decades, a number of jump tests based on high-frequency financial data have been developed, while most, if not all, of those tests can sometimes deliver inconsistent results in practice. Their performance depends crucially on: (i) the choice of sampling methods and frequencies, and (ii) the assumption about measurement errors or, more precisely, the market microstructure noise.

In this chapter, we propose a new nonparametric method to test for jumps in a discretely observed noise-contaminated semimartingale. Different from the common equidistant sampling scheme, we sample the discrete price observations recursively when a symmetric double barrier is breached. The sampling times are determined endogenously by the accumulative tick-by-tick returns, which leads to less information loss compared with an exogenous sampling scheme. To distinguish the barrier "overshoots" caused by discrete Brownian steps and by jumps, we censor the increments between consecutive sampling times with a specific threshold. The standardized test statistic constructed to compare the sample moments of censored and uncensored increments

delivers reliable results for the existence of jumps. Moreover, we illustrate that our new test is robust to weakly dependent market microstructure noise with a two-step noise reduction method inspired by the pre-averging method of Jacod et al. (2009) and the wild bootstrap.

Via both simulation and empirical analyses, we clearly demonstrate the superior performance of our method, which is fairly robust to market microstructure noise, sparse sampling and different tuning parameter choices, and also exhibits fewer spurious detections compared to some commonly used tests constructed from equidistantly sampled observations. Our empirical study based on NYSE-traded stocks provides clear statistical evidence for the presence of jumps, but we conclude that jumps are not as frequent as the results of some competing tests indicate.

Chapter 3: Realized Candlestick Wicks

The discussion about intraday periods with short-lived explosive trends exhibited in asset prices has been thrust into the spotlight since the May 2010 Flash Crash in the U.S. stock market. The usual tenet that, for a semimartingale, volatility dominates the return dynamics under infill asymptotics is not necessarily true if the local drift coefficient diverges at a suitable rate, i.e., the "Drift Burst Hypothesis" of Christensen et al. (2022). Empirical evidence in recent financial literature shows that events like mini flash crashes occur more frequently in recent years, which raises widespread concern about market ineffciency and vulnerability. These market glitches are also a threat to the standard theoretical framework, as a temporary violation of the Itô semimartingale and potentially the no-arbitrage principle, and thereby raise new challenges for the estimation of integrated variance (IV), which serves as the cornerstone of statistical inference with high-frequency financial data.

In this chapter, we develop a novel nonparametric IV estimator that utilizes intraday candlestick information, comprised of the high, low, open, and close prices within short intraday time intervals. Our range-return-difference volatility (RRDV) estimator can exclude excessive return variation induced by short-lived dominant trends and consistently estimate IV from the diffusion component. We demonstrate that our RRDV estimator can provide consistent estimates with variances about four times smaller than those obtained with the differenced-return volatility (DV) estimator of Andersen et al. (2023a). Monte Carlo simulation results confirm the reliable finite-sample performance of RRDV across various scenarios. An empirical illustration on the SPDR S&P 500 ETF Trust (SPY) indicates that the robustness of RRDV in

the presence of extreme price movements contributes to a substantial reduction in occurrences of extremely misleading forecasts and, consequently, improves prediction accuracy when it is integrated within some standard framework of volatility forecasting.

Chapter 4: Decoupling Interday and Intraday Volatility Dynamics with Price Durations

Since the autoregressive conditional duration (ACD) model of Engle and Russell (1998), some studies highlight the feasibility of a parametric structure for duration-based volatility estimators, which enables more flexible inference on intraday volatility. The parametric duration-based estimators can utilize data beyond the estimation window to improve parameter estimation, and potentially achieve more accurate volatility estimates (Tse and Yang, 2012). However, the incorporation of intraday durations beyond a specific day will introduce complexities. Specifically, the durations between consecutive sampling times (same as Chapter 2) with the same threshold for different days will encompass different daily volatility dynamics, which leads to challenges in both model estimation and the analysis of volatility patterns.

In this chapter, we introduce an innovative semiparametric method to (i) nonparametrically decompose the daily and intraday volatility dynamics inherent in the durations obtained across multiple days, and (ii) parametrically estimate both the spot and integrated volatility based on durations. For each day, we adopt a nonparametrically predicted threshold to maintain a relatively consistent number of durations. As the interday persistence of volatility is subsumed into the thresholds, the durations from each day preserve only intraday volatility dynamics. Moreover, we derive a relationship between spot volatility and the conditional density of durations under some mild conditions, which provides an opportunity to estimate the volatility with some parametric duration models. Simulation results demonstrate superior finite-sample performance of our duration-based estimators for both spot and integrated volatility compared to some selected competitors. An empirical application based on intraday SPY transaction data highlights the improved forecasting accuracy of the standard HAR model augmented with our duration-based IV estimator. An intraday analysis based on our spot volatility estimator reveals an immediate and substantial impact of FOMC news announcements on volatility.

Chapter 2

Testing for Jumps in a Discretely Observed Price Process with Endogenous Sampling Times[1]

2.1 Introduction

There exists a consensus in the financial literature that modeling asset price dynamics requires the specification of different components. In addition to the stochastic volatility component which accommodates the persistence of volatility, "jumps" in asset prices serve as an explanation for abnormal large variations which play an important role in the tail behavior of return distributions. Jumps are believed to contain predictive information, such that the correct identification of jumps usually leads to improved price or volatility forecasts and portfolio outcomes (see, e.g., Yan, 2011, Jiang and Yao, 2013, Cremers et al., 2015, for empirical applications using daily or monthly financial data, and Andersen et al., 2007a, Corsi et al., 2010, Nolte and Xu, 2015, Bollerslev et al., 2015, 2020, Pelger, 2020, for those using high-frequency intraday data). The increased availability of high-frequency financial data has further motivated the development of methodologies designed to test the model specification based on a discretely observed semimartingale.

Over the past two decades, a number of nonparametric jump tests have been developed.

[1]This chapter corresponds to Li et al. (2024a), resubmitted to the *Journal of Econometrics*.

Starting from the seminal work of Barndorff-Nielsen and Shephard (2004), most of these tests are constructed on jump-robust measures of returns or their variations, see, e.g., Huang and Tauchen (2005), Barndorff-Nielsen and Shephard (2006), Andersen et al. (2007c), Jiang and Oomen (2008), Lee and Mykland (2008), Aït-Sahalia and Jacod (2009), Corsi et al. (2010), Podolskij and Ziggel (2010), Andersen et al. (2012), Lee and Mykland (2012), and Aït-Sahalia et al. (2012), among others. Some recent works focus on modified versions of these tests when conventional assumptions are violated, see, e.g., Laurent and Shi (2020) and Kolokolov and Renò (2024), and tests for co-jumps in a collection of assets, see, e.g, Bibinger and Winkelmann (2015) and Caporin et al. (2017).

Despite the theoretical developments in the literature, these jump tests in practice can sometimes deliver inconsistent results. Theodosiou and Žikeš (2011), Dumitru and Urga (2012), and Maneesoonthorn et al. (2020) conduct comparisons of various tests based on Monte Carlo simulations and real-world high-frequency data. These papers convincingly show that the performances of various jump tests depend crucially on: (i) the choice of sampling interval, and (ii) the assumption about market microstructure noise. For the first issue, a large sampling interval is typically needed for most classical tests to alleviate the impact of noise, but it also has a detrimental effect on their statistical power. As a result, it is difficult to determine an appropriate sampling interval for these tests in practice. For the second issue, Dumitru and Urga (2012) illustrate that ignoring even an independent and identically distributed (i.i.d.) additive noise can result in significant size distortion for the "star performers" in the literature. It is obvious that a more intricate noise specification, such as those discussed in Kalnina and Linton (2008), Bandi and Russell (2008), Aït-Sahalia et al. (2011), Hautsch and Podolskij (2013), Jacod et al. (2017), Li et al. (2020), Da and Xiu (2021), and Li and Linton (2022), can further muddle this issue.

In this chapter, we introduce an innovative nonparametric method to test for jumps in a discretely observed semimartingale. Different from the conventional practice of sampling observations at equidistant intervals in calendar time, our methodology adopts a path-dependent approach to sample tick-by-tick observations, inspired by the works of Engle and Russell (1998), Andersen et al. (2008), Fukasawa and Rosenbaum (2012), Vetter and Zwingmann (2017), and Hong et al. (2023): Sampling times are recursively determined by the first exit time of price movements from a symmetric barrier since the previous sampled observation. This endogenous

sampling scheme is tailored to be sensitive to discontinuities. Specifically, jumps of sizes larger than the barrier width will immediately trigger the stopping rule and induce large "overshoots" or threshold exceedances. To distinguish between threshold exceedances caused by discrete Brownian steps and those by jumps, we censor the returns between consecutive sampling times with a specific threshold,[2] and construct a standardized test statistic to measure the potential distortion caused by disproportionately large overshoots on the sample moment of returns. Furthermore, we develop a two-step noise reduction method inspired by the pre-averaging approach of Jacod et al. (2009) and the wild bootstrap introduced by Wu (1986) to mitigate the impact of weakly dependent market microstructure noise.

Simulation results reveal that our new high-frequency jump test exhibits reliable finite-sample size and power performance across various aggregation levels, and its performance is robust to measurement errors simulated with a realistically calibrated specification. A comparison with traditional tests constructed from equidistantly sampled observations and some noise-robust versions based on ultra-high-frequency data is conducted thereafter. We find that (i) most calendar-time-sampled tests exhibit less consistent performance across different sampling frequencies and are poorly sized in the presence of noise, which is in line with the Monte Carlo results of Dumitru and Urga (2012) and Maneesoonthorn et al. (2020), and (ii) while noise-robust tests maintain reliable sizes, their power performance still lags behind our test across a wide range of simulation settings. In an empirical application, our test is applied to transaction data of 10 selected stocks listed on the New York Stock Exchange (NYSE). Clear statistical evidence of jumps is found for all selected stocks, with jumps occurring on approximately 10% to 15% of trading days. Furthermore, the test rejections are highly robust to the correction of spurious detections based on the method of Bajgrowicz et al. (2016).

The remainder of this chapter is structured as follows: Section 2.2 lays out the basic setup and key assumptions. Section 2.3 discusses the test statistic and its asymptotic theory, along with the noise reduction technique. Section 2.4 assesses the finite-sample performance of our new test with Monte Carlo simulations. After discussing the empirical application for selected NYSE stocks in Section 2.5, we conclude in Section 2.6. All proofs and additional materials

[2] Related works about the boundary crossing problems for random walks, especially those with Gaussian steps, include Rogozin (1964), Lorden (1970), Lotov (1996), and Khaniyev and Kucuk (2004). The idea of censored increments in this chapter was inspired by the truncated realized volatility of Mancini (2009), which is the first work that utilizes the systematic observation error as an effective way to eliminate the impact of jumps.

can be found in Appendix A.

2.2 Setting and Assumptions

We consider a one-dimensional underlying process $X = (X_t)_{t\geq 0}$ for the efficient logarithmic price of a financial asset. We assume that X follows a possibly discontinuous Itô semimartingale defined on a filtered probability space $(\Omega, \mathcal{F}, (\mathcal{F}_t)_{t\geq 0}, \mathbb{P})$:

$$\begin{aligned} X &= X' + X'', \\ X'_t &= X_0 + \int_0^t \mu_s ds + \int_0^t \sigma_s dW_s, \\ X''_t &= \int_0^t \int_{|\delta|\geq u} \delta(s,x) \underline{p}(ds,dx), \end{aligned} \tag{2.1}$$

where t stands for time, W is a standard Brownian motion, $\underline{p}(dt,dx)$ is a Poisson random measure on $\mathbb{R}_+ \times \mathbb{R}$ with a compensator $\underline{q}(dt,dx) = dt \otimes \lambda(dx)$, and λ is a σ-finite measure on $\mathbb{R}_+$. We assume that X satisfies the following regularity conditions:

Assumption 2.1. (i) The process μ is optional and locally bounded;
(ii) The process σ is càdlàg (i.e., right-continuous with left limits), adapted, and strictly positive;
(iii) There exists a sequence $(\tau_m)_{m\geq 1}$ of stopping times increasing to ∞, and a sequence $(K_m)_{m\geq 1}$ of finite constants, such that it holds for each $m \geq 1$ that $\mathbb{E}[|\sigma_{t\wedge\tau_m} - \sigma_{s\wedge\tau_m}|^2] \leq K_m|t-s|$ for all $s,t \in [0,T]$ with some finite T;
(iv) The function $\delta(\omega,t,x)$ on $\Omega \times \mathbb{R}_+ \times \mathbb{R}$ is predictable;
(v) There is a localizing sequence $(\tau_n)_{n\geq 1}$ of stopping times increasing to ∞, and a sequence $(f_n)_{n\geq 1}$ of deterministic nonnegative functions on $\mathbb{R}$, which satisfies $|\delta(\omega,t,x)| \wedge 1 \leq f_n(x)$ for all (ω,t,x) with $t \leq \tau_n(\omega)$, and $\int_{\mathbb{R}} |f_n|^r \lambda(dx) < \infty$ for some $r \in [0,1)$.

Remark 2.1. Assumption 2.1 entails some very mild technical conditions that the coefficients in Eq. (2.1) should meet. Condition (iii) states that the spot volatility process is locally 1/2-Hölder continuous under the L_2-norm. The smoothness condition is satisfied whenever σ is an Itô semimartingale, or a long memory process driven by a fractional Brownian motion (Bollerslev et al., 2021). The parameter r in Condition (v) sets a bound on the degree of jump activity, which can be interpreted as a generalized version of the Blumenthal-Getoor index for a Lévy process. With some $r \in [0,1)$, we consider jumps of both finite and infinite activities, but

restrict them to be of finite variation, i.e., they are absolutely summable, such that in Eq. (2.1) we dispense with the integral with $\underline{p} - \underline{q}$, see Jacod et al. (2019) for more details.

Remark 2.2. For the pure jump process X'' in Eq. (2.1), integrating $\delta(s, x)$ over the range $(-\infty, -u] \cup [u, \infty)$ for some $u > 0$ removes all jumps of sizes smaller than u. For any fixed u, X'' is a finite-activity jump process. As $u \to 0$, X'' retains both "big" and "small" jumps, such that it converges pathwise to a process of infinite-activity jumps with finite variation. As only discrete observations of the realized sample path $X(\omega)$ are available, we shall assume a slightly higher order in probability for u compared to X' as the number of observations increases, which excludes the very small jumps relative to the increments of X'. Further clarification will be provided in Section 2.2.1 after detailing our observation scheme.

The quadratic variation (QV) of X over a finite interval $[0, t]$ is defined as

$$[X, X]_t = \int_0^t \sigma_s^2 ds + \sum_{0 \le s \le t} (\Delta X_s)^2, \quad \text{with } \Delta X_t = X_t - X_{t-}, \tag{2.2}$$

where the integrated variance (IV), $\int_0^t \sigma_s^2 ds$, summarizes the variation from X'.

Testing for jumps is a procedure to answer the fundamental question of whether the realized sample path $X(\omega)$ is continuous or not over a finite time interval, e.g., $(0, 1)$.[3] Technically speaking, we decompose the sample space Ω into two complementary subsets:

$$\begin{aligned} \Omega' &= \{\omega : X_t''(\omega) = 0, \forall t \in (0, 1)\}, \\ \Omega'' &= \{\omega : X_t''(\omega) \neq 0, \exists t \in (0, 1)\}, \end{aligned} \tag{2.3}$$

where Ω' (resp. Ω'') represents the null hypothesis (resp. alternative hypothesis) for a jump test, which assesses the plausibility of these two hypotheses based on discrete observations of $X(\omega)$.

2.2.1 Observation Scheme

We now describe how observations take place.[4] At stage n, we assume that the successive observations of $X(\omega)$ occur at times $0 = t_{n,0} < t_{n,1} < \dots$ for a sequence $(t_{n,i})$ of discrete times

[3] We restrict the alternative hypothesis to contain at least one jump on $(0, 1)$ as it is not feasible for a test to identify jumps occurring right at both end-points of the interval.

[4] We would like to distinguish the terms "observation scheme" and "sampling scheme" in this chapter. We allow both tick-level and sampled observations to form discrete-time processes, and the term "sampling" refers to a subsampling or subset selection procedure for the discrete observations at the highest frequency.

over a fixed interval (such as a trading day), which is normalized to the unit interval $[0,1]$. We set

$$N_t^n = \sum_{i\geq 1} \mathbb{1}_{\{t_{n,i}\leq t\}} \qquad \text{and} \qquad \Delta_{n,i} = t_{n,i} - t_{n,i-1}, \tag{2.4}$$

where $N \equiv N_1^n$ stands for the number of observations on $(0,1]$, and $\Delta_{n,i}$ is the i-th inter-observation lag at stage n. It is easily seen from the empirical tick-level data that the observation times are far from evenly spaced and usually dependent on $X(\omega)$ itself. Our assumption for the observation scheme over $[0,1]$ is outlined as follows:

Assumption 2.2. Let Δ_n be a positive sequence of real numbers satisfying $\Delta_n \to 0$ as $n \to \infty$. We define an intensity process of observations $\lambda = (\lambda_t)_{0\leq t\leq 1}$ with $\lambda_t = K\sigma_t^2$ for some $K > 0$. There exists a localizing sequence $(\tau_m)_{m\geq 1}$ of stopping times and positive constants $K_{m,p}$ and κ such that:

(i) With $(\mathcal{F}_t^n)_{t\geq 0}$ the smallest filtration containing $(\mathcal{F}_t)_{t\geq 0}$ and with respect to which all observation times $t_{n,i}$ are stopping times, for each $i = 1, 2, \ldots$, the variable $\Delta_{n,i}$ is, conditionally on $\mathcal{F}_{i-1}^n \equiv \mathcal{F}_{t_{n,i-1}}^n$, independent of $\mathcal{F}_\infty = \bigvee_{t\geq 0} \mathcal{F}_t$.

(ii) With the restriction $\{t_{i-1} < \tau_m\}$, we have for all $p \geq 2$,

$$\begin{aligned} \mathbb{E}[|\Delta_{n,i}\lambda_{t_{n,i-1}} - \Delta_n||\mathcal{F}_{i-1}^n] &\leq K_{m,1}\Delta_n^{2+\kappa}, \\ \mathbb{E}[|\Delta_{n,i}\lambda_{t_{n,i-1}}|^p|\mathcal{F}_{i-1}^n] &\leq K_{m,p}\Delta_n^p. \end{aligned} \tag{2.5}$$

A useful consequence of this Assumption is the following convergence in probability:

$$\Delta_n N_t^n \xrightarrow{\mathbb{P}} \tau(t) = \int_0^t \sigma_s^2 ds. \tag{2.6}$$

Remark 2.3. Assumption 2.2 is inspired by Assumption (O) of Jacod et al. (2017) and Assumption (O-ρ, ρ') of Jacod et al. (2019). The process λ controls for the "spot" observation arrival rates, and the unobserved Δ_n can be interpreted as an "average mesh size" between successive observations. Our choice of the intensity $\lambda = K\sigma^2$ implies higher observation frequencies of $X(\omega)$ during periods of high local volatility, which captures the diurnal patterns of transaction activities and intraday volatility. This is motivated by the empirical evidence of the E-mini S&P 500 futures contract in Andersen et al. (2018), which illustrates a notable similarity in the intraday U-shaped patterns of one-minute transaction counts and return

variation, where the pronounced spikes, typically align with market openings or announcements, roughly coincide. Note that λ is defined up to scale, which allows $K = 1$ to be set without loss of generality (by scaling Δ_n correspondingly), see further discussion in Jacod et al. (2017).

Remark 2.4. With the convergence result in Eq. (2.6), Assumption 2.2 implies a time-changed regular observation scheme under infill asymptotics: As $n \to \infty$, the observation time $t_{n,i}$ converges to $\breve{t}_{n,i} = \inf\{t \in [0,1] : \tau(t) = i\Delta_n\}$. This limiting observation scheme corresponds to Example 2.2 in Jacod et al. (2017). In contrast to the calendar time t, the "intrinsic time" $\tau(t)$ evolves endogenously with respect to the variation from X'. The time change induces a certain level of endogeneity, and extends the commonly assumed equidistant observation scheme in high-frequency financial econometrics literature (Li et al., 2014; Dimitriadis and Halbleib, 2022; Dimitriadis et al., 2023). With the irregular mesh sizes $\Delta_{n,i}$ regulated by Condition (ii), the deviation of $(t_{n,i})$ from $(\breve{t}_{n,i})$ vanishes as $n \to \infty$, and has no impact on the limit theorems derived in the next section. Further discussion on this matter can be found in Remark 2.7 and Appendix A.1.1.

We now revisit the Itô semimartingale in Eq. (2.1): Under the assumed observation scheme, we consider a sequence of processes defined on the same probability space $(\Omega, \mathcal{F}, (\mathcal{F}_t)_{t\geq 0}, \mathbb{P})$:

$$X_t^n = X_t' + \int_0^t \int_{|\delta|\geq u_n} \delta(s,x)\underline{p}(ds,dx), \tag{2.7}$$

and we choose a sequence u_n of real numbers satisfying

$$\frac{u_n}{\sqrt{\Delta_n}} \to \infty \qquad \text{and} \qquad u_n \Delta_n^{\beta-1/2} \to 0, \tag{2.8}$$

for any $0 < \beta \leq 1/2$. The choice of u_n of a slightly higher order than $\sqrt{\Delta_n}$ guarantees that, as $n \to \infty$, the integral with Poisson measure $\underline{p}$ in Eq. (2.7) retains both "big" and "small" jumps but excludes the very small ones of order $O_p(\sqrt{\Delta_n})$, i.e., the local alternative in the literature (see Remark 10.27, Aït-Sahalia and Jacod, 2014). Our test is designed to identify the existence of both the finite-activity and local-to-infinite-activity jumps which dominate the X' increments.

2.2.2 Price Duration Sampling

Sparse sampling is widely adopted in both the financial econometrics literature and by practitioners to mitigate the impact of market microstructure noise, with some popular choices like 1-minute and 5-minute sampling in calendar time (Aït-Sahalia et al., 2005; Liu et al., 2015). However, such sparse sampling aggregates a substantial amount of tick-level returns exogenously, which dilutes the relative size of jumps and inevitably reduces the power of jump tests. This phenomenon is evident in the Monte Carlo results of Dumitru and Urga (2012) and Maneesoonthorn et al. (2020): Nearly all traditional tests constructed from calendar-time-sampled returns exhibit rapid power loss as sampling becomes much sparser.[5]

In response to this issue, a path-dependent sampling scheme seems a natural solution. We consider a stochastic and endogenous sampling scheme for all observations of $X(\omega)$ on $[0,1]$: Let $(X_i)_{0\le i\le N}$ collect all observations under Assumption 2.2. With a selected barrier width $c>0$, the price duration sampling (PDS) is defined as the following sampling algorithm:

1. Set $\Pi_0^{(c)}=0$.
2. For $j=1,2,\dots,$ sample X_i for all $i=\Pi_j^{(c)}$ that are decided recursively by

$$\Pi_j^{(c)}=\inf\{\Pi_{j-1}^{(c)}<i\le N:|X_i-X_{\Pi_{j-1}^{(c)}}|\ge c\}. \tag{2.9}$$

We therefore obtain a subsequence $X^{(c)}=(X_{\Pi_j^{(c)}})_{0\le j\le N^{(c)}}$, where $N^{(c)}=\max_{j\ge1}\{\Pi_j^{(c)}\le N\}$ counts the total number of sampled observations. Moreover, we define the PDS returns as the increments of $X^{(c)}$, i.e., $r_j^{(c)}=X_{\Pi_j^{(c)}}-X_{\Pi_{j-1}^{(c)}}$ for all $j\in\{1,2,\dots,N^{(c)}\}$.

Remark 2.5. The above sampling algorithm is a discrete-time version of PDS in Hong et al. (2023). The idea of sampling financial observations based on hitting or exit times was initially proposed by Engle and Russell (1998), and has been further developed since then (Gerhard and Hautsch, 2002; Andersen et al., 2008; Tse and Yang, 2012; Fukasawa and Rosenbaum, 2012; Vetter and Zwingmann, 2017; Hong et al., 2023). While previous studies have primarily focused on volatility estimation based on this alternative sampling scheme, our contribution stands

[5] Some noise-robust tests constructed from filtered data, such as those proposed by Lee and Mykland (2012) and Aït-Sahalia et al. (2012), can utilize all available observations without sampling. As alternative methods that exploit data more sufficiently than classical approaches, we compare their finite-sample performance with our method through simulations in Section 2.4.

out as the first to demonstrate that this scheme can be exploited to construct more effective high-frequency jump tests.

This endogenous sampling scheme is designed to be highly sensitive to the presence of jumps. Fig. 2.1 demonstrates some examples when $X(\omega)$ is continuous and discontinuous, respectively. When $X(\omega)$ is continuous, each sampled return under PDS ("PDS return", i.e., first ladder height with respect to c) consists of the barrier width c and a small threshold exceedance attributed to the discreteness of price observations. When $X(\omega)$ is discontinuous, any single jump larger than c will always trigger an exit-time event in Eq. (2.9), and induce a large "overshoot".

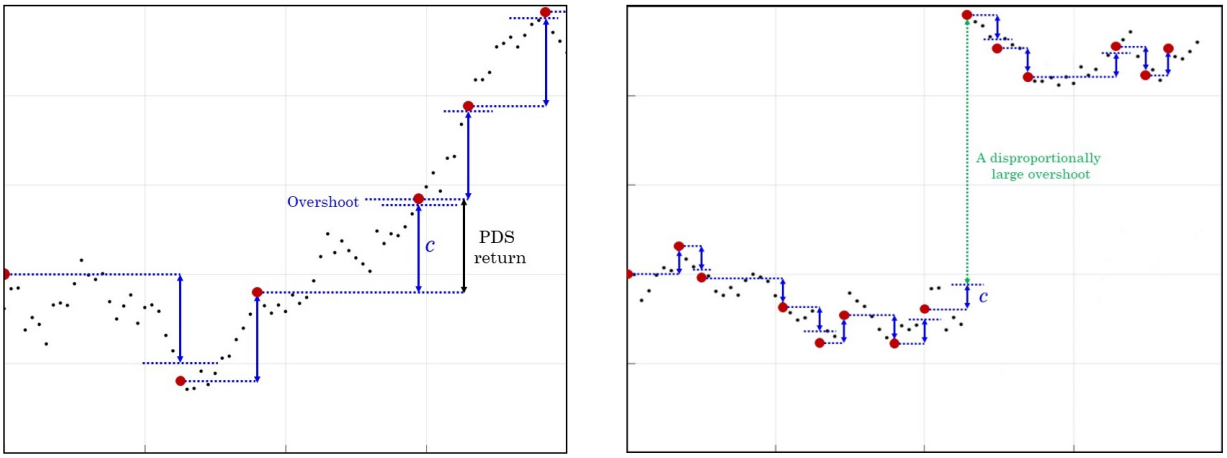

Fig. 2.1 Examples of PDS when $X(\omega)$ is continuous and discontinuous, respectively. Jumps will almost surely lead to the sampling of next available observation, and induce a large overshoot.

The discrepancy between threshold exceedances induced by continuous price increments and jumps can be exploited to construct more powerful jump tests. We provide some preliminary evidence for the impact of different sampling schemes on the power of jump tests with a simple Monte Carlo experiment for an idealized test: We simulate a standard Gaussian random walk with a fixed number of i.i.d. increments (corresponding to the limiting observation scheme in Remark 2.4), and a fixed-size jump is randomly inserted into each simulated path. We then obtain sampled returns with both PDS and equidistant sampling across a wide range of sampling frequencies. For any (PDS or equidistantly) sampled return, we reject the null hypothesis of no jump if the absolute return exceeds its theoretical 95% quantile under the null. This test maintains the correct size by construction for any sampling frequency. When a fixed-size jump is randomly inserted, the sampling frequency inversely controls the "signal-to-noise" ratio, as

the jump size gets diluted by the size of aggregated returns over that interval. This allows us to effectively compare the local power performance of the test under the two sampling schemes.

Fig. 2.2 reports the power curves of the test under both sampling schemes (under the alternative hypothesis that the tested interval contains a jump). We observe that both curves decay towards the nominal level of 5% as the sampling becomes more sparse. However, the test based on PDS returns exhibits uniformly better power than the one based on equidistantly sampled returns across all common sampling frequencies. Intuitively, this power gain is attributed to the sensitivity of our sampling algorithm to jumps, which ensures the jump size information is effectively preserved in the threshold exceedance. By contrast, the equidistant sampling scheme aggregates returns exogenously, where the jump size is diluted much more quickly by the decreasing sampling frequency relative to the PDS case. This advantageous property of PDS contributes to a diminished probability of committing a Type II error, and thereby serves as the main motivation for the new statistical test proposed in the next section.

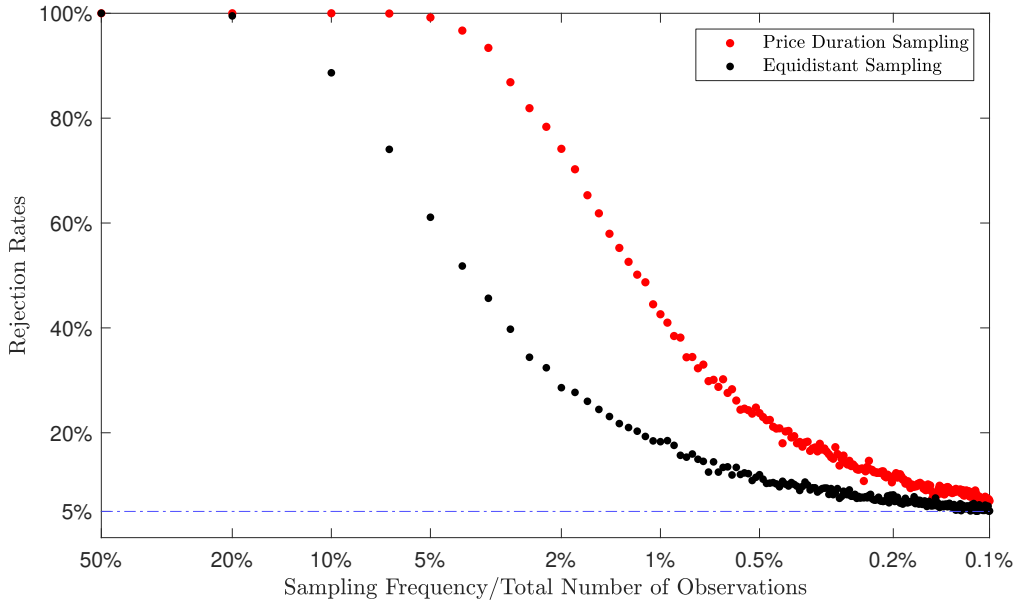

Fig. 2.2 Rejection rates under two different sampling schemes. We simulate 2000 random walk paths with 10^6 standard normal steps. A jump of fixed size 10 are randomly inserted in each path. Under two different sampling schemes, the absolute returns containing jumps are compared with the 95% quantiles of absolute sampled returns under the null.

We now formally introduce our asymptotic setting under PDS. We let the barrier width c shrink proportionally to $\sqrt{\Delta_n}$ under infill asymptotics:

$$c \equiv c_n = m\sqrt{\Delta_n}, \quad \text{for some constant } m > 0. \tag{2.10}$$

When $X(\omega)$ is continuous, each absolute PDS return $|r_i^{(c)}|$ is a sum of the barrier width c and a small threshold exceedance caused by the discreteness of observations, which satisfies

$$1 \leq \frac{|r_i^{(c)}|}{c} = O_p(1), \quad \text{for all } i \in \{1, 2, \ldots, N^{(c)}\}. \tag{2.11}$$

Jumps of a higher asymptotic order than $\sqrt{\Delta_n}$ will almost surely trigger the stopping rule in Eq. (2.9), and induce some disproportionally large PDS returns with

$$\frac{|r_i^{(c)}|}{c} \xrightarrow{\text{a.s.}} \infty. \tag{2.12}$$

To distinguish between the "small" overshoots induced by continuous price increments and the "big" overshoots caused by jumps, we censor the (absolute) PDS returns with a threshold $\varphi_\epsilon(c)$ that shrinks to zero at the same rate $\sqrt{\Delta_n}$ as the barrier width c, i.e., for all $i \in \{1, 2, \ldots, N^{(c)}\}$,

$$|\overline{r}_i^{(c)}| = |r_i^{(c)}| \wedge \varphi_\epsilon(c), \quad \text{where } \varphi_\epsilon(c) = c\,(1+\epsilon) \text{ for some constant } \epsilon > 0. \tag{2.13}$$

Remark 2.6. The idea of censored returns originates from the truncated realized volatility (TRV) estimator of Mancini (2009), while the fixed choice of ϵ in Eq. (2.13) is unconventional in the literature. Different from the standard truncation threshold of a slightly higher order than $\sqrt{\Delta_n}$, our selected threshold $\varphi_\epsilon(c) \asymp \sqrt{\Delta_n}$ affects both the increments from X' and X'' under infill asymptotics. This overcomes the "perfect correlation" issue of TRV and RV (Podolskij and Ziggel, 2010), and enables the construction of feasible test statistics that do not necessarily require consistent IV estimation.[6]

[6] With the standard truncation threshold, the realized moments of truncated and untruncated increments have the same asymptotic distribution if $X(\omega)$ is continuous, such that it is impossible to derive the distribution theory for either the linear or ratio test based on the standard TRV and RV estimators. In this chapter, as our method does not require consistent IV estimation, we can also adopt the truncation technique of Mancini (2009) and discard all absolute PDS returns that are larger than $\varphi_\epsilon(c)$. However, the censoring approach does not change the total number of PDS returns and is therefore more convenient for both our theoretical derivation and empirical implementation.

2.3 Main Results

In this section, we introduce and analyze our new test statistic, which is constructed from the PDS returns between sampled observations collected by $X^{(c)}$. Then we augment the test with an effective noise reduction method to mitigate the impact of market microstructure noise.

2.3.1 Test Statistic

To prepare for the construction of our test statistic, we first introduce the notation for the moments of PDS returns from a standard Gaussian random walk $(Z_i)_{i=0,1,\dots}$ with a barrier width m, which is denoted as $Z_1^{(m)}$:

(i) Absolute moment of $Z_1^{(m)}$: $\mu_\gamma(m) = \mathbb{E}[|Z_1^{(m)}|^\gamma]$,
(ii) Absolute moment of censored $Z_1^{(m)}$: $\overline{\mu}_{\gamma,\epsilon}(m) = \mathbb{E}[|\overline{Z}_1^{(m)}|^\gamma] = \mathbb{E}[(|Z_1^{(m)}| \wedge \varphi_\epsilon(m))^\gamma]$,
(iii) Absolute cross moment of censored and uncensored $Z_1^{(m)}$: $\overline{\rho}_{\gamma,\epsilon}(m) = \mathbb{E}[|Z_1^{(m)}|^\gamma |\overline{Z}_1^{(m)}|^\gamma]$,

and two first-order differentiable and invertible functions:

$$h_\gamma(m) = \frac{\mu_\gamma(m)}{m^\gamma} \qquad \text{and} \qquad \overline{h}_{\gamma,\epsilon}(m) = \frac{\overline{\mu}_{\gamma,\epsilon}(m)}{m^\gamma}, \tag{2.14}$$

with the first-order derivatives $h'_\gamma(m)$ and $\overline{h}'_{\gamma,\epsilon}(m)$, and the inverse functions $h_\gamma^{-1}(x)$ and $\overline{h}_{\gamma,\epsilon}^{-1}(x)$.

We will now proceed to define the testing procedures. For all observations $(X_i)_{0\le i\le N}$ under Assumption 2.2, we obtained the sampled observations in $X^{(c)}$ with the barrier width c that satisfies Eq. (2.10). To assess the distortion resulting from "large" overshoots, we compare the sample moments of uncensored and censored PDS returns normalized by the barrier width c, i.e.,

$$S_2 = \frac{1}{N^{(c)}} \sum_{i=1}^{N^{(c)}} \left(\frac{|r_i^{(c)}|}{c}\right)^2 \quad \text{and} \quad \overline{S}_{2,\epsilon} = \frac{1}{N^{(c)}} \sum_{i=1}^{N^{(c)}} \left(\frac{|\overline{r}_i^{(c)}|}{c}\right)^2, \tag{2.15}$$

with the functions defined in Eq. (2.14):

$$M_c = h_2^{-1}(S_2) \qquad \text{and} \qquad \overline{M}_{c,\epsilon} = \overline{h}_{2,\epsilon}^{-1}\left(\overline{S}_{2,\epsilon}\right). \tag{2.16}$$

Theorem 2.1 (Consistency)**.** With Assumption 2.2 satisfied and $c = m\sqrt{\Delta_n}$, it holds that as

$n \to \infty$,

$$\begin{aligned} (\overline{M}_{c,\epsilon}, M_c)' &\xrightarrow{\mathbb{P}} (m, m)', \qquad \text{if } \omega \in \Omega', \\ (\overline{M}_{c,\epsilon}, M_c)' &\xrightarrow{\mathbb{P}} (m, m^*)', \qquad \text{if } \omega \in \Omega'', \end{aligned} \tag{2.17}$$

where $m^* = h_2^{-1}(\kappa \cdot h_2(m))$ with κ the ratio between QV and IV over $[0, 1]$.

Remark 2.7. The estimators $(\overline{M}_{c,\epsilon}, M_c)'$, constructed from the PDS returns from (i) the observations $(X_i)_{0 \le i \le N}$ on $(t_{n,i})$ with irregular $\Delta_{n,i}$ under Assumption 2.2, and (ii) the Gaussian random walk formed by observations under the limiting observation scheme $(\check{t}_{n,i})$ in Remark 2.4, are shown to have the same limit theorems. These include the law of large numbers (LLN) and the central limit theorem (CLT), both supported by some strong approximation results similarly used in Chernozhukov et al. (2013, 2019), see Appendix A.1.1 for further details. The consistency and asymptotic distribution in Theorem 2.1 and the subsequent Theorem 2.2, respectively, are therefore derived from the random sum LLN and CLT introduced by Anscombe (1952) for randomly indexed random walks (Rényi, 1957; Gut, 2009, 2012). Under the alternative, jumps have no impact on $\overline{M}_{c,\epsilon}$ since $\varphi_\epsilon(c)$ shrinks to zero at the same speed as $\sqrt{\Delta_n}$, while M_c will converge to a different level due to the distortion arising from large overshoots.

Remark 2.8. Whether $X(\omega)$ is continuous or not, once the barrier width c is chosen, a consistent IV estimator should be proportional to the number of sampled observations $N^{(c)}$. Specifically, with a fully observable sample path $X(\omega)$ over $[0, 1]$, the nonparametric duration-based volatility (NPDV) estimator of Hong et al. (2023), i.e., $\widehat{V} = c^2 N^{(c)}$, is shown to be consistent since all absolute PDS returns are exactly c. In a more realistic setting with an infinite number of discrete observations of $X(\omega)$ over $[0, 1]$, we define $\widehat{V}^* = \tilde{c}^2 N^{(c)}$, where $\tilde{c}^2 = c^2 h_2(\overline{M}_{c,\epsilon})$ is corrected for "small" overshoots from discrete Brownian steps with a consistent estimator of m. Even though the estimation of IV is not the primary focus of this work, it contributes to a more accurate duration-based estimator with the discretization error corrected.

Furthermore, both $\overline{M}_{c,\epsilon}$ and M_c are jointly asymptotically normal under the null with a known variance-covariance matrix, which naturally leads to a well-defined ratio test.

Theorem 2.2 (Asymptotic normality)**.** Under the same conditions as in Theorem 2.1, the

estimators $\overline{M}_{c,\epsilon}$ and M_c are jointly normally distributed when $\omega \in \Omega'$:

$$\sqrt{N}\begin{bmatrix}\overline{M}_{c,\epsilon} - m \\ M_c - m\end{bmatrix} \xrightarrow{\mathcal{L}} \mathcal{N}\left(\begin{bmatrix}0\\0\end{bmatrix}, \begin{bmatrix}\phi_{11} & \bullet \\ \phi_{21} & \phi_{22}\end{bmatrix}\right), \tag{2.18}$$

where

$$\phi_{11} = \frac{\mu_2(m)(\overline{\mu}_{4,\epsilon}(m) - \overline{\mu}^2_{2,\epsilon}(m))}{m^4(\overline{h}'_{2,\epsilon}(m))^2}, \tag{2.19}$$

$$\phi_{22} = \frac{\mu_2(m)(\mu_4(m) - \mu_2^2(m))}{m^4(h'_2(m))^2}, \tag{2.20}$$

$$\phi_{21} = \frac{\mu_2(m)(\overline{\rho}_{2,\epsilon}(m) - \mu_2(m)\overline{\mu}_{2,\epsilon}(m))}{m^4(h'_2(m)\overline{h}'_{2,\epsilon}(m))^2}. \tag{2.21}$$

Corollary 2.1. Under the same conditions, the standardized ratio test statistic $T_{c,\epsilon}$ satisfies

$$T_{c,\epsilon} = \frac{\overline{M}_{c,\epsilon}/M_c - 1}{\sqrt{\widehat{V}_\epsilon(\overline{M}_{c,\epsilon})}} \quad \begin{cases} \xrightarrow{\mathcal{L}} \mathcal{N}(0,1) & \text{if } \omega \in \Omega', \\ \xrightarrow{\mathbb{P}} \infty & \text{if } \omega \in \Omega'', \end{cases} \tag{2.22}$$

where the denominator is the estimated standard deviation of $\overline{M}_{c,\epsilon}/M_c$ with

$$\widehat{V}_\epsilon(m) = \frac{1}{m^2 N}(\phi_{11} + \phi_{22} - 2\phi_{21}). \tag{2.23}$$

When $X''(\omega) \equiv 0$ on the interval $(0,1)$, the test statistic $T_{c,\epsilon}$ converges in distribution to a standard normal random variable, which is implied by Theorem 2.2. When $X''(\omega) \neq 0$ for some $t \in (0,1)$, the numerator of $T_{c,\epsilon}$ converges to a finite non-zero level determined by κ, whereas its denominator shrinks to zero as $n \to \infty$. Consequently, the standardized test statistic diverges in the limit, thereby implying the consistency of the test under the alternative hypothesis.

2.3.2 Noise Mitigation

As discussed in Remark 2.7, our asymptotic results derived in Section 2.3.1 are based on the conclusion that our estimators constructed from the sampled returns of (i) the observations on $(t_{n,i})$ under Assumption 2.2, and (ii) the observations on $(\breve{t}_{n,i})$ in Remark 2.4, have the same limit theorems. Since the observations on $(\breve{t}_{n,i})$ form a random walk with all i.i.d. Gaussian steps,

the sampled observations under PDS constitute a stopped random walk (Gut, 2009), which is essential for the applicability of the random sum LLN and CLT of Anscombe (1952). However, this rationale becomes untenable when the observations are contaminated by measurement errors such as market microstructure noise. In this section, we propose an empirically plausible approach to mitigate the noise. With a two-step noise reduction method, we transform the noise-contaminated observations into a sequence of pseudo-observations, which behaves locally like a Gaussian random walk in the limit. Since each sampled return is only determined by finitely many tick-level returns within a local horizon, our test statistic that relies solely on the sample moments of normalized PDS returns remains valid.

To this end, we assume an additive noise term with a weak dependence structure, before which we recall the definition of α-mixing (Fan and Yao, 2003): The α-mixing coefficient of a stationary sequence $(X_i)_{i\in\mathbb{Z}}$ of variables indexed by $i \in \mathbb{Z}$ is defined as

$$\alpha(h) = \sup\{|\mathbb{P}(A \cap B) - \mathbb{P}(A)\mathbb{P}(B)| : A \in \mathcal{F}_i,\, B \in \mathcal{F}^{i+h}\}, \tag{2.24}$$

where the pre- and post-σ-fields are defined as $\mathcal{F}_j = \sigma(\{X_i : i \le j\})$ and $\mathcal{F}^j = \sigma(\{X_i : i \ge j\})$. The process (X_i) is said to be α-mixing if $\alpha(h) \to 0$ as $h \to \infty$.

Assumption 2.3. Let $\varepsilon = (\varepsilon_i)_{0\le i\le N}$ be a stationary sequence with $\mathbb{E}[\varepsilon_i] = 0$ and $\mathbb{E}[|\varepsilon_i|^{2+\delta}] < \infty$ for some $\delta > 0$, where ε_i are identically distributed with the variance σ_ε^2 and the autocovariance function $\Gamma_h = \mathbb{E}[\varepsilon_i\varepsilon_{i+h}]$. The process ε is α-mixing with $\sum_{h=1}^{\infty} \alpha(h)^{\delta/2(2+\delta)} < \infty$, and exogenous to X. The sequence $Y = (Y_i)_{0\le i\le N}$ collects all observations contaminated by noise $Y_i = X_i + \varepsilon_i$, with the log-returns $r_i = Y_i - Y_{i-1}$ for all $1 \le i \le N$.

Remark 2.9. The autocovariance function Γ_h satisfies $\Gamma_0 = \sigma_\varepsilon^2$ and $\Gamma_{-h} = \Gamma_h$. For Γ_h, the standard absolute summability condition, i.e., $\sum_{h\in\mathbb{Z}} |\Gamma_h| < \infty$, is well-known to be sufficient for ergodicity and necessary for α-mixing under stationarity (Ibragimov and Linnik, 1971). Furthermore, the assumed conditions on the $(2+\delta)$-th moment and the α-mixing coefficient $\alpha(h)$ are sufficient for a CLT for the centered, stationary and α-mixing ε (Ibragimov, 1962; Theorem 8.3.7, Durrett, 2019).

Remark 2.10. The additive noise term ε_i summarizes a diverse array of market frictions. An i.i.d. additive noise with non-zero variance, firstly introduced by Zhou (1996), is commonly assumed in earlier literature of high-frequency volatility estimation, see, e.g., Aït-Sahalia et al.

(2005) and Zhang et al. (2005). However, some previous studies including Hansen and Lunde (2006), Ubukata and Oya (2009), and Aït-Sahalia et al. (2011) find empirical evidence of self-dependent noise in financial markets. Recent work by Jacod et al. (2017) summarizes the common statistical properties of market microstructure noise and offers estimators for its autocovariances and autocorrelations, which further confirms this point. Assumption 2.3 allows for a weak dependence structure of the noise. This standard Itô semimartingale plus locally dependent noise framework has been employed by a number of recent studies, see, e.g., Jacod et al. (2017, 2019), Varneskov (2017), Christensen et al. (2022), and Li and Linton (2022).

However, it is worth noting that Assumption 2.3 is in fact more stringent than needed, given that Proposition 2.1 below only necessitates the convergence of the pre-averaged returns defined in Eq. (2.25) to an α-mixing and stationary Gaussian process. This convergence result requires an appropriate limit theorem to hold for a weighted-average of the tick-level returns $r_i = \Delta_i^N Y = \Delta_i^N X + \Delta_i^N \varepsilon$, which is satisfied when the assumed α-mixing and stationary ε is exogenous to X. However, the same result holds when (r_i) itself satisfies such conditions for an appropriate limit theorem, which permits certain dependence structure between X and ε. For brevity, we will stick with the exogenous noise assumption in the analysis henceforward, and examine its potential impact with a more general specification of ε via extensive simulations in Section 2.4.

With the additive noise under Assumption 2.3, the noisy observations clearly do not resemble a Gaussian random walk in the limit. There are two main problems:

(i) The noise term dominates the variance of tick-level returns (r_i) and does not shrink as $n \to \infty$;

(ii) The tick-level returns are no longer independent due to the self-dependence of ε.

We now introduce a two-step noise reduction method which facilitates the construction of a sequence of pseudo-observations with desirable properties:

Step 1: Pre-averaging. We implement the pre-averaging approach of Jacod et al. (2009): We choose a sequence of positive integers k_n satisfying $k_n\sqrt{\Delta_n} = \theta$ for some $\theta > 0$. We calculate log-returns on $(Y_i)_{0\leq i\leq N}$ that are pre-averaged in a local neighborhood of k_n observations:

$$r_i^* = \frac{1}{k_n}\sum_{j=k_n/2+1}^{k_n} Y_{i+j} - \frac{1}{k_n}\sum_{j=1}^{k_n/2} Y_{i+j} = \sum_{j=1}^{k_n-1} g\Big(\frac{j}{k_n}\Big) r_{i+j}, \tag{2.25}$$

where $g(s) = s \wedge (1-s)$, for all $i \in \{1, \ldots, N'\}$ with $N' = N - 2k_n/2 + 2$.

Step 2: Random Sign Flip & Permutation. We compute the "wild-bootstrapped" returns based on the pre-averaged returns $(r_i^*)_{1 \le i \le N'}$ obtained from Step 1:

$$\tilde{r}_i = r^*_{\pi(i)} \delta_{\pi(i)}, \tag{2.26}$$

where $(\delta_i)_{1 \le i \le N'}$ is a sequence of i.i.d. Rademacher random variables,[7] and $\pi : \{1, \ldots, N'\} \mapsto \{1, \ldots, N'\}$ is a uniform random permutation of the index set $\{1, \ldots, N'\}$.

Under the null, we show that the sequence of "wild-bootstrapped" returns $(\tilde{r}_i)_{1 \le i \le N'}$ behaves locally like a sequence of i.i.d. Gaussian random variables:

Proposition 2.1. Let ε, Y follow Assumption 2.3. Under the null hypothesis and as $n \to \infty$, the sequence $(\tilde{r}_i)_{1 \le i \le N'}$ converges in distribution to a sequence of locally independent[8] and identically distributed Gaussian random variables with variances of order $\sqrt{\Delta_n}$.

Remark 2.11. We first discuss why this two-step method can mitigate the impact of noise under the null hypothesis. In Step 1, the standard choice of pre-averaging window balances the orders of X increments and ε, such that the pre-averaged returns $(r_i^*)_{1 \le i \le N'}$ converges to a centered, stationary and self-dependent Gaussian process as $n \to \infty$. The dependence structure of (r_i^*) arises from both the assumed self-dependent ε and overlapping pre-averaging windows. Therefore, we proceed to Step 2 to remove the local dependence, which is inspired by the wild bootstrap introduced by Wu (1986). The random sign flip eliminates serial correlations in (r_i^*). The uniform random permutation assigns equal probability to each of the $N'!$ possible permutations, which ensures that any two variables in $(\tilde{r}_i)_{1 \le i \le N'}$ are independent when their indices are not sufficiently far apart from each other in $\{1, \ldots, N'\}$ under infill asymptotics.

Proposition 2.1 inspires the construction of our test in the presence of noise as follows: We generate a sequence of pseudo-observations $(\tilde{Y}_i)_{0 \le i \le N'}$ as partial sums of $(\tilde{r}_i)$, where $\tilde{Y}_0 = Y_0$ and $\tilde{Y}_i = \sum_{j=1}^{i} \tilde{r}_j$. Next, we choose a sequence of barrier widths $c = m\Delta_n^{1/4}$ and obtain the sampled observations $(\tilde{Y}_i^{(c)})$. Finally, we follow Section 2.3.1 to construct the standardized test statistic $\tilde{T}_{c,\epsilon}$ from $(\tilde{Y}_i^{(c)})$ in place of $(X_i^{(c)})$. Formal establishment of its asymptotic properties requires further assumptions about the noise, and is left for future research. We discuss some

[7] A random variable $\delta \in \{-1, 1\}$ has a Rademacher distribution if $\mathbb{P}(\delta = -1) = \mathbb{P}(\delta = 1) = 1/2$.
[8] A formal definition of local independence is given in Eq. (A.62)

plausible properties of $\tilde{T}_{c,\epsilon}$ in the two Remarks below, which are verified through comprehensive simulations with a realistically calibrated noise specification in the next section.

Remark 2.12. The choice of $c = m\Delta_n^{1/4}$ ensures that the normalized increments $\tilde{r}_i/c$ are invariant to Δ_n, which is analogous to the case without noise. Assuming that $(\tilde{r}_i)_{1\leq i\leq N'}$ is a sequence of i.i.d. centered Gaussian random variables, $(\tilde{Y}_i)_{0\leq i\leq N'}$ forms a genuine Gaussian random walk, and thus the same CLT in Theorem 2.2 would hold for $\tilde{T}_{c,\epsilon}$ under the null. Our simulation results reveal that this CLT still holds for $\tilde{T}_{c,\epsilon}$ constructed from $(\tilde{Y}_i)$. This is because each sampled return is only determined by finitely many increments of $(\tilde{Y}_i)$ within a local horizon, which are indeed asymptotically i.i.d.. Importantly, the convergence rate of $\tilde{T}_{c,\epsilon}$ remains $\sqrt{N}$, which apparently contradicts to the optimal $N^{1/4}$ rate of noise-robust IV estimators (Gloter and Jacod, 2001; Xiu, 2010; Reiß, 2011) that also appear in some noise-robust jump tests (Aït-Sahalia et al., 2012). This discrepancy arises because our test statistic does not rely on a noise-robust IV estimator, but rather on a consistent estimator of the scale-invariant barrier width m, which is identified through the variance of $\tilde{r}_i$. As $\tilde{r}_i$ has the same order as the pre-averaged noise, a consistent estimator of m has the same $\sqrt{N}$ rate as that of a noise variance estimator. Consequently, the estimator of m cannot be translated into a consistent IV estimator in the spirit of Remark 2.8 when noise exists. Nevertheless, this finding also reveals that a noise-robust IV estimator is not a pre-requisite for noise-robust jump tests.

Remark 2.13. When X is discontinuous on $(0, 1)$, we conjecture that our test remains consistent under the alternative hypothesis of local-to-infinite-activity jumps, although it may require a more stringent assumption on u_n in Eq. (2.7). For example, the order of the pre-averaged returns $\tilde{r}_i$ becomes $\Delta_n^{1/4}$, such that u_n needs to satisfy $u_n\Delta_n^{-1/4} \to \infty$ and $u_n\Delta_n^{\beta-1/2} \to 0$ for any $\beta \in (1/4, 1/2]$ as $n \to \infty$ to exclude all jumps that shrink either faster than or equal to the pre-averaged returns from the alternative hypothesis.

2.4 Monte Carlo Simulations

2.4.1 Simulation Design

We simulate an empirically realistic discretized diffusion model for asset prices, which incorporates both time varying tick-variances and transaction activities. Firstly, we simulate a Heston

model for the efficient price process X and obtain its tick-level observations, to which we add jumps with different sizes:

$$\begin{aligned} dX_t &= \Big(\mu - \frac{\sigma_t^2}{2}\Big)dt + \sigma_t dW_t + dX_t'', \quad t \in [0,1] \\ d\sigma_t^2 &= \alpha(\vartheta - \sigma_t^2)dt + \eta\sigma_t dB_t, \end{aligned} \tag{2.27}$$

where $W = (W_t)$ and $B = (B_t)$ are standard Brownian motions with $\mathrm{Corr}(W_t, B_t) = \rho$, and X'' is a compound Poisson process, i.e.,

$$X_t'' = \sum_{i=1}^{N_t} J_i, \tag{2.28}$$

where $N = (N_t)$ is a Poisson process with rate λ, and jump sizes J_i follow a double exponential distribution (Laplace distribution) with the location parameter 0 and the scale parameter b. To generate all tick-level observations, we discretize X equidistantly on $t = i/n$ for $n = 23,400$. Then we modify the observation times $0 \leq t_{n,1} < t_{n,2} < \cdots \leq 1$ following an inhomogeneous Poisson process with the rate

$$\alpha(t) = 1 - \frac{1}{2}\cos 2\pi t, \tag{2.29}$$

where $t \in [0,1]$. The inverted U-shaped rate function $\alpha(t)$ is employed to mimic the empirical feature of more transactions that occur in the early morning and late afternoon than in the middle of the trading day (Jacod et al., 2017). We draw 10,000 simulated price paths for each experiment.

For the additive noise,[9] we denote

$$\varepsilon_i = 2\sqrt{\frac{\sigma_{t_{n,i}}^2}{n}}\left(\omega_i^A + \omega_i^B\sqrt{\frac{\nu-2}{\nu}}\right), \tag{2.30}$$

where ω_i^A are autocorrelated Gaussian random variables defined as

$$\omega_i^A = \phi_i + \sum_{j=1}^{\Lambda}\beta_j\phi_{i-j}, \quad \text{with } \phi_i \sim \text{i.i.d.}\,\mathcal{N}(0,1), \text{ and } \beta_j = \frac{d(1+d)\cdots(j-1+d)}{j!}, \tag{2.31}$$

[9]The simulation design of additive noise mainly follows Aït-Sahalia et al. (2012). In addition, we consider its serial correlation using the method of Jacod et al. (2019).

for $d \in (-0.5, 0.5)$ and a large cutoff value Λ, which form a moving-average series that approximates a fractionally differenced process (Jacod et al., 2019), and ω_i^B are i.i.d. draws from a Student's t distribution with the degree of freedom ν.

The instantaneous standard deviation of the Gaussian-t mixture noise is about four times as much as that of diffusive increments, i.e., $\sqrt{\sigma^2_{t_{n,i}}/n}$, so that the diffusive increments are clearly dominated by the additive noise.[10] This specification of ε_i captures some important features of market microstructure noise in financial markets, e.g., temporal heteroscedasticity, slowly-decaying serial correlation, intraday seasonality, and dependence on the latent prices. The t-distributed noise ω_i^B is introduced to capture the large bouncebacks commonly observed in high-frequency transaction data (Aït-Sahalia et al., 2012). Besides the additive noise, we also consider the rounding errors on the price level, i.e., let the observed prices $e^{Y_i} = e^{X_i+\varepsilon_i}$ be further rounded to cents. The observed logarithmic prices are given as

$$Y_i = \log\left(\left[\frac{e^{X_i+\varepsilon_i}}{0.01}\right] \times 0.01\right), \tag{2.32}$$

where the function $[x]$ rounds a number x to the nearest integer.[11]

The annualized parameters for the Heston model are fixed at $(\mu, \alpha, \vartheta, \eta, \rho) = (0.05, 5, 0.16, 0.5, -0.5)$, where the volatility parameters satisfy the Feller's condition $2\alpha\theta \geq \eta^2$ which ensures the positivity of σ. The parameter choices follow both Aït-Sahalia and Jacod (2009) and Aït-Sahalia et al. (2012), which are calibrated according to the empirical estimates in Aït-Sahalia and Kimmel (2007). For the jump components, we let $\lambda = 1$, and $b = 0.2\sqrt{\theta}$ and $0.4\sqrt{\theta}$ corresponding to moderate and relatively large jump sizes. The moderate (resp. large) jumps contribute about 7% (resp. 25%) of the daily QV on average when noise is absent. For the additive noise term, we let $(d, \Lambda, \nu) = (0.3, 100, 2.5)$ following Aït-Sahalia et al. (2012) and Jacod et al. (2019).

Fig. 2.3 depicts the intraday variation of some market activity variables of a simulated path in the absence of noise, which include the return, number of trades, and annualized RV in

[10] In the simulations, we follow Aït-Sahalia et al. (2012) to truncate the t-distributed ω_i^B at $\pm 50\sqrt{\nu/(\nu-2)}$ to avoid large returns in the absence of jumps, which could lead to very misleading results. Hence, the instantaneous standard deviation of the t-distributed noise $2\omega_i^B\sqrt{\sigma^2_{t_{n,i}}/n}\sqrt{(\nu-2)/\nu}$ is slightly lower than $2\sqrt{\sigma^2_{t_{n,i}}/n}$.

[11] We also consider alternative specifications for the additive heteroscedastic noise, see the results in Appendix A.2.2.

each one-minute interval. Both transaction intensity and return variation exhibit a U-shaped pattern over the trading hours, which is in line with some prior empirical findings (Harris, 1986; Wood et al., 1985; Andersen and Bollerslev, 1997; Andersen et al., 2018, 2019, 2023b). Fig. 2.4 compares the simulated tick-level latent prices and the rounded, noise-contaminated price observations over an intraday episode.

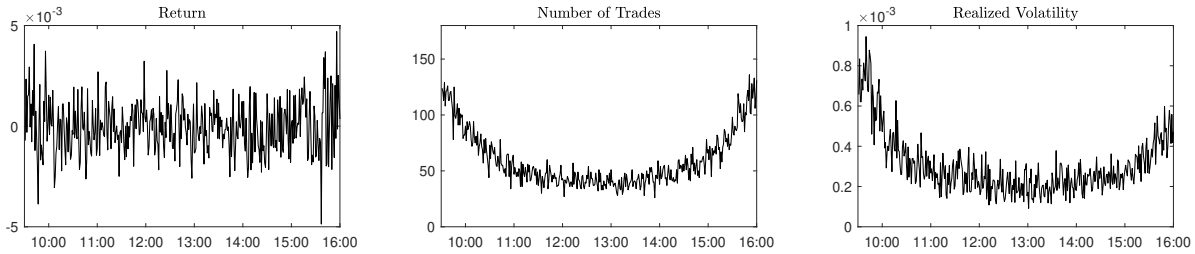

Fig. 2.3 Some market activity variables of simulated price observations. The tick-level observations are simulated with the Heston model in Eq. (2.27), and we assign randomized observation times with an inverted U-shape rate function in Eq. (2.29) to all observations. The returns, numbers of transactions, and annualized RVs are computed at a granularity of one minute.

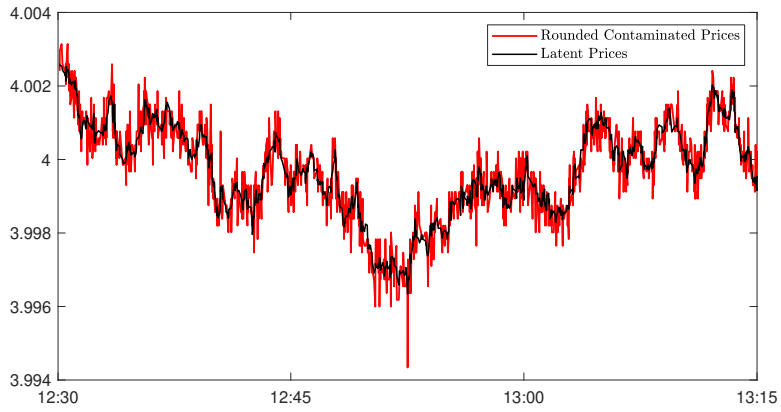

Fig. 2.4 Comparison of the simulated tick-level latent prices and the rounded, noise-contaminated price observations.

2.4.2 Test Performance in the Absence of Market Microstructure Noise

Table 2.1 reports the finite-sample size and size-adjusted power (at 5% nominal level) of the standardized test statistic $T_{c,\epsilon}$ when noise is absent. Tick-level observations are sampled with different PDS barrier widths $c = K\sigma(r_i)$, i.e., K times the standard deviation of tick-by-tick returns, where K ranges from 3 to 10. Different censoring thresholds with $\epsilon \in \{0.05, 0.07, 0.1\}$ are also considered. In Table 2.1, the rejection rates under the null (Panel A) are all closely align with the nominal level. For the finite-sample power under the alternative (Panels B

and C), we find that the rejection rates are fairly robust across different sampling frequencies. Fig. 2.5 compares the finite-sample distributions of our test statistic with the limiting standard normal distribution. Under the null, the finite-sample distribution (solid line) closely resembles the standard normal (shaded area), while the distribution deviates significantly from $\mathcal{N}(0,1)$ when there exist jumps of either moderate or large sizes.

Table 2.1 Finite-sample size and power (%)

Nominal size: 5%	Panel A No Jump				Panel B Moderate Price Jumps				Panel C Large Price Jumps			
		ϵ				ϵ				ϵ		
$c/\sigma(r_i)$	$N^{(c)}$	0.05	0.07	0.10	$N^{(c)}$	0.05	0.07	0.10	$N^{(c)}$	0.05	0.07	0.10
3	1786	5.26	5.31	5.48	1697	58.21	61.68	65.22	1564	76.29	78.47	80.37
4	1100	5.51	5.58	5.89	1043	61.24	64.54	67.46	959	77.95	80.18	81.99
5	744	5.39	5.56	5.77	705	63.01	66.29	69.55	647	79.10	81.00	82.83
6	536	4.99	5.20	5.61	508	63.77	67.13	70.30	466	80.16	82.01	83.92
7	405	5.28	5.56	5.71	383	65.19	68.47	71.07	351	80.59	82.23	84.01
8	316	5.20	5.61	5.93	299	65.86	68.90	72.07	274	80.76	82.51	84.36
9	254	5.28	5.46	6.01	240	66.33	68.88	71.47	220	81.36	82.78	84.42
10	208	5.07	5.29	5.49	197	66.66	69.33	72.16	181	81.20	83.18	84.85

This table reports the finite-sample size and size-adjusted power (%) of 10,000 simulations of the test statistic $T_{c,\epsilon}$ at 5% nominal level in the absence of market microstructure noise. Tick-level observations are sampled with different PDS barrier widths $c = K\sigma(r_i)$, i.e., K times the standard deviation of tick-by-tick returns, where K ranges from 3 to 10. Different censoring thresholds with $\epsilon \in \{0.05, 0.07, 0.1\}$ are considered. $N^{(c)}$ stands for the average sampling frequencies.

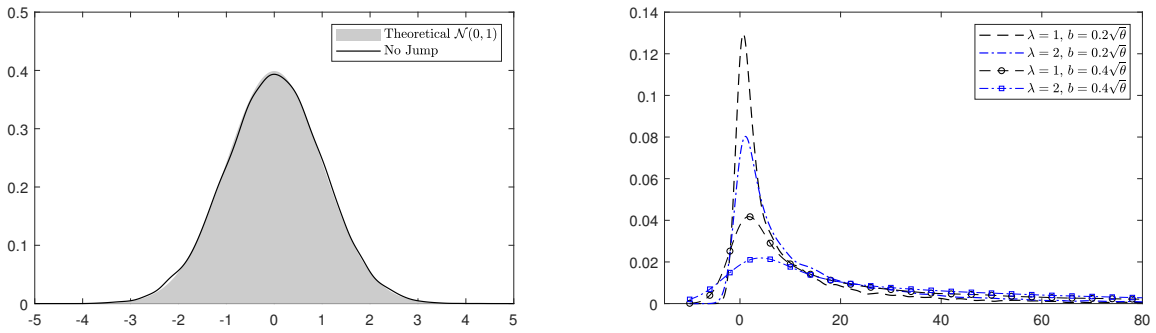

Fig. 2.5 Finite-sample distributions of the standardized test statistic $T_{c,\epsilon}$. We plot the finite-sample distribution under the null (solid line) and compare it with the simulated standard normal (shaded area). Jumps are simulated with a compounded Poisson process with the intensity λ, and their sizes follow a double exponential distribution with the location parameter 0 and the scale parameter b. We consider different parameter choices: (i) $\lambda = 1$, $b = 0.2\sqrt{\theta}$ (dash), (ii) $\lambda = 2$, $b = 0.2\sqrt{\theta}$ (dash-dot), (iii) $\lambda = 1$, $b = 0.4\sqrt{\theta}$ (dash-circle), and (iv) $\lambda = 2$, $b = 0.4\sqrt{\theta}$ (dash-square). In all cases, the PDS barrier width $c = 5\sigma(r_i)$, and the censoring parameter $\epsilon = 0.05$.

2.4.3 Test Performance in the Presence of Market Microstructure Noise

Panel A in Table 2.2 summarizes the finite-sample size (at 5% nominal level) of the standardized test statistic $T_{c,\epsilon}$ constructed from the rounded noise-contaminated observations. We employ the two-step noise reduction method in Section 2.3.2 to construct the sequence of pseudo-observations with three different pre-averaging windows, i.e., $k_n = \lceil \theta\sqrt{N} \rceil$ with $\theta \in \{0.3, 0.4, 0.5\}$. The choices of θ follow the rule of thumb in Hautsch and Podolskij (2013). Similar to the results in the absence of noise, the rejection rates under the null are close to the nominal level across almost all choices of bandwidth c and censoring parameter ϵ. Panels B and C in Table 2.2 report the size-adjusted power under the alternative with moderate and large jumps, respectively. Compared with the simulation results in Table 2.1, the finite-sample power experiences a marginal reduction but remains above 40% for most of the parameter choices. Fig. 2.6 compares the finite-sample distributions of $T_{c,\epsilon}$ with $\mathcal{N}(0,1)$. It is observed that $T_{c,\epsilon}$ is almost a standard normal under the null, but it has a notably larger magnitude than $\mathcal{N}(0,1)$ under the alternative. Compared this with Fig. 2.5, we observe that the right tails of the test statistic become smaller with the same jump specifications. This explains the slightly reduced power of our test in the presence of noise.

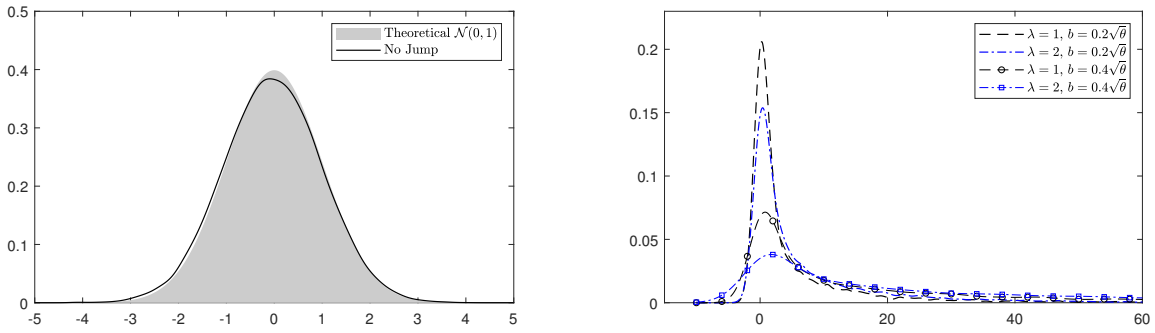

Fig. 2.6 Finite-sample distributions of the standardized test statistic $T_{c,\epsilon}$ in the presence of noise. We plot the finite-sample distribution under the null (solid line) and compare it with the simulated standard normal (shaded area). Jumps are simulated with a compounded Poisson process with the intensity λ, and their sizes follow a double exponential distribution with the location parameter 0 and the scale parameter b. We consider different parameter choices: (i) $\lambda = 1$, $b = 0.2\sqrt{\theta}$ (dash), (ii) $\lambda = 2$, $b = 0.2\sqrt{\theta}$ (dash-dot), (iii) $\lambda = 1$, $b = 0.4\sqrt{\theta}$ (dash-circle), and (iv) $\lambda = 2$, $b = 0.4\sqrt{\theta}$ (dash-square). In all cases, we select the pre-averaging window $k_n = \lceil \theta\sqrt{N} \rceil = 46$ with $\theta = 0.3$, the PDS barrier width $c = 5\sigma(\tilde{r}_i)$, and the censoring parameter $\epsilon = 0.05$.

We then compare the empirical rejection rates of our test with those of 9 classical high-frequency jump tests constructed from equidistantly calendar-time-sampled observations (Table 2.3). These tests include BNS (Barndorff-Nielsen and Shephard, 2006), ABD (Andersen

Table 2.2 Finite-sample size and power (%)

Nominal size: 5%		$\theta = 0.3$				$\theta = 0.4$				$\theta = 0.5$			
			ϵ				ϵ				ϵ		
	$c/\sigma(\tilde{r}_i)$	$N^{(c)}$	0.05	0.07	0.10	$N^{(c)}$	0.05	0.07	0.10	$N^{(c)}$	0.05	0.07	0.10
Panel A No Jump	3	1784	4.90	5.15	5.20	1784	4.80	5.35	5.71	1783	5.06	5.07	5.70
	4	1099	4.84	4.95	5.42	1098	5.29	5.10	5.51	1098	5.14	5.08	5.79
	5	743	4.94	5.01	5.20	743	5.19	5.02	5.57	742	4.81	5.02	5.70
	6	536	4.74	4.89	5.57	536	4.78	5.11	5.58	535	4.96	5.11	5.47
	7	404	4.99	5.11	5.29	404	4.86	5.05	5.76	404	4.86	5.17	5.46
	8	316	5.15	5.37	5.54	316	4.82	5.08	5.43	315	4.81	5.30	5.82
	9	253	5.04	5.41	5.13	254	4.84	5.10	5.63	253	4.96	5.28	5.73
	10	208	5.18	5.10	5.60	208	4.84	5.34	5.54	208	5.04	5.08	5.66
Panel B Moderate Jump	3	1716	46.00	49.28	51.77	1717	44.98	46.84	49.27	1718	43.08	45.18	47.52
	4	1058	45.89	48.56	50.92	1059	43.31	46.76	48.56	1061	41.35	44.77	46.22
	5	717	44.95	47.45	50.42	719	42.99	45.50	47.53	720	40.81	43.12	44.93
	6	519	44.60	46.65	48.86	519	42.82	43.97	47.01	520	40.25	42.06	45.01
	7	392	43.79	45.31	48.98	393	41.00	43.15	46.29	394	40.08	41.95	45.04
	8	307	42.45	45.21	48.64	308	40.97	42.47	46.81	308	39.98	41.03	43.83
	9	247	41.38	43.95	48.57	248	40.54	42.58	45.62	248	38.45	41.21	43.67
	10	203	41.08	44.57	47.51	204	40.04	41.30	45.45	204	38.12	40.03	43.86
Panel C Large Jump	3	1594	68.85	70.38	72.44	1596	68.06	69.14	70.54	1599	66.37	68.54	69.68
	4	983	68.79	70.51	72.17	986	66.37	68.97	70.42	990	65.60	67.26	68.97
	5	668	67.26	69.92	71.80	671	66.37	68.22	69.52	673	65.11	66.50	68.19
	6	484	67.69	69.41	70.48	486	65.92	67.13	69.67	489	64.38	66.05	68.07
	7	367	66.78	68.71	70.81	369	65.14	66.46	68.54	371	63.68	65.35	67.61
	8	288	65.84	68.11	70.24	290	64.22	66.40	68.42	292	62.93	64.89	66.90
	9	233	65.83	67.44	70.32	234	64.08	66.29	68.38	236	62.29	64.68	66.67
	10	192	65.00	66.96	69.70	193	63.44	65.54	68.23	194	61.91	64.12	66.69

This table reports the finite-sample size and size-adjusted power (%) of 10,000 simulations of the test statistic $T_{c,\epsilon}$ at 5% nominal level. All simulated prices are contaminated by the additive Gaussian-t mixture noise and rounding errors. We utilize the two-step noise reduction method in Section 2.3.2 to construct the sequence of pseudo-observations with three different pre-averaging windows, i.e., $k_n = \lceil \theta\sqrt{N} \rceil$ with $\theta \in \{0.3, 0.4, 0.5\}$. The observations are sampled with different PDS barrier widths $c = K\sigma(\tilde{r}_i)$, where K ranges from 3 to 10. Different censoring thresholds with $\epsilon \in \{0.05, 0.07, 0.1\}$ are considered. $N^{(c)}$ stands for the average sampling frequencies.

et al., 2007c), JO (Jiang and Oomen, 2008), LM (Lee and Mykland, 2008), ASJ (Aït-Sahalia and Jacod, 2009), CPR (Corsi et al., 2010), PZ (Podolskij and Ziggel, 2010), MinRV and MedRV (Andersen et al., 2012). The parameter choices for all these tests are determined in accordance with the recommendations from their original literature.[12] Our analysis, in line with the Monte Carlo results of Dumitru and Urga (2012) and Maneesoonthorn et al. (2020), demonstrates that nearly all the tests constructed from equidistantly sampled observations suffer from size distortion and their results become highly unstable under the assumed additive Gaussian-t mixture noise and rounding errors. This noise significantly distorts their finite-sample null distributions, particularly at higher sampling frequencies. It might be interesting to see that

[12] Some parameter choices are reported in Appendix A.2.1.

the size of the JO test is close to the nominal level. However, a closer examination reveals that this is caused by two cancelling distortions due to the mixture of Gaussian and t-distributed noise specification, see Appendix A.2.2 for details. While sparse sampling can alleviate size distortion, it also substantially weakens the power of these tests.

Table 2.3 Finite-sample size and power (%) of other tests

Nominal size: 5%											
	Int. (sec)	N_{spl}	BNS	ABD	JO	LM	ASJ	CPR	PZ	MinRV	MedRV
Panel A No Jump	5	4680	0.33	98.53	6.19	98.40	99.98	33.39	89.61	0.00	0.00
	15	1560	0.42	71.96	5.23	71.12	99.42	18.20	52.91	0.00	0.12
	30	780	3.30	45.63	5.25	46.82	76.71	13.02	30.25	0.99	2.53
	60	390	5.16	28.49	5.75	30.82	29.50	8.47	19.57	3.35	5.30
	120	195	6.46	21.02	8.08	17.73	10.60	7.86	16.76	4.78	6.91
	180	130	6.90	18.61	8.95	15.10	7.52	8.05	15.96	5.29	8.16
	300	78	7.65	15.93	10.87	12.12	4.84	8.97	15.58	5.34	8.98
Panel B Moderate Jump	5	4680	30.08	99.58	31.95	15.80	97.25	10.93	12.40	16.91	26.45
	15	1560	36.42	88.73	36.33	24.78	94.76	21.13	20.59	32.89	36.17
	30	780	33.20	74.27	33.89	32.00	77.29	28.64	28.39	28.95	33.25
	60	390	28.25	61.69	28.25	36.63	45.44	29.58	37.36	24.96	28.61
	120	195	21.64	48.76	20.90	32.73	24.43	24.18	30.47	20.07	23.51
	180	130	17.40	42.22	17.16	28.97	16.57	19.34	25.51	16.34	19.42
	300	78	13.83	33.48	11.33	20.56	11.44	15.93	19.09	13.32	14.74
Panel C Large Jump	5	4680	56.35	99.81	59.11	43.00	95.12	32.58	36.63	42.72	53.55
	15	1560	60.94	93.98	61.18	52.39	95.31	47.32	47.58	58.68	60.84
	30	780	59.06	86.29	59.05	58.46	83.73	54.54	55.57	54.79	58.43
	60	390	54.36	78.40	54.57	62.78	59.83	56.25	62.88	50.60	54.90
	120	195	46.78	70.17	46.16	58.81	36.76	50.12	56.74	44.11	49.20
	180	130	41.21	64.64	40.86	54.93	26.94	44.83	51.91	39.32	44.13
	300	78	34.07	55.92	33.19	45.73	16.14	38.76	43.76	33.66	37.49

This table reports the finite-sample size and size-adjusted power (%) of 10,000 simulations of 9 classical tests at 5% nominal level: BNS (Barndorff-Nielsen and Shephard, 2006), ABD (Andersen et al., 2007c), JO (Jiang and Oomen, 2008), LM (Lee and Mykland, 2008), ASJ (Aït-Sahalia and Jacod, 2009), CPR (Corsi et al., 2010), PZ (Podolskij and Ziggel, 2010), MinRV and MedRV (Andersen et al., 2012). All these tests are constructed on observations equidistantly sampled with various intervals in calendar time: 5, 15, 30, 60, 120, 180 and 300 seconds, and "N_{spl}" stands for the sampling frequencies.

For more appropriate benchmarks when the noise is present, we also consider some noise-robust versions of classical tests (Table 2.4) constructed from ultra-high-frequency data: the noise-adjusted PZ (Podolskij and Ziggel, 2010), LM12 (Lee and Mykland, 2012), and ASJL (Aït-Sahalia et al., 2012). Similar to our test, all these noise-robust tests rely on the pre-averaging approach of Jacod et al. (2009) to "pre-filter" the noise-contaminated observations.[13] The "optimal" tuning parameters for those tests are selected by minimizing the absolute distance

[13]With a simplified i.i.d. noise specification, Andersen et al. (2007c) introduce an "event time" correction of ABD, and Jiang and Oomen (2008) propose an analytically modified form of JO. However, both of them cannot achieve comparable performance under the simulated Gaussian-t mixture noise.

between the nominal size and the empirical size with the simulated tick-level noise-contaminated observations.[14]

Table 2.4 Finite-sample size and power (%) of other noise-robust tests

Nominal size: 5%					
	Int. (sec)	N_{spl}	PZ*	LM12	ASJL
No Jump	tick	23400	5.29	5.03	5.12
	5	4680	4.96	8.83	8.79
Moderate Jump	tick	23400	38.57	22.70	38.22
	5	4680	30.38	18.79	17.66
Large Jump	tick	23400	64.78	40.76	63.50
	5	7680	56.49	31.38	41.96

This table reports the finite-sample size and size-adjusted power (%) of 10,000 simulations of 3 noise-robust tests at 5% nominal level: noise-adjusted PZ (Podolskij and Ziggel, 2010), LM12 (Lee and Mykland, 2012), and ASJL (Aït-Sahalia et al., 2012). All these tests are constructed on tick-level and 5-second-sampled observations. The tuning parameters for those tests are selected by minimizing the absolute distance between the nominal size and the empirical size with the simulated tick-level noise-contaminated observations.

As illustrated in Table 2.2, our PDS-based test demonstrates robustness across various parameter choices: (i) barrier width c, (ii) censoring parameter ϵ, and (iii) pre-averaging window $k_n = \lceil \theta\sqrt{N} \rceil$, even when we consider such a complicated and realistic noise specification. Furthermore, our test remains competitive and, often superior, to those noise-robust tests with optimal parameter choices. While we refrain from providing optimal parameter choices, we offer recommended ranges for practitioners:

(i) Choose c as a multiple of the standard deviation of $\tilde{r}_i$, i.e., $c = K\sigma(\tilde{r}_i)$, with $3 \leq K \leq 10$.

(ii) Choose ϵ in $[0.03, 0.15]$.

(iii) Choose the pre-averaging window $k_n = \lceil \theta\sqrt{N} \rceil$ with $\theta \in [0.2, 0.8]$.

Through extensive simulation studies with different specifications of market frictions, we believe that the recommended parameter choices work reasonably well in finite samples when the number of intraday tick-level observations is no less than 10,000. Additional simulation results can be found in Appendix A.2.2.

[14] Note that the optimal tuning parameters are not empirically feasible in practice. Therefore, the results presented should be interpreted as theoretical upper bounds for these benchmark tests.

2.5 Empirical Analysis

In this section, we employ our new jump test on the high-frequency transaction data of 10 stocks listed on the New York Stock Exchange (NYSE): American Express (AXP), Boeing (BA), Disney (DIS), IBM, Johnson & Johnson (JNJ), JP Morgan (JPM), Merck (MRK), McDonald's (MCD), Procter & Gamble (PG), and Walmart (WMT). Our Trade and Quote (TAQ) dataset includes all transactions from 9:30 am to 4:00 pm on each trading day in 2020. As is standard in empirical research involving high-frequency financial data, we apply filters, as outlined in Barndorff-Nielsen et al. (2009), to eliminate clear data errors, remove all transactions in the original record that are later corrected, cancelled or otherwise invalidated, and keep transactions on NYSE only. Table 2.5 reports descriptive statistics of trades on these selected NYSE stocks, which include the number of trades, observed transaction prices in dollar terms, and intraday log-returns in basis points. Our PDS-based test utilizes the same tuning parameters as those in Section 2.4: the PDS barrier width $c = K\sigma(\tilde{r}_i)$ with K ranging from 4 to 6, the censoring parameter $\epsilon = 0.05$, and three pre-averaging windows $k_n = \lceil \theta\sqrt{N} \rceil$ with $\theta \in \{0.3, 0.4, 0.5\}$.

Table 2.6 reports the proportions of trading days with rejections in 2020, as determined by our PDS-based test. For the selected stocks, the proportions of trading days with identified jumps are no more than 20%, with only AXP and MCD identified to exhibit over 15% of trading days containing jumps. There is little variation of the rejection rates across different stocks, and the results are relatively stable with different parameter choices. For each stock, there is a slight decrease in the percentage of identified jumps when we employ a larger barrier width c for PDS, i.e., sample less frequently. To visualize the testing results for the selected stocks in 2020, we aggregate all stock-day outcomes, which yields a total of 2530 stock-day pairs. Fig. 2.7 illustrates the empirical distributions of the standardized test statistic (solid line) and compares it with the standard normal distribution $\mathcal{N}(0, 1)$. Relative to the limiting distribution under the null hypothesis of no jump (shaded area), the empirical distribution of our test statistic deviates slightly towards the right side, but maintainss a bell shape centered around 0.5.

To eliminate spurious detections due to the multiple testing issue, Bajgrowicz et al. (2016) propose a formal treatment of the over-identification bias with double asymptotics when the jump tests are applied over a sample of many days. We apply their thresholding methods

Table 2.5 Descriptive statistics of daily trades on selected NYSE stocks

Stock		AXP	BA	DIS	IBM	JNJ
Number of trades	Min	3171	10556	9785	5047	6383
	Max	59273	245802	125550	49178	71733
	Mean	19351	55314	37962	17818	22966
	Std Dev	9205	38352	20390	8265	11561
Trasaction prices	Min	67.03	89.00	79.07	90.56	109.16
	Max	138.16	349.45	183.40	158.78	157.66
	Mean	100.88	181.46	121.78	123.16	143.33
	Std Dev	14.72	51.15	20.12	11.57	8.53
Intraday log-returns (1×10^{-4})	Min	−123.24	−163.29	−100.49	−143.49	−110.04
	Max	97.48	129.22	75.30	143.49	200.25
	Mean	0.00	0.00	0.00	0.00	0.00
	Std Dev	1.78	1.85	1.17	1.44	1.23
Stock		JPM	MRK	MCD	PG	WMT
Number of trades	Min	12593	5787	3968	7516	9845
	Max	156987	71570	55024	76337	90546
	Mean	44738	22833	16096	23224	26148
	Std Dev	25335	11058	7838	10422	13032
Trasaction prices	Min	76.92	65.26	124.23	94.31	102.00
	Max	141.10	92.14	231.91	146.92	153.60
	Mean	103.17	79.86	195.17	125.19	128.55
	Std Dev	14.28	4.55	21.74	11.63	12.04
Intraday log-returns (1×10^{-4})	Min	−103.80	−177.00	−154.39	−132.25	−305.08
	Max	103.80	117.50	142.80	207.58	190.19
	Mean	0.00	0.00	0.00	0.00	0.00
	Std Dev	1.06	1.26	1.74	1.33	1.13

This table contains summary statistics for the number of trades, observed transaction prices in dollars, and intraday log-returns in basis points for 10 selected NYSE stocks in 2020. Data are collected from the TAQ database which includes all transactions from 9:30 am to 4:00 pm in each trading day. We apply filters, as outlined in Barndorff-Nielsen et al. (2009), to eliminate clear data errors, remove all transactions in the original record that are later corrected, cancelled or otherwise invalidated, and keep transactions on NYSE only.

Table 2.6 Empirical rejection rates (%) for selected NYSE stocks

k_n	$c/\sigma(\tilde{r}_i)$	AXP	BA	DIS	IBM	JNJ	JPM	MRK	MCD	PG	WMT
$\theta = 0.3$	4	17.00	10.67	9.88	13.04	13.83	10.67	10.67	16.60	13.44	11.07
	5	15.81	10.67	9.49	12.25	11.86	10.67	10.28	16.21	11.86	10.67
	6	14.23	9.88	9.09	12.25	11.46	10.28	9.88	15.02	11.86	11.07
$\theta = 0.4$	4	16.21	9.88	10.28	13.44	12.65	10.67	9.88	15.81	12.65	12.25
	5	15.02	9.88	9.49	12.25	12.25	10.67	9.49	15.42	11.86	11.07
	6	14.23	9.49	9.49	11.46	11.07	9.88	9.49	14.23	11.46	10.28
$\theta = 0.5$	4	15.81	10.28	10.28	12.25	13.04	10.28	10.28	15.81	12.25	11.46
	5	14.23	9.09	9.88	12.25	11.46	9.49	9.09	15.02	11.86	10.67
	6	13.44	8.70	9.09	11.46	11.07	9.88	9.09	14.62	11.07	10.67

This table reports the proportions of days with jumps identified by the PDS-based test for 10 NYSE stocks in 2020. We use three pre-averaging windows $k_n = \lceil \theta\sqrt{N} \rceil$ with $\theta \in \{0.3, 0.4, 0.5\}$, different PDS barrier widths $c = K\sigma(\tilde{r}_i)$, i.e., the integer multiple of the standard deviation of pre-averaged returns, with K ranging from 4 to 6, and the censoring parameter $\epsilon = 0.05$. The total number of trading days is 253.

to our results: (i) the universal threshold $\sqrt{2 \ln 253}$, and (ii) the threshold based on the false

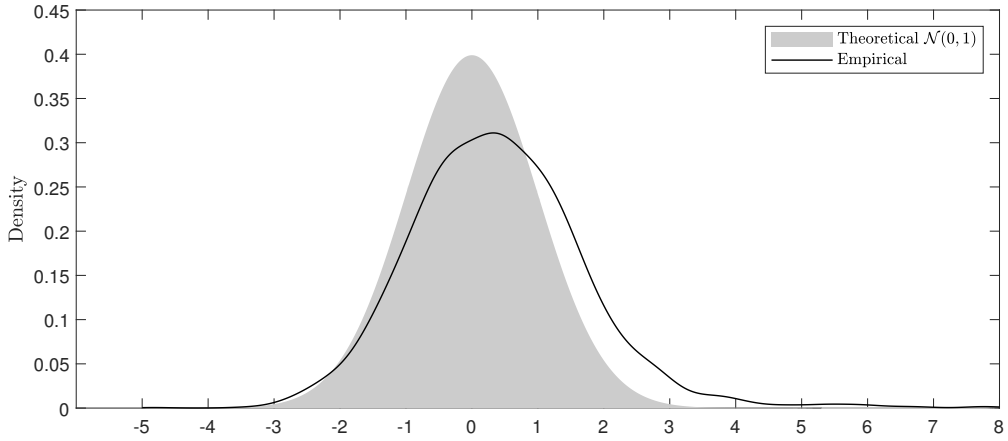

Fig. 2.7 Testing results for selected NYSE stocks in 2020. We plot the empirical distribution of the standardized test statistic for all 2530 stock-day pairs and, for comparison, the simulated standard normal distribution (shaded area). We use the PDS barrier width $c = 4\sigma(\tilde{r}_i)$, the censoring parameter $\epsilon = 0.05$, and the pre-averaging window $k_n = \lceil \theta\sqrt{N} \rceil$ with $\theta = 0.3$, which corresponds to the first row in Table 2.6.

discovery rate (FDR).[15] The adjusted results of our test for all selected stocks are reported in Table 2.7.[16] It is noteworthy that our testing results are fairly robust to the control of spurious detections, which underscores the empirical reliability of our PDS-based test.

2.6 Conclusions

This chapter introduces a novel nonparametric high-frequency jump test for a discretely observed Itô semimartingale. Our approach utilizes a path-dependent sampling strategy for the tick-level price observations. The key intuition behind the construction of our test relies on the fact that, different from a continuous price increase or decrease over a certain time interval, a discontinuous shift with a larger magnitude will always trigger an exit-time event and induce a disproportionately large threshold exceedance under infill asymptotics. Additionally, a two-step noise reduction technique is designed to alleviate the impact of weakly dependent market microstructure noise. Through extensive simulations, we validate the reliable finite-sample

[15] For the vector of one-side test statistics $(S_1, S_2, \ldots, S_N)'$ which converge to i.i.d. standard normal random variables under the null, the universal threshold is $\sqrt{2 \ln N}$ (Bajgrowicz et al., 2016). The data-adaptive FDR threshold is determined from the observed p-value distribution by the Benjamini–Hochberg procedure.

[16] See empirical results without and with the control of spurious detections for other calendar-time-sampling-based and noise-robust tests in Appendix A.2.3. Our test demonstrates somewhat similar performance to some noise-robust tests, but it stands out as the most robust to spurious detections, which further proves its reliability.

Table 2.7 Adjusted empirical rejection rates (%) for selected NYSE stocks

	k_n	$c/\sigma(\tilde{r}_i)$	AXP	BA	DIS	IBM	JNJ	JPM	MRK	MCD	PG	WMT
Panel A Universal threshold	$\theta = 0.3$	4	15.02	9.49	9.09	12.25	12.25	7.91	9.49	14.62	11.07	9.49
		5	13.83	9.88	8.70	11.07	10.28	8.30	9.09	14.62	9.88	8.70
		6	12.65	8.70	8.30	11.07	10.28	7.91	8.70	13.44	9.88	9.09
	$\theta = 0.4$	4	14.23	8.70	9.49	12.25	11.07	8.30	8.70	14.23	10.28	9.88
		5	13.44	8.70	8.70	11.46	11.07	8.30	8.30	13.83	9.88	9.09
		6	13.04	8.70	8.70	10.67	9.88	7.91	8.30	12.65	9.49	8.70
	$\theta = 0.5$	4	13.83	9.09	9.09	11.46	11.86	8.30	9.09	13.83	10.28	9.49
		5	12.65	8.30	9.09	11.07	10.28	7.51	7.91	13.44	9.88	8.70
		6	11.86	7.91	8.30	10.67	9.88	7.51	8.30	13.04	9.49	9.09
Panel B FDR threshold	$\theta = 0.3$	4	13.44	9.09	8.70	11.86	11.07	7.11	9.09	13.44	9.88	8.70
		5	12.65	9.49	8.70	11.07	9.88	7.51	8.70	13.44	9.09	8.30
		6	11.86	8.30	8.30	10.67	9.88	7.51	8.30	12.65	9.09	8.30
	$\theta = 0.4$	4	13.04	8.70	9.09	11.86	10.28	7.51	8.30	13.04	9.88	9.09
		5	12.25	8.30	8.30	11.07	10.67	7.51	8.30	12.65	9.09	8.70
		6	12.25	8.70	8.30	9.88	9.49	7.51	7.91	11.86	9.09	8.30
	$\theta = 0.5$	4	12.65	9.09	8.30	11.07	11.07	7.51	9.09	12.25	9.09	9.09
		5	11.46	7.91	8.70	10.67	9.49	7.11	7.91	12.25	9.09	7.91
		6	11.07	7.91	8.30	10.28	9.49	6.72	7.91	12.25	9.09	8.30

This table reports the proportions of days with jumps identified by the PDS-based test for 10 NYSE stocks in 2020, with the control of spurious detections using (i) the universal threshold and (ii) the FDR threshold of Bajgrowicz et al. (2016). We use three pre-averaging windows $k_n = \lceil \theta\sqrt{N} \rceil$ with $\theta \in \{0.3, 0.4, 0.5\}$, different PDS barrier widths $c = K\sigma(\tilde{r}_i)$, i.e., the integer multiple of the standard deviation of pre-averaged returns, with K ranging from 4 to 6, and the censoring parameter $\epsilon = 0.05$. The total number of trading days is 253.

performance of our test under empirically realistic specifications for price observations, which is convincingly superior to a comprehensive collection of "classical" methods. The Monte Carlo results demonstrate that the performance of our test is robust to various aggregation levels and tuning parameter choices. An empirical analysis of NYSE-traded stocks provides strong statistical evidence for jumps across all selected stocks, and the results are robust to the correction of spurious detections. This methodology stands as the first exploration of the duration-based approach to test for jumps, which offers a robust and easy-to-implement tool for researchers and practitioners.

Chapter 3

Realized Candlestick Wicks[1]

3.1 Introduction

The discussion about intraday periods with extreme high-frequency return persistence was brought back to the fore by the May 2010 "flash crash" in the U.S. stock market (Kirilenko et al., 2017; Menkveld and Yueshen, 2019). The crash originated in E-mini S&P 500 future contracts, and led to an extraordinarily rapid decline by 5-6% and a V-shaped recovery of U.S. equity indices in 30 minutes. It swiftly spread to almost 8,000 individual stocks and exchange traded funds (ETFs), and echoed internationally (CFTC and SEC, 2010). Prices with short-lived locally explosive trends and returns with highly positive autocorrelations exhibit compelling short-horizon predictability.[2] "Gradual jumps" identified by Barndorff-Nielsen et al. (2009) also have similar characteristics. These sharp but "continuous" price movements explain to a large extent the reason for spurious detection of jumps with sparsely sampled data (Christensen et al., 2014; Bajgrowicz et al., 2016), although they have attracted limited attention. Empirical evidence shows such extreme events like mini flash crashes occur more frequently in recent years, which raises widespread concern about market inefficiency and vulnerability (Golub et al.,

[1] This chapter corresponds to Li et al. (2024c), in revision for the *Journal of Econometrics*. This chapter was previously circulated under the title "Nonparametric Range-Based Estimation of Integrated Variance with Episodic Extreme Return Persistence".

[2] Return predictability induced by temporary deviations from the random walk of log-prices has been intensively discussed in low frequencies (Welch and Goyal, 2008; Rapach and Zhou, 2013; Farmer et al., 2023). Laurent and Shi (2022) develop a real-time Dickey-Fuller detection technique for such deviations with high-frequency intraday data, and find evidence for explosiveness and mean reversion of intraday stock prices. Andersen et al. (2022) empirically illustrate that there often exist locally significant and persistent autocorrelations in high-frequency returns.

2012; Laly and Petitjean, 2020; Flora and Renò, 2022). These market glitches are also a threat to the standard theoretical framework, as a temporary violation of the Itô semimartingale assumption and potentially the no-arbitrage principle (Andersen et al., 2023c). Two recent influential studies, Christensen et al. (2022) and Andersen et al. (2023a), attempt to incorporate the mechanism behind these short-term directional and persistent price movements into the standard Itô semimartingale framework. Christensen et al. (2022) attribute the short-lived explosive trend to a locally unbounded drift, which prevails over volatility and dominates log-returns in the vicinity of explosion points.[3] Andersen et al. (2023a) consider these unusual patterns as outcomes of the temporary disequilibrium after ambiguous information arrivals, i.e., the market price over- or under-reacts to information in an inefficient financial market, and deviates temporarily from the true value.[4]

The existence of such events poses new challenges for the estimation of integrated variance (IV), which serves as the cornerstone of statistical inference with high-frequency financial data (Aït-Sahalia and Jacod, 2014). Since the realized volatility (RV) estimator of Andersen and Bollerslev (1998), the increased data availability motivates the development of nonparametric estimation techniques to mitigate the impact of distinctive data characteristics, either in isolation or in combination. A stream of literature focuses on robust IV estimation when the price process has jumps. There are basically two methods to overcome this problem: the bipower and multipower estimators (Barndorff-Nielsen and Shephard, 2004, 2006; Huang and Tauchen, 2005) and truncated estimators (Mancini, 2009), with some combinations thereof (Vetter, 2010; Corsi et al., 2010). Theoretical innovations on this issue continue to emerge afterwards, see, e.g., Andersen et al. (2012) and Jacod and Todorov (2014, 2018). All the aforementioned tools spotlight merely extreme price movements characterized by a discontinuous component, while the distortion of IV measurement by non-trivial periods with sharp but continuous price movements has long been ignored. Laurent and Shi (2020) visualize the bias of (original and modified) RV and realized bipower variation (RBPV) in the presence of a nonzero drift coefficient. The differenced-return volatility (DV) estimator of Andersen et al. (2023a) is the

[3] See also Flora and Renò (2022), Laurent et al. (2022), Christensen and Kolokolov (2023), Kolokolov (2023), Mancini (2023), and Bellia et al. (2024), for some recent theoretical and empirical studies on drift burst.

[4] The economic interpretation of Andersen et al. (2023a) for such short-lived deviations is based on market participants' sticky expectations, which have been highlighted by literature in both macroeconomics and finance (Coibion and Gorodnichenko, 2015; Bouchaud et al., 2019; Farmer et al., 2023).

first IV estimator robust to this type of episodic Itô semimartingale violation.

This chapter develops an alternative nonparametric estimator which can exclude excessive return variation induced by short-lived dominant trends and consistently estimate IV from the diffusion component. Motivated by the drift-independent variance estimator of Yang and Zhang (2000), we propose the range-return-difference volatility (RRDV) estimator based on intraday "candlestick" information, specifically the high, low, open, and close prices (HLOCs) within short time intervals. The RRDV estimator is constructed from pairwise differences between high-low ranges and absolute open-close returns. This construction based on range-return differences is designed to remove the contribution to total variation from a locally persistent component, which dominates both ranges and returns in the intervals within such non-trivial episodes. Fig. 3.1 illustrates some simulated examples of intraday candlestick charts. The candlesticks have long "real bodies" but small or nearly no "wicks", i.e., *marubozu* candlesticks, when the price movements are locally dominated by either discontinuities or short-lived explosive trends. The pairwise offset between ranges and returns offers the wick-based RRDV estimator a built-in robustness to such extreme events.

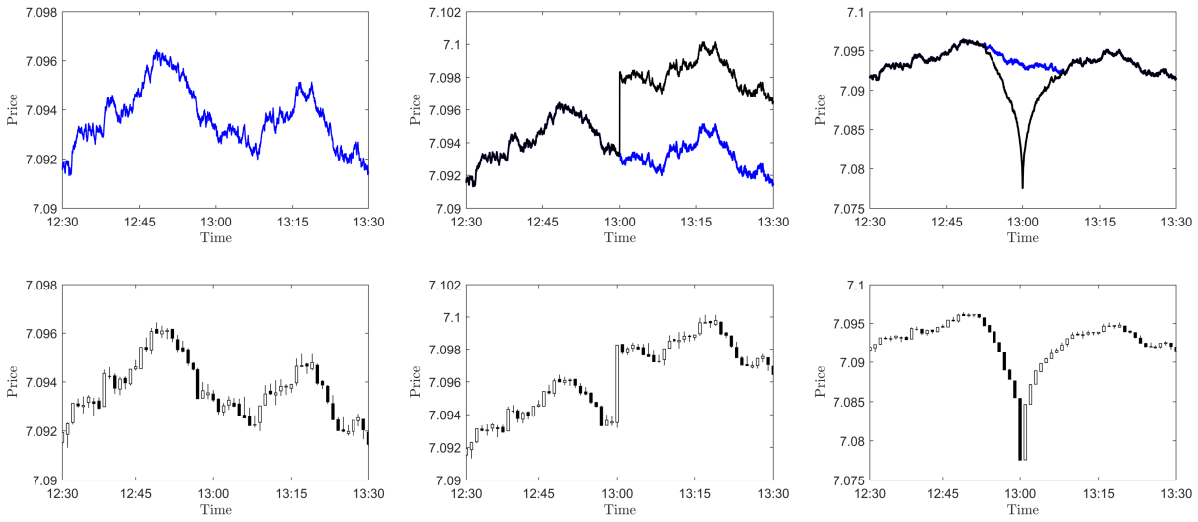

Fig. 3.1 Examples of one-minute intraday candlestick charts for the simulated second-by-second log-prices from different DGPs: continuous (left), discontinuous with a jump (middle), continuous with a V-shaped flash crash (right). White candlesticks indicate upward movements, and black ones denote downward movements.

Different from the DV estimator that is constructed from the first-order differenced returns to offset the excessive return drift in consecutive intervals, RRDV utilizes the candlestick information and implements a similar offset independently within each interval. We derive

the consistency and asymptotic normality of the RRDV estimator under infill asymptotics, which reveals its ability to provide consistent IV estimates with variances approximately four times smaller than those obtained with DV. Importantly, we demonstrate that the presence of jumps with both finite and infinite activities, as well as the episodes of extreme return persistence as modeled by Christensen et al. (2022) and Andersen et al. (2023a), has no impact on the consistency and asymptotic distribution. Simulation results confirm that our new estimator outperforms selected competitors in scenarios with various specifications of extreme directional price movements, with an effective correction for the finite-sample biases. Our empirical application focuses on the prediction of out-of-sample IV estimates of the SPDR S&P 500 ETF Trust (SPY) with the heterogeneous autoregressive (HAR) model of Corsi (2009). We find that the HAR model based on RRDV estimates can achieve smaller forecast errors for both robust and non-robust IV measures than all selected benchmark models, especially on days with continuous or discontinuous extreme events.

From a technical point of view, our estimator is more closely related to the literature on range-based volatility estimation. Since the classical works of Parkinson (1980) and Garman and Klass (1980), a number of studies in this field show the strength of range-based volatility estimators to improve estimation accuracy by extracting more information from realized price paths than return-based measures, see, e.g., Beckers (1983), Ball and Torous (1984), Rogers and Satchell (1991), Kunitomo (1992), Yang and Zhang (2000), Alizadeh et al. (2002), and Brandt and Diebold (2006). The realized range-based volatility (RRV) estimator introduced by Christensen and Podolskij (2007) is the first nonparametric IV measure constructed from high-frequency intraday ranges, which is then extended by Martens and van Dijk (2007), Christensen et al. (2009), and Christensen and Podolskij (2012). More recently, Li et al. (2022) and Bollerslev et al. (2024) introduce the optimal candlestick-based spot volatility estimators with the linear and nonlinear functional forms, respectively, which benefit from the broad availability of intraday candlestick charts. As a fundamental tool in technical analysis that predates the rise of high-frequency data, easy access to intraday candlesticks is now widely available in most online trading applications. This accessibility facilitates the straightforward implementation of candlestick-based inference techniques, rendering them a convenient option for general investors.

The remainder of this chapter is structured as follows: Section 3.2 lays out the basic setup

and introduces the new candlestick-based IV estimator. Section 3.3 discusses its asymptotic behavior under two different specifications of episodic extreme return persistence. Section 3.4 contains finite-sample refinements of our estimator and instructions in practice. Section 3.5 includes an extensive Monte Carlo study that verifies its asymptotic unbiasedness and illustrates the finite-sample performance. After an empirical application of volatility forecasting in Section 3.6, we conclude in Section 3.7. All proofs and additional materials are relegated to Appendix B.

3.2 Volatility Estimation Based on Range-Return Differences

3.2.1 Range-Return-Difference Volatility (RRDV) Estimator

For a finite time interval $[0,t]$, e.g., a trading day, we apply an equidistant partition at $0<\Delta_n<2\Delta_n<\cdots<n\Delta_n\leq t$ to divide it into $n=\lfloor t/\Delta_n\rfloor$ short time intervals. We denote the i-th interval by $I_{n,i}=[(i-1)\Delta_n,i\Delta_n]$. The HLOC over the i-th interval can be expressed respectively as

$$H_i=\sup_{t\in I_{n,i}}X_t,\qquad L_i=\inf_{t\in I_{n,i}}X_t,\qquad O_i=X_{(i-1)\Delta_n},\qquad C_i=X_{i\Delta_n}. \tag{3.1}$$

The high-low range and open-close return are then denoted by

$$w_i=H_i-L_i,\qquad r_i=C_i-O_i. \tag{3.2}$$

The range-return-difference volatility (RRDV) estimator based on the differences between ranges and absolute returns is defined as

$$\widehat{V}_{t,n}=\frac{1}{\Lambda_2}\sum_{i=1}^{n}\left(w_i-|r_i|\right)^2, \tag{3.3}$$

with

$$\Lambda_p=\mathbb{E}\left[\left(\sup_{t,s\in[0,1]}W_t-W_s-|W_1|\right)^p\right], \tag{3.4}$$

where $W=(W_t)_{t\geq0}$ is a standard Brownian motion, and $\Lambda_2=4\ln2-2\approx0.7726$, specifically.

3.2.2 Limit Theorems for Continuous Itô Semimartingales

We consider a continuous Itô semimartingale in a filtered probability space $(\Omega, \mathcal{F}, (\mathcal{F}_t)_{t\geq 0}, \mathbb{P})$:

$$X_t = X_0 + \int_0^t \mu_s ds + \int_0^t \sigma_s dW_s, \tag{3.5}$$

where t stands for time, X_0 is $\mathcal{F}_0$-measurable, $\mu = (\mu_t)_{t\geq 0}$ is a locally bounded and predictable process of drift, $\sigma = (\sigma_t)_{t\geq 0}$ is an adapted, càdlàg and strictly positive (almost surely) process of spot volatility, and $W = (W_t)_{t\geq 0}$ is a standard Brownian motion.

Theorem 3.1 (Consistency)**.** Assume that the efficient price X evolves according to Eq. (3.5) with all traditional conditions satisfied. Then it holds that as $\Delta_n \to 0$,

$$\widehat{V}_{t,n} \xrightarrow{\text{u.c.p.}} \int_0^t \sigma_s^2 ds, \tag{3.6}$$

where $\xrightarrow{\text{u.c.p.}}$ stands for the uniform convergence in probability, i.e., for any processes Z^n, Z we have $Z^n \xrightarrow{\text{u.c.p.}} Z$ if and only if $\sup_{s\leq t} |Z_s^n - Z_s| \xrightarrow{\mathbb{P}} 0$ for all t finite.

Theorem 3.1 indicates that RRDV is a consistent estimator under infill asymptotics when the efficient prices follow a continuous Itô semimartingale. The result is straightforward to prove with the law of large numbers (LLN) for path-dependent functionals of Itô semimartingales, as summarized in Duembgen and Podolskij (2015). To derive an associated central limit theorem (CLT), we need to impose some regularity conditions on σ:

Assumption 3.1. σ does not vanish and follows a continuous Itô semimartingale of the form

$$\sigma_t = \sigma_0 + \int_0^t \tilde{\mu}_s ds + \int_0^t \tilde{\sigma}_s dW_s + \int_0^t \tilde{v}_s dB_s, \tag{3.7}$$

where $\tilde{\mu} = (\tilde{\mu}_t)_{t\geq 0}$, $\tilde{\sigma} = (\tilde{\sigma}_t)_{t\geq 0}$, and $\tilde{v} = (\tilde{v}_t)_{t\geq 0}$ are adapted, càdlàg processes, and $B = (B_t)_{t\geq 0}$ is another Brownian motion independent of W.

Remark 3.1. This assumption rules out possible discontinuities in σ, which is at odds with some empirical evidence, see, e.g., Eraker et al. (2003), Jacod and Todorov (2010), Todorov and Tauchen (2011), and Bandi and Renò (2016). It can be harmlessly relaxed without altering the limit in the next theorem, but needs substantial extra calibration in the proofs. Some relevant discussions can be found in Christensen et al. (2009) and Christensen and Podolskij (2012).

Theorem 3.2 (Asymptotic normality)**.** Assume that the efficient price X follows a continuous Itô semimartingale in Eq. (3.5) with Assumption 3.1 satisfied. Then as $\Delta_n \to 0$, we have

$$\frac{1}{\sqrt{\Delta_n}}\left(\widehat{V}_{t,n} - \int_0^t \sigma_s^2 ds\right) \xrightarrow{\mathcal{L}-\mathrm{s}} \mathcal{MN}\left(0, \Theta \int_0^t \sigma_s^4 ds\right), \tag{3.8}$$

with the variance factor $\Theta = (\Lambda_4 - \Lambda_2^2)/\Lambda_2^2 \approx 0.7245$, and $\Lambda_4 = 24\ln 2 - 12 - 3\zeta(3) \approx 1.0294$, where $\zeta(3) = \sum_{n=1}^{\infty} n^{-3} \approx 1.2021$ is the Riemann's zeta function. We denote by $\xrightarrow{\mathcal{L}-\mathrm{s}}$ the stable convergence in law, and by $\mathcal{MN}$ a mixed normal distribution, i.e., a normal distribution conditional on the realization of its $\mathcal{F}$-conditional variance, which is a random variable.

Remark 3.2. Compared with the DV estimator of Andersen et al. (2023a) which features a variance factor of 3, the asymptotic variance of our candlestick-based RRDV estimator is about four times smaller under infill asymptotics. This result might seem surprising initially, given that Kolokolov et al. (2023) demonstrate that DV attains the variance lower bound of drift-robust IV estimator based on returns from two adjacent blocks. In essence, the improvement of RRDV over DV originates from the additional information contained in high-frequency intraday ranges, which induces a different limiting statistical experiment. This additional information also leads to the diminished variance of the RRV estimator of Christensen and Podolskij (2007) over RV, which is the return-based minimum-variance unbiased estimator (MVUE). Finally, if the robustness to locally explosive trends is not pursued, then one can construct a variance optimal candlestick-based IV estimator in the spirit of Garman and Klass (1980), Li et al. (2022), and Bollerslev et al. (2024). As this is not the main focus of this chapter, we shall leave it for further research.

Remark 3.3. Similar to the limiting distribution of RRV in Christensen and Podolskij (2007), the variance factor Θ in Theorem 3.2 is an infill-asymptotic result based on the presumption that the true HLOCs in all short episodes are observed. In practice, the efficiency of range-based estimators depends on the number of observations used to calculate the high-low range within each interval. See a detailed discussion in Section 3.4.1 about the RRDV estimator constructed from candlesticks formed by a finite number of observations.

For feasible implementation of the asymptotic distribution in Theorem 3.2, we can estimate the integrated quarticity (IQ) with the following range-return difference quarticity (RRDQ)

estimator constructed analogously to RRDV:

$$\widehat{Q}_{t,n} = \frac{n}{\Lambda_4} \sum_{i=1}^{n} (w_i - |r_i|)^4 . \tag{3.9}$$

With techniques similar to Theorem 3.1, we can establish the consistency result for RRDQ:

Corollary 3.1 (Feasible inference)**.** Under the same conditions as in Theorem 3.1, it holds that

$$\widehat{Q}_{t,n} \xrightarrow{\text{u.c.p.}} \int_0^t \sigma_s^4 ds. \tag{3.10}$$

The stable convergence in Theorem 3.2 implies that

$$\sqrt{\frac{n}{\Theta \widehat{Q}_{t,n}}} \left(\widehat{V}_{t,n} - \int_0^t \sigma_s^2 ds \right) \xrightarrow{\mathcal{L}} \mathcal{N}(0,1). \tag{3.11}$$

Remark 3.4. Similar to RRDV, the fourth-moment estimator $\widehat{Q}_{t,n}$ is robust to both discontinuities (in Section 3.2.3) and short-lived locally explosive trends (in Section 3.3). The proofs are analogous and thus omitted here.

3.2.3 Jumps

We examine the behavior of our RRDV estimator constructed on a discontinuous Itô semimartingale defined on $(\Omega, \mathcal{F}, (\mathcal{F}_t)_{t\geq 0}, \mathbb{P})$, e.g., with the Grigelionis (1980) representation:

$$X_t = X_0 + \int_0^t \mu_s ds + \int_0^t \sigma_s dW_s + \left(\delta \mathbb{1}_{\{|\delta|\leq 1\}}\right) \star \left(\underline{p} - \underline{q}\right)_t + \left(\delta \mathbb{1}_{\{|\delta|>1\}}\right) \star \underline{p}_t, \tag{3.12}$$

where $\underline{p} = \underline{p}(dt, dx)$ is a Poisson random measure on $\mathbb{R}_+ \times \mathbb{R}$ with a compensator $\underline{q} = \underline{q}(dt, dx) = dt \otimes \lambda(dx)$, λ is a σ-finite measure on $\mathbb{R}$, and the function $\delta(\omega, t, x)$ on $\Omega \times \mathbb{R}_+ \times \mathbb{R}$ is predictable; see Aït-Sahalia and Jacod (2014) for details regarding the last two integrals.

Assumption 3.2. There exists a sequence $(\tau_n)_{n\geq 1}$ of stopping times increasing to ∞, and a sequence of deterministic nonnegative functions f_n on $\mathbb{R}$ for each n, which satisfies $|\delta(\omega, t, x)| \wedge 1 \leq f_n$ for all (ω, t, x) with $t \leq \tau_n(\omega)$, and $\int_{\mathbb{R}} |f_n|^r \lambda(dx) < \infty$ for some $r \in [0, 1)$.

Remark 3.5. The parameter r sets a bound on the degree of jump activity. With some $r \in [0, 1)$, we consider jumps of both finite and infinite activities, but restrict them to be of

finite variation, i.e., they are absolutely summable, such that in Eq. (3.12) we can dispense with the integral with $\underline{p} - \underline{q}$, see Jacod et al. (2019) for more details.

Jumps of order of magnitude Δ_n^{ϖ} for some $\varpi \in [0, 1/2)$ prevail over the diffusion component and induce non-negligible shifts in $X(\omega)$ under infill asymptotics. We denote by $\Delta X_t = X_t - X_{t-}$ the size of discontinuous shift at time t. The robustness of RRDV in the presence of jumps is shown in the next proposition.

Proposition 3.1 (Jump robustness)**.** Assume that the efficient price X follows a discontinuous Itô semimartingale in Eq. (3.12) with Assumption 3.2 satisfied. Then as $\Delta_n \to 0$,

$$\widehat{V}_{t,n} - \int_0^t \sigma_s^2 ds = O_p\left(\sqrt{\Delta_n}\right), \tag{3.13}$$

where the bias induced by jumps is asymptotically negligible and has no impact on the asymptotic distribution in Theorem 3.2.

Proposition 3.1 indicates the robustness of RRDV to both finite-activity and infinite-activity but finite-variation jumps in the efficient price. In each of the intervals with a nonzero ΔX_t, the discontinuous component in Eq. (3.12) has a higher asymptotic order than the continuous component, and thus dominates both the range and absolute return under infill asymptotics. Consequently, the jumps are mechanically cancelled in the range-return differences. As a result, the contribution from intervals that contain jumps in RRDV is asymptotically negligible and does not affect the consistency and asymptotic normality in Theorems 3.1 and 3.2, respectively.

In contrast, the differencing of returns removes the contribution from similar realizations of a locally persistent term in consecutive intervals, but it retains the unexpected increments from the distinctly less persistent jump component. Therefore, the DV estimator relies on an additional truncation method introduced by Mancini (2009) to discard all unexpectedly large differenced returns that may possibly contain jumps.

As pointed out by Andersen et al. (2023a), market participants may imperfectly react to the shifts in economic fundamentals, and sometimes induce an short-lived deviation between the efficient and observed prices. This phenomenon, referred to as the "gradual jumps" identified by Barndorff-Nielsen et al. (2009) and Hoffmann et al. (2018), will be discussed in the next section as a typical manifestation of short-lived extreme return persistence.

3.3 Extreme Return Persistence

3.3.1 Drift Burst Model

As assumed in Section 3.2.2, the drift $\mu = (\mu_t)_{t\geq 0}$ is locally bounded, so that we can estimate IV consistently under infill asymptotics, because the drift becomes invisible since $\Delta_n \ll \sqrt{\Delta_n}$ in the limit, i.e., for a fixed time point τ, we have

$$\int_{\tau}^{\tau+\Delta_n} \mu_s ds = O_p\left(\Delta_n\right) \quad \text{and} \quad \int_{\tau}^{\tau+\Delta_n} \sigma_s dW_s = O_p\left(\sqrt{\Delta_n}\right), \quad \text{as } \Delta_n \to 0. \tag{3.14}$$

Christensen et al. (2022) point us in a new direction to understand some highly directional price movements over short episodes, in which the unbounded drift prevails over volatility and locally dominates log-returns in the limit, which is summarized in the following assumption.

Assumption 3.3 (Drift burst model)**.** The efficient price X is defined on a filtered probability space $(\Omega, \mathcal{F}, (\mathcal{F}_t)_{t\geq 0}, \mathbb{P})$ and assumed to be a continuous semimartingale described by

$$X_t = X_0 + \int_0^t \mu_s ds + \int_0^t \sigma_s dW_s + H_t, \tag{3.15}$$

with

$$H_t = \int_0^t \mu_s^b ds = \int_0^t \frac{c_s^- \mathbb{1}_{\{s<\tau\}} + c_s^+ \mathbb{1}_{\{s>\tau\}}}{|s-\tau|^\alpha} ds, \tag{3.16}$$

where $\tau \geq 0$, and $1/2 < \alpha < 1$. The coefficients c_t^- and c_t^+ are continuous and twice differentiable deterministic functions. All usual conditions for μ and σ are satisfied.

It is assumed that the bursting drift term μ_t^b has a singularity at the "burst time" τ, and thus explode in the vicinity of τ. The order of magnitude of H_t is given by

$$\int_{\tau-\Delta_n}^{\tau} \frac{c_s^-}{(\tau-s)^\alpha} ds \asymp \int_{\tau}^{\tau+\Delta_n} \frac{c_s^+}{(s-\tau)^\alpha} ds = O_p\left(\Delta_n^{1-\alpha}\right). \tag{3.17}$$

We allow for different drift explosion coefficients c_t^- and c_t^+ before and after τ, and use the same rate of explosion α on both sides for ease of exposition. We restrict $\alpha < 1$ for the continuity of sample paths. When $\alpha > 1/2$, the volatility is completely swamped by the drift in the vicinity of τ, which induces a short-lived return persistence, and biases the nonparametric volatility

estimators constructed from high-frequency intraday returns.[5]

When $1/2 < \alpha < 1$ and $c_\tau^- c_\tau^+ < 0$, the trajectory shows a "V-shape" (or "Λ-shape") in the neighborhood of τ, thanks to a discontinuity in the sign of H_t which locally dominates log-returns (Flora and Renò, 2022). Different drift explosion coefficients c_t^- and c_t^+ can be harmlessly employed to mimic patterns akin to V-shaped flash crashes ($c_\tau^- < 0, c_\tau^+ > 0$) or gradual jumps ($c_\tau^+ = 0$). It will not affect main intuitions.

Proposition 3.2. Assume that the efficient price X follows a continuous semimartingale in Eq. (3.15) and Assumption 3.3 holds with $1/2 < \alpha < 1$. For the RRDV estimator, it holds that

$$\widehat{V}_{t,n} - \int_0^t \sigma_s^2 ds = O_p\left(\Delta_n^{\frac{1}{2\alpha}} \bigvee \sqrt{\Delta_n}\right) = O_p\left(\sqrt{\Delta_n}\right), \quad \forall \alpha \in \left(\frac{1}{2}, 1\right), \tag{3.18}$$

where the bias induced by the drift burst is asymptotically negligible and has no impact on the asymptotic distribution in Theorem 3.2.

Under Assumption 3.3, the drift burst component $H = (H_t)_{t\geq 0}$ dominates the price movement in the vicinity of τ, i.e., the "explosion effect zone", while its impact diminishes as t moves away from τ. Both the range and absolute return in an interval within the effect zone near τ are dominated by a common excessive component, that is, the H increment of a higher asymptotic order than $\sqrt{\Delta_n}$. The pairwise offset between ranges and returns naturally nullifies the impact of H. As a result, the presence of drift burst can only induce an estimation bias of order $O_p(\Delta_n^{1/2\alpha})$ for the RRDV estimator, which is asymptotically negligible and does not affect the CLT result in Theorem 3.2 for all possible $\alpha \in (1/2, 1)$. Over the region not in the vicinity of τ, the invisible H retains the continuous Itô semimartingale assumption with a bias of order $O_p(\sqrt{\Delta_n})$.

The bias result of RRDV in Proposition 3.2 has a similar form as that of DV in Andersen et al. (2023a). We find that the asymptotic order of the RRDV bias under Assumption 3.3 aligns with the bias order $O_p(\sqrt{\Delta_n})$ under the continuous Itô semimartingale assumption, and its upper bound $\sqrt{\Delta_n}$ does not exceed that of the DV bias. Furthermore, the bias result of RRDV remains unaffected by the rate of drift explosion α and does not depend on any parameter

[5] We follow Andersen et al. (2023a) to consider such episodic Itô semimartingale violations with only an exploding drift. It does not necessarily allow local arbitrage opportunities in the specification of Christensen et al. (2022), which accommodates simultaneous drift and volatility bursts with different rates of explosion.

choices, while the DV bias is independent of α only when some conditions for the truncation threshold are satisfied. The result can be extended to the case with stochastically distributed explosion times over $[0, t]$, as illustrated next in Section 3.3.2.

3.3.2 Persistent Noise Model

Andersen et al. (2023a) introduce an alternative specification for the episodic emergence of extreme directional price movements. They consider these complex price patterns as outcomes of market uncertainty caused by imperfect information and irrational market participants.

Assumption 3.4 (Persistent noise model)**.** The observed price X is a combination of the efficient price, modeled as a possibly discontinuous Itô semimartingale in Eq. (3.12), and a component H that accommodates persistent price movements over irregularly spaced episodes:

$$X_t = X_0 + \int_0^t \mu_s ds + \int_0^t \sigma_s dW_s + \sum_{0 \le s \le t} \Delta X_s + H_t. \tag{3.19}$$

We denote by τ_i the first occurrence of the i-th "persistent noise" episode, so that $\tau_1, \tau_2, \ldots, \tau_N \in [0, t)$ form an increasing sequence of stopping times, with N finite almost surely. The persistent noise component is given by

$$H_t = \sum_{i:\tau_i \le t} H_t^{(i)} \mathbb{1}_{\{\epsilon_t^{(i)} \ge 0\}}, \tag{3.20}$$

with $H_t^{(i)}$ defined as

$$H_t^{(i)} = f^{(i)}(\Delta X_{\tau_i}, \eta_{\tau_i}) g^{(i)}(t), \tag{3.21}$$

where $\Delta X_{\tau_i} = X_{\tau_i} - X_{\tau_i^-}$ is the efficient price jump at τ_i, η_{τ_i} is an $\mathcal{F}_{\tau_i}$-measurable random variable, $f^{(i)}$ is a continuous and bounded function, and $g^{(i)}$ has one of the functional forms as follows:

$$g_{gj}^{(i)}(t) = \left[1 - \left(\frac{t - \tau_i}{\overline{\tau}_i - \tau_i}\right)^{\beta}\right] \mathbb{1}_{\{t \in [\tau_i, \overline{\tau}_i]\}}, \tag{3.22}$$

where $0 < \beta < 1/2$, and $\overline{\tau}_i > \tau_i$ is an $\mathcal{F}_{\tau_i}$-measurable random variable, or

$$g_{fc}^{(i)}(t) = c_t^- \left[1 - \left(\frac{\breve{\tau}_i - t}{\breve{\tau}_i - \tau_i}\right)^{\beta^-}\right] \mathbb{1}_{\{t \in [\tau_i, \breve{\tau}_i]\}} + c_t^+ \left[1 - \left(\frac{t - \breve{\tau}_i}{\overline{\tau}_i - \breve{\tau}_i}\right)^{\beta^+}\right] \mathbb{1}_{\{t \in [\breve{\tau}_i, \overline{\tau}_i]\}}, \tag{3.23}$$

where $0 < \beta^-, \beta^+ < 1/2$, the coefficients c_t^- and c_t^+ are continuous and twice differentiable

deterministic function, and $\tau_i < \breve{\tau}_i < \overline{\tau}_i$ are all $\mathcal{F}_{\tau_i}$-measurable random variables. Moreover,

$$\epsilon_t^{(i)} = \sum_{s \in [\tau_i, t]} \Delta \epsilon_s \tag{3.24}$$

is a finite-activity pure jump process with negative jumps.

Remark 3.6. Each of the episodes is activated and terminated by the realizations of τ_i and $\overline{\tau}_i$, or randomly ended by $\epsilon_t^{(i)}$ in the middle. The function $f^{(i)}$ captures the initial market reaction to events with ambiguous information that trigger persistent noise episodes, the random variable η_{τ_i} allows for a random response to such events, and the function $g^{(i)}$ describes the price pattern over a temporary disequilibrium after ambiguous information arrives. Assumption 3.4 allows for two basic forms of $H^{(i)}$ to model market uncertainty in two different scenarios:

I. Market participants underreact (or slowly react) to a shift in fundamentals. In this scenario, there exists $\Delta X_{\tau_i} \neq 0$, the function $g^{(i)}$ takes the form $g_{gj}^{(i)}$ in Eq. (3.22), and $f^{(i)}(\Delta X_{\tau_i}, \eta_{\tau_i}) = -\eta_{\tau_i} \Delta X_{\tau_i}$ with $\eta_{\tau_i} = 1$ or $\eta_{\tau_i} \in (0, 1)$, which partially offsets the efficient price jump at τ_i.

II. Market participants worry about a potential shift in fundamentals. In this scenario, $\Delta X_{\tau_i} = 0$, and the function $g^{(i)}$ takes the form $g_{fc}^{(i)}$ in Eq. (3.23). The deviation from efficient price is (fully or partially) recovered shortly after due to reverse trades by arbitrageurs, which leads to a V-shaped trajectory with a turning point at a random time $\breve{\tau}_i$.

The scenario I and II correspond to two phenomena observed in financial markets, i.e., gradual jumps and flash crashes, respectively. $H^{(i)}$ in scenario II can be viewed as a stochastic extension of the drift burst model in Assumption 3.3, with stochastically distributed explosion times over $[0, t]$.

We next state an analogous result to Proposition 3.2 when the observed prices persistently deviate from the fundamental values due to short-lived market inefficiency.

Proposition 3.3. Assume that the market price X follows a contaminated Itô semimartingale in Eq. (3.19) with finite-activity jumps, i.e., $r = 0$ in Assumption 3.2, and there exists a persistent noise episode $[\tau, \overline{\tau}] \subset [0, t]$. The function $g^{(1)}$ in the noise component $H_t^{(1)}$ takes

either of the two forms in Eqs. (3.22) and (3.23). For the RRDV estimator, it holds that

$$\widehat{V}_{t,n} - \int_0^t \sigma_s^2 ds = \begin{cases} O_p\left(\Delta_n^{\frac{1}{2(1-\beta)}} \bigvee \sqrt{\Delta_n}\right) = O_p\left(\sqrt{\Delta_n}\right), & \forall \beta \in (0, 1/2), \quad \text{when } g^{(1)} = g_{gj}^{(1)}, \\ O_p\left(\Delta_n^{\frac{1}{2(1-\beta^- \wedge \beta^+)}} \bigvee \sqrt{\Delta_n}\right) = O_p\left(\sqrt{\Delta_n}\right), & \forall \beta^{\pm} \in (0, 1/2), \quad \text{when } g^{(1)} = g_{fc}^{(1)}, \end{cases} \tag{3.25}$$

where the bias induced by the persistent noise is asymptotically negligible and has no impact on the asymptotic distribution in Theorem 3.2.

In Proposition 3.3, our discussion is confined to a simplified scenario featuring a single persistent noise episode within the interval $[0, t]$. Similar to the result in Proposition 3.2 with a drift burst, the estimation bias is of order $O_p(\Delta_n^{\frac{1}{2(1-\beta)}})$ with a gradual jump and $O_p(\Delta_n^{\frac{1}{2(1-\beta^- \wedge \beta^+)}})$ with a V-shaped flash crash, respectively, over the "explosion effect zone" where the role of H is no smaller than the diffusion component. The results obtained in the simplified scenario can be straightforwardly extended to more general cases involving a finite number of such episodes with non-overlapping effect zones. Simulation results in Section 3.5 shows that the RRDV estimator remains unbiased in the presence of a gradual jump with an intermittent small flash crash.

Over each short interval in the vicinity of $\breve{\tau}$, the persistent noise H adds the same amount to both range and absolute return. The only exception is the so-called "V" interval in a flash crash, i.e., the interval which accommodates the reversal point $\breve{\tau}$. The range-return difference in the "V" interval is an $O_p(\Delta_n^{\beta^- \wedge \beta^+})$ variable, while its impact is negligible when n approaches infinity. However, a steep "V-shape" could deteriorate the finite-sample performance of RRDV when the interval length is far away from infinitesimal in practice, which shall be discussed in Section 3.4.2.

3.4 Finite-Sample Refinements

3.4.1 Finite-Sample Bias I: Discretization Errors

Variance estimators constructed from high-low ranges often exhibit a systematic downward bias in practice. This issue was initially identified by Garman and Klass (1980), Beckers (1983), and Rogers and Satchell (1991) in the context of daily variance estimation. Range-based IV estimation with intraday observations faces a similar challenge. The source of this downward

bias is the difference between the discretized range calculated from the discrete observations available in practice and the true range originating from a continuous-time process, which is referred to as discretization error. More specifically, since the discretized minimum (maximum) is obtained from a smaller set, it will be greater (smaller) than the continuous minimum (maximum). Consequently, the discretized range includes a negative discretization error. In other words, the scaling factor Λ_2 derived from a standard Brownian motion leads to an over-scaling of the sum of squared discretized range-return differences. Therefore, it is advisable to replace it with a discretized scaling factor based on discretely observed Brownian motion.

To formalize this idea, we introduce some additional notation: We denote by N the number of observations in each interval $((i-1)\Delta_n, i\Delta_n]$, and assume there are totally $Nn+1$ equidistant price observations available over $[0,t]$. We denote the discretized high-low range over the i-th interval by

$$w_{i,N} = H_{i,N} - L_{i,N} = \sup_{j\in\{0,1,\ldots,N\}} X_{(i-1)\Delta_n + j\Delta_n/N} - \inf_{j\in\{0,1,\ldots,N\}} X_{(i-1)\Delta_n + j\Delta_n/N}, \tag{3.26}$$

and then define the discretized RRDV estimator as

$$\widehat{V}_{t,n,N} = \frac{1}{\Lambda_{2,N}} \sum_{i=1}^{n} \left(w_{i,N} - |r_i|\right)^2, \tag{3.27}$$

where $\Lambda_{p,N}$ is the counterpart to Λ_p in Eq. (3.4) when the standard Brownian motion is discretely observed at $t = i/N$ for $i = 0, 1, \ldots, N$ over a unit interval:

$$\Lambda_{p,N} = \mathbb{E}\left[\left(\sup_{i,j\in\{0,1,\ldots,N\}} W_{i/N} - W_{j/N} - |W_1|\right)^p\right]. \tag{3.28}$$

To investigate how the discretization error $\Lambda_{p,N} - \Lambda_p$ evolves across different N, we present the asymptotic expansions for $\Lambda_{2,N}$ and $\Lambda_{4,N}$ as follows:

Proposition 3.4. Assume $W_N = (W_{t,N})_{t\in[0,1]} = (W_{i/N})_{i\in\{0,1,\ldots,N\}}$ is an embedded random walk equidistantly spaced at $N+1$ points over $[0,1]$. The following results hold for $\Lambda_{p,N}$ in Eq. (3.28):

$$\Lambda_{2,N} = \Lambda_2 + \frac{4}{\pi}\zeta\left(\frac{1}{2}\right)\frac{1}{\sqrt{N}} + o\left(\frac{1}{\sqrt{N}}\right), \tag{3.29}$$

$$\Lambda_{4,N} = \Lambda_4 + \left(\frac{48}{\pi} - 4\pi\right)\zeta\left(\frac{1}{2}\right)\frac{1}{\sqrt{N}} + o\left(\frac{1}{\sqrt{N}}\right), \tag{3.30}$$

as $N \to \infty$, where $\zeta(1/2) \approx -1.4604$.

Remark 3.7. The asymptotic expansions in Proposition 3.4 are based on the results in Asmussen et al. (1995), who derive the asymptotic results for Euler discretization errors of one-dimensional reflected Brownian motions, with details summarized in Lemma B.4 in Appendix B.2.7.

Proposition 3.4 indicates that both $\Lambda_{2,N}$ and $\Lambda_{4,N}$, as well as the variance factor $\Theta_N = (\Lambda_{4,N} - \Lambda_{2,N}^2)/\Lambda_{2,N}^2$, can be approximated when N is sufficiently large. This fact inspires us to provide practitioners with polynomial approximations for all factors when a finite N is applied in practice. Fig. 3.2 compares the approximated and simulated values of $\Lambda_{2,N}$ and Θ_N with $11 \leq N \leq 2000$, which confirms the precision of polynomial approximations. Further details on the approximations and practical guidance can be found in Appendix B.3.2.

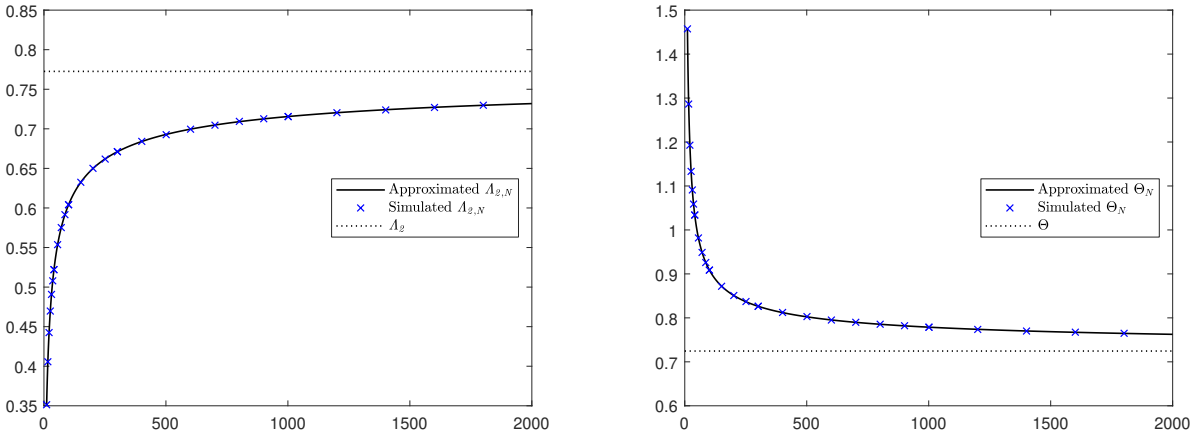

Fig. 3.2 Comparison of approximated and simulated values of $\Lambda_{2,N}$ and Θ_N with $11 \leq N \leq 2000$.

The consistency and asymptotic normality of the discretized RRDV estimator in Eq. (3.27) are summarized in the next corollary. Similar to the discretized RRV in Christensen and Podolskij (2007), the CLT result holds for arbitrary N converging to some integer larger than 1.

Corollary 3.2. Under the same conditions as in Theorem 3.1, it holds that as $\Delta_n \to 0$,

$$\widehat{V}_{t,n,N} \xrightarrow{\text{u.c.p.}} \int_0^t \sigma_s^2 ds. \tag{3.31}$$

Moreover, if Assumption 3.1 holds and $N \to c \in \mathbb{N}^{>1}$, it holds that

$$\frac{1}{\sqrt{\Delta_n}}\left(\widehat{V}_{t,n,N} - \int_0^t \sigma_s^2 ds\right) \xrightarrow{\mathcal{L}-\mathrm{s}} \mathcal{MN}\left(0, \Theta_c \int_0^t \sigma_s^4 ds\right), \tag{3.32}$$

where $\Theta_c = (\Lambda_{4,c} - \Lambda_{2,c}^2)/\Lambda_{2,c}^2$. Finally, the stable convergence implies that

$$\sqrt{\frac{n}{\Theta_N \widehat{Q}_{t,n,N}}}\left(\widehat{V}_{t,n,N} - \int_0^t \sigma_s^2 ds\right) \xrightarrow{\mathcal{L}} \mathcal{N}(0,1), \tag{3.33}$$

where the discretized RRDQ estimator $\widehat{Q}_{t,n,N}$ is given by

$$\widehat{Q}_{t,n,N} = \frac{n}{\Lambda_{4,N}} \sum_{i=1}^{n} (w_{i,N} - |r_i|)^4 \xrightarrow{\text{u.c.p.}} \int_0^t \sigma_s^4 ds. \tag{3.34}$$

The discretized RRDV is undefined when $N \to 1$ because $\Lambda_{2,1} = 0$, unlike RRV that reduces to the standard RV when there are only open and close prices available for all intervals. Furthermore, compared with the DV estimator, the asymptotic variance of the discretized RRDV becomes smaller even when only five observations (including open and close) are available in each interval. Simulation results in Section 3.5.3 demonstrate that the discretized RRDV based on half-a-minute observations (with 1, 2, 3, 5-minute candlestick intervals) can still produce reliable IV estimates, with only a mild increase in finite-sample variance.

The effective correction for discretization errors ensures the reliability of RRDV constructed from discretized candlestick information, i.e., the HLOCs obtained from sparsely or "not-too-finely" sampled price observations within each candlestick interval. The fact that the market microstructure noise becomes more pronounced with higher sampling frequencies has inspired the widespread use of volatility estimators based on sparsely sampled data (Aït-Sahalia et al., 2005). The utilization of discretized HLOCs provides our estimator with a similar robustness to market microstructure noise, without introducing additional complexity for implementation.[6] However, a comprehensive investigation of the asymptotic and finite-sample behavior of range-based estimators constructed from ultra high-frequency or "finely" sampled data with noise contamination requires a more explicit assumption for the noise structure, where the literature is still far from reaching a consensus (Bollerslev et al., 2024). The extension of RRDV in this

[6] Some simulation results are reported in Appendix B.3.5.

direction is left for future research.

3.4.2 Finite-Sample Bias II: V-Shapes

Both models in Section 3.3 can be employed to mimic flash crashes. As commented after Proposition 3.3, the reversal point $\breve{\tau}_i$ (or the explosion time τ in the drift burst model) has no impact on RRDV in the limit, but could deteriorate its finite-sample performance when the interval size is not sufficiently small. An example in Fig. 3.3 illustrates the candlestick patterns around a V-shaped flash crash. In this example, the candlestick in the 5-minute "V" interval has a long lower wick, i.e., the so-called hammer pattern, which potentially introduces a positive bias in the RRDV estimate. This bias becomes particularly pronounced in cases where the V-shape is steep. To mitigate the V-shape bias in finite samples, we augment the RRDV estimator with a truncation threshold for the range-return differences. This augmentation has no impact on the asymptotic results in Sections 3.2 and 3.3, but improves the finite-sample robustness of RRDV to different interval lengths.

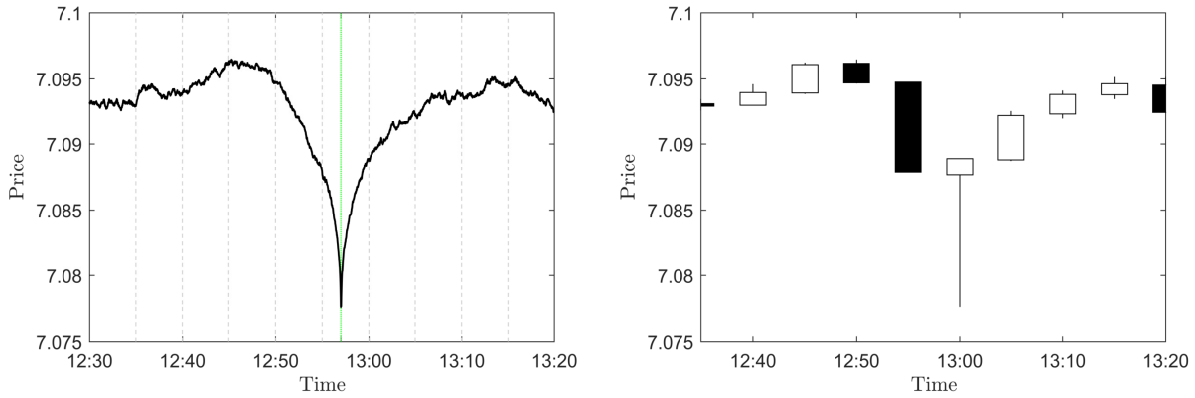

Fig. 3.3 5-minute candlesticks around a simulated V-shaped flash crash.

We employ the classical truncation threshold $\varphi = \zeta \Delta_n^{\varpi}$ with $\varpi \in (0, 1/2)$, initially introduced by Mancini (2009), and set the threshold parameters by using a data-adaptive method. Andersen et al. (2023a) use the truncation threshold for both absolute returns in the truncated realized volatility (TRV) and absolute differenced returns in DV, with

$$\zeta = C_\zeta \sqrt{\mathrm{MedRV}_{t,n}}, \tag{3.35}$$

where $\text{MedRV}_{t,n}$ is the median RV estimator of Andersen et al. (2012), i.e.,

$$\text{MedRV}_{t,n} = \frac{\pi}{6 - 4\sqrt{3} + \pi}\left(\frac{n}{n-2}\right)\sum_{i=2}^{n-1} \text{median}\left(|r_{i-1}|, |r_i|, |r_{i+1}|\right)^2, \tag{3.36}$$

and $C_\zeta^{\text{DV}} = \sqrt{2}C_\zeta^{\text{TRV}} = 3\sqrt{2}$, motivated by the ratio $\sqrt{2}$ between standard deviations of (absolute) differenced and undifferenced i.i.d. Brownian returns. For the RRDV estimator, we truncate the range-return differences with the threshold of the same form, i.e.,

$$\widehat{V}_{t,n,N} = \frac{1}{\Lambda_{2,N}}\sum_{i=1}^{n}\left(w_{i,N} - |r_i|\right)^2 \mathbb{1}_{\left\{w_{i,N} - |r_i| \leq \zeta^{\text{RRDV}}\Delta_n^{\varpi}\right\}}, \tag{3.37}$$

where the parameter ζ^{RRDV} is given by Eq. (3.35) with $C_\zeta^{\text{RRDV}} = 2$, which is approximately the same quantile (99.7%) of range-return differences from a standard Brownian motion.

3.5 Monte Carlo Simulations

This section contains a Monte Carlo study to examine both the asymptotic unbiasedness and the finite-sample performance of the RRDV estimator, which corresponds to the results developed in Sections 3.2 and 3.3.

3.5.1 Simulation Design

We simulate a Heston model for the efficient price process X (Heston, 1993):

$$\begin{aligned} dX_t &= \mu dt + \sigma_t dW_{1,t} + dJ_t, \quad t \in [0,1], \\ d\sigma_t^2 &= \kappa\left(\theta - \sigma_t^2\right)dt + \eta\sigma_t dW_{2,t}, \end{aligned} \tag{3.38}$$

where W_1 and W_2 are standard Brownian motions with $\text{Corr}(W_{1,t}, W_{2,t}) = \rho$, and J is a compound Poisson process, i.e.,

$$J_t = \sum_{i=1}^{N_t} Z_i, \tag{3.39}$$

where N is a Poisson process with rate λ, and Z_i follows a normal distribution $\mathcal{N}(0, \varsigma^2)$. We start with the initial price $X_0 = \ln 1200$, and take the Heston parameters as follows:

$$\begin{aligned} &\mu = 0.05/252, \quad \kappa = 5/252, \quad \theta = 0.0225/252, \quad \eta = 0.4/252, \\ &\rho = -\sqrt{0.5}, \quad \lambda = 1/5, \quad \varsigma = 0.9\%. \end{aligned} \tag{3.40}$$

The volatility parameters satisfy the Feller's condition $2\kappa\theta \geq \eta^2$ which ensures the positivity of σ. The process J simulated with $\lambda = 1/5$ corresponds to one jump per week, and generates around 6.5% of the daily quadratic variation on average.

In this section, we firstly examine the unbiasedness of RRDV in "continuous time": We simulate half-millisecond (0.0005-second) price observations for 2000 days, and construct RRDV on candlestick information in 1, 5, 10, 30-second and 1, 2, 3, 5-minute intervals, respectively. Then we evaluate its finite-sample performance: We simulate one-second and 30-second observations for 10000 days, and construct the candlesticks on 1, 2, 3, and 5-minute intervals, respectively. All simulated observations are equidistantly distributed in $[0, 1]$ which consists of 6.5 hours of trading.

We follow the persistent noise model of Andersen et al. (2023a) to simulate three different patterns of episodic extreme return persistence:[7]

- ***Gradual Jump***: We insert a shift in fundamentals $\Delta X_\tau = 2.5\%$ at $\tau = 0.5$ for all days. For the persistent noise component in Eq. (3.21), we let $i \in \{1\}$, $\tau_1 = \tau$, $f^{(1)}(\Delta X_\tau, \eta_\tau) = -\eta_\tau \Delta X_\tau$ with $\eta_\tau = 1$, $g^{(1)}$ take the form $g^{(1)}_{gj}$ in Eq. (3.22), and $(\tau, \overline{\tau}) = (0.5, 0.59)$.
- ***Flash Crash***: We let $i \in \{1\}$, $\tau_1 = \tau$, $f^{(1)}(\Delta X_\tau, \eta_\tau) = -\eta_\tau$ with $\eta_\tau = 2\%$, $g^{(1)}$ take the form $g^{(1)}_{fc}$ in Eq. (3.23), $(\tau, \breve{\tau}, \overline{\tau}) = (0.41, 0.49, 0.57)$, and $c^{\pm} = 1$.[8]
- ***Gradual Jump + Flash Crash***: We consider two overlapped persistent noise episodes: $i \in \{1, 2\}$. We insert a shift in fundamentals $\Delta X_{\tau_1} = 2.5\%$ at $\tau_1 = 0.5$. We let $f^{(1)}(\Delta X_{\tau_1}, \eta_{\tau_1}) = -\eta_{\tau_1} \Delta X_\tau$ with $\eta_{\tau_1} = 1$, $g^{(1)}$ take the form $g^{(1)}_{gj}$ in Eq. (3.22), and $(\tau_1, \overline{\tau}_1) = (0.5, 0.65)$. For the intermittent (small) flash crash, we assume $f^{(2)}(\Delta X_{\tau_2}, \eta_{\tau_2}) =$

[7] As shown in Eqs. (56) and (57) in Andersen et al. (2023a), there exists an asymptotic correspondence between the two models of episodic extreme return persistence in Section 3.3, and they are equivalent with identical asymptotic analyses when $\beta = 1 - \alpha$. The simulation results with the drift burst model in Eq. (3.15) indicate the same qualitative conclusions.

[8] For flash crashes simulated with $g^{(i)} = g^{(i)}_{fc}$, we stale the observation on $\breve{\tau}_i$ to avoid an unnecessary "jump" on $\breve{\tau}_i$. For example, when $(\tau, \breve{\tau}, \overline{\tau}) = (0.41, 0.49, 0.57) = (9594, 11466, 13338)$ seconds, we truncate the tick-by-tick H increments between 11465 and 11467 seconds.

$-\eta_{\tau_2}$ with $\eta_{\tau_2} = 0.75\%$, $g^{(2)}$ takes the form $g_{fc}^{(2)}$ in Eq. (3.23), and $c^{\pm} = 1$. We assume that the waiting time between τ_1 and τ_2 follows an exponential distribution with rate parameter $\lambda^{\text{Exp}} = 15$, and $(\breve{\tau}_2, \bar{\tau}_2) = (\tau_2 + 0.04, \tau_2 + 0.08)$.

For each scenario, we consider three different choices of parameter $\beta = \beta^{\pm} \in \{0.45, 0.35, 0.25\}$, which controls the steepness of short-lived directional price movement. For example, a smaller β in g_{gj} leads to a steeper gradual jump in observed prices, which is closer to the discontinuous shift in efficient prices, and corresponds to a less sticky expectation of market participants. Fig. 3.4 shows examples of simulated price paths e^X, efficient (in blue) and observed (in black), for all three scenarios with $\beta = \beta^{\pm} = 0.45$.

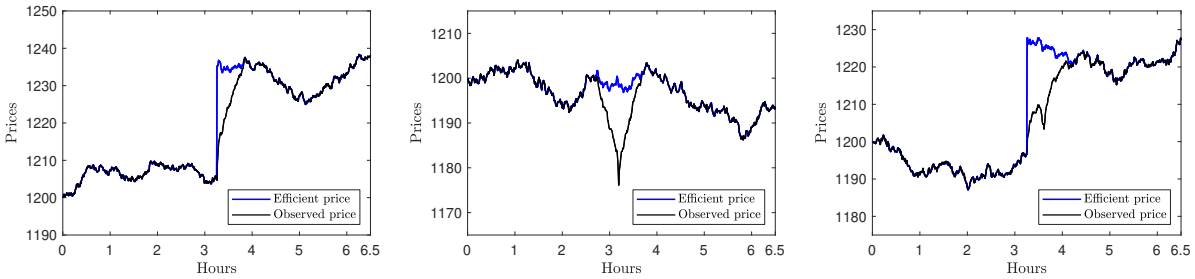

Fig. 3.4 Simulated price paths e^X, efficient (in blue) and observed (in black), with (i) a gradual jump (left), (ii) a flash crash (middle), and (iii) a gradual jump with an intermittent small flash crash (right), respectively. The efficient price X is simulated with the Heston model in Eq. (3.38). The deviation between efficient and observed prices is simulated with the persistent noise model in Assumption 3.4, with all parameters listed above ($\beta = \beta^{\pm} = 0.45$).

3.5.2 Asymptotic Unbiasedness

Table 3.1 reports the relative biases (%) of RRDV in "continuous time" with the simulated half-millisecond observations for 2000 days. In Panel A, we find that the biases have fairly small size when there exists no episodic extreme return persistence. The bias results with $H = 0$ confirm the consistency of our estimator (Section 3.2.2) and its robustness to discontinuities (Section 3.2.3). The existence of gradual jumps leads to only small biases of RRDV constructed from candlesticks with all selected interval lengths, and the biases shrink sufficiently when the number of intervals (resp. the length of intervals) becomes larger (resp. smaller). The V-shaped flash crashes also lead to only negligible biases with small intervals. These bias results in "continuous time" show compelling evidence for the asymptotic unbiasedness of RRDV in

the presence of short-lived explosive trends, as shown in Proposition 3.2 and Proposition 3.3.[9] Fig. 3.5 collects the histograms and QQ plots of estimation errors in some of the Monte Carlo trials, which indicates the close-to-normality of the estimation errors of RRDV in all scenarios.

Table 3.1 Monte Carlo bias results (%)

Panel A: No "V" Bias Correction

		Gradual Jump			Flash Crash			Gradual Jump with an Intermittent Flash Crash		
Interval (sec)	$H = 0$	$\beta = 0.45$	0.35	0.25	$\beta = 0.45$	0.35	0.25	$\beta = 0.45$	0.35	0.25
1	-0.01	-0.15	-0.15	-0.16	-0.19	-0.23	-0.26	-0.15	-0.16	-0.20
5	0.01	-0.47	-0.40	-0.38	-0.72	-0.73	-0.62	-0.61	-0.53	-0.37
10	-0.02	-0.75	-0.77	-0.63	-0.61	0.25	1.72	-0.81	-0.69	-0.49
30	-0.04	-1.89	-1.52	-1.24	-1.38	0.27	2.90	-1.36	-1.06	-0.42
60	0.11	-2.75	-2.25	-1.69	-2.76	-0.91	2.18	-2.27	-0.11	1.23
120	0.12	-3.73	-3.06	-2.44	10.74	22.69	36.21	-0.73	1.11	4.11
180	0.14	-4.58	-3.94	-3.17	10.90	23.50	37.34	-0.70	1.54	5.10
300	0.13	-5.62	-4.88	-3.45	14.38	28.38	43.38	2.45	5.22	5.01

Panel B: With "V" Bias Correction

		Gradual Jump			Flash Crash			Gradual Jump with an Intermittent Flash Crash		
Interval (sec)	$H = 0$	$\beta = 0.45$	0.35	0.25	$\beta = 0.45$	0.35	0.25	$\beta = 0.45$	0.35	0.25
1	-0.80	-0.92	-0.87	-0.80	-0.98	-0.93	-0.90	-0.91	-0.90	-0.87
5	-0.92	-1.18	-1.05	-0.94	-1.34	-1.19	-1.03	-1.22	-1.24	-1.07
10	-0.93	-1.44	-1.27	-1.04	-1.70	-1.60	1.44	-1.48	-1.55	-2.18
30	-0.98	-2.12	-1.86	-1.51	-2.86	-2.54	2.10	-2.03	-2.35	-2.22
60	-0.99	-2.95	-2.52	-2.17	-3.19	-3.34	-3.00	-2.52	-2.65	-2.86
120	-1.26	-3.93	-3.10	-2.59	-6.32	-5.49	-4.34	-3.55	-4.27	-3.92
180	-1.35	-4.53	-3.89	-2.95	-7.60	-6.33	-5.19	-2.99	-4.48	-4.87
300	-1.66	-5.61	-5.07	-4.14	-7.41	-7.84	-6.65	-1.96	-2.81	-3.86

Relative biases (%) of RRDV constructed from 1, 5, 10, 30, 60, 120, 180, and 300-second candlesticks for 2000 days. Panel B reports the relative biases of RRDV with a truncation threshold applied for the range-return differences in all intervals, i.e., $2\sqrt{\Delta_n \mathrm{MedRV}_{t,n}}$, see details in Section 3.4.2. The discretization errors are corrected following the steps in Section 3.4.1. The DGP is the Heston model in Eq. (3.38), and we follow the persistent noise model of Andersen et al. (2023a) to simulate the three different patterns of episodic extreme return persistence.

We notice that the reversal point of the V-shaped flash crash contributes to a positive bias when the intervals are relatively large, and the bias has a larger size when the V-shape is steeper, i.e., with a smaller β. For instance, the relative bias of 5-minute RRDV is 43.38% in the presence of a V-shaped flash crash with $\beta = 0.25$. Panel B of Table 3.1 reports the relative biases of RRDV with a truncation threshold applied for the range-return differences in all intervals, i.e., $2\sqrt{\Delta_n \mathrm{MedRV}_{t,n}}$, as elaborated in Section 3.4.2.[10] Estimating IV with the range-return differences truncated by some right-tail extreme quantile slightly worsen the bias

[9] The bias results of some other IV estimators are presented in Appendix B.3.3.

[10] Theoretically, the truncation threshold should have a higher order than $\sqrt{\Delta_n}$, i.e., $\varpi < 1/2$, while setting $\varpi = 1/2$ for a fixed interval length makes no difference in practice.

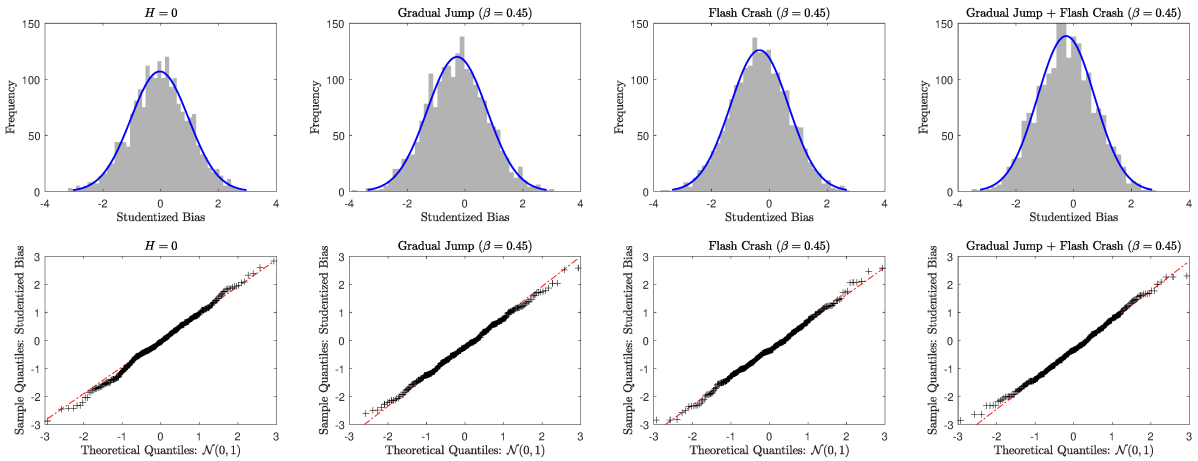

Fig. 3.5 Histograms and QQ plots of studentized estimation errors of one-second RRDV. The estimation errors of RRDV are studentized by the estimates of asymptotic variance in Theorem 3.2, which involves the RRQV estimator in Eq. (3.9). The discretization errors are corrected following the steps in Section 3.4.1. The sample size for QQ plots is 300.

results in "continuous time", but it avoids the significant V-shape bias in finite samples.

3.5.3 Finite-Sample Performance

To evaluate the finite-sample performance of RRDV, we limit the number of observations available in each interval to construct intraday candlesticks: We simulate both second-by-second and half-minute observations, and collect HLOCs in each of the 1, 2, 3, and 5-minute intervals. The RRDV estimators based on HLOCs obtained from 1-second and 30-second data are labeled as "RRDV" and "RRDV*", respectively, in the table of results, where the later corresponds to sparsely or "not-too-finely" sampled data. For the comparative analysis, we consider the truncated realized volatility (TRV) estimator of Mancini (2009):

$$\mathrm{TRV}_{t,n} = \sum_{i=1}^{n} r_i^2 \mathbb{1}_{\{|r_i| \le \zeta^{\mathrm{TRV}} \Delta_n^{\varpi}\}}, \tag{3.41}$$

and the general family of DV estimators in Andersen et al. (2023a):

$$\mathrm{DV}_{1-m,t,n} = \frac{\mathrm{DV}_{t,n}^{(1)} + \mathrm{DV}_{t,n}^{(2)} + \cdots + \mathrm{DV}_{t,n}^{(m)}}{m}, \tag{3.42}$$

where

$$\mathrm{DV}_{t,n}^{(m)} = \frac{1}{2} \sum_{i=m+1}^{n} (r_i - r_{i-m})^2 \mathbb{1}_{\{|r_i - r_{i-m}| \le \zeta^{\mathrm{DV}} \Delta_n^{\varpi}\}}. \tag{3.43}$$

The choice of truncation parameters for TRV, DV and RRDV follows the instructions in Section 3.4.2, with $(C_\zeta^{\text{TRV}}, C_\zeta^{\text{DV}}, C_\zeta^{\text{RRDV}}, \varpi) = (3, 3\sqrt{2}, 2, 1/2)$.[11] Their finite-sample performances are assessed and compared via the root-mean-square error (RMSE), i.e.,

$$\text{RMSE} = \sqrt{\frac{1}{M}\sum_{i=1}^{M}\left(\widehat{V}_{1,n} - \int_0^1 \sigma_t^2 dt\right)^2}, \quad \text{with } M = 10000. \tag{3.44}$$

In Panel A of Table 3.2, we present the RMSEs of all selected IV estimators in the absence of short-lived extreme return persistence. The small RMSEs ($< 2 \times 10^5$) indicate the robustness of all estimators to discontinuities. Compared with other estimators, RRDV has the smallest RMSE results with all selected sampling frequencies, which is consistent with the smallest variance in asymptotic theory. RRDV* based on HLOCs obtained from half-minute data has the largest RMSE with one-minute intervals, while it starts to achieve smaller RMSEs than DV when the length of intervals is extended to two minutes, i.e., there are at lease five observations (open and close included) available in each interval, which is in line with our numerical results in Section 3.4.1. Panel B, C and D in Table 3.2 report the RMSE results in the presence of gradual jumps or/and flash crashes. When there exist local explosive trends, the TRV estimator has larger RMSEs than RRDV and two DV estimators in all scenarios, and the difference becomes more pronounced for "stickier" (less steep) deviations between observed prices and efficient prices, i.e., with larger β's, and for lower sampling frequencies. For the candlestick-based estimators, RRDV* can achieve smaller RMSEs than DV in all cases when the interval length is three minutes or longer, and RRDV based on HLOCs taken from second-by-second observations outperforms all other IV measures across all relevant scenarios.

3.6 Empirical Analysis

In this section, we use the RRDV estimator as the basis for volatility forecasting under the popular heterogeneous autoregressive (HAR) framework for the SPDR S&P 500 ETF Trust (SPY), which is the best-recognized and oldest U.S. listed ETF and by far the most widely

[11] We also consider alternative parameter choices $(C_\zeta^{\text{TRV}}, C_\zeta^{\text{DV}}) = (4, 4\sqrt{2})$ used for comparison in Andersen et al. (2023a). We find that the less aggressive threshold choices will not change the qualitative results and even worsen the finite-sample performance of both estimators when there exists excessive return drift, see Table B.8 in Appendix B.3.4, which is consistent with the Monte Carlo results in Andersen et al. (2023a).

Table 3.2 Monte Carlo RMSE results

Panel A: $H = 0$

Interval	RRDV	RRDV*	TRV	DV	DV_{1-3}
1 min	**0.44**	1.09	0.74	0.84	0.76
2 min	**0.58**	1.02	1.00	1.14	1.03
3 min	**0.69**	1.08	1.22	1.39	1.24
5 min	**0.86**	1.23	1.55	1.77	1.59

Panel B: Gradual Jump

	$\beta = 0.45$					$\beta = 0.35$					$\beta = 0.25$				
Interval	RRDV	RRDV*	TRV	DV	DV_{1-3}	RRDV	RRDV*	TRV	DV	DV_{1-3}	RRDV	RRDV*	TRV	DV	DV_{1-3}
1 min	**0.52**	1.14	1.11	0.80	0.70	**0.50**	1.12	0.96	0.79	0.70	**0.48**	1.11	0.82	0.79	0.70
2 min	**0.69**	1.07	1.95	1.15	1.15	**0.67**	1.06	1.61	1.18	1.07	**0.64**	1.03	1.31	1.11	1.01
3 min	**0.84**	1.18	2.47	1.47	1.34	**0.80**	1.14	2.00	1.38	1.23	**0.78**	1.13	1.64	1.36	1.21
5 min	**1.04**	1.36	3.59	2.14	2.21	**1.02**	1.33	2.86	1.89	1.74	**0.98**	1.30	2.21	1.78	1.61

Panel C: Flash Crash

	$\beta = 0.45$					$\beta = 0.35$					$\beta = 0.25$				
Interval	RRDV	RRDV*	TRV	DV	DV_{1-3}	RRDV	RRDV*	TRV	DV	DV_{1-3}	RRDV	RRDV*	TRV	DV	DV_{1-3}
1 min	**0.52**	1.19	1.74	0.78	0.70	**0.53**	1.16	1.54	0.83	0.75	**0.53**	1.14	1.24	0.82	0.72
2 min	**0.85**	1.21	2.93	1.27	1.12	**0.78**	1.15	2.34	1.27	1.11	**0.72**	1.09	1.77	1.23	1.07
3 min	**1.00**	1.30	4.34	1.55	1.55	**0.93**	1.27	3.47	1.49	1.50	**0.86**	1.19	2.61	1.44	1.42
5 min	**1.18**	1.69	7.00	2.11	2.86	**1.16**	1.59	5.60	2.02	2.68	**1.10**	1.42	4.09	1.98	2.43

Panel D: Gradual Jump with an Intermittent Flash Crash

	$\beta = 0.45$					$\beta = 0.35$					$\beta = 0.25$				
Interval	RRDV	RRDV*	TRV	DV	DV_{1-3}	RRDV	RRDV*	TRV	DV	DV_{1-3}	RRDV	RRDV*	TRV	DV	DV_{1-3}
1 min	**0.51**	1.14	1.28	0.81	0.74	**0.53**	1.15	1.23	0.79	0.71	**0.50**	1.11	1.03	0.79	0.71
2 min	**0.72**	1.12	2.40	1.26	1.55	**0.66**	1.05	2.28	1.27	1.36	**0.68**	1.06	1.59	1.15	1.12
3 min	**0.87**	1.24	3.14	1.72	2.07	**0.78**	1.11	2.89	1.53	1.60	**0.72**	1.14	2.32	1.44	1.51
5 min	**0.95**	1.32	3.71	2.41	2.76	**1.05**	1.40	3.49	2.09	2.30	**0.99**	1.31	2.45	1.81	1.80

RMSE (multiplied by 10^5) of different IV estimators. RRDV and RRDV* are constructed from intraday candlestick information, which is obtained from second-by-second and half-minute observations, respectively. The choice of truncation parameters for TRV, DV and RRDV follows the instructions in Section 3.4.2, with $(C_\zeta^{\mathrm{TRV}}, C_\zeta^{\mathrm{DV}}, C_\zeta^{\mathrm{RRDV}}, \varpi) = (3, 3\sqrt{2}, 2, 1/2)$. The discretization errors of RRDV are corrected following the steps in Section 3.4.1. The DGP is the Heston model in Eq. (3.38). We follow the persistent noise model of Andersen et al. (2023a) to simulate the three different patterns of episodic extreme return persistence.

traded S&P 500 ETF.

3.6.1 Data

We obtain all high-frequency transaction records of SPY from the daily Trade and Quote (TAQ) dataset, with the sample period ranging from January 2, 2014 to December 31, 2021. The tick-by-tick transactions are timestamped in milliseconds until mid-2015 and in microseconds since then.[12] As is standard in empirical research with TAQ data, we use the filters as in Barndorff-Nielsen et al. (2009) to eliminate clear data errors, remove all transactions in the original record that are later corrected, cancelled or otherwise invalidated. In addition, we remove all trading days with an early market closure, and restrict our sample to transactions between 9:41:00 – 16:00:00 Eastern Time (ET) for all individual stocks. The final sample comprises of 1998 days.

3.6.2 Heterogeneous Autoregressive (HAR) Model

The HAR model of Corsi (2009) is designed to parsimoniously capture the dependence structures of return volatility across different horizons, and therefore aims to approximate its long memory that has been extensively confirmed by empirical literature. Renowned for its consistent and remarkable predictive performance, the HAR model serves as the predominant benchmark in volatility forecasting research. In this section, we denote some selected IV measure at day t by $\widehat{V}_t$, and introduce the following moving averages of daily volatility measures as:

$$\widehat{V}_{w,t} = \frac{1}{5}\sum_{i=1}^{5}\widehat{V}_{t-i+1} \qquad \text{and} \qquad \widehat{V}_{m,t} = \frac{1}{22}\sum_{i=1}^{22}\widehat{V}_{t-i+1}, \tag{3.45}$$

where $\widehat{V}_{w,t}$ represents the one-week average and $\widehat{V}_{m,t}$ denotes the one-month average of daily IV estimates, respectively. The standard one-day-ahead HAR model has the following structure:

$$\widehat{V}_t = \omega + \beta_d\widehat{V}_{t-1} + \beta_w\widehat{V}_{w,t-1} + \beta_m\widehat{V}_{m,t-1} + \varepsilon_t, \tag{3.46}$$

[12] We use the SAS code from Holden and Jacobsen (2014) to extract all tick-by-tick transaction records matched with relevant ask/bid quotes from the daily TAQ dataset of WRDS.

which can be easily estimated via ordinary least squares (OLS). As demonstrated by numerous empirical applications in the literature, the implementation of a more refined volatility measure on the right-hand side (RHS) can better exploit the information, and has the potential to significantly improve the predictive accuracy of the HAR model for the left-hand side (LHS) target variable.

In addition to the implementation of better volatility measures in the standard HAR model, a constructive modification of the HAR model structure can also contribute to improved forecasting outcomes. In this section, we consider two important extensions of the original HAR-RV model for the comparative study. One is the HARQ model of Bollerslev et al. (2016). With the motivation that the persistence of RV is affected by the temporal variation in its measurement errors, the HARQ model allows for a time-varying coefficient for the previous day's RV on the RHS, and the coefficient depends on the heteroskedasticity in the error, which is captured by the realized quarticity (RQ):[13]

$$\widehat{V}_t = \omega + \left(\beta_d + \beta_q \sqrt{\mathrm{RQ}_{t-1}}\right) \mathrm{RV}_{t-1} + \beta_w \mathrm{RV}_{w,t-1} + \beta_m \mathrm{RV}_{m,t-1} + \varepsilon_t, \tag{3.47}$$

where

$$\mathrm{RQ}_t = \frac{n}{3} \sum_{i=1}^{n} r_{i,t}^4. \tag{3.48}$$

Inspired by the realized semivariance (RS) introduced by Barndorff-Nielsen et al. (2010), the semivariance HAR (SHAR) model of Patton and Sheppard (2015) stands out as another important HAR-RV modification:

$$\widehat{V}_t = \omega + \beta_d^- \mathrm{RS}_{t-1}^- + \beta_d^+ \mathrm{RS}_{t-1}^+ + \beta_w \mathrm{RV}_{w,t-1} + \beta_m \mathrm{RV}_{m,t-1} + \varepsilon_t, \tag{3.49}$$

where the RS measures are given by

$$\mathrm{RS}_t^- = \sum_{i=1}^{n} r_{i,t}^2 \mathbb{1}_{\{r_{i,t}<0\}} \quad \text{and} \quad \mathrm{RS}_t^+ = \sum_{i=1}^{n} r_{i,t}^2 \mathbb{1}_{\{r_{i,t}>0\}}. \tag{3.50}$$

[13] Following Bollerslev et al. (2016), the "insanity filter" of Swanson and White (1997) is applied: For each rolling or expanding window, the minimum, maximum, and average of in-sample estimates are re-calculated. All one-step-ahead out-of-sample forecasts that are greater (smaller) than the maximum (minimum) in-sample value will be replaced by the in-sample mean.

The intuition that "good" and "bad" volatilities are not created equal motivates the decomposition of the original RV into separate up and downside RS measures. The empirical results in Patton and Sheppard (2015) demonstrate that this decomposition leads to more accurate volatility forecasts, with the "bad" volatility predominantly driving the short-run changes in the future.[14]

3.6.3 Empirical Results

In this section, we estimate the standard HAR model in Eq. (3.46) with various IV measures on the RHS, namely RV, RBPV, TRV, DV, and our RRDV estimator, with an initial in-sample period of the first 1000 days, and forecast one-day-ahead out-of-sample RV, DV, and RRDV. Moreover, we estimate both the HARQ model in Eq. (3.47) and the SHAR model in Eq. (3.49) for the comparison of forecasts. We repeat this procedure of in-sample estimation and out-of-sample forecasting in both a rolling-window (RW) and an expanding-window (EW) fashion, respectively.

All return-based IV measures are constructed from log-returns over 5-minute intervals. For the construction of RRDV based on 5-minute candlesticks, we obtain the corresponding HLOCs from the transaction data, either at the tick level or under previous-tick equidistant sampling. In particular, for the discretized RRDV based on HLOCs from equistantly sampled data, we correct the discretization errors following the steps in Section 3.4.1.

We evaluate the out-of-sample forecasting performance via two widely used loss functions, i.e., the mean squared error (MSE) and the quasi-likelihood (QLIKE) function:

$$\mathrm{MSE}(\theta, h) = (\theta - h)^2 \qquad \text{and} \qquad \mathrm{QLIKE}(\theta, h) = \frac{\theta}{h} - \ln\left(\frac{\theta}{h}\right) - 1, \tag{3.51}$$

where θ and h represent the actual value and the forecast of the target variable, respectively.

Table 3.3 reports the MSE and QLIKE results for one-day-ahead out-of-sample forecasts of three different target volatility measures. Among the standard and modified HAR-RV models, both the HARQ and SHAR models can achieve smaller MSE and QLIKE results than the original HAR-RV model, which demonstrates that the consideration of either the

[14] See Bollerslev (2022) for a comprehensive review of recent financial econometrics research related to "good" and "bad" volatilities constructed from high-frequency intraday data.

Table 3.3 Daily out-of-sample 5-minute HAR volatility forecasts

	RV		DV		RRDV: tick data	
	MSE	QLIKE	MSE	QLIKE	MSE	QLIKE
Panel A: HAR RW Forecasts						
HAR-RV	2.39	0.41	1.57	0.47	1.19	0.30
HARQ	2.35	0.36	1.46	0.40	1.48	0.37
SHAR	2.29	0.39	1.51	0.45	1.04	0.30
HAR-RBPV	2.36	0.41	1.57	0.45	1.20	0.30
HAR-TRV	2.30	0.39	1.51	0.44	1.15	0.28
HAR-DV	2.55	0.40	1.68	0.45	1.32	0.29
HAR-DV$_{1-3}$	2.45	0.39	1.62	0.44	1.24	0.28
HAR-RRDV: tick data	2.17	0.37	1.42	0.42	1.05	0.27
HAR-RRDV: 1-second data	2.16	0.37	1.41	0.42	1.06	0.27
HAR-RRDV: 30-second data	2.09	0.37	1.36	0.42	0.96	0.27
HAR-RRDV: 1-minute data	2.03	0.36	1.31	0.41	0.89	0.27
Panel B: HAR EW Forecasts						
HAR-RV	2.29	0.37	1.51	0.42	1.15	0.29
HARQ	2.27	0.33	1.43	0.38	1.12	0.32
SHAR	2.18	0.35	1.45	0.42	1.02	0.30
HAR-RBPV	2.27	0.36	1.51	0.42	1.16	0.28
HAR-TRV	2.22	0.34	1.45	0.39	1.11	0.26
HAR-DV	2.45	0.35	1.62	0.39	1.27	0.26
HAR-DV$_{1-3}$	2.35	0.34	1.55	0.39	1.19	0.26
HAR-RRDV: tick data	2.10	0.33	1.38	0.38	1.03	0.26
HAR-RRDV: 1-second data	2.09	0.33	1.37	0.37	1.03	0.25
HAR-RRDV: 30-second data	2.03	0.33	1.31	0.37	0.94	0.25
HAR-RRDV: 1-minute data	1.96	0.32	1.26	0.36	0.88	0.25

MSE ($\times 10^8$) and QLIKE of daily out-of-sample volatility forecasts for the SPDR S&P 500 ETF Trust (SPY). The HAR model is re-estimated via OLS in rolling windows and expanding windows, respectively. The fixed (resp. initial) in-sample period for RW (resp. EW) estimation is the first 1000 days. All return-based IV measures are constructed from 5-minute intervals. RRDVs are also constructed from 5-minute candlesticks, in which the HLOCs are obtained from the transaction data either at the tick level or under previous-tick equidistant sampling. The choice of truncation parameters for TRV, DV and RRDV follows the instructions in Section 3.4.2, with $(C_\zeta^{\text{TRV}}, C_\zeta^{\text{DV}}, C_\zeta^{\text{RRDV}}, \varpi) = (3, 3\sqrt{2}, 2, 1/2)$. For RRDVs based on equidistantly sampled observations, the discretization errors are corrected following the steps in Section 3.4.1.

measurement errors in RV or the volatility asymmetry helps to exploit concealed information due to aggregation, and results in more accurate forecasts. Compared with the HAR models augmented with other volatility estimators, the HAR-RRDV model tends to obtain substantially diminished values of both loss functions, and the number of observations available in each candlestick interval seems relatively irrelevant to its predictive capability. Furthermore, the symmetric MSE function penalizes outliers heavily, and is therefore sensitive to excessively misinformative forecasts. The MSE results in Table 3.3 suggest that the HAR-RRDV model can effectively reduce the occurrence of extremely inaccurate forecasts in both left and right tails.

To further explore the reason for the reduced forecast errors of HAR-RRDV, we partition

the entire out-of-sample period into complimentary subsets of days based on two criteria, respectively: (i) days with and without jumps, as well as (ii) days exhibiting episodes of extreme return persistence or not. The presence of discontinuities and persistent noise is identified using the nonparametric tests of Aït-Sahalia et al. (2012) and Andersen et al. (2023a), respectively.[15]

Table 3.4 MSEs on days with/without discontinuities and episodic extreme return persistence

	RV				DV				RRDV: tick data			
	Jumps		Per. Noise		Jumps		Per. Noise		Jumps		Per. Noise	
	Yes	No	Yes	No	Yes	No	Yes	No	Yes	No	Yes	No
Panel A: HAR RW Forecasts												
HAR-RV	7.24	0.24	11.01	1.52	4.61	0.23	6.51	1.08	3.24	0.28	2.93	1.01
HARQ	7.05	0.27	10.73	1.51	4.16	0.26	6.34	0.97	4.13	0.31	2.86	1.34
SHAR	6.90	0.25	10.12	1.50	4.40	0.23	5.73	1.09	3.06	0.16	2.50	0.90
HAR-RBPV	7.17	0.23	10.92	1.50	4.61	0.22	6.45	1.07	3.36	0.24	2.89	1.03
HAR-TRV	6.93	0.25	10.81	1.45	4.39	0.24	6.38	1.02	3.10	0.28	2.84	0.98
HAR-DV	7.76	0.24	10.80	1.72	4.96	0.23	6.37	1.21	3.70	0.26	2.82	1.17
HAR-DV$_{1-3}$	7.42	0.25	10.76	1.61	4.75	0.24	6.34	1.14	3.45	0.26	2.84	1.08
HAR-RRDV: tick data	6.46	0.27	9.93	1.39	4.07	0.25	5.81	0.98	2.73	0.31	2.49	0.91
HAR-RRDV: 1-second data	6.45	0.26	9.77	1.39	4.06	0.24	5.70	0.98	2.68	0.33	2.43	0.92
HAR-RRDV: 30-second data	6.21	0.28	9.63	1.33	3.86	0.25	5.60	0.93	2.42	0.32	2.37	0.82
HAR-RRDV: 1-minute data	6.07	0.23	9.72	1.25	3.75	0.23	5.65	0.87	2.25	0.29	2.40	0.74
Panel B: HAR EW Forecasts												
HAR-RV	6.98	0.22	11.35	1.38	4.45	0.20	6.73	0.98	3.12	0.27	3.03	0.96
HARQ	6.83	0.25	10.99	1.39	4.15	0.23	6.49	0.93	2.99	0.29	2.91	0.94
SHAR	6.08	0.23	10.39	1.36	4.25	0.21	5.95	1.00	2.96	0.16	2.60	0.86
HAR-RBPV	6.94	0.21	11.22	1.38	4.47	0.20	6.65	0.99	3.24	0.24	2.97	0.97
HAR-TRV	6.72	0.23	11.12	1.32	4.27	0.21	6.58	0.94	3.00	0.27	2.93	0.93
HAR-DV	7.50	0.23	11.11	1.59	4.81	0.21	6.58	1.12	3.56	0.26	2.91	1.11
HAR-DV$_{1-3}$	7.16	0.25	11.12	1.47	4.59	0.21	6.57	1.05	3.31	0.26	2.94	1.02
HAR-RRDV: tick data	6.28	0.25	10.16	1.29	3.97	0.23	5.96	0.92	2.65	0.31	2.55	0.87
HAR-RRDV: 1-second data	6.25	0.25	10.00	1.30	3.94	0.23	5.86	0.91	2.60	0.33	2.49	0.88
HAR-RRDV: 30-second data	6.03	0.26	9.83	1.24	3.76	0.23	5.75	0.87	2.35	0.31	2.43	0.79
HAR-RRDV: 1-minute data	5.90	0.22	10.08	1.15	3.65	0.21	5.90	0.80	2.21	0.29	2.50	0.71

This table reports the MSE ($\times 10^8$) results of daily out-of-sample volatility forecasts for the SPDR S&P 500 ETF Trust (SPY) on the days with or without jumps and persistent noise. Jumps and persistent noise are identified with the nonparametric tests of Aït-Sahalia et al. (2012) and Andersen et al. (2023a), respectively. The HAR model is re-estimated via OLS in rolling windows and expanding windows, respectively. The fixed (resp. initial) in-sample period for RW (resp. EW) estimation is the first 1000 days. All return-based IV measures are constructed from 5-minute intervals. RRDVs are also constructed from 5-minute candlesticks, in which the HLOCs are obtained from the transaction data either at the tick level or under previous-tick equidistant sampling. The choice of truncation parameters for TRV, DV and RRDV follows the instructions in Section 3.4.2, with $(C_\zeta^{\mathrm{TRV}}, C_\zeta^{\mathrm{DV}}, C_\zeta^{\mathrm{RRDV}}, \varpi) = (3, 3\sqrt{2}, 2, 1/2)$. For RRDVs based on equidistantly sampled observations, the discretization errors are corrected following the steps in Section 3.4.1.

In Table 3.4, the MSE results for all selected HAR models are presented within these

[15] For the test statistic of Aït-Sahalia et al. (2012), we select the pre-averaging window $k_n = \lfloor \sqrt{n} \rfloor$ and the truncation level $C = 5$. To identify the presence of persistent noise, we construct the test statistic $T_t^n(2)$ of Andersen et al. (2023a) from one-minute pre-averaged and winsorized returns. The selected critical values for those two tests are -1.645 and 1.645, respectively.

classifications. There is a notable reduction in MSEs across all selected models on days without discontinuities or excessive return drift. This observation indicates that the presence of extreme events potentially distorts the estimation of dependence structures in volatility and consequently leads to uniformly worsened forecasts. Among the three target IV measures on the LHS, we find that the one-day-ahead forecasts of RRDV exhibit superior accuracy when there exist either "discontinuous" or "continuous" extreme events, with all chosen RHS variables. Meanwhile, the RV predictions are more vulnerable to both discontinuities and short-lived explosive trends, resulting in substantially larger forecast errors. For each of the target variables on the LHS, the HAR-RRDV model demonstrates the least vulnerability to extreme events and generates the most accurate one-day-ahead forecasts. These collective observations suggest that the robustness of our RRDV estimator in the presence of extreme price movements contributes to the predictive capability when it is integrated within some standard framework of volatility forecasting.

3.7 Conclusions

Motivated by both the statistical superiority of range-based estimation and the broader availability of intraday candlesticks for general investors, we introduce a novel nonparametric candlestick-based estimator for integrated variance (IV) in this chapter, namely the range-return-difference volatility (RRDV) estimator. The RRDV estimator is designed to mitigate the impact of short-lived explosive trends that locally dominate price movements, such as gradual jumps and flash crashes. By modeling these "continuous" extreme events from two perspectives: (i) a locally unbounded drift component (Christensen et al., 2022), and (ii) sticky expectations of market participants (Andersen et al., 2023a), we demonstrate that RRDV can consistently estimate IV with variances about four times smaller than those obtained with the differenced-return volatility (DV) estimator introduced by Andersen et al. (2023a). Our simulation results underscore the reliable finite-sample performance of RRDV across various relevant scenarios. An empirical illustration of volatility forecasting shows that the HAR-RRDV model can effectively reduce the occurrence of extremely misleading forecasts and improve forecasting accuracy according to standard out-of-sample loss functions.

Chapter 4

Decoupling Interday and Intraday Volatility Dynamics with Price Durations[1]

4.1 Introduction

Volatility is an important topic in financial econometrics and a crucial input for any asset pricing, portfolio allocation and risk management framework (Taylor, 2005). It is usually considered as a latent process that describes the return variability over a local horizon, and thus requires estimation from price observations. The increased availability of high-frequency financial data has motivated a shift of volatility estimation techniques from monthly or daily frequencies, such as the GARCH models (Engle, 1982; Bollerslev, 1986) and stochastic volatility models (Taylor, 1982, 1986, 1994), to various high-frequency volatility measures (Aït-Sahalia and Jacod, 2014). As the most representative and widely applied high-frequency volatility estimator, the realized volatility (RV) introduced by Andersen and Bollerslev (1998) is constructed by summing up all squared intraday log-returns, and is well-known to be a consistent and efficient estimator of the integrated variance (IV) of a univariate Itô semimartingale over fixed time intervals. The return-based RV estimator has well-established statistical properties and can be modified to accommodate more accurate volatility measures that are robust to various market frictions,

[1] This chapter corresponds to Li et al. (2024b), submitted to the *Journal of Time Series Analysis*.

e.g., Barndorff-Nielsen and Shephard (2004), Jacod et al. (2009), and Mancini (2009).

The seminal work of Engle and Russell (1998) provides a compelling approach to volatility estimation as an alternative to the return-based methods. Unlike the RV-type estimators that measure the magnitude of price changes over a given time interval, this alternative method measures the time it takes for the price to change by a certain size, i.e., a selected threshold. Since the autoregressive conditional duration (ACD) model of Engle and Russell (1998), the duration-based volatility estimation has been further developed, e.g., Gerhard and Hautsch (2002), Andersen et al. (2008), Tse and Yang (2012), Fukasawa and Rosenbaum (2012), Vetter and Zwingmann (2017), Li et al. (2019, 2021), Hong et al. (2023), and Pelletier and Wei (2023). Specifically, some studies highlight the feasibility of a parametric structure for duration-based volatility estimators, which enables more flexible intraday inference on local volatility. While the nonparametric nature of RV-type estimators provides convenience in construction, it also limits their applicability in situations with limited data availability, e.g., for spot volatility estimation. As summarized by Tse and Yang (2012), the parametric duration-based estimators can benefit from the data beyond the estimation window to enhance parameter estimates, and potentially achieve more accurate volatility estimates. Furthermore, the parametric structure facilitates the inclusion of other covariates such as seasonality, which can not only improve the quality of volatility estimation, but also provide a framework to further explore the relation between volatility and other covariates at a high-frequency level.

The existence of market frictions requires the utilization of "not-too-finely" sampled data, which further restricts the data availability for both return- and duration-based methods in practice (Aït-Sahalia et al., 2005; Liu et al., 2015). For example, both Andersen et al. (2008) and Hong et al. (2023) recommend a moderate to large threshold to ensure a small number of durations relative to the available price observations on each day. Although the parametric structure offers the flexibility to estimate the duration models, e.g., the ACD model of Engle and Russell (1998), with the data beyond a specific day, the incorporation of intraday durations across multiple days introduces complexities. Specifically, the durations obtained with the same threshold from different days will encompass different daily volatility dynamics, which leads to challenges in both model estimation and the analysis of volatility patterns. Although there has been extensive investigations on either daily or intraday volatility dynamics in the literature, a joint analysis of both is nearly infeasible due to their fundamentally different characteristics.

In this chapter, we introduce an innovative semiparametric method to (i) nonparametrically disentangle the daily and intraday volatility dynamics inherent in the durations obtained across multiple days, and (ii) parametrically estimate both the spot and integrated volatility based on durations. For each day, we adopt a nonparametrically predicted threshold to maintain a relatively consistent number of durations. We utilize the fact that, with a fixed number of durations, each daily IV should be proportional to the corresponding squared threshold (Hong et al., 2023), and therefore employ some standard predictive models for one-day-ahead IV measures to determine the "daily" thresholds. Since the interday persistence of volatility is subsumed into the daily thresholds, the durations from each day preserve only intraday volatility dynamics. This decomposition homogenizes the durations from different days, and alleviates the long-run persistence in the duration series. Furthermore, we derive a relationship between spot volatility and the conditional density of durations under some mild conditions, which provides an opportunity to estimate the volatility with some parametric duration models.

Simulation results reveal that our new duration-based method exhibits reliable finite-sample performance for both the spot volatility and IV estimation. We compare our duration-based estimators with both the localized return-based estimator of Foster and Nelson (1996) and some innovative candlestick-based estimators of Li et al. (2022) for spot volatility estimation, as well as with several RV-type estimators for IV estimation. We find that our duration-based estimators can achieve smaller finite-sample biases and exhibit greater robustness to extreme price movements, such as price jumps, when compared to the selected competitors. In our first empirical application, we focus on the prediction of out-of-sample IV estimates of the SPDR S&P 500 ETF Trust (SPY) with the heterogeneous autoregressive (HAR) model of Corsi (2009). We find that the HAR model based on our duration-based IV estimator outperforms most of the selected benchmark models with smaller forecast errors, which is further validated by a Diebold-Mariano test. Furthermore, we conduct an intraday analysis to assess the short-term impact of regular press releases made by the Federal Reserve, i.e., the Federal Open Market Committee (FOMC) news announcements, based on our spot volatility estimator. Our results reveal that the FOMC announcements have an instant and substantial impact on spot volatility, evidenced by a significant volatility spike around 14:00 on FOMC days.

The remainder of this chapter is structured as follows: Section 4.2 introduces our semiparametric estimation procedure, which includes both the nonparametric threshold prediction

and the parametric volatility estimation. Section 4.3 presents an extensive Monte Carlo study to illustrate the finite-sample performance of both our duration-based spot and integrated volatility estimation techniques. After some empirical applications for both daily and intraday volatility of SPY in Section 4.4, we conclude in Section 4.5. All proofs can be found in the Appendix C.

4.2 Econometric Framework

We consider a one-dimensional underlying process $X = (X_t)_{t\geq 0}$ for the efficient logarithmic price of a financial asset. We assume that X follows a semimartingale defined on a filtered probability space $(\Omega, \mathcal{F}, (\mathcal{F}_t)_{t\geq 0}, \mathbb{P})$:

$$X_t = X_0 + \int_0^t \sigma_s dW_s + J_t, \tag{4.1}$$

where t stands for time, $W = (W_t)_{t\geq 0}$ is a standard Brownian motion, $\sigma = (\sigma_t)_{t\geq 0}$ is a càdlàg $\mathcal{F}_t$-adapted process assumed to be locally bounded and bounded away from zero. We assume that X is observed on $[0,T)\cup[T,2T)\cup\ldots\cup[(d-1)T, dT)\cup\ldots$, where the interval $[(d-1)T, dT)$ represents the d-th trading day of length $T > 0$. Price movements during market closures are modeled as jumps occurring at dT, i.e., $\Delta X_d = X_{dT} - X_{dT-}$, and are cumulatively incorporated into the discontinuous component $J_t = \sum_{d=1}^{\lfloor t/T\rfloor} \Delta X_d$. We assume $T \equiv 1$ for ease of notation in subsequent discussions.

Remark 4.1. We do not consider the price jumps during the regular trading sessions due to the natural robustness of duration-based methods to finite-activity jumps. Some relevant discussions can be found in Andersen et al. (2008), Tse and Yang (2012), Hong et al. (2023), Pelletier and Wei (2023), as well as in Chapter 2.

We are interested in the estimation of the spot variance σ_t^2 for some t as well as the integrated variance (IV) over some interval $[s,t]$:

$$V(s,t) = \int_s^t \sigma_u^2 du. \tag{4.2}$$

When the interval $[s,t] = [d-1,d]$ is one trading day, we write $V_d \equiv V(d-1,d)$ as the IV for day d and $V(t) \equiv V(0,t)$ to denote the IV process up to time t. To construct an estimator for

$V(t)$, we extend the duration-based methods of Tse and Yang (2012) and Hong et al. (2023). In contrast to those return-based estimators that fix a time interval Δ and measure the change in X, the duration-based estimators fix a threshold $\delta > 0$ and measure the durations when X increases or decreases by δ. Specifically, we generalize the price duration sampling (PDS) method of Hong et al. (2023) by incorporating a time-varying sampling threshold. We choose a sequence of "daily" thresholds $(\delta_d)_{d=1,2,\ldots}$, where each δ_d is positive and adapted to the information $\mathcal{F}_{d-1}$ available up to time $d-1$. We then sample price observations within each trading day based on the following stopping rule:

$$\tau_{d,0} = d-1, \qquad \tau_{d,i} = \inf_{\tau_{d,i-1}<t\leq d} \left\{ \left| X_t - X_{\tau_{d,i-1}} \right| \geq \delta_d \right\}, \tag{4.3}$$

with the convention that $\inf\{\varnothing\} = \infty$. Consequently, for each day d, we obtain a sequence of sampling times $(\tau_{d,i})_{0\leq i\leq N_d}$, where $\tau_{d,i}$ denotes the i-th price event, $x_{d,i} = \tau_{d,i} - \tau_{d,i-1}$ the i-th inter-event price duration, and $N_d = \sum_{i\geq 0} \mathbb{1}_{\{\tau_{d,i}\in(d-1,d]\}}$ counts the number of price events within the d-th day.

In essence, when the realized sample path $X(\omega)$ is fully observable, the absolute return between each pair of consecutive sampled price observations equals δ_d, i.e., $|X_{\tau_{d,i}} - X_{\tau_{d,i-1}}| = \delta_d$ for all $1 \leq i \leq N_d$. Consequently, N_d can be interpreted as the "frequency" of price path changes by δ_d, which is proportional to the nonparametric duration-based IV estimator proposed by Hong et al. (2023). This argument is formalized by Theorem 1 of Hong et al. (2023), which implies that

$$N_d = \frac{V_d}{\delta_d^2} + M_d + o_p(1), \tag{4.4}$$

where $(M_d)_{d=1,2,\ldots}$ is a Gaussian martingale difference sequence, and $o_p(1)$ vanishes as $\delta_d \to 0$. By taking conditional expectations on both sides of Eq. (4.4), the $\mathcal{F}_{d-1}$-adaptedness of δ_d further implies:

$$\mathbb{E}[N_d|\mathcal{F}_{d-1}] = \frac{\mathbb{E}[V_d|\mathcal{F}_{d-1}]}{\delta_d^2} + o(1). \tag{4.5}$$

Therefore, for a fixed $\delta_d \equiv \delta$, $\mathbb{E}[N_d|\mathcal{F}_{d-1}] \propto \mathbb{E}[V_d|\mathcal{F}_{d-1}]$, implying that the daily price event counts effectively capture the volatility dynamics on a daily horizon. This can be further modeled parametrically based on the durations or intensities of point processes (Engle and Russell, 1998; Tse and Yang, 2012; Hong et al., 2023).

As an important innovation of this chapter, we notice that one does not need to choose a fixed δ. Specifically, an adaptive choice of $\hat{\delta}_d^2 = K^{-1}\mathbb{E}[V_d|\mathcal{F}_{d-1}]$ for some constant K ensures an expectation of K price events on day d, i.e., $\mathbb{E}[N_d|\mathcal{F}_{d-1}] = K + o(1)$.

The adaptive choice of $\hat{\delta}_d$ has two advantages over a constant δ. Firstly, it offers a natural control for the daily sampling frequencies. In practice, the full trajectory of $X(\omega)$ is not available, and can only be observed on a grid of discrete times with the contamination of market microstructure noise. Previous studies on duration-based estimators recommend selecting a moderate to large δ such that the sampling frequency will be small enough relative to the total number of observations (Andersen et al., 2008; Li et al., 2021; Hong et al., 2023). However, achieving such "not-too-finely" sampling is only possible on an average sense with a fixed δ. As shown in Eq. (4.5), the expected daily sampling frequency depends on the daily IV, which could vary substantially across multiple days. With an appropriate choice of K, the adaptive threshold $\hat{\delta}_d$ enables direct control of the expected sampling frequency for each day, which provides uniform protection against market imperfections on a daily basis.

Secondly, the construction of $\hat{\delta}_d$ suggests that $K\hat{\delta}_d^2$ could be interpreted as the mean squared error (MSE) optimal forecast of V_d. The persistence of volatility dynamics at the daily level has been extensively studied in the literature (Corsi, 2009; Gatheral et al., 2018), and these benchmark models provide empirically reliable methods to construct $\hat{\delta}_d$ that fully reflects the daily volatility dynamics. For example, since the squared threshold is essentially a scaled version of RV, some predictive models for one-day-ahead RV, such as the HAR model of Corsi (2009), can be easily applied. As a result, the sampling times $(\tau_{d,i})_{0\le i\le N_d}$ within each day only preserve intraday volatility dynamics, as the interday persistence in the IV process is subsumed into the adaptive thresholds $(\hat{\delta}_d)_{d=1,2,\dots}$. This decomposition allows us to model interday and intraday volatility separately, which greatly increases the flexibility of the point-process-based parametric volatility models of Hong et al. (2023) and Pelletier and Wei (2023). It also considerably simplifies the econometric analysis, offering a more straightforward understanding of the volatility dynamics over an extended period spanning multiple days.

4.2.1 Spot and Integrated Volatility Estimation with Price Durations

We proceed to explain how we estimate both spot and integrated variances from the observed price durations $(x_{d,i})_{1\le i\le N_d}$ based on some $\mathcal{F}_{d-1}$-adapted threshold. We denote $\mathcal{F}_{d,i}$ as the

filtration generated by X up to the sampling time $\tau_{d,i}$. We shall show that the $\mathcal{F}_{d,i-1}$-conditional density of $x_{d,i}$ is linked mechanically to the spot variance σ^2 of the continuous martingale X.

To this end, we introduce some additional notation: Let $V_{d,i} = V(d-1, d-1+\tau_{d,i})$ denote the IV accumulated up to the i-th price event on day d, and thus $\Delta_{d,i}V = V_{d,i} - V_{d,i-1}$ represents the i-th duration in the IV clock. The sequence of IV increments $(\Delta_{d,i}V)_{1\le i\le N_d}$ possesses the following important property:

Proposition 4.1. Assume $(\Delta_{d,i}V)_{1\le i\le N_d}$ is generated from the price model in Eq. (4.1) with the $\mathcal{F}_{d-1}$-adapted threshold δ_d. Then it holds that

$$\Delta_{d,i}V = \delta_d^2 Z_i, \tag{4.6}$$

where $(Z_i)_{1\le i\le N_d}$ is a sequence of independent and identically distributed (i.i.d.) positive random variables such that for all i, $Z_i \overset{\mathcal{L}}{=} \inf_{t>0}\{|B_t| \ge 1\}$ for some standard Brownian motion B with Z_i independent of $\mathcal{F}_{d,i-1}$.

Remark 4.2. Proposition 4.1 stems from the well-known Dambis-Dubins-Schwarz theorem that all continuous martingales are time-changed Brownian motions under the IV clock, or the business time (Barndorff-Nielsen and Shiryaev, 2015). As the price events commute with time changes, $(\Delta_{d,i}V)_{1\le i\le N_d}$ is, up to a constant scaling, identical in distribution to $(Z_i)_{1\le i\le N_d}$. The i.i.d.-ness thus follows from the strong Markov property and the time homogeneity of the Brownian motion. The density of Z_i is well-known in the literature with the following probability density function (PDF) and cumulative distribution function (CDF):

$$f_Z(z) = \sum_{k=-\infty}^{\infty} \frac{2(1+4k)}{\sqrt{2\pi}z^{3/2}} e^{-\frac{(1+4k)^2}{2z}}, \tag{4.7}$$

$$F_Z(z) = 2 - 2\sum_{k=-\infty}^{\infty} \operatorname{erf}\frac{1+4k}{\sqrt{2z}}, \tag{4.8}$$

where $\operatorname{erf} x = (2/\sqrt{\pi})\int_0^x e^{-t^2}dt$ is the error function (Andersen et al., 2008). In particular, we have $\mathbb{E}[Z_i] = \mathbb{E}[Z_i|\mathcal{F}_{d,i-1}] = 1$, which implies that the expected IV increment between two price events is precisely δ_d^2 for all continuous martingales, i.e., $\mathbb{E}[\Delta_{d,i}V|\mathcal{F}_{d,i-1}] = \delta_d^2$.

A key observation from Proposition 4.1 is that the IV-based time change converts $x_{d,i}$ into $\Delta_{d,i}V$ for each i, where the latter is, conditioning on $\mathcal{F}_{d,i-1}$, an i.i.d. duration in the IV

clock. Therefore, one naturally expects that the $\mathcal{F}_{d,i-1}$-conditional distribution of $x_{d,i}$ contains information about IV. To formalize this link, we define a counting process $N_d(t) = \sum_{i\geq 1} \mathbb{1}_{\{\tau_{d,i}\leq t\}}$ which counts the number of price events on day d up to time $t \in [d, d+1]$, and a piecewise constant price process $\overline{X}_t \equiv X_{\tau_{d,N_d(t)}}$, which is constant on each inter-event interval $[\tau_{d,i}, \tau_{d,i+1})$. Let $\overline{\mathcal{F}}_t \subset \mathcal{F}_t$ denote the natural filtration generated by $\overline{X}_t$, and similarly denote $\overline{\mathcal{F}}_{d,i} \equiv \overline{\mathcal{F}}_{\tau_{d,i}}$. We have the following result:

Proposition 4.2. Under the same conditions as in Proposition 4.1, we assume that $V(t)$ is adapted to $\overline{\mathcal{F}}_t$. Let $\Delta_{d,i}V(h) = V(\tau_{d,i-1}, \tau_{d,i-1}+h)$ denote the IV increment over the interval $[\tau_{d,i-1}, \tau_{d,i-1}+h]$. Let $f(h|\overline{\mathcal{F}}_{d,i-1})$ and $F(h|\overline{\mathcal{F}}_{d,i-1})$ denote the $\overline{\mathcal{F}}_{d,i-1}$-conditional PDF and CDF of $x_{d,i}$, respectively. For all d, i, it holds for all $h \in (0, x_{d,i}]$ that:

$$\Delta_{d,i}V(h) = \delta_d^2 G_{d,i}(h), \tag{4.9}$$

where $G_{d,i}(h) = F_Z^{-1}(F(h|\overline{\mathcal{F}}_{d,i-1}))$ and $F_Z^{-1}(\cdot)$ is the inverse function of the CDF in Eq. (4.8). Furthermore, for almost all $h \in (0, x_{d,i}]$, we have:

$$\sigma^2_{\tau_{d,i-1}+h} = \frac{\delta_d^2 f(h|\overline{\mathcal{F}}_{d,i-1})}{f_Z(G_{d,i}(h))}. \tag{4.10}$$

Remark 4.3. The use of the restricted filtration $\overline{\mathcal{F}}_t$ instead of $\mathcal{F}_t$ as well as the $\overline{\mathcal{F}}_t$-adaptedness of $V(t)$ require some elaboration. First, to reflect the PDS procedure on X, it is natural to consider the filtration generated only by sampled observations. This restriction is implicit in the existing work (Tse and Yang, 2012; Hong et al., 2023), which is intended to avoid using the full (potentially noisy) price paths in $\mathcal{F}_t$. The adaptedness of $V(t)$ to $\overline{\mathcal{F}}_t$ also ensures the validity of Proposition 4.1.[2] More importantly, it ensures that $V(t)$ for $\tau_{d,i-1} \leq t \leq \tau_{d,i}$ is $\overline{\mathcal{F}}_{d,i-1}$-predictable. This allows us to construct an observation-driven model for a continuous-time stochastic process, which can be easily estimated based on standard econometric tools. We show via simulations that one can still make valid inference about $V(t)$ conditioning on $\overline{\mathcal{F}}_t$ even when $V(t)$ is a fully stochastic volatility process that violates this restriction.

Proposition 4.2 leads to the following representation of IV over any finite interval $[s, t]$ in

[2]Note that Proposition 4.1 does not hold under $\mathcal{F}_t$ in the sense that Z_i is not i.i.d. when one conditions on $\mathcal{F}_t$ for $t \in (\tau_{d,i-1}, \tau_{d,i})$, as knowing the value of X_t after $\tau_{d,i-1}$ immediately changes the conditional density of Z_i. This is not a problem for $\overline{\mathcal{F}}_t$, since it does not contain the value of X_t between price events.

day d:

$$V(s,t) = \delta_d^2 \left[\sum_{i=N_d(s)}^{N_d(t)} G_{d,i}(x_{d,i}) - G_{d,N_d(s)}(s - \tau_{d,N_d(s)}) + G_{d,N_d(t)+1}(t - \tau_{d,N_d(t)}) \right], \tag{4.11}$$

where the last two terms correct for the (left and right) edge effects due to a mismatch between the interval $[s,t]$ and $[\tau_{d,N_d(s)}, \tau_{d,N_d(t)}]$. Taking $[s,t] = [d-1,d]$ gives the IV for day d, where the left correction is no longer needed. The right correction, termed the "end-of-day" correction in Hong et al. (2023), typically exhibits a smaller magnitude compared to the leading term and is often ignored in practical applications.

However, Proposition 4.2 only identifies the spot variance σ_t^2 for almost all t up to a Lebesgue null set. Intuitively, this is due to the fact that the spot variance process is identified through IV, whose value does not change by altering σ_t^2 on a Lebesgue null set. This also indicates that the point-wise result in Proposition 4.2 may not be very informative about the spot volatility at finitely many t. Instead, we propose to approximate σ_t by the localized IV over the interval $[t, t+h]$ for some small $h > 0$:

$$\bar{\sigma}_t = \sqrt{\frac{1}{h} V(t, t+h)}, \tag{4.12}$$

where $V(s,t)$ is given in Eq. (4.11). This smooths out any potential point-wise divergence from Eq. (4.10), which is adopted in our simulation and empirical analyses.

As an interesting special case of Proposition 4.2, we derive a condition for σ^2 to be almost everywhere piecewise constant:

Corollary 4.1. Suppose there exists a sequence of positive random variables $(\gamma_{d,i})$ with $\gamma_{d,i} \in \overline{\mathcal{F}}_{d,i}$. If $x_{d,i}$ satisfies $\gamma_{d,i-1} x_{d,i} = \delta_d^2 Z_i$ for all d and i, then it holds for almost all $h \in (0, x_{d,i}]$ that:

$$\sigma^2_{\tau_{d,i-1}+h} = \gamma_{d,i-1}. \tag{4.13}$$

Corollary 4.1 suggests that σ^2 is almost everywhere piecewise constant on $[\tau_{d,i-1}, \tau_{d,i}]$ if $x_{d,i}$ is proportional to Z_i conditioning on $\overline{\mathcal{F}}_{d,i-1}$. This is at odds with some of the existing point-process-based volatility estimators in the literature, to which we shall turn. The existing methods, e.g., Hautsch (2011), Tse and Yang (2012), and Hong et al. (2023), typically adhere to two equivalent methodologies: the duration-based method of Engle and Russell (1998), and the intensity-based method of Gerhard and Hautsch (2002). Both methods employ a heuristic

argument that each price event contributes δ_d^2 to V_d, and thus decompose the spot variance multiplicatively as the product of the squared threshold δ_d^2 and the intensity or hazard rate of price events, i.e.,

$$\tilde{\sigma}^2_{\tau_{d,i-1}+h} = \delta_d^2 \, \hbar(h|\overline{\mathcal{F}}_{d,i-1}), \qquad h \in (0, x_{d,i}], \tag{4.14}$$

where $\hbar(h|\overline{\mathcal{F}}_{d,i-1})$ is the $\overline{\mathcal{F}}_{d,i-1}$-conditional hazard function of the price events at time $\tau_{d,i-1}+h$, as defined in Daley and Vere-Jones (2003):

$$\hbar(h|\overline{\mathcal{F}}_{d,i-1}) = \frac{f(h|\overline{\mathcal{F}}_{d,i-1})}{1 - F(h|\overline{\mathcal{F}}_{d,i-1})}. \tag{4.15}$$

This model offers a convenient formulation for the spot variance in a multiplicative structure.

Despite this relatively simpler specification of $\tilde{\sigma}_t^2$, this decomposition cannot hold for the continuous martingale in Eq. (4.1). With the spot variance in Eq. (4.14), the IV increment between $\tau_{d,i-1}$ and $\tau_{d,i}$ is given by

$$\Delta_{d,i}\tilde{V} = \int_{\tau_{d,i-1}}^{\tau_{d,i}} \tilde{\sigma}_s^2 ds = \delta_d^2 \int_0^{x_{d,i}} \hbar(h|\mathcal{F}_{d,i-1}) dh = -\delta_d^2 \ln(1 - F(x_{d,i}|\overline{\mathcal{F}}_{d,i-1}))). \tag{4.16}$$

In this case, with a copula transformation argument, $\Delta_{d,i}\tilde{V}$ follows an exponential distribution with the intensity parameter δ_d^2, which clearly contradicts Corollary 4.1. Specifically, this would imply that the likelihood of a Brownian motion to exit a symmetric barrier $[-\delta_d, \delta_d]$ is time invariant, which is clearly impossible by the continuity of the Brownian motion. Therefore, $\tilde{\sigma}^2$ cannot coincide with the spot variance process of a continuous martingale.

Taking a different approach, Pelletier and Wei (2023) adopt the local volatility approximation of Andersen et al. (2008) and assume that σ is piecewise constant on all intervals of the form $[\tau_{d,i-1}, \tau_{d,i})$. Jointly with Proposition 4.1, it implies that, for each $1 \leq i \leq N_d$,

$$x_{d,i} \overset{\mathcal{L}}{=} \frac{\delta_d^2}{\sigma^2_{\tau_{d,i-1}}} Z_i. \tag{4.17}$$

The difference between the above result and our Corollary 4.1 is two-fold. On the one hand, Pelletier and Wei (2023) allow $\sigma^2_{\tau_{d,i-1}}$ to depend on concurrent information up to time $\tau_{d,i}$ through an additional stochastic component, while our Corollary 4.1 requires $\sigma^2_{\tau_{d,i-1}}$ to be adapted to $\overline{\mathcal{F}}_{d,i-1}$. This can be considered as a stochastic extension of our approach, which can potentially provide more flexibility to model the volatility dynamics. However, the resulting

model becomes fully parameter-driven, which requires computationally intensive estimation techniques and considerably complicates its empirical implementation (Koopman et al., 2016). On the other hand, Proposition 4.2 demonstrates that the piecewise constant assumption can be relaxed to a piecewise adaptedness condition, which allows for a more flexible specification for σ even within our observation-driven framework. We will thus focus on Proposition 4.2 in developing volatility models and leave the generalization to a fully parameter-driven model for future research.

4.2.2 A Semiparametric Model for Daily and Intraday Volatility Dynamics

In this section, we describe our econometric model for both the "daily" thresholds $(\delta_d)_{1\leq d\leq D}$ and the intraday price durations $x_{d,i}$, where D denotes the total number of trading days in the in-sample period. We start with a model for $(\delta_d)_{1\leq d\leq D}$: Let $K \in \mathbb{Z}^+$ denote a predetermined "target" sampling frequency. The realized K-adaptive threshold on the d-th day is defined as

$$\delta_d = \sup_{\delta>0} \operatorname*{argmin}_{\delta} |K - N_d|, \tag{4.18}$$

where the supremum is taken to ensure the uniqueness of $\hat{\delta}_d$. Intuitively, δ_d is the largest threshold that generates a sampling frequency N_d closest to K, which can be easily constructed with the price observations on day d in practice. Note that $K\delta_d^2$ actually serves as a daily IV estimator and can be treated as a proxy for V_d. Based on a burn-in sample of $(\delta_d)_{-h\leq d\leq 0}$, we estimate the HAR model of Corsi (2009):

$$\delta_d^2 = \omega_0 + \omega_1\delta_{d-1}^2 + \omega_2 \sum_{i=1}^{5} \delta_{d-i}^2 + \omega_3 \sum_{i=1}^{22} \delta_{d-i}^2 + \epsilon_d, \tag{4.19}$$

which can be easily estimated via ordinary least squares (OLS). The HAR model is designed to parsimoniously capture the dependence structure of IV across different horizons, and therefore aims to approximate its long memory which has been extensively confirmed by empirical literature. Renowned for its consistent and remarkable predictive performance, the HAR model serves as the predominant benchmark in modeling and forecasting daily IV dynamics. With the parameter estimates $\hat{\boldsymbol{\omega}} = (\hat{\omega}_0, \hat{\omega}_1, \hat{\omega}_2, \hat{\omega}_3)$, we set $\hat{\delta}_1^2$ as the one-step-ahead forecast of δ_1^2 with

the optimal MSE:

$$\hat{\delta}_1^2 = \mathbb{E}[\delta_1^2|\mathcal{F}_0] = \hat{\omega}_0 + \hat{\omega}_1\delta_0^2 + \hat{\omega}_2\sum_{i=1}^{5}\delta_{1-i}^2 + \hat{\omega}_3\sum_{i=1}^{22}\delta_{1-i}^2, \tag{4.20}$$

and the values of $(\hat{\delta}_d)_{2\le d\le D}$ can be obtained with recursive model estimation and prediction in a rolling-window fashion. The construction of $\hat{\delta}_d$ ensures that $\hat{\delta}_d^2 = \mathbb{E}[\delta_d^2|\mathcal{F}_{d-1}] \approx K^{-1}\mathbb{E}[V_d|\mathcal{F}_{d-1}]$, which is the desired threshold adaptive to daily volatility dynamics.

With the sequence of thresholds $(\hat{\delta}_d)_{1\le d\le D}$, we obtain all durations across all D days, which can be modeled parametrically with standard duration-based point process models (Hautsch, 2011). Among many possible choices, we consider the simple log-ACD-GARCH model as follows:

$$\begin{aligned}
\ln x_{d,i} &= \Psi_{d,i} + s_{d,i} + \varepsilon_{d,i}, \quad \varepsilon_{d,i} = \sqrt{h_{d,i}}u_{d,i},\\
\Psi_{d,i} &= \sum_{j=1}^{p}\phi_j\Psi_{d,i-j} + \sum_{j=1}^{q}\theta_j\varepsilon_{d,i-j},\\
h_{d,i} &= \tilde{s}_{d,i} + \sum_{j=1}^{p^*}\alpha_j\varepsilon_{d,i-j}^2 + \sum_{j=1}^{q^*}\beta_j h_{d,i-j},
\end{aligned} \tag{4.21}$$

where $(u_{d,i})$ is a sequence of i.i.d. random variables with zero mean and unit variance, with a parametric PDF $f_u(x;\boldsymbol{\gamma})$ governed by the parameter vector $\boldsymbol{\gamma}$. The processes $(\Psi_{d,i})$ and $(h_{d,i})$ are standard conditional mean and variance specifications used in ACD- and GARCH-type models, which are both $\overline{\mathcal{F}}_{d,i-1}$-predictable. The variables $s_{d,i}$ and $\tilde{s}_{d,i}$ are also $\overline{\mathcal{F}}_{d,i-1}$-predictable components that capture the seasonality in the mean and variance of log-durations, respectively, and are specified in flexible Fourier forms following Andersen and Bollerslev (1997). For example, a Q-th-order flexible-Fourier-form specification for $s_{d,i}$ is given by

$$s_{d,i} = \nu_0 + \nu_1\bar{\tau}_{d,i-1} + \sum_{j=1}^{Q}(\nu_{c,j}\cos(2\pi j\cdot\bar{\tau}_{d,i-1}) + \nu_{s,j}\sin(2\pi j\cdot\bar{\tau}_{d,i-1})), \tag{4.22}$$

where the parameters $\{\nu_0,\nu_1,\nu_{c,1},...,\nu_{c,Q},\nu_{s,1},...,\nu_{s,Q}\}$ for $s_{d,i}$, and similarly $\{\tilde{\nu}_0,\tilde{\nu}_1,\tilde{\nu}_{c,1},...,\tilde{\nu}_{c,Q},\tilde{\nu}_{s,1},...,\tilde{\nu}_{s,Q}\}$ for $\tilde{s}_{d,i}$, are jointly estimated with other model parameters. We follow Hautsch (2011) to reset the autoregressive structure of $\ln x_{d,i}$ and $h_{d,i}$ in Eq. (4.21) at the beginning of each trading day, as we do not expect the end-of-day duration to impact the first duration of

the subsequent day.

Given that the log-ACD-GARCH model in Eq. (4.21) is in essence a variant of the celebrated GARCH model of Engle (1982) and Bollerslev (1986), its related estimation techniques and asymptotic properties are well-understood in the literature. Specifically, since the $\mathcal{F}_{d,i-1}$-conditional density of $x_{d,i}$ is determined by $f_u(x;\boldsymbol{\gamma})$, all model parameters can be jointly estimated with standard maximum likelihood estimation (MLE). Under the correct model specification and standard regularity conditions (see, e.g., Amemiya, 1985), the MLE estimator is consistent and asymptotically normal as the number of days $D \to \infty$.

Furthermore, the volatility dynamics implied by the log-ACD-GARCH model in Eq. (4.21) need some discussions. The $\overline{\mathcal{F}}_{d,i-1}$-predictability of $\Psi_{d,i}$, $s_{d,i}$, and $h_{d,i}$ indicates that

$$\mathbb{E}[x_{d,i}|\overline{\mathcal{F}}_{d,i-1}] = e^{\Psi_{d,i}+s_{d,i}}\mathbb{E}[e^{\sqrt{h_{d,i}}u_{d,i}}|\overline{\mathcal{F}}_{d,i-1}]. \tag{4.23}$$

The term $e^{\Psi_{d,i}+s_{d,i}}$ multiplicatively captures the autoregressive structure and seasonality of intraday price durations. The GARCH-type conditional variance $h_{d,i}$ further allows non-multiplicative autoregressive structure and seasonality to be modeled through the conditional moment generating function of $u_{d,i}$. As an important special case, we let $u_{d,i} \sim \ln Z_i - \mathbb{E}[\ln Z_i]$, where Z_i is defined in Proposition 4.1, and $h_{d,i} = 1$, then by Eq. (4.17) we have

$$x_{d,i} = e^{\Psi_{d,i}+s_{d,i}}Z_i \qquad \text{and} \qquad \sigma^2_{\tau_{d,i-1}} = \delta_d^2 e^{-\Psi_{d,i}-s_{d,i}}, \tag{4.24}$$

where $\ln Z_i$ can be subsumed into the seasonality factor $s_{d,i}$. This implies that σ is piecewise constant on $[\tau_{d,i-1}, \tau_{d,i})$, and can be viewed as a càdlàg (i.e., right-continuous with left limits) process in continuous time that is only updated when the sampling occurs. The changed value of σ on $\tau_{d,i}$ depends on both the self-dependence structure $e^{-\Psi_{d,i}}$ and the seasonal pattern $e^{-s_{d,i}}$. Furthermore, by adopting different density assumptions of $u_{d,i}$ with the further inclusion of the conditional variance component $h_{d,i}$, our model allows the spot volatility to be time-varying, which further enriches the intraday volatility dynamics implied by duration-based models.

4.3 Simulation Results

This section contains a Monte Carlo study to examine the finite-sample performance of the semiparametric volatility model, which corresponds to the results developed in Sections 4.2.1 and 4.2.2.

4.3.1 Simulation Design

We simulate a Heston model for the efficient price process X (Heston, 1993):

$$\begin{aligned} dX_t &= \mu dt + \breve{\sigma}_t dW_{1,t} + dJ_t, \quad \breve{\sigma}_t = \sigma_t \sigma_{u,t}, \\ d\sigma_t^2 &= \alpha \left(\theta_d - \sigma_t^2\right) dt + \eta \sigma_t dW_{2,t}, \end{aligned} \tag{4.25}$$

where W_1 and W_2 are standard Brownian motions with $\text{Corr}(W_{1,t}, W_{2,t}) = \rho$, and J is a compound Poisson process, i.e.,

$$J_t = \sum_{i=1}^{N_t} D_i, \tag{4.26}$$

where N is a Poisson process with rate λ, and D_i follows a normal distribution $\mathcal{N}(0, \varsigma^2)$. For the spot volatility $\breve{\sigma}_t = \sigma_t \sigma_{u,t}$, we follow Hasbrouck (1999), Andersen et al. (2012), and Christensen et al. (2018) to model the diurnal pattern of intraday volatility in $\sigma_{u,t}$ with a sum of two exponentials:

$$\sigma_{u,t} = C + Ae^{-a_1 t} + Be^{-a_2(1-t)}. \tag{4.27}$$

We set $A = 0.75$, $B = 0.25$, $C = 0.88929188$, and $a_1 = a_2 = 10$. This realistically calibrated specification produces a pronounced, asymmetric reverse J-shape in $\sigma_{u,t}$, with variance at $t = 0$ (resp. $t = 1$) more than three times (resp. about 1.5 times) the midday variance ($t = 1/2$).

The annualized parameters for Eq. (4.25) are fixed at $(\mu, \alpha, \theta_0, \eta, \rho) = (0.05, 5, 0.16, 0.5, -0.5)$, where the volatility parameters satisfy the Feller's condition $2\alpha\theta_0 \geq \eta^2$ which ensures the positivity of σ. The parameter choices follow both Aït-Sahalia and Jacod (2009) and Aït-Sahalia et al. (2012), which are calibrated according to the empirical estimates in Aït-Sahalia and Kimmel (2007). Specifically, for the annualized daily variance parameter θ_d, we assume a HAR structure as follows:

$$\theta_d = \omega_0 + \omega_1 \theta_{d-1} + \omega_2 \sum_{i=1}^{5} \theta_{d-i} + \omega_3 \sum_{i=1}^{22} \theta_{d-i} + \epsilon_d^\theta, \quad \text{with } \epsilon_d^\theta \sim \text{i.i.d. } \mathcal{N}(0, \kappa^2), \tag{4.28}$$

where $(\omega_0, \omega_1, \omega_2, \omega_3, \kappa) = (0.03, 0.2, 0.4/5, 0.2/22, 0.03)$. Additionally, the process J simulated with $\lambda = 1/5$ and $\varsigma = 2\%$ implies an average of one jump per week, and the jump variation is about 20% of the daily IV on average, which is consistent with Andersen et al. (2023a). Fig. 4.1 illustrates the intraday variation of returns and annualized RVs of a simulated path in each one-minute interval. The return variation exhibits an asymmetric U-shaped or reverse J-shaped pattern over the trading hours, which is in line with some prior empirical findings (Harris, 1986; Wood et al., 1985; Andersen and Bollerslev, 1997; Christensen et al., 2018; Andersen et al., 2018, 2019, 2023b).

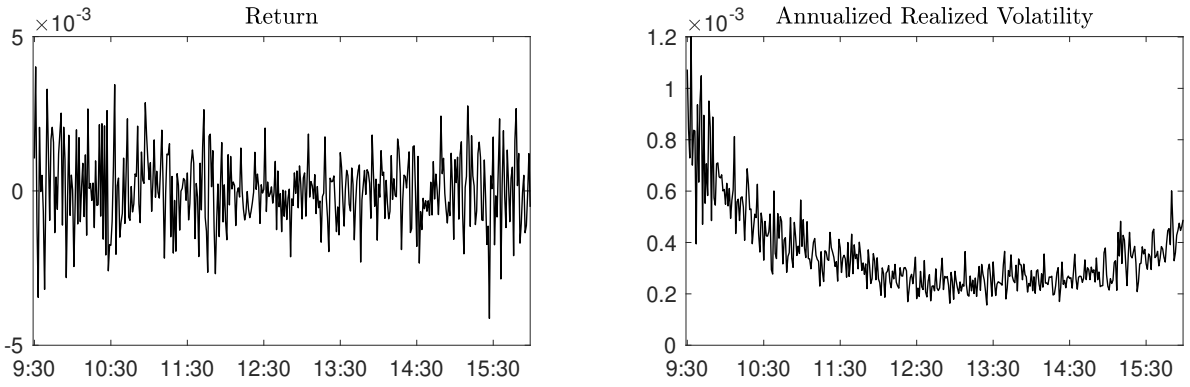

Fig. 4.1 Intraday variation of returns and annualized RVs of a simulated Heston process. The tick-level observations are simulated with the Heston model in Eq. (4.25), with a pronounced, asymmetric reverse J-shape exhibited in spot volatility. The returns and annualized RVs are computed at a granularity of one minute.

We simulate second-by-second observations for 500 consecutive days. The realized K-adaptive thresholds over the first 200 days, i.e., the burn-in sample $\{-h, \ldots, 0\}$, are used to estimate the HAR model in Eq. (4.19) and predict the threshold $\hat{\delta}_1$ for the 201-st day. In this section, we focus on both the spot volatility and IV estimation for the last 300 days.

4.3.2 Model Estimation

For the K-adaptive thresholds, we consider three different values of K, i.e., $K = 78$, 39, and 26, for the burn-in sample, which correspond to similar levels of sparsity of 5, 10 and 15-minute calendar-time sampling, respectively. The durations observed in the last 300 days are obtained with the predicted thresholds from the HAR model in Eq. (4.19) estimated in a rolling-window fashion. As mentioned in Section 4.2, by controlling the daily K-adaptive thresholds, we remove the interday volatility dynamics from the sequence of durations across all 300 days. To obtain the conditional CDF of durations, we estimate the log-ACD-GARCH model in Eq. (4.21) with

MLE (with $u_{d,i}$ assumed as a standard Gaussian white noise). Table 4.1 reports the mean and standard deviation of the estimated parameters for the log-ACD-GARCH model, where we select the lags $(1,1)$ for both the ACD and GARCH parts, with second-order flexible-Fourier-form specifications for both seasonality terms s and $\tilde{s}$.[3]

Table 4.1 Parameter estimates of the log-ACD-GARCH model

Parameters	$K=78$	$K=39$	$K=26$	Parameters	$K=78$	$K=39$	$K=26$
ϕ_1	0.8776	0.7291	0.7283	α_1	0.0012	0.0029	0.0017
	(0.0134)	(0.0292)	(0.0314)		(0.0044)	(0.0059)	(0.0081)
θ_1	-0.8018	-0.6315	-0.6357	β_1	0.8418	0.8739	0.8009
	(0.0185)	(0.0311)	(0.0345)		(0.2040)	(0.1270)	(0.0692)
ν_0	2.1313	3.6763	4.1018	$\tilde{\nu}_0$	-0.0403	0.1693	-0.8568
	(0.1346)	(0.2959)	(0.8327)		(0.1339)	(0.1897)	(0.4269)
ν_1	-2.0959	-3.4849	-3.7677	$\tilde{\nu}_1$	0.0195	-0.1225	0.9965
	(0.1488)	(0.2944)	(0.8411)		(0.1419)	(0.2011)	(0.4285)
$\nu_{c,1}$	0.1749	0.2815	0.3137	$\tilde{\nu}_{c,1}$	-0.0052	0.0124	-0.1045
	(0.0119)	(0.0304)	(0.0892)		(0.0138)	(0.0216)	(0.0454)
$\nu_{c,2}$	0.0194	0.0679	0.1277	$\tilde{\nu}_{c,2}$	-0.0075	0.0192	0.0492
	(0.0095)	(0.0109)	(0.0145)		(0.0098)	(0.0132)	(0.0150)
$\nu_{s,1}$	0.0307	0.0475	0.0440	$\tilde{\nu}_{s,1}$	0.0006	0.0132	-0.0258
	(0.0043)	(0.0102)	(0.0273)		(0.0052)	(0.0076)	(0.0156)
$\nu_{s,2}$	0.0099	0.0345	0.0676	$\tilde{\nu}_{s,2}$	-0.0008	0.0091	0.0523
	(0.0045)	(0.0080)	(0.0115)		(0.0039)	(0.0126)	(0.0130)
Total No. of durations	23218	11327	7292				
log-likelihood	-28526	-14145	-9297				

This table reports the parameter estimates (standard errors in parentheses) for the log-ACD-GARCH model in Eq. (4.21). The white noise $u_{d,i}$ is assumed to follow a standard normal distribution. We select the lags $(1,1)$ for both the ACD and GARCH components, and utilize the second-order flexible-Fourier-form specifications in Eq. (4.22) with $Q=2$ for both seasonality terms s and $\tilde{s}$.

4.3.3 Spot Volatility Estimation

In this section, we utilize the results in Section 4.2.1 to estimate the intraday spot volatility. For some intraday interval $[s, s+\Delta]$, we estimate the average spot volatility with a local IV estimator:

$$\widehat{\bar{\sigma}}(s, s+\Delta) = \sqrt{\frac{1}{\Delta}\widehat{V}(s, s+\Delta)}, \tag{4.29}$$

where $V(s, s+\Delta)$ is defined in Eq. (4.11), and can be estimated with the conditional CDFs of price durations with both the left and right correction. Fig. 4.2 illustrates an example of spot volatility estimation for each equidistant intervals with $\Delta = 5$ minutes, 30 minutes, and one

[3] Additional simulation results, including those with different distributions of $u_{d,i}$, various choices of ACD and GARCH lags, and different values of $Q \geq 1$ for the seasonality terms, which do not alter the qualitative results throughout this section, are available upon request.

hour. The solid line represents a simulated path of the spot volatility process $\breve{\sigma}$ from the Heston model in Eq. (4.25). All annualized spot volatility estimates are calculated from Eq. (4.29), with all durations obtained with the daily K-adaptive thresholds for $K = 78$.

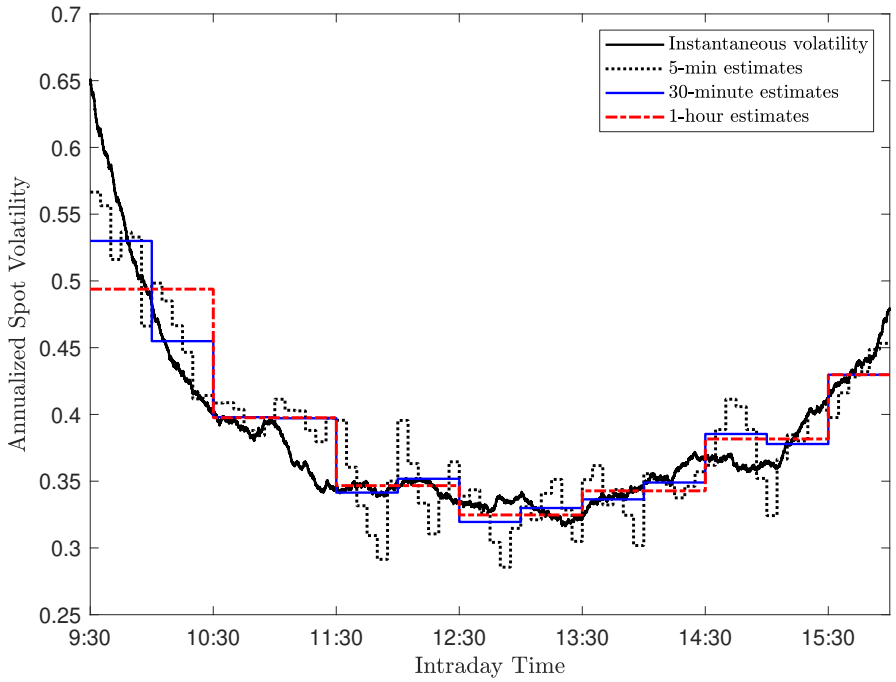

Fig. 4.2 Annualized spot volatility estimates for each equidistant intervals with $\Delta = 5$ minutes, 30 minutes, and one hour. The durations are obtained with the K-adaptive threshold with $K = 78$.

To evaluate the finite-sample performance of our spot volatility estimator, we compare it with some conventional and recently developed innovative estimators. The first benchmark we consider is the classical spot volatility estimator introduced by Foster and Nelson (1996), which is a localized version of RV (Barndorff-Nielsen and Shephard, 2002; Andersen et al., 2003a). Suppose there are k_n price observations with the lag Δ_n over the block $[s, s+\Delta]$, i.e., $\Delta = k_n\Delta_n$. The localized RV estimator is defined as

$$\widehat{\widehat{\sigma}}(s, s+\Delta) = \sqrt{\frac{1}{\Delta}\sum_{i=1}^{k_n} r_i^2}, \tag{4.30}$$

where $r_i = X_{s+i\Delta_n} - X_{s+(i-1)\Delta_n}$ is the i-th return between consecutive observations. Another easy-to-implement benchmark is the optimal candlestick (OK) estimator of Li et al. (2022).

Based on a single candlestick over the block $[s, s+\Delta]$, we have

$$\widehat{\widehat{\sigma}}(s, s+\Delta) = \frac{1}{\sqrt{\Delta}} \left(0.811 w(s, s+\Delta) - 0.369 |r(s, s+\Delta)|\right), \tag{4.31}$$

where $w(s,t)$ and $r(s,t)$ represent the range and return over $[s,t]$, respectively:

$$w(s,t) = \sup_{s \le \tau, \tau' \le t} |X_\tau - X_{\tau'}| \quad \text{and} \quad r(s,t) = X_t - X_s. \tag{4.32}$$

We also consider a local average version by aggregating k candlesticks over multiple small intervals, which demonstrates superior finite-sample performance than the one based on a single candlestick:

$$\widehat{\widehat{\sigma}}(s, s+\Delta) = \frac{1}{k} \sum_{i=1}^{k} \frac{1}{\sqrt{h}} (0.811 w(s+(i-1)h, s+ih) - 0.369 |r(s+(i-1)h, s+ih)|), \tag{4.33}$$

where $h = \Delta/k$ denotes the length of all k subintervals. Their finite-sample performances are assessed and compared via the relative absolute bias and the root-mean-square error (RMSE), i.e., for each spot volatility estimate $\widehat{\widehat{\sigma}}_i$ over the i-th interval,

$$\text{Relative absolute bias} = \frac{1}{N} \sum_{i=1}^{N} \frac{|\widehat{\widehat{\sigma}}_i - \bar{\sigma}_i|}{\bar{\sigma}_i} \quad \text{and} \quad \text{RMSE} = \sqrt{\frac{1}{N} \sum_{i=1}^{N} (\widehat{\widehat{\sigma}}_i - \bar{\sigma}_i)^2}, \tag{4.34}$$

where N = number of intervals every day $\times$ 300 days, and the "true value" $\bar{\sigma}_i$ is the local average of all annualized spot volatilities (tick-level) over each interval.[4]

Table 4.2 reports the relative absolute biases (%) and RMSE results of our duration-based estimator with three different levels of K (78, 39, and 26), the classical local-RV-based estimator (with all second-by-second observations), and the OK estimators based on both a single candlestick and multiple one-minute candlesticks. Compared with the other estimators, the relative absolute biases of our duration-based estimator are similar to those of the localized RV and multiple-candlestick-based OK estimator. However, our estimator consistently exhibits the smallest RMSE across all choices of estimation windows. Furthermore, the RMSE function penalizes outliers heavily, and is therefore sensitive to excessively misinformative estimates.

[4] We can also use the "true" σ_t sampled at the mid-point of each interval, which has nearly no impact on the results in Table 4.2, and does not alter our conclusions.

To further investigate the sensitivity of different spot volatility estimators to price jumps, we conduct a simple Monte Carlo experiment: We insert a jump of a fixed size 2% (one standard deviation ς of the jump size variable D_i) at 13:00 on the same day illustrated in Fig. 4.2. As shown in Fig. 4.3, such a discontinuous shift in the price process has nearly no impact on our duration-based estimator, but can severely bias the localized RV and candlestick-based estimates over the block in which the jump occurs. We conclude that the natural robustness of duration-based methods to jumps enhances our estimator's ability to capture spot volatility dynamics.

Table 4.2 Monte Carlo results for spot volatility estimation

Panel A: Relative Absolute Bias (%)						
Interval (minutes)	$\hat{\sigma}_{K=78}$	$\hat{\sigma}_{K=39}$	$\hat{\sigma}_{K=26}$	local RV	OK (single)	OK (multiple)
5	8.96	10.12	11.15	10.45	21.11	13.82
10	8.68	9.92	10.94	9.90	21.02	12.43
15	8.49	9.65	10.88	9.78	20.99	12.07
30	8.11	9.17	10.24	9.82	20.09	11.77
60	7.80	8.85	9.70	9.93	20.02	11.74
Panel B: RMSE ($\times 10^2$)						
Interval (minutes)	$\hat{\sigma}_{K=78}$	$\hat{\sigma}_{K=39}$	$\hat{\sigma}_{K=26}$	local RV	OK (single)	OK (multiple)
5	4.57	5.23	5.61	12.38	11.25	6.67
10	4.32	5.14	5.53	11.86	11.11	5.64
15	4.17	4.76	5.24	11.51	10.99	5.26
30	3.93	4.31	4.92	10.83	10.84	4.86
60	3.77	4.17	4.65	9.61	10.57	4.74

This table reports the relative absolute biases (%) and RMSE results of the duration-based estimators with three different levels of K (78, 39, and 26), the classical local-RV-based estimator (with all second-by-second observations), and the OK estimators based on both a single candlestick and multiple consecutive one-minute candlesticks. The relative absolute biases and RMSE results are calculated based on the annualized spot volatility estimate and the local average of all tick-level spot volatilities (as true value) over each interval.

4.3.4 Integrated Variance Estimation

Similar to the localized IV estimator used in Section 4.3.3, the theoretical results in Section 4.2.1 can also be employed to estimate the daily IV:

$$V_d \equiv V(d-1,d) = \delta_d^2 \left[\sum_{i=1}^{N_d} G_{d,i}(x_{d,i}) + G_{d,N_d+1}(d - \tau_{d,N_d}) \right], \tag{4.35}$$

where the second term in the summand represents the "end-of-day" correction between the last price event and the market closing time. We compute all durations between price events across the 300-day period with the predicted K-adaptive thresholds for $K = 78$, 39, and 26,

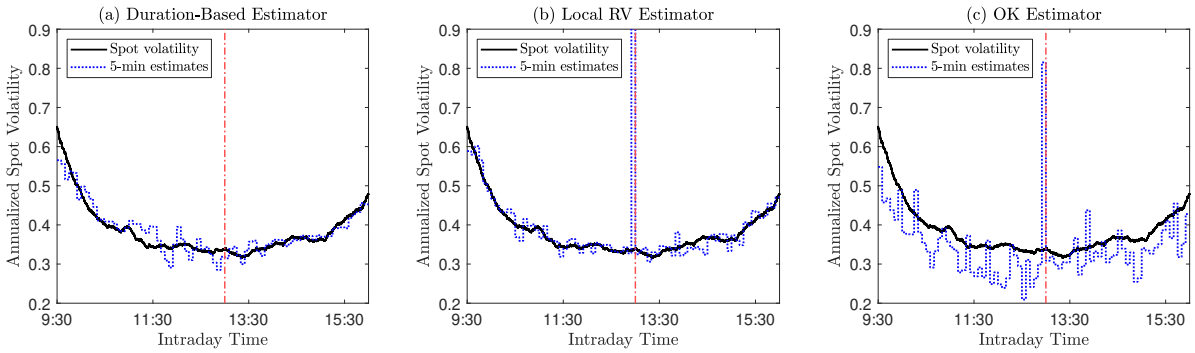

Fig. 4.3 Comparisons of 5-minute spot volatility estimates when there exist jumps. A jump of a 2% fixed size(one standard deviation ς of the jump size variable D_i) is inserted at 13:00 (highlighted by the red dash-dot line) on the same day illustrated in Fig. 4.2. The durations are obtained with the K-adaptive threshold with $K = 78$. The local RV estimator in (b) are constructed from all available second-by-second observations. The OK estimator in (c) uses five consecutive one-minute candlesticks to compute each 5-minute volatility estimate.

and then estimate the daily IV based on the conditional CDFs of each duration. For the comparative analysis, we consider the daily RV, the realized bipower variation (RBPV) of Barndorff-Nielsen and Shephard (2004), and the truncated realized volatility (TRV) of Mancini (2009) as benchmarks:

$$\mathrm{RV}_d = \sum_{i=1}^{n} r_{d,i}^2, \tag{4.36}$$

$$\mathrm{RBPV}_d = \frac{\pi}{2}\left(\frac{n}{n-1}\right)\sum_{i=2}^{n} |r_{d,i}||r_{d,i-1}|, \tag{4.37}$$

$$\mathrm{TRV}_d = \sum_{i=1}^{n} r_{d,i}^2 \mathbb{1}_{\{|r_{d,i}|\leq\varphi\}}, \tag{4.38}$$

where Δ_n stands for the length of sampling intervals, and $n = (d-(d-1))/\Delta_n = \Delta_n^{-1}$ is the number of sampled returns over the day d. We construct all three calendar-time-based IV estimators from 5, 10, and 15-minute sampled returns, which correspond to the selected sampling frequencies of the adaptive PDS. For the TRV estimator, we employ the classical truncation threshold $\varphi = \zeta\Delta_n^{\varpi}$ with $\varpi \in (0, 1/2)$, and set the threshold parameters with a data-adaptive method:

$$\zeta = C\sqrt{\mathrm{MedRV}_d}, \tag{4.39}$$

where we choose $C = 3$, and MedRV is the median RV estimator of Andersen et al. (2012):

$$\text{MedRV}_d = \frac{\pi}{6 - 4\sqrt{3} + \pi}\left(\frac{n}{n-2}\right)\sum_{i=2}^{n-1}\text{median}(|r_{d,i-1}|, |r_{d,i}|, |r_{d,i+1}|)^2. \tag{4.40}$$

Table 4.3 reports the relative absolute bias (%) and RMSE results for the annualized IV estimates. Our duration-based estimator achieves both the smallest relative absolute bias and RMSE across all selected sampling frequencies. While the jump-robust RBPV and TRV estimators have better finite-sample performance than the traditional RV estimator, their bias and RMSE results are still slightly larger than those of our duration-based estimator. This highlights the robustness and effectiveness of the duration-based method as an alternative to the return-based approaches in high-frequency volatility estimation.

Table 4.3 Monte Carlo results for IV estimation

Panel A: Relative Absolute Bias (%)				
Sampling Frequency	$\widehat{V}_d$	RV	RBPV	TRV
78	13.11	24.38	15.61	14.75
39	15.06	29.21	22.17	20.81
26	16.09	32.28	25.96	24.00
Panel B: RMSE ($\times 10^2$)				
Sampling Frequency	$\widehat{V}_d$	RV	RBPV	TRV
78	2.57	7.70	3.08	2.79
39	2.73	8.35	4.22	3.99
26	2.85	8.84	4.99	4.52

This table reports the relative absolute biases (%) and RMSE results of the duration-based IV estimator, RV, RBPV, and TRV. The bias and RMSE results are calculated based on the annualized IV estimates for 300 days.

4.4 Empirical Analysis

In this section, we first utilize our duration-based IV estimator as the basis for daily volatility forecasting under the HAR framework for the SPDR S&P 500 ETF Trust (SPY), which is the best-recognized and oldest U.S. listed ETF and by far the most widely traded S&P 500 ETF. Subsequently, we employ our duration-based spot volatility estimator to assess how intraday volatility responds to some specific macroeconomic events, such as FOMC news announcements.

4.4.1 Overview

We obtain all high-frequency transaction records of SPY from the daily Trade and Quote (TAQ) dataset, with the sample period ranging from January 2, 2014 to December 30, 2022. The tick-by-tick transactions are timestamped in milliseconds until mid-2015 and in microseconds since then.[5] As is standard in empirical research with TAQ data, we use the filters as in Barndorff-Nielsen et al. (2009) to eliminate data errors, remove all transactions in the original record that are later corrected, cancelled or otherwise invalidated. In addition, we remove all trading days with an early market closure, and restrict our sample to transactions between 9:31:00 – 16:00:00 Eastern Time (ET) for all individual stocks.

To obtain the durations with the adaptive PDS, we utilize all trading days from January 2014 to December 2016 as the burn-in period, which allows us to predict the first K-adaptive daily threshold in 2017. Fig. 4.4 compares the autocorrelations of log-durations (from 2017 to 2022, 1499 days in total) obtained with the predicted daily thresholds (with $K = 78$) to those obtained with a fixed threshold for all days. It is notable that the utilization of daily adaptive thresholds effectively alleviates the long memory observed in log-durations over extended multi-day periods.

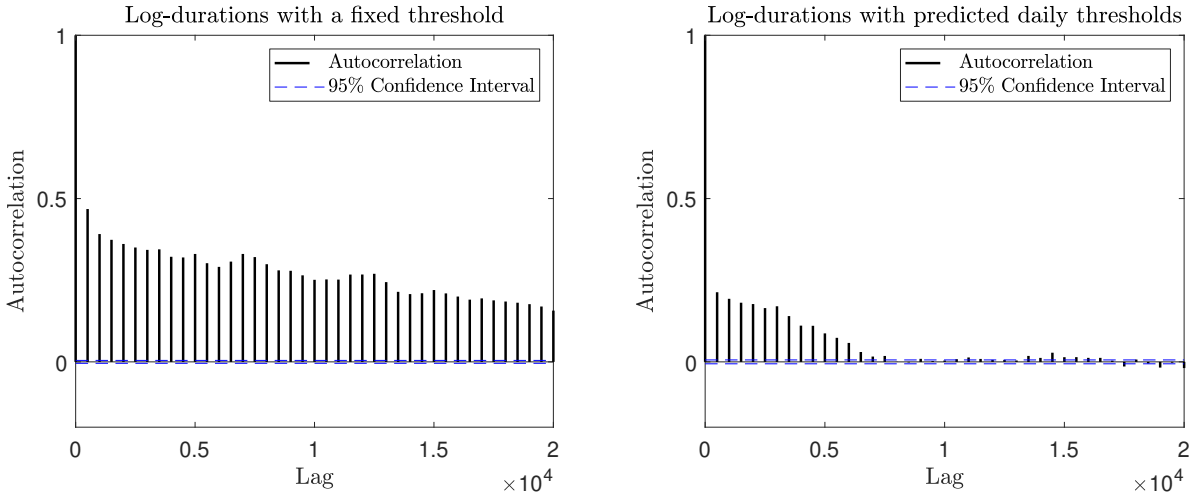

Fig. 4.4 Correlograms of log-durations obtained with (a) a fixed threshold and (b) the predicted daily thresholds with $K = 78$. We choose the fixed threshold as the mean value of ex post K-adaptive thresholds in Eq. (4.18) for all days.

[5] We use the SAS code from Holden and Jacobsen (2014) to extract all tick-by-tick transaction records matched with relevant ask/bid quotes from the daily TAQ dataset available on the Wharton Research Data Services (WRDS).

As a representative, we estimate the log-ACD-GARCH model in Eq. (4.21) via MLE with all log-durations from 2017 to 2022. In line with Section 4.3, we select the lags $(1, 1)$ for both the ACD and GARCH parts, with second-order flexible-Fourier-form specifications for both seasonality terms s and $\tilde{s}$. The parameter estimates (with standard errors) are reported in Table 4.4.[6] All parameters in both ACD and GARCH components are statistically significant. Both the conditional means and variances demonstrate strong positive autocorrelation. For the intraday seasonality terms s and $\tilde{s}$, most of the estimated parameters in the first sine-cosine summand ($\nu_{c,1}$, $\nu_{s,1}$, $\tilde{\nu}_{c,1}$) are significant. Fig. 4.5 illustrates the intraday seasonality for the conditional mean and variance of durations (with $K = 78$), respectively.

Table 4.4 Parameter estimates of the log-ACD-GARCH model

Parameters	$K = 78$	$K = 39$	$K = 26$	Parameters	$K = 78$	$K = 39$	$K = 26$
ϕ_1	0.9775	0.9230	0.9158	α_1	0.0719	0.0897	0.0453
	(0.0008)	(0.0024)	(0.0031)		(0.0024)	(0.0046)	(0.0083)
θ_1	-0.7635	-0.6623	-0.6346	β_1	0.7943	0.6010	0.8773
	(0.0028)	(0.0055)	(0.0070)		(0.0087)	(0.0219)	(0.0369)
ν_0	1.4627	2.5488	2.9599	$\tilde{\nu}_0$	-0.9218	-0.9035	-0.8982
	(0.0562)	(0.2976)	(0.1069)		(0.1082)	(0.0420)	(0.0188)
ν_1	-1.5425	-2.5510	-2.8900	$\tilde{\nu}_1$	0.9999	0.9994	0.9999
	(0.0565)	(0.3017)	(0.0349)		(0.1086)	(0.0345)	(0.0685)
$\nu_{c,1}$	0.1305	0.1988	0.2236	$\tilde{\nu}_{c,1}$	-0.1109	-0.1548	-0.1004
	(0.0059)	(0.0311)	(0.0077)		(0.0112)	(0.0078)	(0.0034)
$\nu_{c,2}$	-0.0005	0.0456	0.0877	$\tilde{\nu}_{c,2}$	0.0249	0.0171	0.0411
	(0.0023)	(0.0053)	(0.0499)		(0.0032)	(0.0090)	(0.0246)
$\nu_{s,1}$	0.0329	0.0585	0.0670	$\tilde{\nu}_{s,1}$	-0.0097	0.0052	-0.0141
	(0.0022)	(0.0099)	(0.0167)		(0.0037)	(0.0059)	(0.0083)
$\nu_{s,2}$	-0.0035	0.0192	0.0291	$\tilde{\nu}_{s,2}$	0.0239	0.0605	0.0238
	(0.0018)	(0.0042)	(0.0188)		(0.0027)	(0.0070)	(0.0062)
Total No. of durations	111715	52017	34078				
log-likelihood	-169462	-79914	-53267				

This table reports the parameter estimates (standard errors in parentheses) for the log-ACD-GARCH model in Eq. (4.21). The white noise $u_{d,i}$ is assumed to follow a standard normal distribution. We select the lags $(1, 1)$ for both the ACD and GARCH components, and utilize the second-order flexible-Fourier-form specifications in Eq. (4.22) with $Q = 2$ for both seasonality terms s and $\tilde{s}$.

[6] Additional results with various choices of ACD and GARCH lags, and $Q \geq 1$ for the seasonality terms, which do not alter the qualitative results throughout this section, are available upon request.

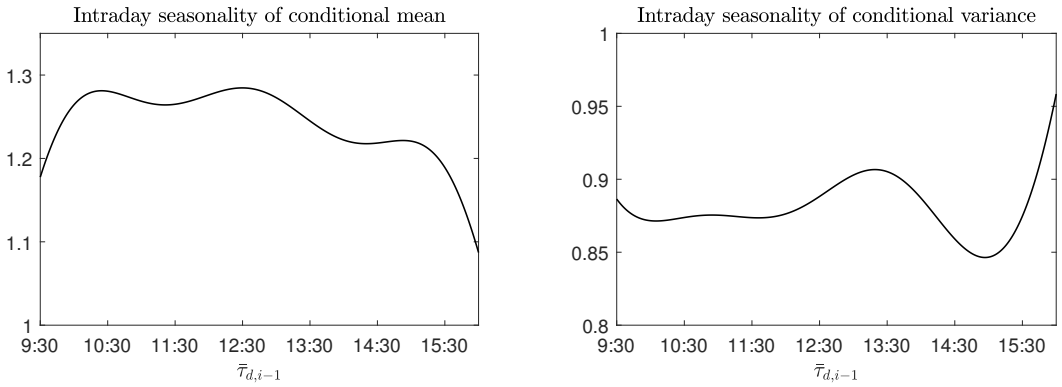

Fig. 4.5 Intraday seasonality $\exp(s_{d,i})$ and $\exp(\tilde{s}_{d,i})$ for the conditional mean and variance of durations (with $K = 78$). The parameter estimates are reported in Table 4.4.

4.4.2 Daily Volatility Forecasting

We denote some selected IV measure at day d by $\widehat{V}_d$, and define the multi-day moving averages of daily volatility measures as follows:

$$\widehat{V}_d^{(w)} = \frac{1}{5}\sum_{d=1}^{5}\widehat{V}_{d-i+1} \qquad \text{and} \qquad \widehat{V}_d^{(m)} = \frac{1}{22}\sum_{d=1}^{22}\widehat{V}_{d-i+1}, \tag{4.41}$$

where $\widehat{V}_d^{(w)}$ represents the one-week average and $\widehat{V}_d^{(m)}$ denotes the one-month average of daily IV estimates, respectively. The standard one-day-ahead HAR model has the following structure:

$$\widehat{V}_d = \omega + \beta^{(d)}\widehat{V}_{d-1} + \beta^{(w)}\widehat{V}_{d-1}^{(w)} + \beta^{(m)}\widehat{V}_{d-1}^{(m)} + \varepsilon_d. \tag{4.42}$$

As demonstrated by numerous empirical applications in the literature, the implementation of a more refined volatility measure on the right-hand side (RHS) can better exploit the information, and has the potential to significantly improve the predictive accuracy of the HAR model for the left-hand side (LHS) target variable. In this section, we compare the predictability of HAR models augmented with different IV measures, including our duration-based IV estimator.

To construct our duration-based IV estimator based on the adaptive PDS, we utilize all trading days from January 2014 to December 2016 as the burn-in period, which allows us to forecast the first K-adaptive daily threshold in 2017. The initial in-sample period includes 1000 days from January 3, 2017. We estimate the log-ACD-GARCH model in Eq. (4.21) (with the same lag choices as in Section 4.4.1) to obtain all IV estimates in the initial in-sample

period, and then forecast the first out-of-sample IV (on the 1001-th day) with the HAR model in Eq. (4.42). This procedure of in-sample estimation and out-of-sample forecasting is repeated in both rolling-window (RW) and expanding-window (EW) fashion. For the actual values of out-of-sample IV estimates on subsequent days, we repeatedly re-estimate the log-ACD-GARCH model with all durations in the corresponding "in-sample plus one day" period.

Similar to Section 4.3, we consider three different values of K (78, 39, and 26), which correspond to similar levels of sparsity of 5, 10 and 15-minute sampling for return-based IV estimators. In addition to the standard HAR model augmented with our duration-based estimator and some return-based measures, we also consider two important extensions of the original HAR-RV model of Corsi (2009): One is the HARQ model of Bollerslev et al. (2016). It allows for a time-varying coefficient for the daily RV on the RHS, which also depends on the heteroskedasticity in the error, captured by the realized quarticity (RQ) estimator:[7]

$$\widehat{V}_d = \omega + \left(\beta^{(d)} + \beta^{(q)}\sqrt{\mathrm{RQ}_{d-1}}\right)\mathrm{RV}_{d-1} + \beta^{(w)}\mathrm{RV}_{d-1}^{(w)} + \beta^{(m)}\mathrm{RV}_{d-1}^{(m)} + \varepsilon_d, \tag{4.43}$$

where $\mathrm{RQ}_d = 3^{-1}n\sum_{i=1}^{n} r_{d,i}^4$. Inspired by the intuition that "good" and "bad" volatilities have different effects, the semivariance HAR (SHAR) model of Patton and Sheppard (2015) stands out as another important HAR-RV modification:

$$\widehat{V}_d = \omega + \beta_-^{(d)}\mathrm{RS}_{d-1}^- + \beta_+^{(d)}\mathrm{RS}_{d-1}^+ + \beta^{(w)}\mathrm{RV}_{d-1}^{(w)} + \beta^{(m)}\mathrm{RV}_{d-1}^{(m)} + \varepsilon_d, \tag{4.44}$$

where the realized semivariances (RS) are introduced by Barndorff-Nielsen et al. (2010):

$$\mathrm{RS}_d^- = \sum_{i=1}^{n} r_{d,i}^2 \mathbb{1}_{\{r_{d,i}<0\}}, \tag{4.45}$$

$$\mathrm{RS}_d^+ = \sum_{i=1}^{n} r_{d,i}^2 \mathbb{1}_{\{r_{d,i}>0\}}. \tag{4.46}$$

We evaluate the out-of-sample forecasting performance via two widely used loss functions, i.e.,

[7] Following Bollerslev et al. (2016), the "insanity filter" of Swanson and White (1997) is applied: For each rolling or expanding window, the minimum, maximum, and average of in-sample estimates are re-calculated. All one-step-ahead out-of-sample forecasts that are greater (smaller) than the maximum (minimum) in-sample value will be replaced by the in-sample mean.

the mean squared error (MSE) and the quasi-likelihood (QLIKE) function:

$$\text{MSE}(\theta, h) = (\theta - h)^2, \tag{4.47}$$

$$\text{QLIKE}(\theta, h) = \frac{\theta}{h} - \ln\left(\frac{\theta}{h}\right) - 1, \tag{4.48}$$

where θ and h represent the actual value and the forecast of the target variable, respectively.

Table 4.5 reports the MSE and QLIKE results for one-day-ahead out-of-sample forecasts of two different target IV measures: RV and our duration-based IV estimator. For 5-minute and 10-minute RV forecasts, both the HARQ and SHAR models produce lower QLIKE results compared to the original HAR-RV model, while the HARQ model tends to obtain more misinformative forecasts in the tails, as indicated by its higher MSE results. However, this advantage of both HAR-RV modifications disappears when we forecast the 15-minute RV and our duration-based IV estimator across all considered sampling frequencies. Compared with the HAR models augmented with other volatility estimators, the HAR model based on our duration-based IV estimator ("duration-based HAR") consistently obtains substantially diminished MSE and relatively lower QLIKE results. The HAR-TRV model performs the best among all alternatives, which achieves the second smallest MSE results in all cases. As the MSE function penalizes outliers heavily and is sensitive to excessively inaccurate forecasts, the MSE results in Table 4.5 suggest that the duration-based HAR model can effectively reduce the occurrence of extremely misinformative forecasts in both left and right tails.

Table 4.6 presents the p-values of the modified Diebold-Mariano test (with Newey-West HAC standard errors) based on MSE for the null hypothesis that the accuracy of duration-based HAR forecasts is inferior to the forecasts from an alternative HAR model. For the duration-based forecasts with $K = 78$, the Diebold-Mariano test indicates rejection at the 1% significance level for all return-based HAR alternatives, except for HAR-TRV, where rejection occurs at the 10% level. For the duration-based forecasts with $K = 39$ and 26, most of the entries in Panels B and C of Table 4.6 are well below 50%, which indicates a preference for the duration-based HAR forecasts, although with less robust statistical significance compared to the $K = 78$ case.

Table 4.5 Daily out-of-sample HAR volatility forecasts

	RV				Duration-based $\widehat{V}_d$			
	RW		EW		RW		EW	
	MSE	QLIKE	MSE	QLIKE	MSE	QLIKE	MSE	QLIKE
HAR-RV-5 min	3.85	0.37	3.86	0.35	2.12	0.17	2.11	0.17
HARQ-5 min	4.10	0.32	4.07	0.31	2.42	0.18	2.32	0.17
SHAR-5 min	3.85	0.36	3.85	0.34	2.12	0.17	2.11	0.16
HAR-RBPV-5 min	3.89	0.38	3.90	0.36	2.14	0.18	2.12	0.17
HAR-TRV-5 min	3.72	0.35	3.73	0.33	1.96	0.15	1.96	0.15
HAR-Duration ($K = 78$)	3.43	0.35	3.44	0.33	1.74	0.16	1.74	0.15
HAR-RV-10 min	3.64	0.39	3.64	0.37	1.60	0.12	1.59	0.12
HARQ-10 min	3.95	0.35	3.91	0.34	1.85	0.12	1.74	0.12
SHAR-10 min	3.59	0.37	3.58	0.35	1.73	0.12	1.64	0.12
HAR-RBPV-10 min	3.83	0.36	3.82	0.35	1.90	0.14	1.85	0.14
HAR-TRV-10 min	3.73	0.36	3.73	0.34	1.64	0.11	1.62	0.11
HAR-Duration ($K = 39$)	3.37	0.36	3.37	0.35	1.44	0.12	1.43	0.11
HAR-RV-15 min	4.32	0.42	4.32	0.40	2.00	0.10	1.98	0.10
HARQ-15 min	4.16	0.45	4.18	0.42	1.82	0.12	1.82	0.11
SHAR-15 min	4.51	0.44	4.41	0.42	2.20	0.11	2.09	0.10
HAR-RBPV-15 min	4.15	0.41	4.14	0.40	1.90	0.11	1.88	0.11
HAR-TRV-15 min	3.86	0.44	3.87	0.41	1.62	0.10	1.62	0.10
HAR-Duration ($K = 26$)	3.79	0.42	3.79	0.39	1.51	0.10	1.51	0.10

This table reports the MSE ($\times 10^4$) and QLIKE results of daily out-of-sample volatility forecasts for the SPDR S&P 500 ETF Trust (SPY). The HAR model is re-estimated via OLS in rolling windows and expanding windows, respectively. The fixed (resp. initial) in-sample period for RW (resp. EW) estimation is the first 1000 days. For the actual values of out-of-sample duration-based IV estimates on subsequent days, we re-estimate the log-ACD-GARCH model with all durations in each corresponding "in-sample plus one day" period.

4.4.3 Intraday Volatility Dynamics Around FOMC Announcements

The short-term impact of macroeconomic news announcements on high-frequency intraday price, volume and volatility dynamics has received a lot of attention from the financial economics and econometrics literature (Andersen et al., 2003b, 2007b; Lee and Mykland, 2008, 2012; Bollerslev et al., 2018, 2021). Some recent macroeconomics literature also identifies monetary shocks based on the assumption that the market volatility tends to spike during specific public news announcements such as those associated with FOMC meetings (Nakamura and Steinsson, 2018). Here we apply our duration-based spot volatility estimator to examine the short-term impact of FOMC news announcements on intraday volatility dynamics.

We split our sample period from 2017 to 2022 (with the burn-in period excluded) into two subsets: 98 days with pre-scheduled FOMC announcements ("FOMC days"), and those without FOMC announcements ("non-FOMC days"). Fig. 4.6 demonstrates the average annualized spot volatility estimates for each 5-minute intervals on FOMC and non-FOMC days, respectively. We clearly observe an instant and substantial volatility spike around 14:00 ET on FOMC days,

Table 4.6 Diebold-Mariano p-values for duration-based volatility forecasts

	RV		Duration-based $\widehat{V}_d$	
	RW	EW	RW	EW
Panel A: HAR-Duration ($K = 78$):				
HAR-RV-5 min	0.0013	0.0014	0.0034	0.0038
HARQ-5 min	0.0004	0.0004	0.0004	0.0005
SHAR-5 min	0.0017	0.0039	0.0046	0.0068
HAR-RBRV-5 min	0.0005	0.0006	0.0012	0.0014
HAR-TRV-5 min	0.0256	0.0251	0.0873	0.0863
Panel B: HAR-Duration ($K = 39$):				
HAR-RV-10 min	0.0977	0.0963	0.2222	0.2276
HARQ-10 min	0.0076	0.0098	0.0212	0.0459
SHAR-10 min	0.1742	0.2234	0.1074	0.1565
HAR-RBRV-10 min	0.0276	0.0307	0.0201	0.0236
HAR-TRV-10 min	0.0855	0.0855	0.1971	0.2113
Panel C: HAR-Duration ($K = 26$):				
HAR-RV-15 min	0.0372	0.0366	0.0499	0.0514
HARQ-15 min	0.1197	0.0989	0.1256	0.1083
SHAR-15 min	0.0116	0.0194	0.0137	0.0227
HAR-RBRV-15 min	0.0600	0.0633	0.0130	0.0151
HAR-TRV-15 min	0.7462	0.6955	0.4750	0.4561

This table reports the p-values of the modified Diebold-Mariano test (with Newey-West HAC standard errors) based on MSE. The null hypothesis is that the accuracy of duration-based HAR forecasts is inferior to the forecasts from an alternative HAR model.

but it is absent on non-FOMC days, which is in line with the findings in Bollerslev et al. (2021). Moreover, the volatility after the FOMC announcements remains significantly higher compared to non-FOMC days.

Additionally, the estimated spot volatilities in all 5-minute blocks display a clear asymmetric U-shaped or reverse J-shaped pattern over the trading hours, which is consistent with both our simulation specifications in Section 4.3 and empirical evidence in the literature, e.g., Christensen et al. (2018), and Andersen et al. (2018, 2019, 2023b).

4.5 Conclusions

This chapter introduces a novel semiparametric framework for duration-based volatility estimation. We employ daily adaptive thresholds to separate daily volatility dynamics from the intraday durations over an extended period spanning multiple days. Both spot and integrated volatility estimators are formulated based on a classical parametric duration model. This methodology to disentangle daily and intraday volatility dynamics greatly enhances the data availability for model estimation, which overcomes the limitations of sparse sampling widely

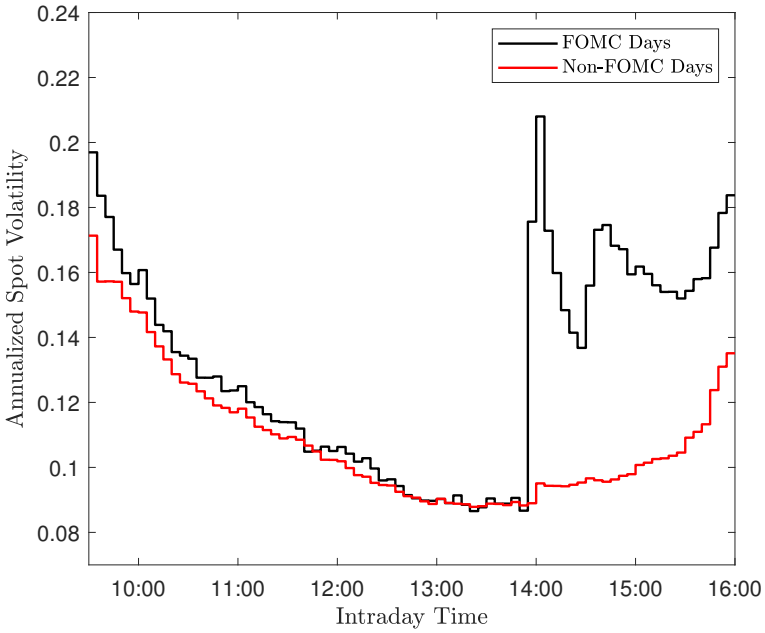

Fig. 4.6 Annualized spot volatility estimates for each equidistant intervals with $\Delta = 5$ minutes. The durations are obtained with the K-adaptive threshold with $K = 78$.

adopted in both the financial econometrics literature and by practitioners, and potentially leads to more accurate volatility estimates. The simulation results demonstrate the superior finite-sample performance of our duration-based volatility estimators compared to selected competitors. In an empirical illustration of daily volatility forecasting, we observe that the HAR model augmented with our duration-based IV estimator can effectively reduce the occurrence of extremely misleading forecasts, and improves forecasting accuracy according to standard out-of-sample loss functions. Furthermore, based on our spot volatility estimator, we identify an immediate and substantial short-term impact of FOMC news announcements on intraday volatility.

References

Aït-Sahalia, Y. and Jacod, J. (2009). Testing for jumps in a discretely observed process. *Annals of Statistics*, 37(1):184–222.

Aït-Sahalia, Y. and Jacod, J. (2014). *High-Frequency Financial Econometrics*. Princeton University Press.

Aït-Sahalia, Y., Jacod, J., and Li, J. (2012). Testing for jumps in noisy high frequency data. *Journal of Econometrics*, 168(2):207–222.

Aït-Sahalia, Y. and Kimmel, R. (2007). Maximum likelihood estimation of stochastic volatility models. *Journal of Financial Economics*, 83(2):413–452.

Aït-Sahalia, Y., Mykland, P. A., and Zhang, L. (2005). How often to sample a continuous-time process in the presence of market microstructure noise. *Review of Financial Studies*, 18(2):351–416.

Aït-Sahalia, Y., Mykland, P. A., and Zhang, L. (2011). Ultra high frequency volatility estimation with dependent microstructure noise. *Journal of Econometrics*, 160(1):160–175.

Alizadeh, S., Brandt, M. W., and Diebold, F. X. (2002). Range-based estimation of stochastic volatility models. *Journal of Finance*, 57(3):1047–1091.

Amemiya, T. (1985). *Advanced Econometrics*. Harvard University Press.

Andersen, T. G., Archakov, I., Cebiroglu, G., and Hautsch, N. (2022). Local mispricing and microstructural noise: A parametric perspective. *Journal of Econometrics*, 230(2):510–534.

Andersen, T. G. and Bollerslev, T. (1997). Intraday periodicity and volatility persistence in financial markets. *Journal of Empirical Finance*, 4(2-3):115–158.

Andersen, T. G. and Bollerslev, T. (1998). Answering the skeptics: Yes, standard volatility models do provide accurate forecasts. *International Economic Review*, 39(4):885–905.

Andersen, T. G., Bollerslev, T., and Diebold, F. X. (2007a). Roughing it up: Including jump components in the measurement, modeling, and forecasting of return volatility. *Review of Economics and Statistics*, 89(4):701–720.

Andersen, T. G., Bollerslev, T., Diebold, F. X., and Labys, P. (2003a). Modeling and forecasting realized volatility. *Econometrica*, 71(2):579–625.

Andersen, T. G., Bollerslev, T., Diebold, F. X., and Vega, C. (2003b). Micro effects of macro announcements: Real-time price discovery in foreign exchange. *American Economic Review*, 93(1):38–62.

Andersen, T. G., Bollerslev, T., Diebold, F. X., and Vega, C. (2007b). Real-time price discovery in global stock, bond and foreign exchange markets. *Journal of International Economics*, 73(2):251–277.

Andersen, T. G., Bollerslev, T., and Dobrev, D. (2007c). No-arbitrage semi-martingale restrictions for continuous-time volatility models subject to leverage effects, jumps and i.i.d. noise: Theory and testable distributional implications. *Journal of Econometrics*, 138(1):125–180.

Andersen, T. G., Bondarenko, O., Kyle, A. S., and Obizhaeva, A. A. (2018). Intraday trading invariance in the E-mini S&P 500 futures market. Working Paper.

Andersen, T. G., Dobrev, D., and Schaumburg, E. (2008). Duration-based volatility estimation. Working Paper.

Andersen, T. G., Dobrev, D., and Schaumburg, E. (2012). Jump-robust volatility estimation using nearest neighbor truncation. *Journal of Econometrics*, 169(1):75–93.

Andersen, T. G., Li, Y., Todorov, V., and Zhou, B. (2023a). Volatility measurement with pockets of extreme return persistence. *Journal of Econometrics*, 237(2):105439.

Andersen, T. G., Su, T., Todorov, V., and Zhang, Z. (2023b). Intraday periodic volatility curves. *Journal of the American Statistical Association*, forthcoming.

Andersen, T. G., Thyrsgaard, M., and Todorov, V. (2019). Time-varying periodicity in intraday volatility. *Journal of the American Statistical Association*, 114(528):1695–1707.

Andersen, T. G., Todorov, V., and Zhou, B. (2023c). Real-time detection of local no-arbitrage violations. Working Paper.

Anscombe, F. J. (1952). Large-sample theory of sequential estimation. *Mathematical Proceedings of the Cambridge Philosophical Society*, 48(4):600–607.

Asmussen, S., Glynn, P., and Pitman, J. (1995). Discretization error in simulation of one-dimensional reflecting Brownian motion. *Annals of Applied Probability*, 5(4):875–896.

Bajgrowicz, P., Scaillet, O., and Treccani, A. (2016). Jumps in high-frequency data: Spurious detections, dynamics, and news. *Management Science*, 62(8):2198–2217.

Ball, C. A. and Torous, W. N. (1984). The maximum likelihood estimation of security price volatility: Theory, evidence, and application to option pricing. *Journal of Business*, 57(1):97–112.

Bandi, F. M. and Renò, R. (2016). Price and volatility co-jumps. *Journal of Financial Economics*, 119(1):107–146.

Bandi, F. M. and Russell, J. R. (2008). Microstructure noise, realized variance, and optimal sampling. *Review of Economic Studies*, 75(2):339–369.

Barndorff-Nielsen, O. E., Hansen, P. R., Lunde, A., and Shephard, N. (2009). Realized kernels in practice: Trades and quotes. *Econometrics Journal*, 12(3):1–32.

Barndorff-Nielsen, O. E., Kinnebrock, S., and Shephard, N. (2010). Measuring downside risk – realised semivariance. in T. Bollerslev, J. Russell, and M. Watson, eds., *Volatility and Time Series Econometrics: Essays in Honor of Robert F. Engle*, New York: Oxford University Press, 2010.

Barndorff-Nielsen, O. E. and Shephard, N. (2002). Econometric analysis of realized volatility and its use in estimating stochastic volatility models. *Journal of the Royal Statistical Society Series B: Statistical Methodology*, 64(2):253–280.

Barndorff-Nielsen, O. E. and Shephard, N. (2004). Power and bipower variation with stochastic volatility and jumps. *Journal of Financial Econometrics*, 2(1):1–37.

Barndorff-Nielsen, O. E. and Shephard, N. (2006). Econometrics of testing for jumps in financial economics using bipower variation. *Journal of Financial Econometrics*, 4(1):1–30.

Barndorff-Nielsen, O. E. and Shiryaev, A. N. (2015). *Change of Time and Change of Measure*. World Scientific Publishing.

Beckers, S. (1983). Variances of security price returns based on high, low, and closing prices. *Journal of Business*, 56(1):97–112.

Bellia, M., Christensen, K., Kolokolov, A., Pelizzon, L., and Renò, R. (2024). Do designated market makers provide liquidity during extreme price movements? Working Paper.

Bibinger, M. and Winkelmann, L. (2015). Econometrics of co-jumps in high-frequency data with noise. *Journal of Econometrics*, 184(2):361–378.

Bollerslev, T. (1986). Generalized autoregressive conditional heteroskedasticity. *Journal of Econometrics*, 31(3):307–327.

Bollerslev, T. (2022). Realized semi(co)variation: Signs that all volatilities are not created equal. *Journal of Financial Econometrics*, 20(2):219–252.

Bollerslev, T., Li, J., and Li, Q. (2024). Optimal nonparametric range-based volatility estimation. *Journal of Econometrics*, 238(1):105548.

Bollerslev, T., Li, J., and Liao, Z. (2021). Fixed-k inference for volatility. *Quantitative Economics*, 12(4):1053–1084.

Bollerslev, T., Li, J., and Xue, Y. (2018). Volume, volatility, and public news announcements. *Review of Economic Studies*, 85(4):2005–2041.

Bollerslev, T., Li, S. Z., and Zhao, B. (2020). Good volatility, bad volatility, and the cross section of stock returns. *Journal of Financial and Quantitative Analysis*, 55(3):751–781.

Bollerslev, T., Patton, A. J., and Quaedvlieg, R. (2016). Exploiting the errors: A simple approach for improved volatility forecasting. *Journal of Econometrics*, 192(1):1–18.

Bollerslev, T., Todorov, V., and Xu, L. (2015). Tail risk premia and return predictability. *Journal of Financial Economics*, 118(1):113–134.

Borodin, A. N. and Salminen, P. (2002). *Handbook of Brownian Motion: Facts and Formulae*. Springer, Second edition.

Bouchaud, J.-P., Krueger, P., Landier, A., and Thesmar, D. (2019). Sticky expectations and the profitability anomaly. *Journal of Finance*, 74(2):639–674.

Brandt, M. W. and Diebold, F. X. (2006). A no-arbitrage approach to range-based estimation of return covariances and correlations. *Journal of Business*, 79(1):61–74.

Caporin, M., Kolokolov, A., and Renò, R. (2017). Systemic co-jumps. *Journal of Financial Economics*, 126(3):563–591.

CFTC and SEC (2010). Findings regarding the market events of May 6, 2010: Report of the staffs of the CFTC and SEC to the Joint Advisory Committee on Emerging Regulatory Issues. Available at https://www.sec.gov/files/marketevents-report.pdf.

Chernozhukov, V., Chetverikov, D., and Kato, K. (2013). Gaussian approximations and multiplier bootstrap for maxima of sums of high-dimensional random vectors. *Annals of Statistics*, 41(6):2786–2819.

Chernozhukov, V., Chetverikov, D., and Kato, K. (2019). Inference on causal and structural parameters using many moment inequalities. *Review of Economic Studies*, 86(5):1867–1900.

Christensen, K., Hounyo, U., and Podolskij, M. (2018). Is the diurnal pattern sufficient to explain intraday variation in volatility? A nonparametric assessment. *Journal of Econometrics*, 205(2):336–362.

Christensen, K. and Kolokolov, A. (2023). An unbounded intensity model for point process. Working Paper.

Christensen, K., Oomen, R., and Renò, R. (2022). The drift burst hypothesis. *Journal of Econometrics*, 227(2):461–497.

Christensen, K., Oomen, R. C., and Podolskij, M. (2014). Fact or friction: Jumps at ultra high frequency. *Journal of Financial Economics*, 114(3):576–599.

Christensen, K. and Podolskij, M. (2007). Realized range-based estimation of integrated variance. *Journal of Econometrics*, 141(2):323–349.

Christensen, K. and Podolskij, M. (2012). Asymptotic theory of range-based multipower variation. *Journal of Financial Econometrics*, 10(3):417–456.

Christensen, K., Podolskij, M., and Vetter, M. (2009). Bias-correcting the realized range-based variance in the presence of market microstructure noise. *Finance and Stochastics*, 13(2):239–268.

Coibion, O. and Gorodnichenko, Y. (2015). Information rigidity and the expectations formation process: A simple framework and new facts. *American Economic Review*, 105(8):2644–2678.

Corsi, F. (2009). A simple approximate long-memory model of realized volatility. *Journal of Financial Econometrics*, 7(2):174–196.

Corsi, F., Pirino, D., and Renò, R. (2010). Threshold bipower variation and the impact of jumps on volatility forecasting. *Journal of Econometrics*, 159(2):276–288.

Cremers, M., Halling, M., and Weinbaum, D. (2015). Aggregate jump and volatility risk in the cross-section of stock returns. *Journal of Finance*, 70(2):577–614.

Da, R. and Xiu, D. (2021). When moving-average models meet high-frequency data: Uniform inference on volatility. *Econometrica*, 89(6):2787–2825.

Daley, D. J. and Vere-Jones, D. (2003). *An Introduction to the Theory of Point Processes, Volume I: Elementary Theory and Methods*. Springer, 2nd Edition.

Dieker, A. and Lagos, G. (2017). On the Euler discretization error of Brownian motion about random times. Working Paper.

Dimitriadis, T. and Halbleib, R. (2022). Realized quantiles. *Journal of Business & Economic Statistics*, 40(3):1346–1361.

Dimitriadis, T., Halbleib, R., Polivka, J., Rennspies, J., Streicher, S., and Wolter, A. F. (2023). Efficient sampling for realized variance estimation in time-changed diffusion models. Working Paper.

Duembgen, M. and Podolskij, M. (2015). High-frequency asymptotics for path-dependent functionals of Itô semimartingales. *Stochastic Processes and their Applications*, 125(4):1195–1217.

Dumitru, A.-M. and Urga, G. (2012). Identifying jumps in financial assets: A comparison between nonparametric jump tests. *Journal of Business & Economic Statistics*, 30(2):242–255.

Durrett, R. (2019). *Probability: Theory and Examples*. Cambridge University Press, Fifth edition.

Engle, R. F. (1982). Autoregressive nditional heteroscedasticity with estimates of the variance of United Kingdom inflation. *Econometrica*, 50(4):987–1007.

Engle, R. F. and Russell, J. R. (1998). Autoregressive conditional duration: A new model for irregularly spaced transaction data. *Econometrica*, 66(5):1127–1162.

Eraker, B., Johannes, M., and Polson, N. (2003). The impact of jumps in volatility and returns. *Journal of Finance*, 58(3):1269–1300.

Fan, J. and Yao, Q. (2003). *Nonlinear Time Series: Nonparametric and Parametric Methods*. Springer.

Farmer, L., Schmidt, L., and Timmermann, A. (2023). Pockets of predictability. *Journal of Finance*, 78(3):1279–1341.

Feller, W. (1951). The asymptotic distribution of the range of sums of independent random variables. *Annals of Mathematical Statistics*, 22(3):427–432.

Flora, M. and Renò, R. (2022). V-shapes. Working Paper.

Foster, D. P. and Nelson, D. B. (1996). Continuous record asymptotics for rolling sample variance estimators. *Econometrica*, 64(1):139.

Fukasawa, M. and Rosenbaum, M. (2012). Central limit theorems for realized volatility under hitting times of an irregular grid. *Stochastic Processes and their Applications*, 122(12):3901–3920.

Garman, M. B. and Klass, M. J. (1980). On the estimation of security price volatilities from historical data. *Journal of Business*, 53(1):67–78.

Gatheral, J., Jaisson, T., and Rosenbaum, M. (2018). Volatility is rough. *Quantitative Finance*, 18(6):933–949.

Gerhard, F. and Hautsch, N. (2002). Volatility estimation on the basis of price intensities. *Journal of Empirical Finance*, 9(1):57–89.

Gloter, A. and Jacod, J. (2001). Diffusions with measurement errors. I. Local asymptotic normality. *ESAIM: Probability and Statistics*, 5:225–242.

Golub, A., Keane, J., and Poon, S.-H. (2012). High frequency trading and mini flash crashes. Working Paper.

Grigelionis, B. (1980). A martingale approach to the statistical problems of point processes. *Scandinavian Journal of Statistics*, 7(4):190–196.

Gut, A. (2009). *Stopped Random Walks: Limit Theorems and Applications*. Springer, Second edition.

Gut, A. (2012). Anscombe's theorem 60 years later. *Sequential Analysis*, 31(3):368–396.

Hansen, P. R. and Lunde, A. (2006). Realized variance and market microstructure noise. *Journal of Business & Economic Statistics*, 24(2):127–161.

Harris, L. (1986). A transaction data study of weekly and intradaily patterns in stock returns. *Journal of Financial Economics*, 16(1):99–117.

Hasbrouck, J. (1999). The dynamics of discrete bid and ask quotes. *Journal of Finance*, 54(6):2109–2142.

Hautsch, N. (2011). *Econometrics of Financial High-Frequency Data*. Springer.

Hautsch, N. and Podolskij, M. (2013). Preaveraging-based estimation of quadratic variation in the presence of noise and jumps: Theory, implementation, and empirical evidence. *Journal of Business & Economic Statistics*, 31(2):165–183.

Heston, S. L. (1993). A closed-form solution for options with stochastic volatility with applications to bond and currency options. *Review of Financial Studies*, 6(2):327–343.

Hoffmann, M., Vetter, M., and Dette, H. (2018). Nonparametric inference of gradual changes in the jump behaviour of time-continuous processes. *Stochastic Processes and their Applications*, 128(11):3679–3723.

Holden, C. W. and Jacobsen, S. (2014). Liquidity measurement problems in fast, competitive markets: Expensive and cheap solutions. *Journal of Finance*, 69(4):1747–1785.

Hong, S. Y., Nolte, I., Taylor, S. J., and Zhao, X. (2023). Volatility estimation and forecasts based on price durations. *Journal of Financial Econometrics*, 21(1):106–144.

Huang, X. and Tauchen, G. (2005). The relative contribution of jumps to total price variance. *Journal of Financial Econometrics*, 3(4):456–499.

Ibragimov, I. A. (1962). Some limit theorems for stationary processes. *Theory of Probability & Its Applications*, 7(4):349–382.

Ibragimov, I. A. and Linnik, Y. V. (1971). *Independent and Stationary Sequences of Random Variables*. Wolters-Noordhoff.

Jacod, J., Li, Y., Mykland, P. A., Podolskij, M., and Vetter, M. (2009). Microstructure noise in the continuous case: The pre-averaging approach. *Stochastic Processes and their Applications*, 119(7):2249–2276.

Jacod, J., Li, Y., and Zheng, X. (2017). Statistical properties of microstructure noise. *Econometrica*, 85(4):1133–1174.

Jacod, J., Li, Y., and Zheng, X. (2019). Estimating the integrated volatility with tick observations. *Journal of Econometrics*, 208(1):80–100.

Jacod, J. and Todorov, V. (2010). Do price and volatility jump together? *Annals of Applied Probability*, 20(4):1425–1469.

Jacod, J. and Todorov, V. (2014). Efficient estimation of integrated volatility in presence of infinite variation jumps. *Annals of Statistics*, 42(3):1029–1069.

Jacod, J. and Todorov, V. (2018). Limit theorems for integrated local empirical characteristic exponents from noisy high-frequency data with application to volatility and jump activity estimation. *Annals of Applied Probability*, 28(1):511–576.

Jiang, G. J. and Oomen, R. C. (2008). Testing for jumps when asset prices are observed with noise – a "swap variance" approach. *Journal of Econometrics*, 144(2):352–370.

Jiang, G. J. and Yao, T. (2013). Stock price jumps and cross-sectional return predictability. *Journal of Financial and Quantitative Analysis*, 48(5):1519–1544.

Kalnina, I. and Linton, O. (2008). Estimating quadratic variation consistently in the presence of endogenous and diurnal measurement error. *Journal of Econometrics*, 147(1):47–59.

Khaniyev, T. and Kucuk, Z. (2004). Asymptotic expansions for the moments of the Gaussian random walk with two barriers. *Statistics & Probability Letters*, 69(1):91–103.

Kirilenko, A., Kyle, A. S., Samadi, M., and Tuzun, T. (2017). The flash crash: High-frequency trading in an electronic market. *Journal of Finance*, 72(3):967–998.

Kolokolov, A. (2023). Cryptocrashes. Working Paper.

Kolokolov, A. and Renò, R. (2024). Jumps or staleness? *Journal of Business & Economic Statistics*, 24(2):516–532.

Kolokolov, A., Renò, R., and Zoi, P. (2023). BUMVU estimators. Working Paper.

Koopman, S. J., Lucas, A., and Scharth, M. (2016). Predicting time-varying parameters with parameter-driven and observation-driven models. *Review of Economics and Statistics*, 98(1):97–110.

Kunitomo, N. (1992). Improving the Parkinson method of estimating security price volatilities. *Journal of Business*, 65(2):295–302.

Laly, F. and Petitjean, M. (2020). Mini flash crashes: Review, taxonomy and policy responses. *Bulletin of Economic Research*, 72(3):251–271.

Laurent, S., Renò, R., and Shi, S. (2022). Realized drift. Working Paper.

Laurent, S. and Shi, S. (2020). Volatility estimation and jump detection for drift-diffusion processes. *Journal of Econometrics*, 217(2):259–290.

Laurent, S. and Shi, S. (2022). Unit root test with high-frequency data. *Econometric Theory*, 38(1):113–171.

Lee, S. S. and Mykland, P. A. (2008). Jumps in financial markets: a new nonparametric test and jump dynamics. *Review of Financial Studies*, 21(6):2535–2563.

Lee, S. S. and Mykland, P. A. (2012). Jumps in equilibrium prices and market microstructure noise. *Journal of Econometrics*, 168(2):396–406.

Li, J., Wang, D., and Zhang, Q. (2022). Reading the candlesticks: An OK estimator for volatility. *Review of Economics and Statistics*, forthcoming.

Li, Q., Li, Y., Nolte, I., Nolte, S., and Yu, S. (2024a). Testing for jumps in a discretely observed price process with endogenous sampling times. Working Paper.

Li, Y., Mykland, P. A., Renault, E., Zhang, L., and Zheng, X. (2014). Realized volatility when sampling times are possibly endogenous. *Econometric Theory*, 30(3):580–605.

Li, Y., Nolte, I., and Nolte, S. (2019). Renewal based volatility estimation. Working Paper.

Li, Y., Nolte, I., and Nolte, S. (2021). High-frequency volatility modeling: A Markov-switching autoregressive conditional intensity model. *Journal of Economic Dynamics and Control*, 124:104077.

Li, Y., Nolte, I., Nolte, S., and Yu, S. (2024b). Decoupling interday and intraday volatility dynamics with price durations. Working Paper.

Li, Y., Nolte, I., Nolte, S., and Yu, S. (2024c). Realized candlestick wicks. Working Paper.

Li, Z. M., Laeven, R. J., and Vellekoop, M. H. (2020). Dependent microstructure noise and integrated volatility estimation from high-frequency data. *Journal of Econometrics*, 215(2):536–558.

Li, Z. M. and Linton, O. (2022). A ReMeDI for microstructure noise. *Econometrica*, 90(1):367–389.

Liu, L. Y., Patton, A. J., and Sheppard, K. (2015). Does anything beat 5-minute RV? a comparison of realized measures across multiple asset classes. *Journal of Econometrics*, 187(1):293–311.

Lorden, G. (1970). On excess over the boundary. *Annals of Mathematical Statistics*, 41(2):520–527.

Lotov, V. I. (1996). On some boundary crossing problems for Gaussian random walks. *Annals of Probability*, 24(4):2154–2171.

Mancini, C. (2009). Non-parametric threshold estimation for models with stochastic diffusion coefficient and jumps. *Scandinavian Journal of Statistics*, 36(2):270–296.

Mancini, C. (2023). Drift burst test statistic in the presence of infinite variation jumps. *Stochastic Processes and their Applications*, 163:535–591.

Maneesoonthorn, W., Martin, G. M., and Forbes, C. S. (2020). High-frequency jump tests: Which test should we use? *Journal of Econometrics*, 219(2):478–487.

Martens, M. and van Dijk, D. (2007). Measuring volatility with the realized range. *Journal of Econometrics*, 138(1):181–207.

Meilijson, I. (2011). The Garman-Klass volatility estimator revisited. *Revstat*, 9(3):199–212.

Menkveld, A. J. and Yueshen, B. Z. (2019). The flash crash: A cautionary tale about highly fragmented markets. *Management Science*, 65(10):4470–4488.

Nakamura, E. and Steinsson, J. (2018). High-frequency identification of monetary non-neutrality: the information effect. *Quarterly Journal of Economics*, 133(3):1283–1330.

Nolte, I. and Xu, Q. (2015). The economic value of volatility timing with realized jumps. *Journal of Empirical Finance*, 34:45–59.

Parkinson, M. (1980). The extreme value method for estimating the variance of the rate of return. *Journal of Business*, 53(1):61–65.

Patton, A. J. and Sheppard, K. (2015). Good volatility, bad volatility: Signed jumps and the persistence of volatility. *Review of Economics and Statistics*, 97(3):683–697.

Pelger, M. (2020). Understanding systematic risk: A high-frequency approach. *Journal of Finance*, 75(4):2179–2220.

Pelletier, D. and Wei, W. (2023). A stochastic price duration model for estimating high-frequency volatility. *Journal of Financial Econometrics*, forthcoming.

Podolskij, M. and Ziggel, D. (2010). New tests for jumps in semimartingale models. *Statistical Inference for Stochastic Processes*, 13(1):15–41.

Rapach, D. and Zhou, G. (2013). Forecasting stock returns. in G. Elliott and A. Timmermann, eds., *Handbook of Economic Forecasting: Volume 2, Part A*, Amsterdam: Elsevier, 2013.

Reiß, M. (2011). Asymptotic equivalence for inference on the volatility from noisy observations. *Annals of Statistics*, 39(2):772–802.

Rényi, A. (1957). On the asymptotic distribution of the sum of a random number of independent random variables. *Acta Mathematica Academiae Scientiarum Hungarica*, 8:193–199.

Rogers, L. C. G. and Satchell, S. E. (1991). Estimating variance from high, low and closing prices. *Annals of Applied Probability*, 1(4):504–512.

Rogozin, B. A. (1964). On the distribution of the first jump. *Theory of Probability & Its Applications*, 9(3):450–465.

Swanson, N. R. and White, H. (1997). Forecasting economic time series using flexible versus fixed specification and linear versus nonlinear econometric models. *International Journal of Forecasting*, 13(4):439–461.

Taylor, S. J. (1982). Financial returns modelled by the product of two stochastic processes – A study of the daily sugar prices 1961-75. In Anderson, O. D., ed., *Time Series Analysis: Theory and Practice*. Vol. 1, North-Holland, 203–226.

Taylor, S. J. (1986). *Modelling Financial Time Series*. Chichester: John Wiley.

Taylor, S. J. (1994). Modeling stochastic volatility: A review and comparative study. *Mathematical Finance*, 4(2):183–204.

Taylor, S. J. (2005). *Asset Price Dynamics, Volatility, and Prediction*. Princeton University Press.

Theodosiou, M. and Žikeš, F. (2011). A comprehensive comparison of alternative tests for jumps in asset prices. Working Paper.

Todorov, V. and Tauchen, G. (2011). Volatility jumps. *Journal of Business & Economic Statistics*, 29(3):356–371.

Tse, Y.-K. and Yang, T. T. (2012). Estimation of high-frequency volatility: An autoregressive conditional duration approach. *Journal of Business & Economic Statistics*, 30(4):533–545.

Ubukata, M. and Oya, K. (2009). Estimation and testing for dependence in market microstructure noise. *Journal of Financial Econometrics*, 7(2):106–151.

Varneskov, R. T. (2017). Estimating the quadratic variation spectrum of noisy asset prices using generalized flat-top realized kernels. *Econometric Theory*, 33(6):1457–1501.

Vetter, M. (2010). Limit theorems for bipower variation of semimartingales. *Stochastic Processes and their Applications*, 120(1):22–38.

Vetter, M. and Zwingmann, T. (2017). A note on central limit theorems for quadratic variation in case of endogenous observation times. *Electronic Journal of Statistics*, 11(1):963–980.

Welch, I. and Goyal, A. (2008). A comprehensive look at the empirical performance of equity premium prediction. *Review of Financial Studies*, 21(4):1455–1508.

Wood, R. A., McInish, T. H., and Ord, J. K. (1985). An investigation of transactions data for NYSE stocks. *Journal of Finance*, 40(3):723–739.

Wu, C.-F. J. (1986). Jackknife, bootstrap and other resampling methods in regression analysis. *Annals of Statistics*, 14(4):1261–1295.

Xiu, D. (2010). Quasi-maximum likelihood estimation of volatility with high frequency data. *Journal of Econometrics*, 159(1):235–250.

Yan, S. (2011). Jump risk, stock returns, and slope of implied volatility smile. *Journal of Financial Economics*, 99(1):216–233.

Yang, D. and Zhang, Q. (2000). Drift-independent volatility estimation based on high, low, open, and close prices. *Journal of Business*, 73(3):477–492.

Zhang, L., Mykland, P. A., and Aït-Sahalia, Y. (2005). A tale of two time scales: Determining integrated volatility with noisy high-frequency data. *Journal of the American Statistical Association*, 100(472):1394–1411.

Zhou, B. (1996). High-frequency data and volatility in foreign-exchange rates. *Journal of Business & Economic Statistics*, 14(1):45–52.

Appendix A

Appendix to Chapter 2

A.1 Proofs

A.1.1 Proof of Theorems 2.1 and 2.2

Proof. Firstly, we demonstrate that the difference between the limiting behavior of functionals of squared normalized PDS returns $|r_i^{(c)}/c|^2$ (i) under Assumption 2.2 and (ii) under the time-changed regular observation scheme in Remark 2.4 becomes negligible under infill asymptotics.

In all the sequel, the positive constants K and K' varies from line to line, but never depends on n, N, and $N^{(c)}$, and the various indices i, j. Unless specifically stated, we assume $X(\omega)$ is continuous, i.e., $\omega \in \Omega'$.

Similar to the Assumption (S-HON) of Jacod et al. (2019), we impose the following stronger assumption without loss of generality by a classical localization procedure:

Assumption A.1. We have Assumptions 2.1 and 2.2 with $\tau_1 = \infty$. Moreover, the function δ and the processes μ, σ, λ, X are bounded, and we have $N \leq K\Delta_n^{-1}$ and $\mathbb{E}[\Delta_{n,i}^p] \leq K'\Delta_n^p$.

A.1.1.1 Intrinsic time

With an absolutely continuous time change from the calendar time t to intrinsic time $\tau(t)$:

$$t \mapsto \tau(t) = \int_0^t \sigma_s^2 ds, \tag{A.1}$$

the intrinsic-time counterpart of X adapted to $(\mathcal{F}_t)_{t\geq 0}$ is

$$\widetilde{X}_{\tau(t)} = \widetilde{X}_0 + \int_0^{\tau(t)} \widetilde{\mu}_s ds + \widetilde{W}_{\tau(t)}, \tag{A.2}$$

where $\widetilde{\mu}$ is time-changed processes corresponding to μ in Eq. (2.1), and $\widetilde{W} = (\widetilde{W}_\tau)_{\tau\geq 0}$ is a Brownian motion evolving in intrinsic time. The relation $\widetilde{X}_{\tau(t)} = X_t$ holds for all t, and the τ-time process $\widetilde{X} = (\widetilde{X}_{\tau(t)})_{t\geq 0}$ is adapted to $(\widetilde{\mathcal{F}}_{\tau(t)})_{t\geq 0}$ with the τ-time σ-algebra satisfying $\widetilde{\mathcal{F}}_{\tau(t)} = \mathcal{F}_t$ (Lemma 1.2, Barndorff-Nielsen and Shiryaev, 2015). Particularly, when X is a calendar-time local martingale, $\widetilde{X}$ is an intrinsic-time Brownian motion (with an initial condition), which is implied by the Dambis-Dubins-Schwarz theorem. To simplify our discussions and avoid unnecessary complications, we assume the drift coefficient $\mu = 0$, which does not affect our asymptotic results.

A.1.1.2 Observation schemes

We start with two sequences of observations of $X(\omega)$:

(I) Under Assumption 2.2: X_{t_i}, for all $i = 0, 1, 2, \ldots, N$,

(II) Equidistant observations in intrinsic time: $\widetilde{X}_{i\Delta_n}$, for all $i = 0, 1, 2, \ldots, N$.

For the ease of notation, we denote $t_i \equiv t_{n,i}$ under Assumption 2.2, and $\check{t}_i \equiv \tau^{-1}(i\Delta_n)$. The increments between successive observations are denoted by

$$r_i = X_{t_i} - X_{t_{i-1}} \qquad \text{and} \qquad \check{r}_i = X_{\check{t}_i} - X_{\check{t}_{i-1}}, \tag{A.3}$$

for all $i \in \{1, 2, \ldots, N\}$. Lemma A.1 of Jacod et al. (2017) indicates the sequence (I) is an $(\mathcal{F}_t^n)$-martingale with Gaussian increments. Different from the independent but not identically distributed increments r_i, the increments $\check{r}_i$ are i.i.d. normal with zero mean and variance Δ_n, which make the sequence (II) a homogenous Gaussian random walk.

Remark A.1. We assume both sequences have the same number $N \equiv N_1^n$ of observations. Assumption A.1 and Eq. (2.6) indicate that $T = \tau^{-1}(N\Delta_n)$ is bounded and $T \xrightarrow{\mathbb{P}} 1$ as $n \to \infty$. Moreover, by the triangle inequality and law of iterated expectations, Assumption 2.2 further implies $\mathbb{E}[|N\Delta_n - \tau(1)|] \leq K\Delta_n$, hence $|T - 1| = O_p(\Delta_n)$. That being said, the probability of jump occurrence in the "differenced part" of observation interval is negligible, see more

discussions in Section 2.3 of Aït-Sahalia and Jacod (2009). To fix ideas, let $\delta \to 0$, then $\mathbb{P}(X''_t \neq 0 \text{ for some } t \in [0,T] \triangle [0,1]) \leq \mathbb{P}(|T-1| > \delta) + \mathbb{P}(X''_t \neq 0 \text{ for some } t \in [1-\delta, 1+\delta]) = o(1)$, since we only assume potential jumps in $(0,1)$.

For each sequence of observations, we conduct the PDS with the barrier width $c = m\sqrt{\Delta_n}$. We denote the squared PDS returns from each sequence of sampled observations by

$$\begin{aligned} R_i &= (r_i^{(c)})^2, \qquad i \in \{1,2,...,N^{(c)}\}, \\ \breve{R}_i &= (\breve{r}_i^{(c)})^2, \qquad i \in \{1,2,...,\breve{N}^{(c)}\}. \end{aligned} \tag{A.4}$$

Note that the PDS returns $\breve{r}_i^{(c)}$ are i.i.d., as implied by the strong Markov property of the Gaussian random walk (II) and the symmetric feature of the stopping rule in Eq. (2.9).

A.1.1.3 Some lemmas

We define two supremum processes $(Y_j)_{1\leq j\leq N}$ and $(\breve{Y}_j)_{1\leq j\leq N}$ as

$$Y_j = \sup_{1\leq i\leq j} |X_{t_i}| \qquad \text{and} \qquad \breve{Y}_j = \sup_{1\leq i\leq j} |X_{\breve{t}_i}|. \tag{A.5}$$

Lemma A.1. For any fixed $1 \leq j \leq N$, it holds for the supremum processes that

$$|Y_j - \breve{Y}_j| = O_p(j^2 \Delta_n^{1+\kappa/2} \sqrt{L_n}), \tag{A.6}$$

where for the ease of notation, $L_n \equiv \log N \asymp \log(\Delta_n^{-1})$.

Proof. Let $\mathcal{D}_n \equiv \sigma(\Delta_{n,1}, \Delta_{n,2}, \ldots)$ denote the σ-algebra generated by observation times. Note that by the triangle inequality of ℓ_∞-norm

$$\begin{aligned} |Y_j - \breve{Y}_j| &= \Big| \max_{1\leq i\leq j} |X_{t_i}| - \max_{1\leq i\leq j} |X_{\breve{t}_i}| \Big| \\ &\leq \max_{1\leq i\leq j} |X_{t_i} - X_{\breve{t}_i}|. \end{aligned} \tag{A.7}$$

Note that by definition, we have with probability approaching 1,

$$\begin{aligned} X_{t_i} - X_{\check{t}_i} &= \sum_{\ell=1}^{i}\Big(\int_{t_{\ell-1}}^{t_\ell} \sigma_s dW_s - \int_{\check{t}_{\ell-1}}^{\check{t}_\ell} \sigma_s dW_s\Big) \\ &= \sum_{\ell=1}^{i}(\sigma_{t_{\ell-1}}(W_{t_\ell} - W_{t_{\ell-1}}) - \sigma_{\check{t}_{\ell-1}}(W_{\check{t}_\ell} - W_{\check{t}_{\ell-1}})) \\ &+ \sum_{\ell=1}^{i}\Big(\int_{t_{\ell-1}}^{t_\ell} (\sigma_s - \sigma_{t_{\ell-1}})dW_s - \int_{\check{t}_{\ell-1}}^{\check{t}_\ell} (\sigma_s - \sigma_{\check{t}_{\ell-1}})dW_s\Big) \\ &\equiv A_{n,i}^{(1)} + A_{n,i}^{(2)}. \end{aligned} \tag{A.8}$$

For the first term, by the maximal inequality of Gaussian variables, we have

$$\mathbb{E}\Big[\max_{1\le i\le j} |A_{n,i}^{(1)}|\Big|\mathcal{D}_n\Big] \le K\sqrt{L_n \max_{1\le i\le j}\Big|\sum_{\ell=1}^{i}(\Delta_{n,\ell}\lambda_{t_{\ell-1}} - \Delta_n)\Big|}. \tag{A.9}$$

For the right hand side, note that by the triangle inequality and Assumption 2.2 (ii),

$$\max_{1\le i\le j}\Big|\sum_{\ell=1}^{i}\mathbb{E}[|\Delta_{n,\ell}\lambda_{t_{\ell-1}} - \Delta_n||\mathcal{F}_{\ell-1}^n]\Big| \le Kj\Delta_n^{2+\kappa}. \tag{A.10}$$

Combining Eq. (A.9) and Eq. (A.10), it follows the law of iterated expectation that

$$\max_{1\le i\le j}|A_{n,i}^{(1)}| = O_p(j\Delta_n^{1+\kappa/2}\sqrt{L_n}). \tag{A.11}$$

For the second term in Eq. (A.8), by the maximal inequality, we have

$$\mathbb{E}\Big[\max_{1\le i\le j}|A_{n,i}^{(2)}|\Big] \le Kj\max_{1\le i\le j}\mathbb{E}[|A_{n,i}^{(2)}|] \le Kj^2\Delta_n^{3/2+\kappa/2}, \tag{A.12}$$

where the last step is by the Burkholder-Davis-Gundy inequality and smoothness of σ regulated by Assumption 2.1 (iii). The proof of required statement is completed by the triangle inequality and Eqs. (A.7), (A.8), (A.11) and (A.12). □

We define the first sampled observations for both sequences:

$$X_1^{(c)} = X_{\Pi_1^{(c)}} \qquad \text{and} \qquad \check{X}_1^{(c)} = X_{\tau^{-1}(\check{\Pi}_1^{(c)}\Delta_n)}, \tag{A.13}$$

which means that the $\Pi_1^{(c)}$-th and the $\breve{\Pi}_1^{(c)}$-th observations in (I) and (II), respectively, are the first to breach the symmetric double barrier. Lemma A.2 indicates that the first exit times of both sequences coincide with probability approaching 1 under infill asymptotics.

Lemma A.2. For $c = m\sqrt{\Delta_n}$, let $\overline{N}^{(c)} \equiv N^{(c)} \wedge \breve{N}^{(c)}$.

(i) For all integer $p \geq 1$, $\mathbb{E}[(\breve{\Pi}_1^{(c)})^p] < \infty$.

(ii) The first exit times for both sequences (I) and (II) satisfy

$$\mathbb{P}\Big(\max_{1 \leq i \leq \overline{N}^{(c)}} |\Pi_i^{(c)} - \breve{\Pi}_i^{(c)}| \geq 1 \Big) \leq K \Delta_n^{\kappa/2} \sqrt{L_n}. \tag{A.14}$$

Proof. (i) Note that $\breve{\Pi}_1^{(c)}$ has the same distribution as the number of steps for a standard Gaussian random walk $(Z_i)_{i=1,2,\ldots}$ to exit the double barrier $(-m, m)$. Let $h = \inf\{\tau : \widetilde{W}_\tau \notin (-m, m)\}$ denote the first exit time of the time-changed Brownian motion $\widetilde{W}$ from $(-m, m)$, then it is clear that $\breve{\Pi}_1^{(c)} - 1 \leq h$ by the continuity of Brownian motion, thus $\mathbb{E}[(\breve{\Pi}_1^{(c)} - 1)^p] \leq \mathbb{E}[h^p]$ for all $p > 0$. The Laplace transform of h is well-known in the literature, see, e.g., Eq. (3.0.1) in Borodin and Salminen (2002): $\mathbb{E}[e^{-\lambda h}] = \cosh^{-1}\sqrt{2\lambda} m$, and its Maclaurin series implies that $\mathbb{E}[h^p] < \infty$ for all integer $p \geq 1$. This completes the proof.

(ii) We start from the first term. By definition, we have

$$\mathbb{P}(\Pi_1^{(c)} \geq k) = \mathbb{P}(Y_k \leq c) \quad \text{and} \quad \mathbb{P}(\breve{\Pi}_1^{(c)} \geq k) = \mathbb{P}(\breve{Y}_k \leq c). \tag{A.15}$$

Let $\epsilon > 0$ be a positive number that can be arbitrarily small but not depend on N, it follows Lemma A.1 and the Markov inequality that

$$\begin{aligned}
\mathbb{P}(\Pi_1^{(c)} - \breve{\Pi}_1^{(c)} \geq 1) &= \sum_{k=1}^{N} \mathbb{P}(\breve{\Pi}_1^{(c)} = k) \mathbb{P}(\Pi_1^{(c)} > k | \breve{\Pi}_1^{(c)} = k) \\
&\leq \sum_{k=1}^{N} \mathbb{P}(\breve{\Pi}_1^{(c)} = k) \mathbb{P}(\breve{Y}_k - Y_k > \epsilon) \\
&\leq K \Delta_n^{1+\kappa/2} \sqrt{L_n} \Big[\sum_{k=1}^{N} k^2 \mathbb{P}(\breve{\Pi}_1^{(c)} = k) \Big] \\
&\leq K \Delta_n^{1+\kappa/2} \sqrt{L_n},
\end{aligned} \tag{A.16}$$

where the last line uses $\sum_{k=1}^{N} k^2 \mathbb{P}(\breve{\Pi}_1^{(c)} = k) \leq \mathbb{E}[(\breve{\Pi}_1^{(c)})^2] \leq K$ by Lemma A.2 (i). Similarly, we

can also show

$$\mathbb{P}(\breve{\Pi}_1^{(c)} - \Pi_1^{(c)} \geq 1) \leq K\Delta_n^{1+\kappa/2}\sqrt{L_n}. \tag{A.17}$$

Combining above results, we have

$$\mathbb{P}(|\Pi_1^{(c)} - \breve{\Pi}_1^{(c)}| \geq 1) \leq K\Delta_n^{1+\kappa/2}\sqrt{L_n}. \tag{A.18}$$

Now, note that for any $2 \leq q \leq \overline{N}^{(c)}$, we have

$$\begin{aligned}\mathbb{P}\Big(\max_{1\leq i\leq q}|\Pi_i^{(c)} - \breve{\Pi}_i^{(c)}| \geq 1\Big) \leq \mathbb{P}\Big(\max_{1\leq i\leq q-1}|\Pi_i^{(c)} - \breve{\Pi}_i^{(c)}| \geq 1\Big) \\ + \mathbb{P}(|\Pi_q^{(c)} - \breve{\Pi}_q^{(c)}| \geq 1 | \Pi_i^{(c)} = \breve{\Pi}_i^{(c)} \text{ for all } 1 \leq i \leq q-1).\end{aligned} \tag{A.19}$$

By the renewal property, we have $\Pi_q^{(c)} - \breve{\Pi}_q^{(c)} \overset{\mathcal{L}}{=} \Pi_1^{(c)} - \breve{\Pi}_1^{(c)}$ conditional on $\Pi_i^{(c)} = \breve{\Pi}_i^{(c)}$ for all $1 \leq i \leq q-1$. Therefore, using a same argument as in driving Eq. (A.18), we can show the second term is bounded by $K\Delta_n^{1+\kappa/2}\sqrt{L_n}$. Applying the above argument recursively, we have

$$\begin{aligned}\mathbb{P}\Big(\max_{1\leq i\leq \overline{N}^{(c)}}|\Pi_i^{(c)} - \breve{\Pi}_i^{(c)}| \geq 1\Big) &\leq K\overline{N}^{(c)}\Delta_n^{1+\kappa/2}\sqrt{L_n} \\ &\leq K\Delta_n^{\kappa/2}\sqrt{L_n},\end{aligned} \tag{A.20}$$

for which we use $\overline{N}^{(c)} \asymp \Delta_n^{-1}$. The proof is then completed. □

Lemma A.3. Strong approximation for sampled return, it holds that

$$\mathbb{P}\Big(\max_{1\leq i\leq \overline{N}^{(c)}}|r_i^{(c)} - \breve{r}_i^{(c)}| > K\Delta_n^{1+\kappa/8}\Big) \leq K'\Delta_n^{\kappa/8}\sqrt{L_n}. \tag{A.21}$$

Proof. It follows the maximal inequality of Gaussian variables that

$$\mathbb{E}\Big[\max_{1\leq i\leq N}|r_i - \breve{r}_i|\Big|\mathcal{D}_n\Big] \leq K\sqrt{L_n}\max_{1\leq i\leq N}\sqrt{|\mathbb{E}[\Delta_{n,i}\lambda_{t_{i-1}}|\mathcal{F}_{i-1}^n] - \Delta_n|} \leq K\Delta_n^{1+\kappa/2}\sqrt{L_n}. \tag{A.22}$$

Let $E_n \equiv \{\Pi_i^{(c)} = \breve{\Pi}_i^{(c)} \text{ for all } 1 \leq i \leq N^{(c)} = \breve{N}^{(c)}\}$, we have $\mathbb{P}(E_n^{\complement}) \leq K\Delta_n^{\kappa/2}\sqrt{L_n}$ by Lemma A.2 (ii). Note that by the maximal inequality, we have for any $p > 1$,

$$\mathbb{E}\Big[\max_{1\leq i\leq \breve{N}^{(c)}}|\breve{\Pi}_i^{(c)} - \breve{\Pi}_{i-1}^{(c)}|^p\Big] \leq \breve{N}^{(c)}\max_{1\leq i\leq \breve{N}^{(c)}}\mathbb{E}[|\breve{\Pi}_i^{(c)} - \breve{\Pi}_{i-1}^{(c)}|^p] \leq K_p\Delta_n^{-1}, \tag{A.23}$$

where the last step is by Lemma A.2 (i). Taking $p > 4/\kappa$ gives

$$\mathbb{E}\Big[\max_{1\le i\le \breve{N}^{(c)}} |\breve{\Pi}_i^{(c)} - \breve{\Pi}_{i-1}^{(c)}|^2\Big] \le K\Delta_n^{-\kappa/2}. \tag{A.24}$$

Moreover, by Cauchy-Schwarz inequality, we obtain

$$\begin{aligned}\mathbb{E}\Big[\max_{1\le i\le \breve{N}^{(c)}} |r_i^{(c)} - \breve{r}_i^{(c)}|\Big|E_n\Big] &\le \sqrt{\mathbb{E}\Big[\max_{1\le i\le \breve{N}^{(c)}} |\breve{\Pi}_i^{(c)} - \breve{\Pi}_{i-1}^{(c)}|^2\Big]\mathbb{E}\Big[\max_{1\le \ell\le n} |r_\ell - \breve{r}_\ell|^2\Big]} \\ &\le K\Delta_n^{1+\kappa/4}\sqrt{L_n}.\end{aligned} \tag{A.25}$$

Therefore, we have

$$\begin{aligned}&\mathbb{P}\Big(\max_{1\le i\le \overline{N}^{(c)}} |r_i^{(c)} - \breve{r}_i^{(c)}| > K\Delta_n^{1+\kappa/8}\Big) \\ &\le \mathbb{P}\Big(\max_{1\le i\le \breve{N}^{(c)}} |r_i^{(c)} - \breve{r}_i^{(c)}| > K\Delta_n^{1+\kappa/8}\Big|E_n\Big) + \mathbb{P}(E_n^{\complement}) \\ &\le K'(\Delta_n^{\kappa/8}\sqrt{L_n} + \Delta_n^{\kappa/2}\sqrt{L_n}).\end{aligned} \tag{A.26}$$

This completes the proof. □

Lemma A.3 shows the statistics constructed from sampled returns under observation schemes (I) and (II) are equivalent up to a $\Delta_n^{-1-\kappa/8}$ normalization, which is sufficient for the $c^{-1} \asymp \Delta_n^{-1/2}$ $\sqrt{\breve{N}^{(c)}} \asymp \Delta_n^{-1/2}$ order in conventional CLT. The requirement is only $\kappa > 0$.

The above type of strong approximation results are similarly used in, e.g., the proof of Theorem 5.1 in Chernozhukov et al. (2013) and the proof of Theorem 4.3 in Chernozhukov et al. (2019). It allows us to focus on the limiting behavior of functionals of $\breve{R}_i/c^2$, the result can be sufficiently extended to those of R_i/c^2. To fix ideas, consider a possibly multi-dimensional Lipschitz function $f(\cdot)$. Suppose that

$$\frac{1}{\breve{N}^{(c)}}\sum_{i=1}^{\breve{N}^{(c)}} f\Big(\frac{\breve{R}_i}{c^2}\Big) \xrightarrow{\mathbb{P}} \mu_f, \quad \text{and} \quad \frac{1}{\sqrt{\breve{N}^{(c)}}}\sum_{i=1}^{\breve{N}^{(c)}}\Big(f\Big(\frac{\breve{R}_i}{c^2}\Big) - \mu_f\Big) \xrightarrow{\mathcal{L}} \mathcal{N}(0, \Sigma_f). \tag{A.27}$$

Let $E_n' \equiv \{\Pi_i^{(c)} = \breve{\Pi}_i^{(c)} \text{ for all } 1 \le i \le \breve{N}^{(c)}\} \cap \{\max_{1\le i\le \breve{N}^{(c)}} |R_i - \breve{R}_i|/c^2 > K\Delta_n^{1/2+\kappa/16}\}$. Note that $a^2 - b^2 = (a-b)^2 + 2b(a-b)$, it follows triangle inequality that

$$\max_{1\le i\le \breve{N}^{(c)}} |R_i - \breve{R}_i| \le \Big(\max_{1\le i\le \breve{N}^{(c)}} |r_i^{(c)} - \breve{r}_i^{(c)}|\Big)^2 + 2\Big(\max_{1\le i\le \breve{N}^{(c)}} |\breve{r}_i^{(c)}|\Big)\Big(\max_{1\le i\le \breve{N}^{(c)}} |r_i^{(c)} - \breve{r}_i^{(c)}|\Big). \tag{A.28}$$

Note that $\max_{1\le i\le \breve{N}^{(c)}} |\breve{r}_i^{(c)}| = O_p(\Delta_n^{1/2}\sqrt{L_n}) = o_p(\Delta_n^{1/2-\kappa/16})$ by the maximal inequality of sub-Gaussian variables. Then it follows Lemma A.2 (ii), Lemma A.3, and Eq. (A.28) that $\mathbb{P}(E_n') \ge 1 - K\Delta_n^{\kappa/8}\sqrt{L_n}$. Therefore, for each $\varepsilon > 0$,

$$\begin{aligned}
&\mathbb{P}\Big(\Big\|\frac{1}{N^{(c)}}\sum_{i=1}^{N^{(c)}} f\Big(\frac{R_i}{c^2}\Big) - \mu_f\Big\| > \varepsilon\Big) \\
&\le \mathbb{P}\Big(\Big\|\frac{1}{\breve{N}^{(c)}}\sum_{i=1}^{\breve{N}^{(c)}} f\Big(\frac{\breve{R}_i}{c^2}\Big) - \mu_f\Big\| > \frac{\varepsilon}{2}\Big) + \mathbb{P}\Big(\Big\|\frac{1}{N^{(c)}}\sum_{i=1}^{N^{(c)}} f\Big(\frac{R_i}{c^2}\Big) - \frac{1}{\breve{N}^{(c)}}\sum_{i=1}^{\breve{N}^{(c)}} f\Big(\frac{\breve{R}_i}{c^2}\Big)\Big\| > \frac{\varepsilon}{2}\Big) \\
&\le \mathbb{P}\Big(\Big\|\frac{1}{\breve{N}^{(c)}}\sum_{i=1}^{\breve{N}^{(c)}} f\Big(\frac{\breve{R}_i}{c^2}\Big) - \mu_f\Big\| > \frac{\varepsilon}{2}\Big) + \mathbb{P}\Big(K\max_{1\le i\le \breve{N}^{(c)}}\frac{|R_i - \breve{R}_i|}{c^2} > \frac{\varepsilon}{2}\Big| E_n'\Big) + \mathbb{P}(E_n'^{\complement}) \\
&= \mathbb{P}\Big(\Big\|\frac{1}{\breve{N}^{(c)}}\sum_{i=1}^{\breve{N}^{(c)}} f\Big(\frac{\breve{R}_i}{c^2}\Big) - \mu_f\Big\| > \frac{\varepsilon}{2}\Big) + K\Delta_n^{\kappa/8}\sqrt{L_n}.
\end{aligned} \tag{A.29}$$

Let $Z \sim \mathcal{N}(0, \Sigma_f)$. For each $A \subset \mathbb{R}^{\dim(f)}$ and $\varepsilon > 0$, let $A^\varepsilon \equiv \{x \in \mathbb{R}^{\dim(f)} : \inf_{y\in A}\|x-y\| \le \varepsilon\}$ denote the ε-enlargement of A, then we have

$$\begin{aligned}
&\mathbb{P}\Big(\frac{1}{\sqrt{N^{(c)}}}\sum_{i=1}^{N^{(c)}}\Big(f\Big(\frac{R_i}{c^2}\Big) - \mu_f\Big) \in A\Big) \\
&\le \mathbb{P}\Big(\frac{1}{\sqrt{\breve{N}^{(c)}}}\sum_{i=1}^{\breve{N}^{(c)}}\Big(f\Big(\frac{\breve{R}_i}{c^2}\Big) - \mu_f\Big) \in A^\varepsilon\Big) + \mathbb{P}\Big(\Big\|\frac{1}{\sqrt{N^{(c)}}}\sum_{i=1}^{N^{(c)}} f\Big(\frac{R_i}{c^2}\Big) - \frac{1}{\sqrt{\breve{N}^{(c)}}}\sum_{i=1}^{\breve{N}^{(c)}} f\Big(\frac{\breve{R}_i}{c^2}\Big)\Big\| > \varepsilon\Big) \\
&\le \mathbb{P}\Big(\frac{1}{\sqrt{\breve{N}^{(c)}}}\sum_{i=1}^{\breve{N}^{(c)}}\Big(f\Big(\frac{\breve{R}_i}{c^2}\Big) - \mu_f\Big) \in A^\varepsilon\Big) + \mathbb{P}\Big(K\sqrt{\breve{N}^{(c)}}\max_{1\le i\le \breve{N}^{(c)}}\frac{|R_i - \breve{R}_i|}{c^2} > \varepsilon\Big| E_n'\Big) + \mathbb{P}(E_n'^{\complement}) \\
&= \mathbb{P}(Z \in A) + \mathbb{P}(Z \in A^\varepsilon \setminus A) + K\Delta_n^{\kappa/8}\sqrt{L_n}.
\end{aligned} \tag{A.30}$$

Taking $\varepsilon \to 0$, the right-hand side becomes $\mathbb{P}(Z \in A) + o(1)$. Similarly, one can show

$$\mathbb{P}\Big(\frac{1}{\sqrt{N^{(c)}}}\sum_{i=1}^{N^{(c)}}\Big(f\Big(\frac{R_i}{c^2}\Big) - \mu_f\Big) \in A\Big) \ge \mathbb{P}(Z \in A) - o(1). \tag{A.31}$$

This shows the same CLT holds. Therefore, our attention is restricted to the limit theorems of the test statistics constructed from $(\breve{r}_i^{(c)})_{1\le i\le \breve{N}^{(c)}}$. For ease of notation, we shall drop the breve mark ($\breve{}$) in the subsequent proofs.

A.1.1.4 Proof of Theorem 2.1

Under the null. As randomly indexed partial sums of i.i.d. random variables, the PDS returns $r_i^{(c)}$ for all $1 \leq i \leq N^{(c)}$ form a stopped random walk. To consider the departure from ordinary limit theorems that hold for processes with fixed indices, some previous studies extend the standard results to accommodate randomly indexed random walks, see, e.g., Anscombe (1952), Rényi (1957), and Gut (2009, 2012).

Note that the condition specified in Anscombe's theorem (Theorem 1, Rényi, 1957; Theorem 2.2 and 2.3, Gut, 2012) is satisfied by the strong law for renewal processes, i.e., as $n \to \infty$,

$$\frac{N^{(c)}}{N} \xrightarrow{\text{a.s.}} \mathbb{E}[\Pi_1^{(c)}] = \frac{1}{\mu_2(m)}, \tag{A.32}$$

such that the random sum LLN implies, jointly with the continuous mapping theorem, that

$$\frac{\sum_{i=1}^{N^{(c)}} R_i}{c^2 N^{(c)}} \xrightarrow{\mathbb{P}} h_2(m) \quad \text{and} \quad \frac{\sum_{i=1}^{N^{(c)}} \overline{R}_i}{c^2 N^{(c)}} \xrightarrow{\mathbb{P}} \overline{h}_{2,\epsilon}(m). \tag{A.33}$$

The consistency of both $\overline{M}_{c,\epsilon}$ and M_c in Eq. (2.17) is a direct result of the continuous mapping theorem from Eq. (A.33).

Under the Alternative. We denote by (Λ_t^n) the counting process of all jumps in (X_t^n) in Eq. (2.7), then Λ_t^n is bounded for each n, and for all n, we have

$$\sum_{0 \leq s \leq t} |\Delta X_t^n|^r < \infty, \tag{A.34}$$

which implies for large enough n (such that $u_n \to 0$),

$$u_n^r \Lambda_t^n \leq \sum_{0 \leq s \leq t} |\Delta X_t^n|^r < \infty, \tag{A.35}$$

from which one can deduce that $\Lambda_t^n = O_p(\Delta_n^{-r/2})$ for all fixed t.

When $X(\omega)$ is discontinuous within $(0,1)$, we denote by $\{s_1, s_2 \ldots, s_\Lambda\}$ the sequence of all jump times in chronological order, where $\Lambda \equiv \Lambda_1^n(\omega)$ counts the number of all discontinuities on $(0,1]$. We define

$$k^-(s) = \inf_{0 \leq i \leq n} \{t_i \geq s : |t_i - s|\} \qquad \text{and} \qquad k^+(s) = \inf_{0 \leq i \leq n} \{t_i < s : |t_i - s|\} \tag{A.36}$$

as the index of the first observations no earlier than and strictly before s, respectively. We split the sequence of observations $(X_{t_i})_{0\le i\le N}$ into $\Lambda+1$ segments with $i=k^+(s_j)$ for all $1\le j\le \Lambda$ as cutoff points. As $N\to\infty$, we have $k^+(s_j)-k^+(s_{j-1})\to\infty$ (also, $k^+(s_1)\to\infty$), since any intervals of length of order Δ_n mostly contain a single jump of size larger than u_n, see Section 2.3 of Aït-Sahalia and Jacod (2009).

For each segment $(X_{t_i})_{k^+(s_{j-1})\le i\le k^+(s_j)}$, we obtain the PDS returns $(r_i^{(c)})_{N_{j-1}^{(c)}+1\le i\le N_j^{(c)}}$ with the barrier width $c=m\sqrt{\Delta_n}$. For each $i\in A_n=\{N_1^{(c)},N_2^{(c)},\dots,N_\Lambda^{(c)}\}$, the PDS return $|r_i^{(c)}|\ge u\gg c$ contains jumps and will be censored by $\varphi_\epsilon(c)$. For all $i\notin A_n$, the PDS return $r_i^{(c)}$ contains only aggregated Brownian increments. For the censored PDS returns, we have

$$\frac{\sum_{i=1}^{N^{(c)}}\overline{R}_i}{c^2N^{(c)}}=\frac{\sum_{i\notin A_n}\overline{R}_i}{c^2N^{(c)}}+\frac{\sum_{i\in A_n}\overline{R}_i}{c^2N^{(c)}}. \tag{A.37}$$

For the first term above, since the cardinality of A_n is $\Lambda=O_p(\Delta_n^{-r/2})\ll\Delta_n^{-1}\asymp N^{(c)}$, we have

$$\frac{\sum_{i\notin A_n}\overline{R}_i}{c^2N^{(c)}}=\frac{N^{(c)}-\Lambda}{N^{(c)}}\frac{\sum_{i\notin A_n}\overline{R}_i}{c^2(N^{(c)}-\Lambda)},\quad \text{where } \frac{N^{(c)}-\Lambda}{N^{(c)}}\xrightarrow{\text{a.s.}}1, \tag{A.38}$$

such that it coincides with the limit theorems under the null. For the second term, it holds that

$$\frac{\sum_{i\in A_n}\overline{R}_i}{c^2N^{(c)}}\le K\frac{\Lambda}{N^{(c)}}\le K'\Delta_n^{1-r/2}, \tag{A.39}$$

which has no impact on the LLN result. It still vanishes after multiplying by $\sqrt{N^{(c)}}\asymp\Delta_n^{-1/2}$ for any $r\in[0,1)$, and thus does not affect the CLT.

For uncensored PDS returns, it holds that as $n\to\infty$,

$$\frac{\sum_{i=1}^{N^{(c)}}R_i}{c^2N^{(c)}}\xrightarrow{\mathbb{P}}\frac{h_2(m)[X,X]_1}{\tau(1)},\quad \text{where } \tau(1)=\int_0^1\sigma_s^2ds, \tag{A.40}$$

because $\sum_{i=1}^{N^{(c)}}R_i\xrightarrow{\mathbb{P}}[X,X]_1$ and $c^2N^{(c)}\xrightarrow{\mathbb{P}}\tau(1)/h_2(m)$. This completes the proof.

A.1.1.5 Proof of Theorem 2.2

As mentioned in Appendix A.1.1.4, the condition in Anscombe's theorem is satisfied. The random index version of Lindeberg-Lévy CLT (Theorem 2.3, Gut, 2012) can be applied to verify the asymptotic normality of $(\overline{M}_{c,\epsilon},M_c)'$. We start with an i.i.d. two-dimensional random

vector

$$X_i = \left(\frac{\overline{R}_i}{c^2}, \frac{R_i}{c^2}\right)', \tag{A.41}$$

with the mean vector

$$\mathbb{E}[X_i] \xrightarrow{\mathbb{P}} \mu = (\overline{h}_{2,\epsilon}(m), h_2(m))', \tag{A.42}$$

and a 2×2 variance-covariance matrix (among the components of the vector):

$$\mathrm{Var}(X_i) \xrightarrow{\mathbb{P}} \Sigma, \tag{A.43}$$

where

$$\Sigma = m^{-4} \begin{bmatrix} \overline{\mu}_{4,\epsilon}(m) - \overline{\mu}^2_{2,\epsilon}(m) & \overline{\rho}_{2,\epsilon}(m) - \mu_2(m)\overline{\mu}_{2,\epsilon}(m) \\ \overline{\rho}_{2,\epsilon}(m) - \mu_2(m)\overline{\mu}_{2,\epsilon}(m) & \mu_4(m) - \mu_2^2(m) \end{bmatrix}. \tag{A.44}$$

The functions in Σ, i.e., μ, $\overline{\mu}$, and $\overline{\rho}$, are defined in Section 2.3.1.

For the sample mean vector

$$\overline{X} = \frac{1}{N^{(c)}} \sum_{i=1}^{N^{(c)}} X_i = \left(\frac{1}{N^{(c)}} \sum_{i=1}^{N^{(c)}} \frac{\overline{R}_i}{c^2}, \frac{1}{N^{(c)}} \sum_{i=1}^{N^{(c)}} \frac{R_i}{c^2}\right)' = (\overline{S}_{2,\epsilon}, S_2)', \tag{A.45}$$

where the summation of these vectors is being done component-wise. The random sum Lindeberg-Lévy CLT implies that as $n \to \infty$,

$$\sqrt{N^{(c)}}(\overline{X} - \mu) \xrightarrow{\mathcal{L}} \mathcal{N}(0, \Sigma), \tag{A.46}$$

and

$$\sqrt{N}(\overline{X} - \mu) \xrightarrow{\mathcal{L}} \mathcal{N}(0, \mu_2(m)\Sigma). \tag{A.47}$$

Therefore, for the random vector $f(\overline{X}) = (\overline{M}_{c,\epsilon}, M_c)'$ with the vector function

$$f\left(\begin{bmatrix} x \\ y \end{bmatrix}\right) = \begin{bmatrix} \overline{h}^{-1}_{2,\epsilon}(x) \\ h_2^{-1}(y) \end{bmatrix}, \tag{A.48}$$

it holds that

$$\sqrt{N}(f(\overline{X}) - m) \xrightarrow{\mathcal{L}} \mathcal{N}(0,\ \mu_2(m)\nabla f(\mu)'\Sigma\nabla f(\mu)), \tag{A.49}$$

by the multivariate delta method, where

$$\nabla f(\mu) = ((\overline{h}'_{2,\epsilon}(\overline{h}^{-1}_{2,\epsilon}(\overline{h}_{2,\epsilon}(m))))^{-1}, (h'_2(h_2^{-1}(h_2^{-1}(m))))^{-1}) = ((\overline{h}'_{2,\epsilon}(m))^{-1}, (h'_2(m))^{-1}). \quad \text{(A.50)}$$

This completes the proof.

□

A.1.2 Proof of Proposition 2.1

Proof. We first prove that the sequence of pre-averaged returns $(r_i^*)_{1\leq i\leq N'}$ converges in law to a centered stationary Gaussian process with desired variance under infill asymptotics for each i. We assume $k_n = 2k$ for simplicity, and expand r_i^* in terms of $\Delta_j^N X = X_j - X_{j-1}$ and ε_j:

$$\begin{aligned} r_i^* &= \frac{1}{k_n}\sum_{j=1}^{k}(X_{i+k+j} - X_{i+j}) + \frac{1}{k_n}\sum_{j=1}^{k}(\varepsilon_{i+k+j} - \varepsilon_{i+j}) \\ &= \underbrace{\sum_{j=1}^{k_n} g\Big(\frac{j}{2k}\Big)\Delta_{i+j}^N X}_{A_i} + \underbrace{\frac{1}{k_n}\sum_{j=1}^{k}(\varepsilon_{i+k+j} - \varepsilon_{i+j})}_{B_i}, \end{aligned} \quad \text{(A.51)}$$

where $g(s) = s \wedge (1-s)$ is the triangular kernel weighting function. Under Assumption 2.2 and by the strong approximation result in Eq. (A.22), we deduce that A_i converges in probability to $\sum_{j=1}^{k_n} g(\frac{j}{2k})\breve{r}_{i+j}$, which is a linear combination of i.i.d. centered Gaussian random variables. The α-mixing ε with the conditions in Assumption 2.3 indidates a CLT under weak dependence (Ibragimov, 1962; Theorem 8.3.7, Durrett, 2019), which implies the asymptotic Gaussianity of B_i. The independence between X and ε implies that r_i^* converges in distribution to a centered Gaussian random variable for all i.

We now identify the limiting law of (r_i^*) by calculating its variance kernel explicitly, which also establishes the stationarity of the limiting Gaussian process. With $\mathrm{Corr}(X_j, \varepsilon_{j'}) = 0$ for any $0 \leq j, j' \leq N$, we have $\mathrm{Var}(r_i^*) = \mathrm{Var}(A_i) + \mathrm{Var}(B_i)$ with

$$\mathrm{Var}(A_i) = \sum_{j=1}^{k_n} g^2\Big(\frac{j}{k_n}\Big)(\Delta_n + o(\Delta_n)) = \frac{k_n\Delta_n}{12} + o(\sqrt{\Delta_n}). \quad \text{(A.52)}$$

For the additive noise term, we define the partial sum of ε as

$$S_{n,h} = \sum_{i=1}^{h} \varepsilon_{n+i}, \tag{A.53}$$

and start with the following results for some $\lambda \geq h$:

$$\mathrm{Var}(S_{n,h}) = \sum_{m=1-h}^{h-1} (h - |m|)\Gamma_m = h \sum_{m=1-h}^{h-1} \Big(1 - \Big|\frac{m}{h}\Big|\Big)\Gamma_m, \tag{A.54}$$

$$\begin{aligned} \mathrm{Cov}(S_{n,h}, S_{n+\lambda,h}) = \mathbb{E}[S_{n,h}S_{n+\lambda,h}] &= \sum_{i=0}^{h-1}\sum_{j=0}^{h-1} \mathrm{Cov}(\varepsilon_{n+i}, \varepsilon_{n+\lambda+i+j}) \\ &= \sum_{m=1-h}^{h-1} (h - |m|)\Gamma_{m+\lambda} = h \sum_{m=1-h}^{h-1} \Big(1 - \Big|\frac{m}{h}\Big|\Big)\Gamma_{m+\lambda}, \end{aligned} \tag{A.55}$$

where the weight $1 - |m/h|$ is the Bartlett kernel. Therefore, we have

$$\begin{aligned} \mathrm{Var}(B_i) &= \frac{1}{4k^2}\mathrm{Var}(S_{i+k,k} - S_{i,k}) \\ &= \frac{1}{4k^2}\mathrm{Var}(S_{i+k,k}) + \frac{1}{4k^2}\mathrm{Var}(S_{i,k}) - 2\mathrm{Cov}(S_{i+k,k}, S_{i,k}) \\ &= \frac{1}{2k}\sum_{m=1-k}^{k-1} \Big(1 - \Big|\frac{m}{k}\Big|\Big)\Gamma_m - \frac{1}{2k}\sum_{m=1-k}^{k-1} \Big(1 - \Big|\frac{m}{k}\Big|\Big)\Gamma_{m+k} \end{aligned} \tag{A.56}$$

of the order $\sqrt{\Delta_n}$ by the absolute summability of Γ_m, which is implied by the α-mixing property of ε under Assumption 2.3 (Ibragimov and Linnik, 1971). Since $k_n \asymp \sqrt{N}$, both $\mathrm{Var}(A_i)$ and $\mathrm{Var}(B_i)$ are of the order $\sqrt{\Delta_n}$, such that we can ignore all terms with order smaller than $\sqrt{\Delta_n}$, which yields $\mathrm{Var}(r_i^*) = \mathrm{Var}(A_i) + \mathrm{Var}(B_i) \asymp \sqrt{\Delta_n}$.

With the time-invariant first moment and finite second moment of r_i^* for all time, in order to prove the weak stationarity of (r_i^*), we need to make sure that the autocovariance $\mathrm{Cov}(r_i^*, r_{i+\lambda}^*)$ does not vary with i. Here we firstly deal with the autocovariance of A_i. It suffices to examine the autocovariance for non-negative integer-valued lags λ, as the autocovariance function is always symmetric.

$$\mathrm{Cov}(A_i, A_{i+\lambda}) = \mathbb{E}[A_i A_{i+\lambda}] = \mathbb{E}\left[\sum_{j=1}^{k_n} g\Big(\frac{j}{k_n}\Big)\Delta_{i+j}^N X \sum_{\eta=1}^{k_n} g\Big(\frac{\eta}{k_n}\Big)\Delta_{i+\lambda+\eta}^N X\right]. \tag{A.57}$$

When $\lambda \geq k_n$, $\mathrm{Cov}(A_i, A_{i+\lambda}) = 0$. When $1 \leq \lambda \leq k_n - 1$, we have

$$\begin{aligned}\mathrm{Cov}(A_i, A_{i+\lambda}) &= \mathbb{E}\left[\sum_{j=1}^{k_n-\lambda} g\Big(\frac{j}{k_n}\Big) g\Big(\frac{j+\lambda}{k_n}\Big)(\Delta^N_{i+\lambda+j} X)^2\right] \\ &= \sum_{j=1}^{k_n-\lambda} g\Big(\frac{j}{k_n}\Big) g\Big(\frac{j+\lambda}{k_n}\Big)\mathbb{E}[(\Delta^N_{i+\lambda+j} X)^2] = O(\sqrt{\Delta_n}).\end{aligned} \tag{A.58}$$

For the noise term, we have the lag-λ autocovariance

$$\begin{aligned}&\mathrm{Cov}(B_i, B_{i+\lambda}) = \frac{1}{4k^2}\mathbb{E}[(S_{i+k,k} - S_{i,k})(S_{i+k+\lambda,k} - S_{i+\lambda,k})] \\ &= \frac{1}{4k^2}\left(\mathbb{E}[S_{i+k,k}S_{i+k+\lambda,k}] + \mathbb{E}[S_{i,k}S_{i+\lambda,k}] - \mathbb{E}[S_{i+k,k}S_{i+\lambda,k}] - \mathbb{E}[S_{i,k}S_{i+k+\lambda,k}]\right) \\ &= \frac{1}{2k}\sum_{m=1-k}^{k-1}\Big(1 - \Big|\frac{m}{k}\Big|\Big)\Gamma_{m+\lambda} - \frac{1}{4k}\sum_{m=1-k}^{k-1}\Big(1 - \Big|\frac{m}{k}\Big|\Big)\Gamma_{m+\lambda-k} - \frac{1}{4k}\sum_{m=1-k}^{k-1}\Big(1 - \Big|\frac{m}{k}\Big|\Big)\Gamma_{m+\lambda+k} \\ &= O(\sqrt{\Delta_n}),\end{aligned} \tag{A.59}$$

by the absolute summability of Γ_m. In the limit, both the covariances are finite and time-invariant (not depend on i) for all possible $\lambda \in \mathbb{N}$, which implies the weak stationarity of (r^*_i) in the limit, as desired.

For Step 2, we first demonstrate how the random sign flip eliminates serial correlations in (r^*_i). Let $F(x) = \mathbb{P}(r^*_i \leq x)$ denote the CDF of r^*_i. It is obvious that the product $\delta_i r^*_i$ is a Gaussian random variable with the same distribution:

$$\begin{aligned}\mathbb{P}(\delta_i r^*_i \leq x) &= \mathbb{P}(\delta_i = 1)\mathbb{P}(\delta_i r^*_i \leq x | \delta_i = 1) + \mathbb{P}(\delta_i = -1)\mathbb{P}(\delta_i r^*_i \leq x | \delta_i = -1) \\ &= \frac{1}{2}\mathbb{P}(r^*_i \leq x) + \frac{1}{2}\mathbb{P}(r^*_i \geq -x) = F(x),\end{aligned} \tag{A.60}$$

and the autocovariance function for any $i \in \{1, \ldots, N' - \lambda\}$ satisfies

$$\mathrm{Cov}(\delta_i r^*_i, \delta_{i+\lambda} r^*_{i+\lambda}) = \mathbb{E}[\delta_i \delta_{i+\lambda} r^*_i r^*_{i+\lambda}] = \mathbb{E}[\delta_i]\mathbb{E}[\delta_{i+\lambda}]\mathrm{Cov}(r^*_i, r^*_{i+\lambda}) = 0. \tag{A.61}$$

Next, we establish that, following the uniform random permutation $\pi : \{1, \ldots, N'\} \mapsto \{1, \ldots, N'\}$, any two variables in $(\tilde{r}_i)_{1 \leq i \leq N'}$ are independent when their indices are not sufficiently distant from each other each other in $\{1, \ldots, N'\}$ under infill asymptotics. We start with a formal definition of the local independence for a discrete-time stochastic process: The

process $X = (X_i)_{1\le i\le n}$ is said to be locally independent if

$$\begin{aligned} &\lim_{n\to\infty} \sup_{\substack{1\le i,j\le n\\ 1\le|i-j|\le \Lambda_n}} \mathbb{P}(X_i \text{ and } X_j \text{ are dependent}) = 0, \\ \text{or}\quad &\lim_{n\to\infty} \sup_{\substack{1\le i,j\le n\\ 1\le|i-j|\le \Lambda_n}} \{|\mathbb{P}(A\cap B) - \mathbb{P}(A)\mathbb{P}(B)| : A\in\sigma(X_i), B\in\sigma(X_j)\} = 0, \end{aligned} \tag{A.62}$$

where $\Lambda_n \asymp n^{\varpi}$ for some $\varpi \in (0,1)$, such that X_i is independent to other variables in X whose indices fall within the interval $[i-\Lambda_n, i+\Lambda_n]$. In our case, we need to verify

$$\lim_{n\to\infty} \sup_{\substack{1\le i,j\le N'\\ 1\le|i-j|\le \Lambda_n}} \mathbb{P}(\tilde{r}_i \text{ and } \tilde{r}_j \text{ are dependent}) = 0. \tag{A.63}$$

The fact that $(\varepsilon_i)_{0\le i\le N}$ is α-mixing implies that

$$\alpha(\Lambda_n) = \sup\{|\mathbb{P}(A\cap B) - \mathbb{P}(A)\mathbb{P}(B)| : A\in\sigma(\varepsilon_i), B\in\sigma(\varepsilon_{i+\Lambda_n})\} \to 0, \tag{A.64}$$

as $n\to\infty$, thus ε_i and ε_j are asymptotically independent if $|i-j|\ge\Lambda_n$.

With the uniform random permutation, we denote

$$\tilde{r}_i = r^*_{\pi(i)}\delta_{\pi(i)} \quad \text{and} \quad \tilde{r}_j = r^*_{\pi(j)}\delta_{\pi(j)} \tag{A.65}$$

where $\pi(i)$, $\pi(j)$ are the corresponding indices of the products before permutation. Therefore, for all $1\le i,j\le N'$ and $1\le|i-j|\le\Lambda_n$, $\tilde{r}_i$ and $\tilde{r}_j$ are independent if the corresponding indices $\pi(i)$ and $\pi(j)$ are sufficiently far apart from one another:

$$\begin{aligned} \mathbb{P}(\tilde{r}_i \text{ and } \tilde{r}_j \text{ are dependent}) &= \mathbb{P}(r^*_{\pi(i)} \text{ and } r^*_{\pi(j)} \text{ are dependent}) \\ &= \mathbb{P}(\sigma(\{\varepsilon_{\pi(i)+\ell} : 0\le\ell\le k_n\}) \text{ and } \sigma(\{\varepsilon_{\pi(j)+\ell} : 0\le\ell\le k_n\}) \text{ are dependent}) \\ &\le 2\mathbb{P}(\pi(i)+1\le\pi(j)\le\pi(i)+k_n+\Lambda_n) \\ &= \frac{2(k_n+\Lambda_n)}{N'-1} = O(\Delta_n^{\gamma}), \quad \text{where } \gamma = 1-\max\Big\{\frac{1}{2},\varpi\Big\}. \end{aligned} \tag{A.66}$$

For a sequence of N' variables, the uniform random permutation ensures that each of the $N'!$ possible permutations are equally likely and that each "ball" $r^*_{\pi(i)}\delta_{\pi(i)}$ has an equal chance of

being placed into any "box" i, which has become a question of classical probability. As $n \to \infty$, $\tilde{r}_i$ and $\tilde{r}_j$ with $1 \leq |i-j| \leq \Lambda_n$ are asymptotically independent. This completes the proof.

□

A.2 Supplementary Results

A.2.1 Parameter Choices for Other Tests

For other tests constructed in Sections 2.4 and 2.5, we clarify some specific parameter choices:

LM: For the local realized bipower variation, we consider the window size $K = \sqrt{252N}$, where N is the number of sampled observations.

ASJ: For the multipower variations constructed on two different sampling intervals δ and $k\delta$, we select $p = 4$ and $k = 2$, which satisfies the requirement.

CPR: For the auxiliary local variance estimator, we employ the nonparametric filter of length $2L+1$ with $L = 25$ and a Gaussian kernel, which follows the recommendation in Appendix B of Corsi et al. (2010).

PZ: We employ the truncated realised power variation with $p = 4$ and the truncation threshold $cN^{-\varpi}$, where c and ϖ follow the recommendation in Section 5 of Podolskij and Ziggel (2010). For the noise-adjusted version, we select the pre-averaging window $k_n = 0.5\lfloor\sqrt{N}\rfloor$.

LM12: We select the pre-averaging window $k_n = 0.4\lfloor\sqrt{N}\rfloor$, which minimizes the absolute distance between the nominal size and the empirical size with the simulated tick-level noise-contaminated observations.

ASJL: We select the pre-averaging window $k_n = 0.9\lfloor\sqrt{N}\rfloor$ based on the simulated noise-contaminated data, and the truncation level $C = 5$.

A.2.2 Simulation Results with Other Noise Specifications

In addition to the simulation results in Section 2.4, we consider three other specifications for the additive noise that follows Aït-Sahalia et al. (2012) as robustness checks:

(i) Gaussian noise:

$$\varepsilon_i = 2Z_i\sqrt{\frac{\sigma^2_{t_{n,i}}}{n}}, \tag{A.67}$$

where Z_i are i.i.d. draws from a standard normal distribution, see Tables A.1 to A.3.

(ii) Autocorrelated Gaussian noise:

$$\varepsilon_i = 2\omega_i^A \sqrt{\frac{\sigma^2_{t_{n,i}}}{n}}, \tag{A.68}$$

where ω_i^A is an autocorrelated Gaussian defined in Eq. (2.31), see Tables A.4 to A.6.

(iii) t-distributed noise:

$$\varepsilon_i = 2\omega_i^B \sqrt{\frac{\nu-2}{\nu}} \sqrt{\frac{\sigma^2_{t_{n,i}}}{n}}, \tag{A.69}$$

where ω_i^B are i.i.d. draws from a Student's t distribution with the degree of freedom ν, see Tables A.7 to A.9.

Table A.1 Finite-sample size and power (%) under Gaussian noise

Nominal size: 5%		$\theta = 0.3$				$\theta = 0.4$				$\theta = 0.5$			
			ϵ				ϵ				ϵ		
	$c/\sigma(\tilde{r}_i)$	$N^{(c)}$	0.05	0.07	0.10	$N^{(c)}$	0.05	0.07	0.10	$N^{(c)}$	0.05	0.07	0.10
Panel A No Jump	3	1785	4.90	5.21	5.35	1783	5.07	5.05	5.76	1783	5.01	5.07	5.70
	4	1099	5.33	5.03	5.49	1098	4.93	5.14	5.81	1098	5.24	5.21	5.62
	5	743	4.71	5.14	5.33	743	5.18	5.28	5.43	742	5.10	5.70	5.27
	6	535	5.26	5.01	5.49	535	4.63	4.89	5.53	535	4.82	5.47	5.13
	7	404	4.71	4.99	5.19	404	4.61	5.55	5.62	404	5.17	5.18	5.08
	8	316	4.83	4.79	5.59	315	4.83	5.23	5.73	315	5.08	5.12	5.30
	9	254	5.44	4.80	5.30	253	5.22	5.00	5.38	253	5.20	5.20	5.73
	10	208	4.93	5.31	5.71	208	4.98	5.41	5.68	208	5.18	5.28	5.75
Panel B Moderate Jump	3	1715	47.74	49.52	50.82	1716	44.73	47.04	49.52	1718	42.85	45.35	47.45
	4	1058	46.68	48.74	50.80	1059	43.38	46.51	48.46	1061	41.71	44.74	46.93
	5	717	45.27	47.51	50.26	718	43.27	45.29	48.09	720	41.23	43.10	45.95
	6	518	44.45	47.15	49.63	519	43.24	44.57	46.91	520	41.10	42.06	45.13
	7	392	44.91	46.79	49.45	393	42.51	43.70	46.51	394	40.31	41.96	44.21
	8	307	42.82	46.95	49.09	308	41.76	43.10	45.84	308	39.45	40.95	44.10
	9	247	42.13	45.59	48.45	248	40.81	42.65	46.06	248	38.43	40.97	43.46
	10	203	41.42	44.81	48.32	204	40.32	41.82	46.46	204	38.26	40.44	43.70
Panel C Large Jump	3	1587	69.98	71.41	73.31	1589	68.18	69.74	71.08	1594	67.26	68.39	69.95
	4	979	68.91	71.10	72.74	982	67.81	69.39	70.89	985	65.92	67.49	69.41
	5	665	68.80	70.14	72.20	668	66.75	69.09	70.32	670	65.28	66.87	69.25
	6	482	67.64	69.69	71.54	485	66.71	68.34	69.77	487	64.99	66.15	68.20
	7	365	67.61	69.10	71.27	368	65.47	66.78	69.89	370	63.94	65.80	67.99
	8	287	67.37	68.95	71.00	289	65.11	66.62	68.93	291	64.21	65.45	66.91
	9	232	65.90	69.22	70.84	234	64.78	66.60	68.88	235	63.87	64.83	67.73
	10	191	65.47	68.02	70.71	193	64.23	65.74	68.45	194	63.14	64.76	67.56

This table reports the finite-sample size and size-adjusted power (%) of 10,000 simulations of the test statistic $T_{c,\epsilon}$ at 5% nominal level. All simulated prices are contaminated by the additive Gaussian noise and rounding errors. We utilize the two-step noise reduction method in Section 2.3.2 to construct the sequence of pseudo-observations with three different pre-averaging windows, i.e., $k_n = \lceil \theta\sqrt{N} \rceil$ with $\theta \in \{0.3, 0.4, 0.5\}$. The observations are sampled with different PDS barrier widths $c = K\sigma(\tilde{r}_i)$, where K ranges from 3 to 10. Different censoring thresholds with $\epsilon \in \{0.05, 0.07, 0.1\}$ are considered. $N^{(c)}$ stands for the average sampling frequencies.

Table A.2 Finite-sample size and power (%) of other tests under Gaussian noise

Nominal size: 5%											
	Int. (sec)	N_{spl}	BNS	ABD	JO	LM	ASJ	CPR	PZ	MinRV	MedRV
Panel A No Jump	5	4680	0.23	20.28	1.06	14.02	100.00	0.37	5.59	0.00	0.00
	15	1560	4.93	26.64	3.70	22.26	93.73	5.43	9.91	0.91	2.89
	30	780	7.88	26.93	5.02	29.32	38.68	8.42	12.55	4.04	6.35
	60	390	7.69	23.90	6.23	27.86	13.10	8.26	14.47	5.37	7.14
	120	195	7.49	20.82	8.07	17.76	7.10	8.02	16.23	5.71	7.93
	180	130	7.91	18.97	9.05	15.11	5.36	8.70	16.12	5.78	8.78
	300	78	7.74	15.54	10.98	11.96	4.22	8.70	14.91	5.67	9.12
Panel B Moderate Jump	5	4680	44.28	76.55	51.82	69.09	99.76	47.13	66.49	40.11	45.46
	15	1560	40.43	73.96	44.90	60.35	92.97	43.88	61.13	37.19	41.85
	30	780	36.17	68.73	38.30	51.11	65.25	39.14	52.79	33.48	36.97
	60	390	29.52	60.12	30.92	42.23	37.60	32.97	43.63	27.36	31.32
	120	195	21.55	50.01	22.20	36.06	22.08	24.92	32.72	21.00	24.32
	180	130	17.48	42.85	17.40	30.52	14.55	20.17	26.98	17.02	20.84
	300	78	15.27	34.45	11.91	21.62	11.67	17.54	19.96	14.36	16.51
Panel C Large Jump	5	4680	68.50	87.98	74.10	84.55	99.83	70.65	82.69	64.96	68.91
	15	1560	65.66	86.64	69.37	79.03	95.72	68.29	79.36	62.52	66.47
	30	780	61.28	83.55	64.47	73.60	78.16	64.28	74.79	58.50	62.36
	60	390	55.16	79.09	57.63	67.45	57.04	58.50	68.70	52.97	57.53
	120	195	46.02	71.16	48.22	61.94	36.07	50.16	59.34	44.72	49.98
	180	130	41.61	65.42	42.27	56.76	26.63	45.35	53.82	40.37	44.59
	300	78	35.12	57.46	33.77	46.86	17.83	39.24	45.27	34.30	38.21

This table reports the finite-sample size and size-adjusted power (%) of 10,000 simulations of 9 classical tests at 5% nominal level: BNS (Barndorff-Nielsen and Shephard, 2006), ABD (Andersen et al., 2007c), JO (Jiang and Oomen, 2008), LM (Lee and Mykland, 2008), ASJ (Aït-Sahalia and Jacod, 2009), CPR (Corsi et al., 2010), PZ (Podolskij and Ziggel, 2010), MinRV and MedRV (Andersen et al., 2012). All these tests are constructed on observations equidistantly sampled with various intervals in calendar time: 5, 15, 30, 60, 120, 180 and 300 seconds, and "N_{spl}" stands for the sampling frequencies.

Table A.3 Finite-sample size and power (%) of other noise-robust tests under Gaussian noise

Nominal size: 5%					
	Int. (sec)	N_{spl}	PZ*	LM12	ASJL
No Jump	tick	23400	5.10	3.27	5.12
	5	4680	4.93	8.59	8.79
Moderate Jump	tick	23400	39.34	24.12	38.06
	5	4680	29.96	18.97	16.88
Large Jump	tick	23400	64.18	39.18	62.90
	5	7680	56.03	32.23	41.41

This table reports the finite-sample size and size-adjusted power (%) of 10,000 simulations of 3 noise-robust tests at 5% nominal level: noise-adjusted PZ (Podolskij and Ziggel, 2010), LM12 (Lee and Mykland, 2012), and ASJL (Aït-Sahalia et al., 2012). All these tests are constructed on tick-level and 5-second-sampled observations. The tuning parameters for those tests are selected by minimizing the absolute distance between the nominal size and the empirical size with the simulated tick-level noise-contaminated observations.

Table A.4 Finite-sample size and power (%) under autocorrelated Gaussian noise

Nominal size: 5%		$\theta = 0.3$				$\theta = 0.4$				$\theta = 0.5$			
			ϵ				ϵ				ϵ		
	$c/\sigma(\tilde{r}_i)$	$N^{(c)}$	0.05	0.07	0.10	$N^{(c)}$	0.05	0.07	0.10	$N^{(c)}$	0.05	0.07	0.10
Panel A No Jump	3	1785	4.85	5.28	5.39	1784	5.14	5.34	5.69	1783	5.38	5.70	5.84
	4	1099	5.02	5.36	5.34	1099	5.05	4.94	5.32	1097	5.23	5.62	5.69
	5	743	4.84	5.45	4.96	743	4.82	5.58	5.37	743	5.41	5.64	6.07
	6	536	4.71	5.14	5.30	536	4.87	5.32	5.23	535	4.73	5.33	5.63
	7	404	5.21	5.36	5.44	404	5.11	4.91	5.60	404	5.20	5.02	5.45
	8	316	4.74	5.21	5.50	316	4.91	4.79	5.74	316	4.75	5.17	5.41
	9	253	4.56	5.05	5.37	254	4.92	5.16	5.35	253	4.86	5.36	5.32
	10	208	4.87	5.45	5.33	208	5.01	5.48	5.77	208	5.36	5.42	5.75
Panel B Moderate Jump	3	1715	47.02	49.41	52.39	1717	45.14	47.22	49.69	1719	43.27	45.53	48.29
	4	1058	46.22	48.63	51.34	1059	43.97	46.88	48.80	1061	42.70	44.28	47.16
	5	717	45.80	47.83	51.35	719	43.38	45.64	48.35	720	40.70	43.64	45.82
	6	518	45.25	46.85	49.59	519	41.62	45.13	47.71	520	40.83	42.25	45.93
	7	392	43.53	46.57	48.48	393	41.06	44.33	46.80	394	39.47	42.48	45.30
	8	307	43.39	45.85	49.41	308	41.95	43.80	46.44	309	39.25	41.64	44.64
	9	247	43.28	45.83	48.46	248	40.78	43.20	46.57	248	39.04	40.64	45.10
	10	203	42.70	44.97	48.27	204	40.26	41.86	45.96	204	38.51	40.48	43.28
Panel C Large Jump	3	1587	69.39	70.70	72.91	1590	67.87	69.33	71.27	1594	66.82	68.17	70.24
	4	979	68.87	70.46	72.68	983	66.80	69.17	70.63	985	65.84	67.74	69.17
	5	665	67.98	70.11	72.16	668	66.93	68.16	70.27	671	65.21	66.26	68.55
	6	482	68.20	69.38	71.78	485	65.87	67.95	69.81	487	64.66	66.04	67.63
	7	366	66.57	68.81	71.08	368	65.20	67.12	68.95	370	64.53	66.31	67.93
	8	287	67.04	69.14	71.08	289	64.39	66.85	69.28	291	63.97	65.09	67.34
	9	232	66.01	68.47	70.40	234	64.17	66.33	69.04	235	63.15	64.93	67.69
	10	191	66.15	67.95	70.27	193	63.67	65.80	68.23	194	62.39	64.69	67.11

This table reports the finite-sample size and size-adjusted power (%) of 10,000 simulations of the test statistic $T_{c,\epsilon}$ at 5% nominal level. All simulated prices are contaminated by the additive autocorrelated Gaussian noise and rounding errors. We utilize the two-step noise reduction method in Section 2.3.2 to construct the sequence of pseudo-observations with three different pre-averaging windows, i.e., $k_n = \lceil \theta\sqrt{N} \rceil$ with $\theta \in \{0.3, 0.4, 0.5\}$. The observations are sampled with different PDS barrier widths $c = K\sigma(\tilde{r}_i)$, where K ranges from 3 to 10. Different censoring thresholds with $\epsilon \in \{0.05, 0.07, 0.1\}$ are considered. $N^{(c)}$ stands for the average sampling frequencies.

Table A.5 Finite-sample size and power (%) of other tests under autocorrelated Gaussian noise

Nominal size: 5%											
	Int. (sec)	N_{spl}	BNS	ABD	JO	LM	ASJ	CPR	PZ	MinRV	MedRV
Panel A No Jump	5	4680	0.00	15.38	0.72	10.46	100.00	0.00	5.19	0.00	0.00
	15	1560	2.48	22.98	2.79	19.26	97.34	2.84	8.11	0.40	1.59
	30	780	5.59	24.77	4.27	26.71	47.36	6.32	11.46	2.93	4.99
	60	390	6.84	23.25	5.87	26.53	14.89	7.32	13.67	4.93	6.60
	120	195	7.08	20.54	7.43	17.00	8.51	7.64	15.53	5.55	7.50
	180	130	7.33	17.86	8.53	14.31	5.60	8.09	15.63	5.56	7.98
	300	78	7.92	15.88	10.90	12.15	4.35	9.20	15.09	5.73	9.55
Panel B Moderate Jump	5	4680	42.34	73.62	49.60	68.05	99.81	45.64	64.41	37.27	42.66
	15	1560	39.11	71.47	43.61	59.86	93.84	42.79	60.18	36.30	40.82
	30	780	36.35	66.97	37.43	50.10	66.10	40.00	52.66	32.51	37.08
	60	390	28.49	59.32	29.46	41.52	39.38	32.06	43.30	26.18	30.62
	120	195	22.16	48.88	21.09	34.90	21.09	25.48	32.18	20.48	23.39
	180	130	17.80	41.66	16.58	29.83	15.66	20.78	25.61	17.18	19.83
	300	78	13.36	32.57	11.19	19.64	10.68	14.91	18.07	12.98	14.99
Panel C Large Jump	5	4680	66.02	86.02	71.75	83.05	99.73	68.49	80.74	61.79	66.31
	15	1560	63.75	85.06	67.48	78.59	95.40	66.49	78.52	61.00	64.90
	30	780	60.36	82.44	62.07	72.40	78.66	63.52	73.58	57.06	61.05
	60	390	53.77	76.70	55.08	65.78	56.45	57.05	67.04	51.59	55.26
	120	195	46.55	68.90	46.82	60.23	35.58	49.80	57.96	44.44	48.75
	180	130	40.73	64.47	41.31	55.31	24.87	44.99	51.75	39.56	44.64
	300	78	33.58	56.01	32.74	44.99	16.57	37.28	42.89	32.71	36.46

This table reports the finite-sample size and size-adjusted power (%) of 10,000 simulations of 9 classical tests at 5% nominal level: BNS (Barndorff-Nielsen and Shephard, 2006), ABD (Andersen et al., 2007c), JO (Jiang and Oomen, 2008), LM (Lee and Mykland, 2008), ASJ (Aït-Sahalia and Jacod, 2009), CPR (Corsi et al., 2010), PZ (Podolskij and Ziggel, 2010), MinRV and MedRV (Andersen et al., 2012). All these tests are constructed on observations equidistantly sampled with various intervals in calendar time: 5, 15, 30, 60, 120, 180 and 300 seconds, and "N_{spl}" stands for the sampling frequencies.

Table A.6 Finite-sample size and power (%) of other noise-robust tests under autocorrelated Gaussian noise

Nominal size: 5%					
	Int. (sec)	N_{spl}	PZ*	LM12	ASJL
No Jump	tick	23400	5.06	2.91	5.19
	5	4680	4.98	8.10	8.92
Moderate Jump	tick	23400	38.51	21.87	37.46
	5	4680	29.10	18.91	17.09
Large Jump	tick	23400	65.58	39.64	63.69
	5	7680	55.98	32.62	41.88

This table reports the finite-sample size and size-adjusted power (%) of 10,000 simulations of 3 noise-robust tests at 5% nominal level: noise-adjusted PZ (Podolskij and Ziggel, 2010), LM12 (Lee and Mykland, 2012), and ASJL (Aït-Sahalia et al., 2012). All these tests are constructed on tick-level and 5-second-sampled observations. The tuning parameters for those tests are selected by minimizing the absolute distance between the nominal size and the empirical size with the simulated tick-level noise-contaminated observations.

Table A.7 Finite-sample size and power (%) under t-distributed noise

Nominal size: 5%		$\theta = 0.3$				$\theta = 0.4$				$\theta = 0.5$			
			ϵ				ϵ				ϵ		
	$c/\sigma(\tilde{r}_i)$	$N^{(c)}$	0.05	0.07	0.10	$N^{(c)}$	0.05	0.07	0.10	$N^{(c)}$	0.05	0.07	0.10
Panel A No Jump	3	1785	4.74	5.28	5.54	1784	5.25	5.01	5.79	1783	5.04	5.38	5.73
	4	1100	5.01	5.04	5.40	1098	5.05	5.00	5.78	1098	5.05	5.10	5.61
	5	743	4.62	4.85	5.29	743	4.77	5.04	5.51	743	4.60	5.31	5.82
	6	536	4.93	5.01	5.35	535	4.67	5.01	5.42	535	4.81	5.44	5.81
	7	404	4.83	5.08	5.22	404	4.81	5.04	5.48	403	5.24	5.58	5.67
	8	316	4.86	5.34	5.27	316	4.91	5.22	5.67	316	4.88	5.15	5.70
	9	254	4.77	5.42	5.24	253	5.13	5.41	5.39	253	4.83	5.01	5.72
	10	208	5.12	5.37	5.64	208	5.27	5.56	5.77	208	4.93	5.62	5.84
Panel B Moderate Jump	3	1716	46.47	48.75	50.70	1718	44.29	46.93	48.39	1718	42.42	45.03	46.94
	4	1058	45.56	48.39	50.84	1060	43.27	45.47	47.73	1061	41.57	43.20	45.28
	5	717	45.09	47.07	50.32	719	42.73	45.48	47.82	720	40.67	42.31	45.21
	6	519	44.78	46.46	48.26	519	41.76	44.18	46.61	521	40.50	42.15	44.40
	7	392	44.00	45.75	48.66	393	40.80	43.60	46.14	394	39.99	41.48	43.88
	8	307	42.56	44.26	48.15	308	40.08	42.59	45.58	308	39.08	41.55	43.25
	9	247	42.79	44.68	48.11	248	39.44	41.88	45.47	248	38.55	41.12	42.51
	10	203	41.21	44.19	46.88	204	39.69	41.62	44.87	204	37.62	39.87	42.92
Panel C Large Jump	3	1585	70.44	71.21	73.23	1589	68.58	70.69	72.01	1592	66.90	68.86	70.80
	4	978	69.91	71.37	73.07	981	68.25	69.64	71.07	985	66.59	68.75	69.66
	5	664	69.36	71.15	72.79	668	67.65	69.30	71.08	670	66.09	67.79	69.56
	6	481	68.75	70.43	72.67	484	66.82	68.64	70.50	487	65.24	66.70	68.72
	7	365	68.08	69.77	71.74	368	65.70	67.87	69.97	370	64.57	66.43	68.83
	8	287	67.67	68.95	70.93	289	65.10	68.12	69.69	291	63.77	66.09	67.83
	9	232	66.89	68.86	71.66	234	64.52	66.96	69.63	235	63.39	66.10	67.81
	10	191	66.21	68.25	70.90	192	64.24	66.28	69.49	194	62.52	64.96	67.43

This table reports the finite-sample size and size-adjusted power (%) of 10,000 simulations of the test statistic $T_{c,\epsilon}$ at 5% nominal level. All simulated prices are contaminated by the additive t-distributed noise and rounding errors. We utilize the two-step noise reduction method in Section 2.3.2 to construct the sequence of pseudo-observations with three different pre-averaging windows, i.e., $k_n = \lceil \theta\sqrt{N} \rceil$ with $\theta \in \{0.3, 0.4, 0.5\}$. The observations are sampled with different PDS barrier widths $c = K\sigma(\tilde{r}_i)$, where K ranges from 3 to 10. Different censoring thresholds with $\epsilon \in \{0.05, 0.07, 0.1\}$ are considered. $N^{(c)}$ stands for the average sampling frequencies.

Table A.8 Finite-sample size and power (%) of other tests under t-distributed noise

	Int. (sec)	N_{spl}	BNS	ABD	JO	LM	ASJ	CPR	PZ	MinRV	MedRV
Panel A No Jump	5	4680	58.90	100.00	15.85	100.00	99.92	99.87	99.70	0.12	0.02
	15	1560	12.76	90.37	10.10	89.87	92.05	56.23	72.27	0.71	2.19
	30	780	8.89	59.49	7.81	62.42	44.91	24.70	40.96	3.06	5.18
	60	390	7.25	35.24	7.38	38.66	16.35	11.91	24.07	4.49	7.09
	120	195	7.23	23.72	8.22	20.16	7.68	8.87	18.31	5.11	7.38
	180	130	7.37	19.82	8.99	16.35	5.38	8.42	17.48	5.30	8.46
	300	78	7.34	15.19	10.83	11.47	4.33	8.64	14.86	5.22	8.55
Panel B Moderate Jump	5	4680	37.49	100.00	37.05	17.64	99.97	11.25	13.71	39.54	41.12
	15	1560	40.61	96.71	38.20	25.74	97.85	21.65	20.95	34.45	37.18
	30	780	36.25	82.85	35.77	31.96	70.97	30.82	27.51	31.47	35.67
	60	390	30.11	65.91	29.45	36.41	40.48	30.72	35.36	27.12	31.05
	120	195	22.54	50.98	21.73	34.11	21.92	24.58	30.89	20.59	23.94
	180	130	17.55	43.33	17.67	29.39	14.43	20.16	25.77	16.98	20.66
	300	78	14.49	34.14	12.22	22.25	10.45	16.11	20.07	13.74	17.01
Panel C Large Jump	5	4680	62.75	100.00	63.82	45.20	99.98	31.59	38.22	63.94	65.60
	15	1560	65.71	98.39	64.24	53.45	98.79	47.84	47.73	59.14	61.94
	30	780	61.92	91.00	62.02	59.38	81.94	56.98	54.91	56.36	60.86
	60	390	55.55	82.02	55.88	63.00	57.74	56.36	62.26	52.38	56.60
	120	195	47.62	71.89	47.85	60.48	37.89	51.29	57.77	45.42	50.37
	180	130	41.65	65.87	43.02	55.53	25.61	45.02	52.02	40.67	45.06
	300	78	35.10	57.50	34.13	47.57	16.34	39.19	45.37	34.32	39.24

This table reports the finite-sample size and size-adjusted power (%) of 10,000 simulations of 9 classical tests at 5% nominal level: BNS (Barndorff-Nielsen and Shephard, 2006), ABD (Andersen et al., 2007c), JO (Jiang and Oomen, 2008), LM (Lee and Mykland, 2008), ASJ (Aït-Sahalia and Jacod, 2009), CPR (Corsi et al., 2010), PZ (Podolskij and Ziggel, 2010), MinRV and MedRV (Andersen et al., 2012). All these tests are constructed on observations equidistantly sampled with various intervals in calendar time: 5, 15, 30, 60, 120, 180 and 300 seconds, and "N_{spl}" stands for the sampling frequencies.

Table A.9 Finite-sample size and power (%) of other noise-robust tests under t-distributed noise

Nominal size: 5%					
	Int. (sec)	N_{spl}	PZ*	LM12	ASJL
No Jump	tick	23400	5.07	5.46	6.18
	5	4680	4.64	9.24	8.74
Moderate Jump	tick	23400	39.40	25.31	37.68
	5	4680	29.26	18.76	17.19
Large Jump	tick	23400	65.11	41.81	62.48
	5	7680	55.60	31.85	41.42

This table reports the finite-sample size and size-adjusted power (%) of 10,000 simulations of 3 noise-robust tests at 5% nominal level: noise-adjusted PZ (Podolskij and Ziggel, 2010), LM12 (Lee and Mykland, 2012), and ASJL (Aït-Sahalia et al., 2012). All these tests are constructed on tick-level and 5-second-sampled observations. The tuning parameters for those tests are selected by minimizing the absolute distance between the nominal size and the empirical size with the simulated tick-level noise-contaminated observations.

A.2.3 Supplementary Empirical Results

Table A.10 reports the empirical results for 7 other tests. Based on the simulation results in Tables 2.3 and 2.4, we select four calendar-time-sampling-based tests: BNS, CPR, MinRV and MedRV, with different sampling intervals: 30, 60, 120, and 300 seconds, and we also construct the noise-robust tests PZ*, LM12 and ASJL from tick-by-tick and 5-second data. For most of the selected stocks, the noise-robust ASJL constructed from tick-level observations obtains comparable results to our PDS-based test.

Table A.10 Empirical rejection rates (%) of other tests for selected NYSE stocks

Test	Int. (sec)	AXP	BA	DIS	IBM	JNJ	JPM	MRK	MCD	PG	WMT
BNS	30	32.02	20.55	20.95	28.46	36.36	32.81	49.80	25.69	43.08	32.41
	60	20.16	11.07	19.37	25.69	28.06	24.51	37.55	26.09	31.23	26.88
	120	17.00	16.21	16.21	22.53	27.67	25.30	25.69	23.32	27.27	27.67
	300	18.58	18.58	15.42	19.76	20.16	17.00	23.32	22.13	22.13	22.13
CPR	30	38.34	32.02	35.57	39.13	47.83	38.34	59.29	33.20	52.57	41.11
	60	28.46	16.60	26.88	33.99	40.32	32.41	45.85	29.25	40.32	35.57
	120	25.30	20.16	21.74	30.83	34.78	32.02	33.99	28.85	32.81	33.60
	300	23.32	23.72	21.34	27.67	29.64	22.13	32.81	28.46	30.43	30.83
MinRV	30	22.53	17.39	15.42	18.18	22.92	21.74	27.67	19.76	26.48	21.34
	60	14.23	9.88	15.42	19.76	21.74	16.21	22.92	20.95	22.13	22.13
	120	14.23	12.65	12.65	18.58	18.18	17.79	18.58	19.76	19.76	21.74
	300	13.04	14.62	13.83	17.39	13.04	11.07	15.81	15.42	16.21	14.23
MedRV	30	30.83	23.72	28.46	31.62	37.15	29.64	40.71	29.64	37.94	32.02
	60	20.55	15.81	22.92	28.46	37.15	27.67	33.60	28.85	32.81	30.04
	120	20.55	18.58	18.58	26.48	29.64	26.48	27.27	26.88	28.85	34.78
	300	18.97	17.00	16.60	24.11	21.74	20.55	23.72	24.90	28.06	25.30
PZ*	tick	7.51	6.32	6.32	5.93	6.32	6.72	7.51	5.14	7.51	4.74
	5	31.23	22.92	19.76	26.09	22.13	23.32	23.72	24.90	30.04	31.62
LM12	tick	12.65	4.35	7.51	9.49	12.65	11.46	12.65	9.49	18.58	11.86
	5	32.02	21.34	30.04	37.55	29.25	27.27	38.74	27.67	40.32	35.18
ASJL	tick	15.81	20.16	13.04	13.83	13.83	13.44	15.02	20.55	13.83	15.02
	5	32.02	20.95	29.25	21.34	26.48	21.74	22.92	26.09	30.04	32.41

This table reports the proportions of days with jumps for 10 NYSE stocks in 2020, as identified by the following procedures: BNS (Barndorff-Nielsen and Shephard, 2006), CPR (Corsi et al., 2010), PZ (Podolskij and Ziggel, 2010), MinRV and MedRV (Andersen et al., 2012), PZ* (Podolskij and Ziggel, 2010), LM12 (Lee and Mykland, 2012), and ASJL (Aït-Sahalia et al., 2012). The first 4 tests are constructed from observations equidistantly sampled in calendar time (with the last tick interpolation): 30, 60, 120 and 300 seconds. The noise-adjusted PZ*, LM12, and ASJL are constructed from tick-by-tick and 5-second-sampled data. The total number of trading days is 253.

Table A.11 reports the empirical results for other tests constructed from calendar-time-sampled data, with the control of spurious detections using the thresholding methods in Bajgrowicz et al. (2016): (i) the universal threshold $\sqrt{2\ln 253}$, and (ii) the FDR threshold. We only consider one-sided tests whose limiting distribution is $\mathcal{N}(0,1)$ under the null, which includes the upper-tailed BNS, CPR, MinRV, MedRV, PZ*, and the lower-tailed ASJL, but

excludes the Gumbel-distributed LM12.

Table A.11 Adjusted empirical rejection rate (%) of other tests for selected NYSE stocks

	Test	Int. (sec)	AXP	BA	DIS	IBM	JNJ	JPM	MRK	MCD	PG	WMT
Panel A Universal threshold	BNS	30	24.11	18.18	17.79	23.32	27.67	25.69	33.99	20.95	30.83	22.92
		60	15.81	9.09	15.42	19.37	18.58	18.97	29.25	20.55	24.11	20.16
		120	13.44	13.83	15.02	20.55	22.92	22.13	21.74	17.79	19.37	20.55
		300	15.02	16.21	13.04	15.42	16.21	14.62	19.76	17.79	17.00	20.55
	CPR	30	27.67	27.27	29.64	27.67	31.23	26.88	36.76	23.32	33.99	26.48
		60	22.92	13.83	20.55	25.69	27.67	22.92	31.23	20.95	27.67	24.11
		120	21.34	17.00	19.76	24.90	24.11	27.27	25.69	23.32	23.72	24.51
		300	18.18	20.55	16.60	22.53	23.72	18.18	25.69	22.13	21.74	26.09
	MinRV	30	17.79	16.21	13.44	16.21	19.37	18.18	23.32	16.60	20.55	16.60
		60	11.86	8.30	14.23	15.81	17.79	14.62	20.55	18.97	20.16	18.97
		120	12.25	12.25	12.25	18.18	17.39	17.39	15.02	17.79	16.21	18.97
		300	12.25	13.44	13.44	16.21	12.25	11.07	15.42	13.44	15.02	13.83
	MedRV	30	24.51	21.74	26.09	25.30	26.09	21.74	30.04	22.92	28.46	26.09
		60	17.00	14.23	19.76	23.32	29.64	21.34	24.90	25.69	24.11	22.53
		120	17.39	16.21	17.39	21.34	24.11	24.11	22.53	22.13	22.13	29.64
		300	16.21	15.42	15.02	20.55	18.97	18.97	18.18	20.95	24.51	22.13
	PZ*	tick	5.53	5.53	6.32	3.56	3.56	5.93	5.93	3.95	5.14	3.16
		5	2.77	4.35	1.58	3.95	3.16	2.77	2.77	3.16	3.56	4.74
	ASJL	tick	14.23	18.58	13.04	13.04	13.44	12.25	12.25	19.37	13.44	14.62
		5	26.09	17.39	26.09	18.18	21.34	17.00	18.58	22.53	25.30	24.11
Panel B FDR threshold	BNS	30	14.23	15.02	16.21	14.23	12.25	15.02	9.09	14.62	11.46	11.07
		60	13.04	7.11	12.25	12.65	10.28	14.23	15.02	13.04	14.23	9.09
		120	9.88	13.44	14.62	14.62	13.83	17.39	12.25	15.02	13.83	10.28
		300	13.04	13.04	9.88	12.25	13.83	11.46	12.65	13.44	9.09	16.21
	CPR	30	9.09	15.42	19.37	13.04	11.86	9.09	7.51	12.25	8.30	10.28
		60	14.62	10.67	15.02	15.02	13.04	15.02	12.25	11.46	11.07	9.88
		120	13.83	16.21	16.21	13.04	14.62	16.21	13.04	13.44	13.04	10.67
		300	13.04	16.21	11.46	17.00	13.04	10.28	17.79	15.02	13.44	15.42
	MinRV	30	15.81	14.23	12.65	16.21	12.65	17.39	11.07	14.23	15.02	13.83
		60	10.67	7.51	11.07	12.65	12.65	11.86	13.44	18.58	13.44	14.62
		120	10.67	12.25	12.65	18.18	13.83	16.21	14.23	16.21	14.62	16.21
		300	12.65	11.86	13.44	15.81	12.25	11.07	13.04	13.44	15.02	13.83
	MedRV	30	15.02	19.37	19.76	10.28	16.60	16.60	10.67	16.21	17.39	13.44
		60	13.04	13.04	13.44	11.86	19.76	13.04	13.83	18.18	16.60	11.07
		120	15.42	15.02	13.83	15.42	18.58	21.74	16.21	18.97	12.25	18.58
		300	11.07	13.83	9.49	16.60	13.83	16.60	13.04	13.04	16.60	18.97
	PZ*	tick	5.53	5.53	6.32	3.56	3.56	5.93	5.93	3.95	5.14	3.16
		5	2.77	4.35	1.58	3.95	3.16	2.77	2.77	3.16	3.56	4.74
	ASJL	tick	13.04	16.21	13.04	10.28	13.44	12.25	11.07	17.39	13.44	14.62
		5	15.02	13.44	18.58	15.42	15.42	14.23	12.65	18.58	17.39	14.62

This table reports the proportions of days with jumps for 10 NYSE stocks in 2020, as identified by the following procedures: BNS (Barndorff-Nielsen and Shephard, 2006), CPR (Corsi et al., 2010), PZ (Podolskij and Ziggel, 2010), MinRV and MedRV (Andersen et al., 2012), PZ* (Podolskij and Ziggel, 2010), and ASJL (Aït-Sahalia et al., 2012), with the control of spurious detections using the thresholding methods in Bajgrowicz et al. (2016). The first 4 tests are constructed from observations equidistantly sampled in calendar time (with the last tick interpolation): 30, 60, 120 and 300 seconds. The noise-adjusted PZ* and ASJL are constructed from tick-by-tick and 5-second-sampled data. The total number of trading days is 253.

Appendix B

Appendix to Chapter 3

B.1 Normalized High, Low, and Close

For the standard Brownian motion starting at zero, i.e., $W = (W_t)_{t\geq 0}$, in a filtered probability space $(\Omega, \mathcal{F}, (\mathcal{F}_t)_{t\geq 0}, \mathbb{P})$, we denote the normalized high, low, and close as, respectively,

$$u = \sup_{0\leq t\leq 1} W_t, \qquad d = \inf_{0\leq t\leq 1} W_t, \qquad c = W_1. \tag{B.1}$$

For the range of a standard Brownian motion, i.e., $\omega = u - d$, its probability distribution was firstly proposed by Feller (1951) and its moment generating function was then derived by Parkinson (1980), i.e., for the r-th moment:

$$\mathbb{E}[\omega^r] = \frac{4}{\sqrt{\pi}}\left(1 - \frac{4}{2^r}\right) 2^{\frac{r}{2}} \Gamma\left(\frac{r+1}{2}\right) \zeta(r-1), \tag{B.2}$$

where $\Gamma(x)$ and $\zeta(x)$ are the Gamma and Riemann's zeta functions, respectively. In particular, we have

$$\begin{aligned} \mathbb{E}[\omega] &= 2\sqrt{\frac{2}{\pi}} \approx 1.5958, \qquad & \mathbb{E}[\omega^2] &= 4\ln 2 \approx 2.7726, \\ \mathbb{E}[\omega^3] &= \frac{2}{3}\sqrt{2\pi^3} \approx 5.2499, \qquad & \mathbb{E}[\omega^4] &= 9\zeta(3) \approx 10.8185. \end{aligned} \tag{B.3}$$

Also, Garman and Klass (1980) reveals the following fourth moments of the normalized high, low, close via the generating functions $\mathbb{E}[u^p d^q c^r]$:[1]

$$\mathbb{E}[u^4] = \mathbb{E}[d^4] = \mathbb{E}[c^4] = 3, \qquad \mathbb{E}[u^2c^2] = \mathbb{E}[d^2c^2] = 2, \tag{B.4}$$

$$\mathbb{E}[u^3c] = \mathbb{E}[d^3c] = 2.25, \qquad \mathbb{E}[uc^3] = \mathbb{E}[dc^3] = 1.5, \tag{B.5}$$

$$\mathbb{E}[u^2dc] = \mathbb{E}[ud^2c] = \frac{9}{4} - 2\ln 2 - \frac{7}{8}\zeta(3) \approx -0.1881, \tag{B.6}$$

$$\mathbb{E}[u^2d^2] = 3 - 4\ln 2 \approx 0.2274, \tag{B.7}$$

$$\mathbb{E}[udc^2] = 2 - 2\ln 2 - \frac{7}{8}\zeta(3) \approx -0.4381, \tag{B.8}$$

$$\mathbb{E}[ud^3] = \mathbb{E}[u^3d] = 3 - 3\ln 2 - \frac{9}{8}\zeta(3) \approx -0.4318, \tag{B.9}$$

where $\zeta(3) = \sum_{n=1}^{\infty} n^{-3} \approx 1.2021$. It is straightforward that

$$\mathbb{E}[\omega^2c^2] = \mathbb{E}[(u-d)^2c^2] = \mathbb{E}[u^2c^2] + \mathbb{E}[d^2c^2] - 2\mathbb{E}[udc^2] = 4\ln 2 + \frac{7}{4}\zeta(3) \approx 4.8762. \tag{B.10}$$

When we substitute the normalized close c in above moments with its absolute value $|c|$, it is obvious that the values in Eqs. (B.5) and (B.6) do not follow from Garman and Klass (1980). Different from the Garman-Klass triple (u, d, c), Meilijson (2011) considers $(\tilde{u}, \tilde{d}, |c|)$ where $(\tilde{u}, \tilde{d}) = (u, d)$ if $c \geq 0$ while $(\tilde{u}, \tilde{d}) = -(d, u)$ if $c < 0$, and derives the second and fourth moments as follows:

$$\mathbb{E}[\tilde{u}^2] = \frac{7}{4}, \quad \mathbb{E}[\tilde{d}^2] = \frac{1}{4}, \quad \mathbb{E}[\tilde{u}|c|] = \frac{5}{4}, \quad \mathbb{E}[\tilde{d}|c|] = -\frac{1}{4}, \quad \mathbb{E}[\tilde{u}\tilde{d}] = 1 - 2\ln 2 \approx -0.3863, \tag{B.11}$$

$$\mathbb{E}[\tilde{u}^4] = \frac{93}{16}, \quad \mathbb{E}[\tilde{d}^4] = \frac{3}{16}, \quad \mathbb{E}[\tilde{u}^2|c|^2] = \frac{31}{8}, \quad \mathbb{E}[\tilde{d}^2|c|^2] = \frac{1}{8}, \tag{B.12}$$

$$\mathbb{E}[\tilde{u}^3|c|] = \frac{147}{32}, \quad \mathbb{E}[\tilde{d}^3|c|] = -\frac{3}{32}, \quad \mathbb{E}[\tilde{u}|c|^3] = \frac{27}{8}, \quad \mathbb{E}[\tilde{d}|c|^3] = -\frac{3}{8}, \tag{B.13}$$

$$\mathbb{E}[\tilde{u}^2\tilde{d}^2] = \mathbb{E}[u^2d^2] = 3 - 4\ln 2 \approx 0.2274, \tag{B.14}$$

$$\mathbb{E}[\tilde{u}\tilde{d}|c|^2] = \mathbb{E}[udc^2] = 2 - 2\ln 2 - \frac{7}{8}\zeta(3) \approx -0.4381, \tag{B.15}$$

$$\mathbb{E}[\tilde{u}^3\tilde{d}] + \mathbb{E}[\tilde{u}\tilde{d}^3] = \mathbb{E}[ud(u^2 + d^2)] = 6 - 6\ln 2 - \frac{9}{4}\zeta(3) \approx -0.8635, \tag{B.16}$$

[1] See Appendix C in Garman and Klass (1980).

$$\mathbb{E}[\tilde{u}^2\tilde{d}|c|] + \mathbb{E}[\tilde{u}\tilde{d}^2|c|] = \mathbb{E}[udc(u+d)] = \frac{9}{2} - 4\ln 2 - \frac{7}{4}\zeta(3) \approx -0.3762, \tag{B.17}$$

$$\mathbb{E}[\tilde{u}\tilde{d}^2|c|] = \frac{1}{16}\zeta(3) - 2\ln 2 + \frac{47}{32} \approx 0.1576. \tag{B.18}$$

We can use the above results to obtain the following second and fourth moments of $(\omega, |c|)$:

$$\mathbb{E}[\omega|c|] = \mathbb{E}[(\tilde{u} - \tilde{d})|c|] = \mathbb{E}[\tilde{u}|c|] - \mathbb{E}[\tilde{d}|c|] = \frac{3}{2}, \tag{B.19}$$

$$\mathbb{E}[\omega|c|^3] = \mathbb{E}[(\tilde{u} - \tilde{d})|c|^3] = \mathbb{E}[\tilde{u}|c|^3] - \mathbb{E}[\tilde{d}|c|^3] = \frac{15}{4}, \tag{B.20}$$

$$\begin{aligned}
\mathbb{E}[\omega^3|c|] &= \mathbb{E}[(\tilde{u} - \tilde{d})^3|c|] \\
&= \mathbb{E}[(\tilde{u}^3 - \tilde{d}^3 - 3\tilde{u}^2\tilde{d} + 3\tilde{u}\tilde{d}^2)|c|] \\
&= \mathbb{E}[\tilde{u}^3|c|] - \mathbb{E}[\tilde{d}^3|c|] - 3\mathbb{E}[\tilde{u}^2\tilde{d}|c|] + 3\mathbb{E}[\tilde{u}\tilde{d}^2|c|] \\
&= \frac{147}{32} + \frac{3}{32} - 3\left(\frac{9}{2} - 4\ln 2 - \frac{7}{4}\zeta(3)\right) + 6\left(\frac{1}{16}\zeta(3) - 2\ln 2 + \frac{47}{32}\right) \\
&= \frac{45}{8}\zeta(3) \approx 6.7616.
\end{aligned} \tag{B.21}$$

To calculate the third moments of $(\omega, |c|)$, we derive the analytical expressions for $\mathbb{E}[\tilde{u}^2|c|]$, $\mathbb{E}[\tilde{d}^2|c|]$, $\mathbb{E}[\tilde{u}|c|^2]$, $\mathbb{E}[\tilde{d}|c|^2]$, and $\mathbb{E}[\tilde{u}\tilde{d}|c|]$, which are not available in the literature. For the first four quantities, we obtain the results by integrating the joint densities in Meilijson (2011), i.e.,

$$f_{\tilde{u},|c|}(a,x) = 4(2a - x)\phi(2a - x), \quad 0 < x < a, \tag{B.22}$$

$$f_{\tilde{d},|c|}(b,x) = 4(x - 2b)\phi(x - 2b), \quad b < 0 < x, \tag{B.23}$$

where $\phi(z) = (2\pi)^{-1/2}e^{-z^2/2}$ is the probability density function (PDF) of $\mathcal{N}(0,1)$:

$$\mathbb{E}[\tilde{u}^2|c|] = \frac{17}{3\sqrt{2\pi}} \approx 2.2607, \quad \mathbb{E}[\tilde{d}^2|c|] = \frac{1}{3\sqrt{2\pi}} \approx 0.1330, \tag{B.24}$$

$$\mathbb{E}[\tilde{u}|c|^2] = \frac{7}{3}\sqrt{\frac{2}{\pi}} \approx 1.8617, \quad \mathbb{E}[\tilde{d}|c|^2] = -\frac{1}{3}\sqrt{\frac{2}{\pi}} \approx -0.2660. \tag{B.25}$$

There is one more moment needed, i.e., $\mathbb{E}[\tilde{u}\tilde{d}|c|]$. We start with the infinitesimal event $A = \{W_1 \in (x, x + dx), W_t \in (b, a), \forall t \in [0,1]\}$, where $b < \min\{x, 0\} \leq 0 \leq \max\{x, 0\} < a$, and its

probability $\mathbb{P}(A) = Q(a,b,x)dx$, where

$$Q(a,b,x) = \sum_{j=-\infty}^{\infty} \{\phi(x-2j(a-b)) - \phi(x-2b-2j(a-b))\}. \tag{B.26}$$

The joint density of $(\tilde{u}, \tilde{d}, |c|)$ is then given by $f_{\tilde{u},\tilde{d},|c|}(a,b,x) = -2\partial^2 Q(a,b,x)/\partial a \partial b$, restricted to $b < 0 < x < a$, which is also an infinite series.[2] The summand with $j = 0$ takes value 0 because both two ϕ functions are independent of at least one of a and b, as similar to the second term in the summand with $j = 1$. The required moment can be obtained by solving the triple integral:

$$\begin{aligned}
\mathbb{E}[\tilde{u}\tilde{d}|c|] &= -2\int_0^{\infty}\int_0^{a}\int_{-\infty}^{0} abx \frac{\partial^2 Q(a,b,x)}{\partial a \partial b} dbdxda \\
&= -2\sum_{j\in\mathbb{C}_{\mathbb{Z}}\{0\}} \int_0^{\infty} ada \int_0^{a} xdx \int_{-\infty}^{0} \frac{\partial}{\partial a} b \left[\frac{\partial}{\partial b}\phi(x-2j(a-b))\right. \\
&\qquad \left. -\frac{\partial}{\partial b}\phi(x-2b-2j(a-b))\mathbb{1}_{\{j\neq 1\}}\right] db
\end{aligned} \tag{B.27}$$

We integrate each summand in three univariate steps. The first step will integrate over $b \in (-\infty, 0)$ the product of b and mixed second derivative $\partial^2\phi(x+Ma+Kb)/\partial a\partial b$:

$$\begin{aligned}
\int_{-\infty}^{0} \frac{\partial}{\partial a} b \frac{\partial}{\partial b}\phi(x+Ma+Kb)db &= \frac{\partial}{\partial a}\int_{-\infty}^{0} b\frac{\partial}{\partial b}\phi(x+Ma+Kb)db \\
&= \frac{\partial}{\partial a}\int_{-\infty}^{0} bd\phi(x+Ma+Kb) \\
&= \frac{\partial}{\partial a}\left[b\phi(x+Ma+Kb)\right]_{-\infty}^{0} - \frac{\partial}{\partial a}\int_{-\infty}^{0}\phi(x+Ma+Kb)db \\
&= -\int_{-\infty}^{0}\frac{\partial}{\partial a}\phi(x+Ma+Kb)db \\
&= -M\int_{-\infty}^{0}\phi'(x+Ma+Kb)db \\
&= -\frac{M}{K}\left[\phi(x+Ma+Kb)\right]_{-\infty}^{0} \\
&= -\frac{M}{K}\phi(x+Ma).
\end{aligned} \tag{B.28}$$

[2] See more details in the Appendix of Meilijson (2011).

Then we multiply the above result by x and integrate it over $x \in (0, a)$:

$$\begin{aligned}
&\int_0^a x dx \int_{-\infty}^0 \frac{\partial}{\partial a} b \frac{\partial}{\partial b} \phi(x + Ma + Kb) db \\
&= -\frac{M}{K} \int_0^a x \phi(x + Ma) dx \\
&= -\frac{M}{K} \int_{Ma}^{(M+1)a} y \phi(y) dy + \frac{M^2 a}{K} \int_{Ma}^{(M+1)a} \phi(y) dy \\
&= \frac{M}{K} \int_{Ma}^{(M+1)a} \phi'(y) dy + \frac{M^2 a}{K} \int_{Ma}^{(M+1)a} \phi(y) dy \qquad \text{because } \phi'(z) = -z\phi(z) \\
&= \frac{M}{K} \left[\phi((M+1)a) - \phi(Ma) \right] + \frac{M^2 a}{K} \left[\Phi((M+1)a) - \Phi(Ma) \right] \\
\text{or } &= \frac{M}{K} \left[\phi((M+1)a) - \phi(Ma) \right] - \frac{M^2 a}{K} \left[\Phi^*((M+1)a) - \Phi^*(Ma) \right],
\end{aligned} \tag{B.29}$$

where $\Phi(z) = \int_{-\infty}^z \phi(t) dt = 0.5(1 + \operatorname{erf} z/\sqrt{2})$ is the cumulative distribution function (CDF) of $\mathcal{N}(0, 1)$, and $\Phi^*(z) = 1 - \Phi(z) = 0.5(1 - \operatorname{erf} z/\sqrt{2})$ is the survival function. Finally, this expression is multiplied by a and integrated over $a \in (0, \infty)$. We use the results

$$\int_0^\infty a\phi(aA) da = \int_0^\infty a\phi(-aA) da = \frac{1}{\sqrt{2\pi} A^2}, \tag{B.30}$$

$$\int_0^\infty a^2 \Phi(-aA) da = \int_0^\infty a^2 \Phi^*(aA) da = \frac{1}{3A^3} \sqrt{\frac{2}{\pi}}, \quad \text{with } A > 0, \tag{B.31}$$

to calculate the triple integral of $abx\partial^2 \phi(x + Ma + Kb)/\partial a \partial b$. When $M \in \mathbb{Z}^{>0}$, we have

$$\begin{aligned}
&\int_0^\infty a da \int_0^a x dx \int_{-\infty}^0 \frac{\partial}{\partial a} b \frac{\partial}{\partial b} \phi(x + Ma + Kb) db \\
&= \frac{M}{K} \int_0^\infty a\phi((M+1)a) da - \frac{M}{K} \int_0^\infty a\phi(Ma) da \\
&\qquad + \frac{M^2}{K} \int_0^\infty a^2 \Phi((M+1)a) da - \frac{M^2}{K} \int_0^\infty a^2 \Phi(Ma) da \\
&= \frac{1}{\sqrt{2\pi}} \frac{M}{K} \left[\frac{1}{(M+1)^2} - \frac{1}{M^2} \right] - \frac{1}{3} \sqrt{\frac{2}{\pi}} \frac{M^2}{K} \left[\frac{1}{(M+1)^3} - \frac{1}{M^3} \right] = \mathcal{G}(M, K).
\end{aligned} \tag{B.32}$$

When $M \in \mathbb{Z}^{<-1}$, we have

$$\begin{aligned}
&\int_0^\infty ada \int_0^a xdx \int_{-\infty}^0 \frac{\partial}{\partial a} b \frac{\partial}{\partial b} \phi(x + Ma + Kb) db \\
&= \frac{M}{K} \int_0^\infty a\phi((M+1)a)da - \frac{M}{K} \int_0^\infty a\phi(Ma)da \\
&\qquad - \frac{M^2}{K} \int_0^\infty a^2 \Phi^*((M+1)a)da + \frac{M^2}{K} \int_0^\infty a^2 \Phi^*(Ma)da \\
&= \frac{1}{\sqrt{2\pi}} \frac{M}{K} \left[\frac{1}{(M+1)^2} - \frac{1}{M^2} \right] - \frac{1}{3} \sqrt{\frac{2}{\pi}} \frac{M^2}{K} \left[\frac{1}{(M+1)^3} - \frac{1}{M^3} \right] = \mathcal{G}(M, K).
\end{aligned} \tag{B.33}$$

We now transfer each summand into a rational function of j, by letting M take $-2j$, and K take $2j$ or $2(j-1)$. For summands with $j \in \mathbb{C}_{\mathbb{Z}}\{0, 1\}$, we have

$$\begin{aligned}
&\int_0^\infty ada \int_0^a xdx \int_{-\infty}^0 \frac{\partial}{\partial a} b \left[\frac{\partial}{\partial b} \phi(x - 2j(a-b)) - \frac{\partial}{\partial b} \phi(x - 2b - 2j(a-b)) \right] db \\
&= \mathcal{G}(-2j, 2j) - \mathcal{G}(-2j, 2(j-1)) \\
&= -\frac{1}{\sqrt{2\pi}} \left(1 - \frac{j}{j-1} \right) \left[\frac{1}{(1-2j)^2} - \frac{1}{(2j)^2} \right] - \frac{1}{3} \left(2j - \frac{2j^2}{j-1} \right) \sqrt{\frac{2}{\pi}} \left[\frac{1}{(1-2j)^3} + \frac{1}{(2j)^3} \right] \\
&= \frac{1}{\sqrt{2\pi}} \frac{1}{j-1} \left[\frac{1}{(1-2j)^2} - \frac{1}{(2j)^2} \right] + \frac{2}{3} \frac{j}{j-1} \sqrt{\frac{2}{\pi}} \left[\frac{1}{(1-2j)^3} + \frac{1}{(2j)^3} \right],
\end{aligned} \tag{B.34}$$

and the infinite series

$$\begin{aligned}
\sum_{j \in \mathbb{C}_{\mathbb{Z}}\{0,1\}} \int_0^\infty ada \int_0^a xdx \int_{-\infty}^0 \frac{\partial}{\partial a} b \Big[&\frac{\partial}{\partial b} \phi(x - 2j(a-b)) \\
&- \frac{\partial}{\partial b} \phi(x - 2b - 2j(a-b)) \Big] db = \frac{14\pi^2 - 138}{72\sqrt{2\pi}}.
\end{aligned} \tag{B.35}$$

For summand with $j = 1$, we have

$$\int_0^\infty ada \int_0^a xdx \int_{-\infty}^0 \frac{\partial}{\partial a} b \frac{\partial}{\partial b} \phi(x - 2a + 2b) db = \mathcal{G}(-2, 2) = \frac{5}{12\sqrt{2\pi}}. \tag{B.36}$$

Therefore, the joint moment is calculated by Eq. (B.27):

$$\mathbb{E}[\tilde{u}\tilde{d}|c|] = -2 \left(\frac{5}{12\sqrt{2\pi}} + \frac{14\pi^2 - 138}{72\sqrt{2\pi}} \right) = \frac{54 - 7\pi^2}{18\sqrt{2\pi}} \approx -0.3344. \tag{B.37}$$

Now we can use the results in Eqs. (B.24), (B.25) and (B.37) to calculate the third moments of

$(\omega, |c|)$:

$$\begin{aligned}\mathbb{E}[\omega^2|c|] &= \mathbb{E}[\tilde{u}^2|c|] + \mathbb{E}[\tilde{d}^2|c|] - 2\mathbb{E}[\tilde{u}\tilde{d}|c|] \\ &= \frac{17}{3\sqrt{2\pi}} + \frac{1}{3\sqrt{2\pi}} - 2 \times \frac{54 - 7\pi^2}{18\sqrt{2\pi}} \\ &= \frac{7}{9}\sqrt{\frac{\pi^3}{2}} \approx 3.0624,\end{aligned} \tag{B.38}$$

$$\mathbb{E}[\omega|c|^2] = \mathbb{E}[\tilde{u}|c|^2] - \mathbb{E}[\tilde{d}|c|^2] = \frac{8}{3}\sqrt{\frac{2}{\pi}} \approx 2.1277. \tag{B.39}$$

Moreover, direct calculation of

$$\mathbb{E}[|c|^r] = 2\int_0^\infty \frac{x^r}{\sqrt{2\pi}} e^{-\frac{x^2}{2}} dx \tag{B.40}$$

shows the following moments:

$$\mathbb{E}[|c|] = \sqrt{\frac{2}{\pi}} \approx 0.7979, \quad \mathbb{E}[|c|^2] = 1, \quad \mathbb{E}[|c|^3] = 2\sqrt{\frac{2}{\pi}} \approx 1.5958, \quad \mathbb{E}[|c|^4] = 3. \tag{B.41}$$

For the convenience of further discussion, we denote the moments of $(\omega, |c|)$ by

$$\lambda_{p,r} = \mathbb{E}[\omega^p|c|^r]. \tag{B.42}$$

All $\lambda_{p,r}$ that will be used in Appendix B.2 have been calculated in this section, and are summarized in Table B.1.

B.2 Proofs

B.2.1 Proof of Theorem 3.1

Proof. It is straightforward to prove Theorem 3.1 with the LLN for path-dependent functionals of continuous Itô semimartingales, as summarized in Duembgen and Podolskij (2015). Here we start with some notation. We denote by $C([0,1])$ the space of continuous real valued functions on the interval $[0,1]$, and by $\|\cdot\|_\infty$ the supremum norm on $C([0,1])$. A function $f : C([0,1]) \to \mathbb{R}$ is said to have polynomial growth if $|f(x)| \leq C(1 + \|x\|_\infty^p)$ for some $C, p > 0$.

Definition B.1 (Local uniform continuity)**.** The function $f : C([0,1]) \to \mathbb{R}$ is locally uniformly

Table B.1 Analytical values of $\lambda_{p,r} = \mathbb{E}[\omega^p |c|^r]$

p \ r	0	1	2	3	4
0	1	$\sqrt{\frac{2}{\pi}}$	1	$2\sqrt{\frac{2}{\pi}}$	3
1	$2\sqrt{\frac{2}{\pi}}$	$\frac{3}{2}$	$\frac{8}{3}\sqrt{\frac{2}{\pi}}$	$\frac{15}{4}$	–
2	$4\ln 2$	$\frac{7}{9}\sqrt{\frac{\pi^3}{2}}$	$4\ln 2 + \frac{7}{4}\zeta(3)$	–	–
3	$\frac{2}{3}\sqrt{2\pi^3}$	$\frac{45}{8}\zeta(3)$	–	–	–
4	$9\zeta(3)$	–	–	–	–

This table reports the analytical values of joint moments of $(\omega, |c|)$, i.e., $\lambda_{p,r} = \mathbb{E}[\omega^p |c|^r]$ with $p, r \in \mathbb{N}$ and $0 \leq p + r \leq 4$, where ω (resp. c) is defined as the high-low range (resp. open-close return) of a standard Brownian motion within an unit interval.

continuous if for all $x \in C([0,1])$, there exists a closed ball of radius $K > 0$ centered at 0, i.e., $B_{\leq K}(0)=\{x \in C([0,1]); \|x\|_\infty \leq K\}$,[3] such that for every $\epsilon > 0$, there exists $\delta > 0$, for $x, y \in B_{\leq K}(0)$, $\|x - y\|_\infty \leq \delta$, we have $|f(x) - f(y)| \leq \epsilon$. This locally uniform continuity assumption is satisfied whenever $|f(x) - f(y)| \leq C\|x - y\|_\infty^p$ for all $x, y \in C([0,1])$ and some $C, p > 0$.

Lemma B.1 (Theorem 2.1, Duembgen and Podolskij, 2015)**.** Assume that the efficient price X follows a continuous Itô semimartingale in Eq. (3.5) with all traditional conditions satisfied. Given a function $g : C([0,1]) \to \mathbb{R}$ and a vanishing sequence Δ_n, for the sequence of processes

$$\widehat{V}_{t,n}(g) = \Delta_n \sum_{i=1}^{n} g\left(\frac{d_i^n(X)}{\sqrt{\Delta_n}}\right), \tag{B.43}$$

where $d_i^n(X) = \{X_{(i-1+s)\Delta_n} - X_{(i-1)\Delta_n}; s \in [0,1]\}$, if g is locally uniformly continuous and has polynomial growth, it holds that

$$\widehat{V}_{t,n}(g) \xrightarrow{\text{u.c.p.}} V_t(g) = \int_0^t \rho_{\sigma_\tau}(g) d\tau, \tag{B.44}$$

as $n \to \infty$, where $\rho_z(g) = \mathbb{E}\left[g(\{zW_s; s \in [0,1]\})\right]$ whenever it is finite.

It is obvious that the new HLOC estimator $\widehat{V}_{t,n}$ in Eq. (3.3) can be written in the form of

[3] The notion of locally uniform continuity is slightly different from the usual one that requires uniform continuity on neighbourhoods or compact sets, see more details in Remark 2.1 in Duembgen and Podolskij (2015).

Eq. (B.43) with a specific path-dependent function $g : C([0,1]) \to \mathbb{R}$ of the scaled incremental process:

$$\begin{aligned} g\left(\frac{d_i^n(X)}{\sqrt{\Delta_n}}\right) &= \frac{1}{4\ln 2 - 2}\left\{\sup_{0\le s\le 1}\frac{d_i^n(X)}{\sqrt{\Delta_n}} - \inf_{0\le s\le 1}\frac{d_i^n(X)}{\sqrt{\Delta_n}} - \frac{\left|X_{i\Delta_n} - X_{(i-1)\Delta_n}\right|}{\sqrt{\Delta_n}}\right\}^2 \\ &= \frac{1}{4\ln 2 - 2}\left\{f_1\left(\frac{d_i^n(X)}{\sqrt{\Delta_n}}\right) - f_2\left(\frac{d_i^n(X)}{\sqrt{\Delta_n}}\right)\right\}^2, \end{aligned} \tag{B.45}$$

where

$$f_1(x) = \sup_{0\le s\le 1} x(s) - \inf_{0\le s\le 1} x(s) \quad \text{and} \quad f_2(x) = |x(1) - x(0)|. \tag{B.46}$$

The function $g(x)$ is therefore a linear combination of polynomials of the range $f_1(x)$ and a finite power variation $f_2(x)$, as well as the cross term $f_1(x)f_2(x)$. This path-dependent function has polynomial growth, and is thus locally uniformly continuous. Then the LLN in Lemma B.1 readily applies with

$$\begin{aligned} \int_0^t \rho_{\sigma_\tau}(g)d\tau &= \int_0^t \mathbb{E}\left[g(\{\sigma_\tau W_s; s\in[0,1]\})\right]d\tau \\ &= \frac{1}{4\ln 2 - 2}\int_0^t \mathbb{E}\left[\left(f_1(\{\sigma_\tau W_s; s\in[0,1]\}) - f_2(\{\sigma_\tau W_s; s\in[0,1]\})\right)^2\right]d\tau \\ &= \frac{1}{4\ln 2 - 2}\int_0^t \mathbb{E}\left[\left(\sup_{0\le s\le 1}\sigma_\tau W_s - \inf_{0\le s\le 1}\sigma_\tau W_s - \sigma_\tau\left|W_1 - W_0\right|\right)^2\right]d\tau \\ &= \frac{1}{4\ln 2 - 2}\int_0^t \mathbb{E}\Bigg[\left(\sup_{0\le s\le 1}\sigma_\tau W_s - \inf_{0\le s\le 1}\sigma_\tau W_s\right)^2 + \sigma_\tau^2 W_1^2 \\ &\quad - 2\left(\sup_{0\le s\le 1}\sigma_\tau W_s - \inf_{0\le s\le 1}\sigma_\tau W_s\right)\sigma_\tau\left|W_1\right|\Bigg]d\tau \\ &= \frac{1}{4\ln 2 - 2}\int_0^t \sigma_\tau^2\,\mathbb{E}\left[\omega^2 + c^2 - 2\omega|c|\right]d\tau \\ &= \frac{1}{4\ln 2 - 2}\int_0^t \sigma_\tau^2\left(\lambda_{2,0} + \lambda_{0,2} - 2\lambda_{1,1}\right)d\tau \\ &= \frac{1}{4\ln 2 - 2}\int_0^t \sigma_\tau^2\left(4\ln 2 + 1 - 2\times\frac{3}{2}\right)d\tau \\ &= \int_0^t \sigma_\tau^2 d\tau, \end{aligned} \tag{B.47}$$

where ω, c, and $\lambda_{p,r} = \mathbb{E}[\omega^p|c|^r]$ are defined in Appendix B.1. This completes the proof.

□

B.2.2 Proof of Theorem 3.2

Proof. We denote by $f'_y(x)$ the Gâteaux derivative of f at point x in the direction of y, i.e.,

$$f'_y(x) = \lim_{h \to 0} \frac{f(x+hy) - f(x)}{h}. \tag{B.48}$$

Lemma B.2 (Theorem 2.2, Duembgen and Podolskij, 2015)**.** Assume that the conditions of Lemma B.1 hold and Assumption 3.1 is satisfied. If $g'_y(x)$ for some $\|y\|_\infty \leq 1$ is (i) locally uniformly continuous, and (ii) has polynomial growth, it follows that as $n \to \infty$,

$$\frac{1}{\sqrt{\Delta_n}} \left(\widehat{V}_{t,n}(g) - V_t(g) \right) \xrightarrow{\mathcal{L}-\mathrm{s}} U_t(g), \tag{B.49}$$

where $U_t(g) = \int_0^t u_\tau^{(1)} d\tau + \int_0^t u_\tau^{(2)} dW_\tau + \int_0^t u_\tau^{(3)} dW'_\tau$ with

$$\begin{aligned} u_\tau^{(1)} &= \mu_\tau \rho_{\sigma_\tau}^{(2)}(g') + \frac{1}{2}\tilde{\sigma}_\tau \rho_{\sigma_\tau}^{(3)}(g') - \frac{1}{2}\tilde{\sigma}_\tau \rho_{\sigma_\tau}^{(2)}(g'), \\ u_\tau^{(2)} &= \rho_{\sigma_\tau}^{(1)}(g), \\ u_\tau^{(3)} &= \sqrt{\rho_{\sigma_\tau}(g^2) - \rho_{\sigma_\tau}^2(g) - (\rho_{\sigma_\tau}^{(1)}(g))^2}, \end{aligned} \tag{B.50}$$

and, for $z \in \mathbb{R}$ and $G(x,y) = g'_y(x)$,

$$\begin{aligned} \rho_z^{(1)}(g) &= \mathbb{E}[g(\{zW_s; s \in [0,1]\})W_1], \\ \rho_z^{(2)}(g') &= \mathbb{E}[G(\{zW_s; s \in [0,1]\}, \{s; s \in [0,1]\})], \\ \rho_z^{(3)}(g') &= \mathbb{E}[G(\{zW_s; s \in [0,1]\}, \{W_s^2; s \in [0,1]\})]. \end{aligned} \tag{B.51}$$

The process $W' = (W'_t)_{t \geq 0}$ is a Brownian motion defined on an extension of $(\Omega, \mathcal{F}, (\mathcal{F}_t)_{t \geq 0}, \mathbb{P})$, which is independent of $\mathcal{F}$. This is especially the case when g is an even function, i.e., $g(x) = g(-x)$ for all $x \in C([0,1])$, where it holds that

$$\rho_z^{(1)}(g) = \rho_z^{(2)}(g') = \rho_z^{(3)}(g') = 0, \tag{B.52}$$

for all $z \in \mathbb{R}$, since $W \overset{\mathcal{L}}{=} -W$ and expectations of odd functionals of W are 0, and hence we have

$$U_t(g) = \int_0^t \sqrt{\rho_{\sigma_\tau}(g^2) - \rho_{\sigma_\tau}^2(g)}\, dW'_\tau. \tag{B.53}$$

which is an $\mathcal{F}$-conditional Gaussian martingale with mean 0.

As mentioned in Appendix B.2.1, the path-dependent function $g : C([0,1]) \to \mathbb{R}$ in Eq. (B.45) is a linear combination of f_1^2, f_2^2, and $f_1 f_2$. Even though the stable CLT for $f_2^2(d_i^n(X)/\sqrt{\Delta_n})$ is easily deduced from Lemma B.2 (cf. Example 1 in Section 3, Duembgen and Podolskij, 2015), the result of g cannot be obtained straightforwardly because the range is not Gâteaux differentiable in general.

However, we may replace the Gâteaux derivative by an alternative form for functions which are not Gâteaux differentiable. We consider a range-based functional $\xi(x) = f(f_1(x))$ as an example, where $f : \mathbb{R} \to \mathbb{R}$ is a continuously differentiable function, such that both f and f' have polynomial growth (cf. Example 3 in Section 3, Duembgen and Podolskij, 2015), by applying the following lemma from Christensen and Podolskij (2007):

Lemma B.3. Given two continuous functions $x, y \in C([0,1])$, assume t^* is the only point in $[0,1]$ where the maximum of x is achieved, i.e., $t^* = \operatorname{argmax}_{0\le s\le 1} x(s)$. Then it holds that

$$\lim_{h\to 0} \frac{\sup_{0\le s\le 1}(x(s)+hy(s)) - \sup_{0\le s\le 1} x(s)}{h} = y(t^*). \tag{B.54}$$

In the proofs $x(t)$ plays the role of the Brownian motion, which attains its maximum (resp. minimum) at a unique point almost surely. Let $\bar{t} = \operatorname{argmax}_{0\le s\le 1} W_s$ and $\underline{t} = \operatorname{argmin}_{0\le s\le 1} W_s$. Then Lemma B.2 remains valid when σ is everywhere invertible (Christensen and Podolskij, 2012) with

$$\begin{aligned}
\rho_z^{(1)}(\xi) &= \mathbb{E}\left[f\left(z\left(\sup_{0\le s\le 1} W_s - \inf_{0\le s\le 1} W_s \right)\right) W_1 \right], \\
\rho_z^{(2)}(\xi') &= \mathbb{E}\left[f'\left(z\left(\sup_{0\le s\le 1} W_s - \inf_{0\le s\le 1} W_s \right)\right) (\bar{t} - \underline{t}) \right], \\
\rho_z^{(3)}(\xi') &= \mathbb{E}\left[f'\left(z\left(\sup_{0\le s\le 1} W_s - \inf_{0\le s\le 1} W_s \right)\right) \left(W_{\bar{t}}^2 - W_{\underline{t}}^2 \right) \right],
\end{aligned} \tag{B.55}$$

which extends the asymptotic theory in Lemma B.2 to general functions of the range.

Moreover, the derivative of the cross term $f_1 f_2$ is a linear combination of two separate components which include f_1' and f_2' respectively. It means that for the path-dependent function $g : C([0,1]) \to \mathbb{R}$ in Eq. (B.45) we can obtain the closed-form $\rho_z^{(1)}(g)$, $\rho_z^{(2)}(g')$, and $\rho_z^{(3)}(g')$ for all $z \in \mathbb{R}$, and Eq. (B.52) holds when g is an even function. Therefore, the stable CLT in

Lemma B.2 holds with the limiting process $U_t(g)$ in Eq. (B.53), where the squared integrand is given by

$$\begin{aligned}
\rho_{\sigma_\tau}(g^2) - \rho^2_{\sigma_\tau}(g) &= \mathbb{E}\left[g^2(\{\sigma_\tau W_s; s \in [0,1]\})\right] - (\mathbb{E}\left[g(\{\sigma_\tau W_s; s \in [0,1]\})\right])^2 \\
&= \frac{1}{(4\ln 2 - 2)^2}\Big\{\mathbb{E}\left[(f_1(\{\sigma_\tau W_s; s \in [0,1]\}) - f_2(\{\sigma_\tau W_s; s \in [0,1]\}))^4\right] \\
&- \left(\mathbb{E}\left[(f_1(\{\sigma_\tau W_s; s \in [0,1]\}) - f_2(\{\sigma_\tau W_s; s \in [0,1]\}))^2\right]\right)^2\Big\} \\
&= \frac{1}{(4\ln 2 - 2)^2}\Bigg\{\mathbb{E}\left[\left(\sup_{0\le s\le 1}\sigma_\tau W_s - \inf_{0\le s\le 1}\sigma_\tau W_s - \sigma_\tau |W_1|\right)^4\right] \\
&- \left(\mathbb{E}\left[\left(\sup_{0\le s\le 1}\sigma_\tau W_s - \inf_{0\le s\le 1}\sigma_\tau W_s - \sigma_\tau |W_1|\right)^2\right]\right)^2\Bigg\} \\
&= \frac{\sigma_\tau^4}{(4\ln 2 - 2)^2}\left\{\mathbb{E}\left[(\omega - |c|)^4\right] - \left(\mathbb{E}\left[(\omega - |c|)^2\right]\right)^2\right\} \\
&= \frac{\sigma_\tau^4}{(4\ln 2 - 2)^2}\left\{\mathbb{E}\left[\omega^4 - 4\omega^3|c| + 2\omega^2c^2 - 4\omega|c|^3 + c^4\right] - \left(\mathbb{E}\left[\omega^2 + c^2 - 2\omega|c|\right]\right)^2\right\} \\
&= \frac{\sigma_\tau^4}{(4\ln 2 - 2)^2}\left\{\lambda_{4,0} - 4\lambda_{3,1} + 6\lambda_{2,2} - 4\lambda_{1,3} + \lambda_{0,4} - (\lambda_{2,0} + \lambda_{0,2} - 2\lambda_{1,1})^2\right\} \\
&= \frac{40\ln 2 - 16(\ln 2)^2 - 3\zeta(3) - 16}{(4\ln 2 - 2)^2}\sigma_\tau^4 \approx 0.7245\sigma_\tau^4.
\end{aligned} \tag{B.56}$$

This completes the proof.

□

B.2.3 Proof of Corollary 3.1

Proof. The proof is analogous to that of Theorem 3.1. The RRDQ estimator $\widehat{Q}_{t,n}$ in Eq. (3.9) can be written in the form of Eq. (B.43) with a locally uniformly continuous function $g^2 : C([0,1]) \to \mathbb{R}$ of the scaled incremental process:

$$g^2\left(\frac{d_i^n(X)}{\sqrt{\Delta_n}}\right) = \frac{1}{\Lambda_4}\left\{f_1\left(\frac{d_i^n(X)}{\sqrt{\Delta_n}}\right) - f_2\left(\frac{d_i^n(X)}{\sqrt{\Delta_n}}\right)\right\}^4. \tag{B.57}$$

Then the LLN in Lemma B.1 readily applies with

$$\begin{aligned}
\int_0^t \rho_{\sigma_\tau}(g^2)d\tau &= \int_0^t \mathbb{E}\left[g^2(\{\sigma_\tau W_s; s\in[0,1]\})\right]d\tau \\
&= \frac{1}{\Lambda_4}\int_0^t \mathbb{E}\left[(f_1(\{\sigma_\tau W_s; s\in[0,1]\}) - f_2(\{\sigma_\tau W_s; s\in[0,1]\}))^4\right]d\tau \\
&= \frac{1}{\Lambda_4}\int_0^t \mathbb{E}\left[\left(\sup_{0\le s\le 1}\sigma_\tau W_s - \inf_{0\le s\le 1}\sigma_\tau W_s - \sigma_\tau|W_1|\right)^4\right]d\tau \\
&= \frac{1}{\Lambda_4}\int_0^t \sigma_\tau^4\,\mathbb{E}\left[\omega^4 - 4\omega^3|c| + 2\omega^2c^2 - 4\omega|c|^3 + c^4\right]d\tau \\
&= \frac{1}{\Lambda_4}\int_0^t \sigma_\tau^4\left(\lambda_{4,0} - 4\lambda_{3,1} + 6\lambda_{2,2} - 4\lambda_{1,3} + \lambda_{0,4}\right)d\tau \\
&= \frac{1}{\Lambda_4}\int_0^t \sigma_\tau^4\left(9\zeta(3) - 4\times\frac{45}{8}\zeta(3) + 6\left(4\ln 2 + \frac{7}{4}\zeta(3)\right) - 4\times\frac{15}{4} + 3\right)d\tau \\
&= \frac{1}{\Lambda_4}\int_0^t \sigma_\tau^4\left(24\ln 2 - 12 - 3\zeta(3)\right)d\tau \\
&= \int_0^t \sigma_\tau^4 d\tau.
\end{aligned} \tag{B.58}$$

This completes the proof. □

B.2.4 Proof of Proposition 3.1

Proof. We define the set

$$\Gamma_n = \{1\le i\le n : X \text{ is discontinuous in } I_{n,i}\}, \quad \text{with } k_n = |\Gamma_n|, \tag{B.59}$$

where $|A|$ stands for the cardinality of set A. The absolute summability of $\Delta X_s = X_s - X_{s^-}$ for all $s\in[0,t]$ implies that the number of "visible" realizations of the discontinuous component, i.e., ΔX_s of a larger order of magnitude than $\sqrt{\Delta_n}$, is an $O_p(\Delta_n^\gamma)$ random variable, where

$$\gamma = -\sup_{0\le s\le t}\left\{0\le\varpi<\frac{1}{2} : \Delta X_s \asymp \Delta_n^\varpi\right\}, \tag{B.60}$$

which corresponds to the smallest order of non-negligible jumps on $[0,t]$. It is obvious that k_n is bounded by the number of non-negligible jumps over $[0,t]$, such that we have $k_n = O_p(\Delta_n^\gamma)$.

We decompose the RRDV over $[0,t]$ into two complementary parts:

$$\widehat{V}_{t,n} = \frac{1}{\Lambda_2}\sum_{i\in\Gamma_n}(w_i - |r_i|)^2 + \frac{1}{\Lambda_2}\sum_{i\in\Gamma_n'}(w_i - |r_i|)^2 = \widehat{V}^{(1)}_{t,k_n} + \widehat{V}^{(2)}_{t,n-k_n}. \tag{B.61}$$

For $\widehat{V}^{(1)}_{t,k_n}$, we have

$$w_i = \sup_{\tau,\tau' \in I_{n,i}} \left| \int_\tau^{\tau'} \sigma_s dW_s + \sum_{s \in I_{n,i}} \Delta X_s \right| \leq \sup_{\tau,\tau' \in I_{n,i}} \left| \int_\tau^{\tau'} \sigma_s dW_s \right| + \left| \sum_{s \in I_{n,i}} \Delta X_s \right|, \tag{B.62}$$

$$|r_i| = \left| \int_{(i-1)\Delta_n}^{i\Delta_n} \sigma_s dW_s + \sum_{s \in I_{n,i}} \Delta X_s \right| \geq \left| \sum_{s \in I_{n,i}} \Delta X_s \right| - \left| \int_{(i-1)\Delta_n}^{i\Delta_n} \sigma_s dW_s \right|, \tag{B.63}$$

and thus

$$\begin{aligned} w_i - |r_i| &\leq \sup_{\tau,\tau' \in I_{n,i}} \left| \int_\tau^{\tau'} \sigma_s dW_s \right| + \left| \int_{(i-1)\Delta_n}^{i\Delta_n} \sigma_s dW_s \right| \\ &= \sigma_{(i-1)\Delta_n} \sqrt{\Delta_n} \left(\sup_{\tau,\tau' \in [0,1]} |W_\tau - W_{\tau'}| + |W_1| \right) + o_p\left(\sqrt{\Delta_n}\right) \quad \text{(Euler discretization)} \\ &= O_p\left(\sqrt{\Delta_n}\right). \end{aligned} \tag{B.64}$$

By adding up the squares of range-return differences in all k_n intervals, we have

$$\widehat{V}^{(1)}_{t,k_n} = O_p\left(k_n \Delta_n\right) = O_p\left(\Delta_n^{\gamma+1}\right). \tag{B.65}$$

For the sum of IV over all k_n intervals, we also have

$$\sum_{i \in \Gamma_n} \int_{(i-1)\Delta_n}^{i\Delta_n} \sigma_s^2 ds = O_p\left(k_n \Delta_n\right) = O_p\left(\Delta_n^{\gamma+1}\right). \tag{B.66}$$

With the triangle inequality, the absolute bias satisfies

$$\left| \widehat{V}^{(1)}_{t,k_n} - \sum_{i \in \Gamma_n} \int_{(i-1)\Delta_n}^{i\Delta_n} \sigma_s^2 ds \right| \leq \widehat{V}^{(1)}_{t,k_n} + \sum_{i \in \Gamma_n} \int_{(i-1)\Delta_n}^{i\Delta_n} \sigma_s^2 ds = O_p\left(\Delta_n^{\gamma+1}\right). \tag{B.67}$$

For $\widehat{V}^{(2)}_{t,n-k_n}$, it holds naturally that

$$\widehat{V}^{(2)}_{t,n-k_n} - \sum_{i \in \Gamma'_n} \int_{(i-1)\Delta_n}^{i\Delta_n} \sigma_s^2 ds = O_p\left(\sqrt{\Delta_n}\right). \tag{B.68}$$

The results for $\widehat{V}^{(1)}_{t,k_n}$ and $\widehat{V}^{(2)}_{t,n-k_n}$ in Eqs. (B.67) and (B.68) imply the result in the theorem.

□

B.2.5 Proof of Proposition 3.2

Proof. We follow Andersen et al. (2023a) to assume $\tau = 0$ for simplicity:

$$X_t = X_0 + \int_0^t \mu_s ds + \int_0^t \sigma_s dW_s + H_t, \quad \text{where } H_t = \int_0^t \frac{c_s^+}{s^\alpha} ds, \quad \frac{1}{2} < \alpha < 1. \tag{B.69}$$

The increment of H_t over the i-th interval is given by

$$H_{i\Delta_n} - H_{(i-1)\Delta_n} = \int_{(i-1)\Delta_n}^{i\Delta_n} \frac{c_s^+}{s^\alpha} ds = C_i \Delta_n^{1-\alpha} f(i;\alpha), \tag{B.70}$$

for some constant C_i, where $f(x;\theta) = x^{1-\theta} - (x-1)^{1-\theta}$ is a monotonically decreasing function over $[1,\infty)$ with $f(1;\theta) = 1$ and $\lim_{x\to\infty} f(x;\theta) = 0$ for all $0 < \theta < 1$. There exists an unique integer K_n defined as

$$K_n = \max_i \left\{ i \in \mathbb{Z}^+, 1 \le i \le n : f(i;\alpha) \asymp \Delta_n^{\alpha-\frac{1}{2}} \right\}. \tag{B.71}$$

The mean value theorem indicates

$$f(K_n;\alpha) = K_n^{1-\alpha} - (K_n - 1)^{1-\alpha} = (1-\alpha)(K_n - \varepsilon)^{-\alpha}, \tag{B.72}$$

for some $\varepsilon \in (0,1)$. It is therefore satisfied that

$$K_n \asymp \Delta_n^{\frac{1}{2\alpha}-1}. \tag{B.73}$$

The role of H is no smaller than the diffusion component over the first K_n intervals, while it starts to be swamped by volatility from the (K_n+1)-th interval because its contribution vanishes in the limit. Depending on the asymptotic order of H, we decompose the RRDV over $[0,t]$ into two complementary parts:

$$\widehat{V}_{t,n} = \frac{1}{\Lambda_2} \sum_{i=1}^{K_n} (w_i - |r_i|)^2 + \frac{1}{\Lambda_2} \sum_{i=K_n+1}^{n} (w_i - |r_i|)^2 = \widehat{V}_{[0,K_n\Delta_n]} + \widehat{V}_{[K_n\Delta_n,t]}. \tag{B.74}$$

For all $1 \leq i \leq K_n$, we have

$$w_i = \sup_{\tau,\tau' \in I_{n,i}} \left| \int_\tau^{\tau'} \sigma_s dW_s + H_{\tau'} - H_\tau \right| \leq \sup_{\tau,\tau' \in I_{n,i}} \left| \int_\tau^{\tau'} \sigma_s dW_s \right| + \left| H_{i\Delta_n} - H_{(i-1)\Delta_n} \right|, \quad \text{(B.75)}$$

$$|r_i| = \left| \int_{(i-1)\Delta_n}^{i\Delta_n} \sigma_s dW_s + H_{i\Delta_n} - H_{(i-1)\Delta_n} \right| \geq \left| H_{i\Delta_n} - H_{(i-1)\Delta_n} \right| - \left| \int_{(i-1)\Delta_n}^{i\Delta_n} \sigma_s dW_s \right|, \quad \text{(B.76)}$$

and thus

$$w_i - |r_i| \leq \sup_{\tau,\tau' \in I_{n,i}} \left| \int_\tau^{\tau'} \sigma_s dW_s \right| + \left| \int_{(i-1)\Delta_n}^{i\Delta_n} \sigma_s dW_s \right| = O_p\left(\sqrt{\Delta_n}\right). \quad \text{(B.77)}$$

By adding up all squared range-return differences in the first K_n intervals, we have

$$\widehat{V}_{[0,K_n\Delta_n]} = O_p\left(K_n\Delta_n\right) = O_p\left(\Delta_n^{\frac{1}{2\alpha}}\right). \quad \text{(B.78)}$$

For the IV over the period which accommodates the first K_n intervals, it holds that

$$\int_0^{K_n\Delta_n} \sigma_s^2 ds = O_p\left(K_n\Delta_n\right) = O_p\left(\Delta_n^{\frac{1}{2\alpha}}\right). \quad \text{(B.79)}$$

With the triangle inequality, the absolute bias satisfies

$$\left| \widehat{V}_{[0,K_n\Delta_n]} - \int_0^{K_n\Delta_n} \sigma_s^2 ds \right| \leq \widehat{V}_{[0,K_n\Delta_n]} + \int_0^{K_n\Delta_n} \sigma_s^2 ds = O_p\left(\Delta_n^{\frac{1}{2\alpha}}\right). \quad \text{(B.80)}$$

For $\widehat{V}_{[K_n\Delta_n,t]}$, it holds naturally that

$$\widehat{V}_{[K_n\Delta_n,t]} - \int_{K_n\Delta_n}^t \sigma_s^2 ds = O_p\left(\sqrt{\Delta_n}\right). \quad \text{(B.81)}$$

Since $K_n\Delta_n \to 0$ under infill asymptotics, the RRDV over $[0,t]$ is equivalent to $\widehat{V}_{[K_n\Delta_n,t]}$. The bias results in Eqs. (B.80) and (B.81) show that the bias of RRDV due to drift burst is asymptotically negligible and has no impact on the asymtotic distribution in Theorem 3.2. This completes the proof.

□

B.2.6 Proof of Proposition 3.3

Proof. As an analogous result to Proposition 3.2, the bias of RRDV in the presence of persistent noise can be proved following the same steps with similar simplifying assumptions: There exists one persistent noise episode $[0,1]$, which is triggered by some ambiguous information arriving at time 0, and the funtion $g^{(1)}$ takes the form $g^{(1)}_{gj}$ in Eq. (3.22). The process $\epsilon^{(1)}_t$ in H_t only introduces extra randomness to the duration of persistent noise episode, which shall be harmlessly ignored.

As shown in Eqs. (56) and (57) in Andersen et al. (2023a), there exists an asymptotic correspondence between the two models of episodic extreme return persistence, and they are equivalent with identical asymptotic analyses if we let $\beta = 1-\alpha$. The increment of H_t on the i-th interval is

$$H_{i\Delta_n} - H_{(i-1)\Delta_n} = f^{(1)}(\Delta X_0, \eta)\left[(i-1)^\beta - i^\beta\right]\Delta_n^\beta = \eta\Delta X_0\left[i^\beta - (i-1)^\beta\right]\Delta_n^\beta, \tag{B.82}$$

where $f^{(1)}(\Delta X_0, \eta) = -\eta\Delta X_0$ with $\eta \in (0,1]$. With $\beta = 1-\alpha \in (0,1/2)$, the above persistent noise increment is equivalent to the drift burst increment in Eq. (B.70). Jumps with $r = 0$ induce the bias of order $O_p(\Delta_n^{\gamma+1}) = O_p(\Delta_n)$ with $\gamma = 0$, which has no impact on the bias result of RRDV. The proof from here can proceed following the same steps as the proof of Theorem 5. When the function $g^{(1)} = g^{(1)}_{fc}$, the asymptotic effect of H depends on the smaller of the two parameters β^- and β^+.

□

B.2.7 Proof of Proposition 3.4

Proof. We obtain the asymptotic expansions of $\Lambda_{2,N}$ and $\Lambda_{4,N}$ by specializing the general results in Asmussen et al. (1995) and Dieker and Lagos (2017). Lemma B.4 demonstrates the asymptotic distribution of the Euler discretization error of one-dimensional reflected Brownian motion.

Lemma B.4. We denote a reflected Brownian motion by $\overline{W} = \Gamma W$ with the reflection mapping

$$\Gamma X_t = X_t - \left(\inf_{0\le s\le t} X_s \wedge 0\right), \tag{B.83}$$

where W is a standard Brownian motion that starts from 0. Let $\overline{W}_{t,N}$ be the embedded reflected Brownian motion observed at N discrete points, i.e., at $t_i = it/N$ for $i = 1, 2, \ldots, N$. The Euler discretization error of $\overline{W}_1$, i.e., $\varepsilon_{1,N} = \overline{W}_1 - \overline{W}_{1,N}$, has a weak convergence to a nonzero limit:

$$\sqrt{N}\varepsilon_{1,N} \xrightarrow{\mathcal{L}} \Upsilon, \quad \text{with } \Upsilon = \min_{k\in\mathbb{Z}} R_{U+k}, \tag{B.84}$$

as $N \to \infty$, where $R = (R_t)_{t\geq 0}$ is a two-sided Bessel process of order 3, U is a uniformly distributed random variable on $(0, 1)$ which is independent of R. The scaled discretization error $\sqrt{N}\varepsilon_{1,N}$ is asymptotically independent of W, with the $\mathbb{R} \times C([0, 1])$-valued random pair $(\sqrt{N}\varepsilon_{1,N}, W) \xrightarrow{\mathcal{L}} (\Upsilon, W)$, where Υ is independent of W.

Lemma B.5. The Euler discretization error of $\overline{W}$ satisfies

$$\varepsilon_{1,N} = \inf_{i\in\{0,1,\ldots,N\}} W_{i/N} - \inf_{0\leq t\leq 1} W_t. \tag{B.85}$$

Given a function $g : \mathbb{R} \to \mathbb{R}$ whose first derivative g' exists at $\inf_{0\leq t\leq 1} W_t$ and is non-zero valued, the delta method implies that as $N \to \infty$,

$$\sqrt{N}\left(g\left(\inf_{i\in\{0,1,\ldots,N\}} W_{i/N}\right) - g\left(\inf_{0\leq t\leq 1} W_t\right)\right) \xrightarrow{\mathcal{L}} g'\left(\inf_{0\leq t\leq 1} W_t\right)\Upsilon. \tag{B.86}$$

Therefore, the expected functional values of discretized infimum can be approximated with the polynomial expansion as follows:

$$\mathbb{E}\left[g\left(\inf_{i\in\{0,1,\ldots,N\}} W_{i/N}\right)\right] = \mathbb{E}\left[g\left(\inf_{0\leq t\leq 1} W_t\right)\right] + \mathbb{E}\left[g'\left(\inf_{0\leq t\leq 1} W_t\right)\right]\mathbb{E}[\Upsilon]\frac{1}{\sqrt{N}} + o\left(\frac{1}{\sqrt{N}}\right), \tag{B.87}$$

where

$$\mathbb{E}[\Upsilon] = -\frac{\zeta(1/2)}{\sqrt{2\pi}} \approx 0.5826. \tag{B.88}$$

The results above enable us to derive asymptotic expansions of the moments of $(\omega, |c|)$, i.e., $\lambda_{p,r} = \mathbb{E}[\omega^p|c|^r]$, whose analytical values are summarized in Table B.1, with $p, r \in \mathbb{N}$ and $0 \leq p + r \leq 4$.

Corollary B.1. For the moments of $(\omega, |c|)$ derived in Appendix B.1, i.e., $\lambda_{p,r} = \mathbb{E}[\omega^p|c|^r]$, we

have the following asymptotic result:

$$\lambda_{p,r,N} = \lambda_{p,r} + M_{p,r}\frac{\zeta(1/2)}{\sqrt{2\pi}}\frac{1}{\sqrt{N}} + o\left(\frac{1}{\sqrt{N}}\right), \quad \text{with } M_{p,r} = 2p\lambda_{p-1,r}. \tag{B.89}$$

Proof. It is intuitively clear that the random variable $\varepsilon_{1,N}$ in Lemma B.4, for N large, is solely determined by the behavior of W in a neighborhood of its minimizer $\underline{t}$, i.e., the almost surely unique random time $\underline{t} \in [0,1]$ at which W attains its minimum value $\inf_{0\le t\le 1} W_t$ over the unit interval.

The results in Lemma B.5 are also convenient to switch from infima to suprema, with

$$\varepsilon_{1,N} = \sup_{0\le t\le 1} W_t - \sup_{i\in\{0,1,\dots,N\}} W_{i/N}, \tag{B.90}$$

which is a direct result from sign reversion.

Because the Brownian motion is space-homogeneous and symmetric, it holds that

$$\begin{aligned}
\omega_N - \omega &= \left(\sup_{i\in\{0,1,\dots,N\}} W_{i/N} - \inf_{i\in\{0,1,\dots,N\}} W_{i/N}\right) - \left(\sup_{0\le t\le 1} W_t - \inf_{0\le t\le 1} W_t\right) \\
&= \left(\sup_{i\in\{0,1,\dots,N\}} W_{i/N} - \sup_{0\le t\le 1} W_t\right) - \left(\inf_{i\in\{0,1,\dots,N\}} W_{i/N} - \inf_{0\le t\le 1} W_t\right) \\
&\overset{\mathcal{L}}{=} -2\varepsilon_{1,N},
\end{aligned} \tag{B.91}$$

and therefore

$$\sqrt{N}\left(\omega_N^p - \omega^p\right) \xrightarrow{\mathcal{L}} -2p\omega^{p-1}\Upsilon, \quad \text{as } N\to\infty, \tag{B.92}$$

by the delta method. The equivalence in distribution "$\overset{\mathcal{L}}{=}$" in Eq. (B.91) holds because $\sup_{0\le t\le 1} W_t - \sup_{i\in\{0,1,\dots,N\}} W_{i/N}$ and $\inf_{i\in\{0,1,\dots,N\}} W_{i/N} - \inf_{0\le t\le 1} W_t$ are asymptotically i.i.d..

For the Euler discretization error of the moment $\lambda_{p,r}$, we have

$$\begin{aligned}
\lambda_{p,r,N} - \lambda_{p,r} &= \mathbb{E}[(\omega_N^p - \omega^p)|c|^r] \\
&= -2p\mathbb{E}[\omega^{p-1}|c|^r]\mathbb{E}[\Upsilon]\frac{1}{\sqrt{N}} + o\left(\frac{1}{\sqrt{N}}\right) \\
&= 2p\lambda_{p-1,r}\frac{\zeta(1/2)}{\sqrt{2\pi}}\frac{1}{\sqrt{N}} + o\left(\frac{1}{\sqrt{N}}\right).
\end{aligned} \tag{B.93}$$

This completes the proof of Corollary B.1.

□

Table B.2 lists the values of "bias factor" $M_{p,r}$ for all $1 \leq p \leq 4$ and $0 \leq r \leq 3$.

Table B.2 Bias factor $M_{p,r}$ for discrete moment $\lambda_{p,r,N}$

p \ r	0	1	2	3
1	2	$2\sqrt{\frac{2}{\pi}}$	2	$4\sqrt{\frac{2}{\pi}}$
2	$8\sqrt{\frac{2}{\pi}}$	6	$\frac{32}{3}\sqrt{\frac{2}{\pi}}$	–
3	$24\ln 2$	$\frac{14}{3}\sqrt{\frac{\pi^3}{2}}$	–	–
4	$\frac{16}{3}\sqrt{2\pi^3}$	–	–	–

This table lists the "bias factor" $M_{p,r}$ used in asymptotic expansions of $\lambda_{p,r,N}$ with $1 \leq p \leq 4$ and $0 \leq r \leq 3$. In the polynomial expansion for $\lambda_{p,r,N}$, the coefficient for $N^{-1/2}$ is $M_{p,r}\zeta(1/2)/\sqrt{2\pi}$.

It is now straightforward to obtain the asymptotic expansions of $\Lambda_{2,N}$ and $\Lambda_{4,N}$ in Proposition 3.4:

$$\begin{aligned}
\Lambda_{2,N} &= \lambda_{2,0,N} + \lambda_{0,2} - 2\lambda_{1,1,N} \\
&= \Lambda_2 + (M_{2,0} - 2M_{1,1})\frac{\zeta(1/2)}{\sqrt{2\pi}}\frac{1}{\sqrt{N}} + o\left(\frac{1}{\sqrt{N}}\right) \\
&= \Lambda_2 + 4\sqrt{\frac{2}{\pi}}\frac{\zeta(1/2)}{\sqrt{2\pi}}\frac{1}{\sqrt{N}} + o\left(\frac{1}{\sqrt{N}}\right) \\
&= \Lambda_2 + \frac{4}{\pi}\zeta\left(\frac{1}{2}\right)\frac{1}{\sqrt{N}} + o\left(\frac{1}{\sqrt{N}}\right),
\end{aligned} \tag{B.94}$$

$$\begin{aligned}
\Lambda_{4,N} &= \lambda_{4,0,N} - 4\lambda_{3,1,N} + 6\lambda_{2,2,N} - 4\lambda_{1,3,N} + \lambda_{0,4} \\
&= \Lambda_4 + (M_{4,0} - 4M_{3,1} + 6M_{2,2} - 4M_{1,3})\frac{\zeta(1/2)}{\sqrt{2\pi}}\frac{1}{\sqrt{N}} + o\left(\frac{1}{\sqrt{N}}\right) \\
&= \Lambda_4 + \left(\frac{16}{3}\sqrt{2\pi^3} - \frac{56}{3}\sqrt{\frac{\pi^3}{2}} + 48\sqrt{\frac{2}{\pi}}\right)\frac{\zeta(1/2)}{\sqrt{2\pi}}\frac{1}{\sqrt{N}} + o\left(\frac{1}{\sqrt{N}}\right) \\
&= \Lambda_4 + \left(\frac{48}{\pi} - 4\pi\right)\zeta\left(\frac{1}{2}\right)\frac{1}{\sqrt{N}} + o\left(\frac{1}{\sqrt{N}}\right).
\end{aligned} \tag{B.95}$$

This completes the proof.

□

B.2.8 Proof of Corollary 3.2

Proof. It follows the same steps as the proofs of Theorem 3.1, 3.2, and Corollary 3.1. □

B.3 Supplementary Materials

B.3.1 Simulation Scheme

The numerical results for $(\Lambda_{2,N}, \Lambda_{4,N}, \Theta_N)'$ with different N are calculated from a large number of simulated paths of the standard Brownian motion. Each replication generates a sequence of $N+1$ equidistant observations at $t_i = i/N$ for $i = 0, 1, \ldots, N$. As N is allowed to span any natural number except 0 and 1, we adopt the following simulation scheme to efficiently utilize our computational resources:

i. For $N \in \{2, 3, 4, \ldots, 10\}$, we simulate 10^9 replications of $W_{i/N}$ for $i = 0, 1, \ldots, N$.

ii. For $N \in \{11, 12, 13, \ldots, 200\}$, we simulate 10^8 replications of $W_{i/N}$ for $i = 0, 1, \ldots, N$.

iii. For $N \in \{201, 202, 203, \ldots, 2000, 2005, 2010, \ldots, 5000, 5010, 5020, \ldots, 10^4, 10^5, 10^6, 10^7\}$, we simulate 10^7 replications of $W_{i/N}$ for $i = 0, 1, \ldots, N$.

B.3.2 Discretized Factors

Table B.3 reports the estimation results for the polynomial equation

$$Y_N = \sum_{i=0}^{k} \beta_i N^{-i/2} + \epsilon_N, \tag{B.96}$$

where $Y_N = (\Lambda_{2,N}, \Lambda_{4,N}, \Theta_N)'$ collects the simulated values for all three factors with N ranging from 11 to 10^8. The intercepts $\beta_0 = (\Lambda_2, \Lambda_4, \Theta)'$ and the first two coefficients in the vector β_1 are obtained from the analytical results in Proposition 3.4. We find that a cubic (resp. quartic) approximation works very well across all $N \geq 11$ for $\Lambda_{2,N}$ (resp. $\Lambda_{4,N}$ or Θ_N), as indicated by the root-mean-square error (RMSE) and R^2.

Table B.3 Polynomial regression results for discrete factors

Coefficients	$\Lambda_{2,N}$	$\Lambda_{4,N}$	Θ_N
β_0	Λ_2	Λ_4	Θ
β_1	$4\zeta(1/2)/\pi$	$(48/\pi - 4\pi)\zeta(1/2)$	1.6618
β_2	1.7429	6.8076	1.7371
β_3	-0.6999	-6.3635	1.0395
β_4	–	2.8711	5.4477
RMSE ($\times 10^4$)	0.6088	1.6358	1.3555
R^2	0.9998	0.9999	1.0000

Estimated coefficients for the polynomial regression model $Y_N = \sum_{i=0}^{k} \beta_i N^{-i/2} + \epsilon_N$ with weighted least squares. $Y_N = (\Lambda_{2,N}, \Lambda_{4,N}, \Theta_N)'$ collects the simulated values for all three factors with N ranging from 11 to 10^8. The intercepts β_0 and the first two coefficients in the vector β_1 are from the analytical results in Proposition 3.4.

We next provide a practical instruction on the selection for all factors with different $N \in \mathbb{N}^{>1}$:

- Use the simulated values in Table B.4 for $N \in \{2, 3, \ldots, 10\}$.
- Use the polynomial approximation with coefficients listed in Table B.3 for all $N \geq 11$.

Table B.4 shows the simulated values for $(\Lambda_{2,N}, \Lambda_{4,N}, \Theta_N)'$ with N ranging from 2 to 10, which achieve the highest level of precision within our simulation schemes in Appendix B.3.1.

Table B.4 Simulated values for discrete factors

N	$\Lambda_{2,N}$	$\Lambda_{4,N}$	Θ_N
2	0.0908	0.0567	5.8696
3	0.1486	0.0945	3.2809
4	0.1926	0.1304	2.5170
5	0.2277	0.1631	2.1457
6	0.2567	0.1926	1.9224
7	0.2812	0.2192	1.7712
8	0.3023	0.2432	1.6616
9	0.3206	0.2650	1.5777
10	0.3368	0.2849	1.5110

Simulated values for $\Lambda_{2,N}$, $\Lambda_{4,N}$, and Θ_N with N ranging from 2 to 10. For the detailed simulation scheme, see Appendix B.3.1.

B.3.3 Monte Carlo Bias Results of Other Estimators

In addition to the Monte Carlo bias results in Section 3.5.2, Tables B.5 to B.7 report the relative bias (%) in "continuous time" of the TRV estimator of Mancini (2009) and the two DV estimators of Andersen et al. (2023a), respectively. The choices of truncation parameters for TRV and DV are in line with Section 3.5.3.

Table B.5 Monte Carlo bias results (%): Truncated realized volatility (TRV)

Panel A: $C_\zeta^{\text{TRV}} = 4$

		Gradual Jump			Flash Crash			Gradual Jump with an Intermittent Flash Crash		
Interval (sec)	$H = 0$	$\beta = 0.45$	0.35	0.25	$\beta = 0.45$	0.35	0.25	$\beta = 0.45$	0.35	0.25
1	-0.14	0.51	0.56	0.56	0.85	0.89	0.94	0.58	0.72	0.83
5	-0.18	2.12	2.02	1.80	3.46	3.19	2.88	2.55	2.72	2.60
10	-0.16	3.66	3.36	2.83	6.05	5.39	4.74	4.56	4.58	4.23
30	-0.19	8.83	7.63	5.92	15.07	12.58	9.90	9.96	10.08	9.36
60	-0.27	15.09	12.55	9.14	24.87	19.93	15.29	17.21	15.29	15.83
120	-0.35	27.92	22.02	16.02	42.97	35.15	25.04	34.72	29.33	21.38
180	-0.28	32.40	25.29	16.85	61.86	49.50	35.73	30.59	29.20	21.88
300	-0.39	43.35	31.71	19.63	96.99	78.29	56.19	42.98	31.45	28.53

Panel B: $C_\zeta^{\text{TRV}} = 3$

		Gradual Jump			Flash Crash			Gradual Jump with an Intermittent Flash Crash		
Interval (sec)	$H = 0$	$\beta = 0.45$	0.35	0.25	$\beta = 0.45$	0.35	0.25	$\beta = 0.45$	0.35	0.25
1	-3.06	-2.45	-2.35	-2.25	-2.19	-2.15	-2.05	-2.44	-2.27	-2.10
5	-3.09	-1.02	-1.05	-1.08	0.05	0.03	0.07	-0.73	-0.55	-0.59
10	-3.08	0.29	0.16	-0.17	2.30	1.69	1.27	0.93	0.95	0.75
30	-3.12	4.43	3.56	2.19	9.24	7.24	5.54	5.56	5.27	4.60
60	-3.20	9.36	7.02	4.32	17.76	14.74	11.22	11.10	9.64	8.89
120	-3.29	17.76	13.51	9.09	29.81	22.18	14.27	21.30	19.47	13.72
180	-3.37	22.29	16.48	10.47	44.94	34.00	23.32	23.20	19.37	16.88
300	-3.68	32.41	23.52	14.47	72.39	54.66	37.25	26.24	23.27	24.39

Relative bias (%) of the truncated realized volatility (TRV) estimator of Mancini (2009) constructed from 1, 5, 10, 30, 60, 120, 180, and 300-second intervals for 2000 days. The truncation threshold for returns in all intervals is $C_\zeta^{\text{TRV}}\sqrt{\Delta_n \text{MedRV}_{t,n}}$, with $C_\zeta^{\text{TRV}} = 4$ or 3. The DGP is the Heston model in Eq. (3.38), and we follow the persistent noise model of Andersen et al. (2023a) to simulate the three different patterns of episodic extreme return persistence.

B.3.4 Monte Carlo RMSE Results of Other Estimators

In addition to the comparison of finite-sample performances among RRDV and the main competitors TRV and DV, we also consider two traditional IV estimators, i.e., RV and RBPV, and also TRV and DV with less aggressive choices of truncation threshold. The RMSE results are shown in Table B.8.

Table B.6 Monte Carlo bias results (%): Differenced-return volatility (DV)

Panel A: $C_\zeta^{\mathrm{DV}} = 4\sqrt{2}$

		Gradual Jump			Flash Crash			Gradual Jump with an Intermittent Flash Crash		
Interval (sec)	$H = 0$	$\beta = 0.45$	0.35	0.25	$\beta = 0.45$	0.35	0.25	$\beta = 0.45$	0.35	0.25
1	-0.15	-0.10	-0.09	-0.08	-0.04	-0.09	-0.04	-0.15	-0.11	-0.01
5	-0.22	-0.08	-0.14	-0.01	-0.01	0.09	0.15	0.12	0.16	0.11
10	-0.18	-0.24	-0.23	-0.09	0.53	0.35	0.67	0.46	0.16	0.13
30	-0.24	0.08	-0.23	-0.04	0.37	0.58	1.26	1.65	1.03	0.87
60	-0.39	1.30	-0.41	-0.59	1.59	2.89	4.62	4.60	1.55	1.86
120	-0.50	6.58	6.34	0.76	9.70	9.81	8.61	15.33	12.94	2.99
180	-0.47	8.80	1.21	-1.02	14.43	11.35	9.74	16.16	11.74	2.16
300	-1.02	23.35	8.80	-0.33	30.23	23.24	19.18	40.15	17.62	8.58

Panel B: $C_\zeta^{\mathrm{DV}} = 3\sqrt{2}$

		Gradual Jump			Flash Crash			Gradual Jump with an Intermittent Flash Crash		
Interval (sec)	$H = 0$	$\beta = 0.45$	0.35	0.25	$\beta = 0.45$	0.35	0.25	$\beta = 0.45$	0.35	0.25
1	-3.05	-2.88	-2.81	-2.65	-2.86	-2.83	-2.67	-2.95	-2.90	-2.64
5	-3.12	-2.63	-2.48	-2.22	-2.37	-2.10	-1.75	-2.62	-2.45	-2.21
10	-3.10	-2.47	-2.28	-2.07	-1.76	-1.77	-1.52	-2.14	-1.97	-2.02
30	-3.14	-1.88	-1.69	-1.59	-0.82	-0.70	-0.27	-1.11	-1.26	-1.33
60	-3.32	-1.17	-1.11	-1.45	0.83	1.58	2.17	-0.08	-0.80	-0.72
120	-3.53	1.68	1.79	-0.24	5.51	5.10	3.92	5.21	4.33	1.07
180	-3.56	0.81	-1.65	-2.28	4.49	2.85	2.19	5.49	3.10	0.41
300	-4.15	6.29	-0.81	-2.87	7.30	5.31	4.77	14.24	8.92	3.81

Relative bias (%) of the differenced-return volatility (DV) estimator of Andersen et al. (2023a) constructed from 1, 5, 10, 30, 60, 120, 180, and 300-second intervals for 2000 days. The truncation threshold for all first-order differenced returns is $C_\zeta^{\mathrm{DV}}\sqrt{\Delta_n \mathrm{MedRV}_{t,n}}$, with $C_\zeta^{\mathrm{DV}} = 4\sqrt{2}$ or $3\sqrt{2}$. The DGP is the Heston model in Eq. (3.38), and we follow the persistent noise model of Andersen et al. (2023a) to simulate the three different patterns of episodic extreme return persistence.

Table B.7 Monte Carlo bias results (%): Generalized differenced-return volatility (DV_{1-3})

Panel A: $C_\zeta^{DV} = 4\sqrt{2}$

		Gradual Jump			Flash Crash			Gradual Jump with an Intermittent Flash Crash		
Interval (sec)	$H = 0$	$\beta = 0.45$	0.35	0.25	$\beta = 0.45$	0.35	0.25	$\beta = 0.45$	0.35	0.25
1	-0.15	-0.07	-0.08	-0.06	-0.01	-0.03	0.03	-0.07	-0.05	0.02
5	-0.23	-0.02	-0.03	0.09	0.09	0.12	0.25	0.29	0.37	0.32
10	-0.23	0.12	-0.11	0.23	0.54	0.52	0.76	0.65	0.72	0.81
30	-0.39	0.68	0.71	0.90	1.40	1.42	1.93	2.58	2.63	2.81
60	-0.67	2.21	1.34	1.16	4.32	5.35	6.48	6.65	4.03	5.95
120	-1.18	14.01	9.98	5.26	12.02	10.99	9.50	17.83	19.46	8.14
180	-1.44	12.72	4.62	1.89	24.31	21.09	17.93	26.73	16.28	7.08
300	-2.27	31.54	11.95	3.89	57.17	48.30	38.20	52.08	30.39	14.81

Panel B: $C_\zeta^{DV} = 3\sqrt{2}$

		Gradual Jump			Flash Crash			Gradual Jump with an Intermittent Flash Crash		
Interval (sec)	$H = 0$	$\beta = 0.45$	0.35	0.25	$\beta = 0.45$	0.35	0.25	$\beta = 0.45$	0.35	0.25
1	-3.06	-2.89	-2.80	-2.64	-2.84	-2.80	-2.66	-2.90	-2.82	-2.64
5	-3.13	-2.60	-2.48	-2.22	-2.33	-2.12	-1.74	-2.48	-2.25	-2.17
10	-3.14	-2.39	-2.15	-1.98	-1.77	-1.79	-1.60	-2.03	-1.88	-1.74
30	-3.31	-1.51	-1.33	-1.30	-0.67	-0.53	-0.21	-0.39	-0.29	-0.31
60	-3.62	-0.46	-0.61	-0.94	1.45	1.75	1.74	1.88	1.32	1.81
120	-4.14	5.46	3.46	1.92	5.53	4.83	3.53	9.79	10.25	4.78
180	-4.45	3.92	1.89	-0.04	9.35	7.50	6.52	12.95	9.92	4.50
300	-5.53	11.92	4.57	0.87	24.49	20.74	17.37	27.81	10.57	10.49

Relative bias (%) of the generalized DV_{1-3} estimator of Andersen et al. (2023a) constructed from 1, 5, 10, 30, 60, 120, 180, and 300-second intervals for 2000 days. The truncation threshold for all first-, second-, and third-order differenced returns is $C_\zeta^{DV}\sqrt{\Delta_n \text{MedRV}_{t,n}}$, with $C_\zeta^{DV} = 4\sqrt{2}$ or $3\sqrt{2}$. The DGP is the Heston model in Eq. (3.38), and we follow the persistent noise model of Andersen et al. (2023a) to simulate the three different patterns of episodic extreme return persistence.

Table B.8 Monte Carlo RMSE results of other estimators

Panel A: $H = 0$															
Interval	RV	RBPV	TRV	DV	DV_{1-3}										
1 min	6.59	0.92	0.64	0.79	0.69										
2 min	6.65	1.30	0.91	1.11	0.98										
3 min	6.66	1.63	1.12	1.39	1.21										
5 min	6.73	2.10	1.47	1.81	1.61										
Panel B: Gradual Jump															
	$\beta = 0.45$					$\beta = 0.35$					$\beta = 0.25$				
Interval	RV	RBPV	TRV	DV	DV_{1-3}	RV	RBPV	TRV	DV	DV_{1-3}	RV	RBPV	TRV	DV	DV_{1-3}
1 min	8.32	3.85	1.54	0.83	0.76	10.53	4.51	1.35	0.80	0.72	14.81	5.24	1.11	0.80	0.72
2 min	9.48	6.81	2.81	1.45	1.73	11.67	7.68	2.32	1.36	1.47	15.82	8.62	1.85	1.18	1.17
3 min	13.08	8.79	3.23	1.87	1.95	16.70	9.14	2.65	1.59	1.44	22.62	9.13	1.99	1.41	1.29
5 min	17.61	12.80	4.35	3.41	3.87	21.81	12.55	3.39	2.66	2.55	28.07	11.86	2.46	2.09	1.99
Panel C: Flash Crash															
	$\beta = 0.45$					$\beta = 0.35$					$\beta = 0.25$				
Interval	RV	RBPV	TRV	DV	DV_{1-3}	RV	RBPV	TRV	DV	DV_{1-3}	RV	RBPV	TRV	DV	DV_{1-3}
1 min	8.18	5.16	2.37	0.80	0.82	8.49	5.72	1.95	0.85	0.88	8.42	5.76	1.55	0.91	0.94
2 min	8.63	5.51	4.05	1.48	1.51	8.30	4.77	3.39	1.50	1.48	7.58	3.67	2.60	1.45	1.40
3 min	9.94	8.42	5.75	2.10	2.62	9.36	7.30	4.78	2.00	2.43	8.30	5.61	3.65	1.88	2.19
5 min	12.64	13.28	9.01	3.84	5.62	11.49	11.17	7.46	3.44	4.99	9.65	8.28	5.58	3.04	4.12
Panel D: Gradual Jump with an Intermittent Flash Crash															
	$\beta = 0.45$					$\beta = 0.35$					$\beta = 0.25$				
Interval	RV	RBPV	TRV	DV	DV_{1-3}	RV	RBPV	TRV	DV	DV_{1-3}	RV	RBPV	TRV	DV	DV_{1-3}
1 min	7.98	3.28	1.73	0.90	0.90	9.21	3.89	1.51	0.82	0.81	13.06	4.83	1.40	0.84	0.85
2 min	9.07	5.89	3.45	1.65	2.09	10.13	6.41	2.56	1.50	1.87	14.27	8.08	2.57	1.53	1.72
3 min	11.22	7.30	3.51	2.24	2.72	13.74	7.83	2.91	2.04	2.04	19.83	9.09	2.82	1.85	2.07
5 min	15.40	12.12	5.94	5.60	6.93	17.13	9.23	3.34	3.06	2.76	23.22	10.35	2.65	2.25	2.36

RMSE (multiplied by 10^5) of different IV estimators: RV, RBPV, and also TRV and DV with less aggressive truncation thresholds. The choice of truncation parameters for TRV and DV follows the instructions in Section 3.4.2, with $(C_\zeta^{\text{TRV}}, C_\zeta^{\text{DV}}, \varpi) = (4, 4\sqrt{2}, 1/2)$. The DGP is the Heston model in Eq. (3.38), and we follow the persistent noise model of Andersen et al. (2023a) to simulate the three different patterns of episodic extreme return persistence.

B.3.5 Monte Carlo RMSE Results with Market Microstructure Noise

In order to examine the impact of market microstructure noise on the finite-sample performance of RRDV, we augment the Heston model in Eq. (3.38) with an additive heterogeneous Gaussian noise term, which is in line with the Monte Carlo simulation in Christensen et al. (2022):

$$Y_i = X_i + \epsilon_i, \quad \epsilon_i \sim \text{i.i.d.}\, \mathcal{N}(0, \tilde{\sigma}_i^2), \quad \text{where } \tilde{\sigma}_i = \gamma \sqrt{\frac{\sigma_{t_i}^2}{n}}. \tag{B.97}$$

We set the noise-to-volatility ratio $\gamma = 0.5$, which corresponds to a medium contamination level (Christensen et al., 2014).[4]

Besides the additive noise, we consider the rounding errors on the price level, i.e., let the observed prices $e^{Y_i} = e^{X_i + \epsilon_i}$ be further rounded to cents. The observed logarithmic prices are given as

$$Y_i = \ln\left(\left[\frac{e^{X_i+\epsilon_i}}{0.01}\right] \times 0.01\right), \tag{B.98}$$

where the function $[x]$ rounds a number x to the nearest integer.

Table B.9 reports the RMSEs of all selected IV estimators when there exists the heterogeneous Gaussian noise in Eq. (B.97). For RRDV based on candlestick information obtained from one-second data, it exhibits noticeably elevated RMSEs compared to the noise-free case when the candlestick window is small (1 minute), and performs worse than its competitors. This observation confirms that the range-based estimators are comparatively more susceptible to noise contamination. However, RRDV regains its superiority as the interval extends slightly to 2 minutes. For the "sparse" RRDV* based on HLOCs from half-minute data, the RMSE results do not show significant differences between the noise-free and noisy cases. As discussed in Section 3.4.1, the implementation of effective discretization error correction facilitates the construction of RRDV on sparsely sampled observations, and thus enhance its robustness to market microstructure noise.

[4] A larger noise-to-volatility ratio, e.g., $\gamma = 1$, will not change the qualitative results.

Table B.9 Monte Carlo RMSE results with market microstructure noise

Panel A: $H = 0$

Interval	RRDV	RRDV*	TRV	DV	DV_{1-3}
1 min	1.29	1.18	0.71	0.81	**0.73**
2 min	**0.98**	1.05	0.99	1.14	1.02
3 min	**0.92**	1.11	1.21	1.38	1.24
5 min	**0.96**	1.24	1.55	1.77	1.58

Panel B: Gradual Jump

	$\beta = 0.45$					$\beta = 0.35$					$\beta = 0.25$				
Interval	RRDV	RRDV*	TRV	DV	DV_{1-3}	RRDV	RRDV*	TRV	DV	DV_{1-3}	RRDV	RRDV*	TRV	DV	DV_{1-3}
1 min	1.07	1.12	1.17	0.80	**0.70**	1.13	1.12	1.02	0.80	**0.71**	1.15	1.14	0.87	0.80	**0.71**
2 min	**0.80**	1.05	1.98	1.17	1.18	**0.83**	1.03	1.66	1.21	1.09	**0.88**	1.05	1.34	1.11	1.02
3 min	**0.78**	1.14	2.51	1.49	1.38	**0.81**	1.13	2.05	1.38	1.23	**0.84**	1.12	1.67	1.36	1.22
5 min	**0.93**	1.33	3.61	2.19	2.26	**0.94**	1.30	2.87	1.86	1.73	**0.94**	1.28	2.21	1.80	1.60

Panel C: Flash Crash

	$\beta = 0.45$					$\beta = 0.35$					$\beta = 0.25$				
Interval	RRDV	RRDV*	TRV	DV	DV_{1-3}	RRDV	RRDV*	TRV	DV	DV_{1-3}	RRDV	RRDV*	TRV	DV	DV_{1-3}
1 min	1.05	1.13	1.83	0.82	**0.74**	1.05	1.12	1.60	0.84	**0.75**	1.07	1.12	1.30	0.86	**0.75**
2 min	**0.66**	1.13	2.99	1.32	1.16	**0.71**	1.09	2.39	1.29	1.12	**0.76**	1.04	1.79	1.26	1.10
3 min	**0.74**	1.29	4.37	1.55	1.56	**0.74**	1.20	3.50	1.48	1.50	**0.76**	1.15	2.62	1.44	1.42
5 min	**1.04**	1.73	7.03	2.13	2.90	**0.96**	1.57	5.55	2.03	2.70	**0.94**	1.39	4.06	1.94	2.40

Panel D: Gradual Jump with an Intermittent Flash Crash

	$\beta = 0.45$					$\beta = 0.35$					$\beta = 0.25$				
Interval	RRDV	RRDV*	TRV	DV	DV_{1-3}	RRDV	RRDV*	TRV	DV	DV_{1-3}	RRDV	RRDV*	TRV	DV	DV_{1-3}
1 min	1.12	1.11	1.33	0.82	**0.75**	1.12	1.12	1.28	0.80	**0.76**	1.09	1.15	1.05	0.80	**0.73**
2 min	**0.84**	1.06	2.35	1.30	1.59	**0.83**	1.18	1.99	1.25	1.28	**0.93**	1.05	1.79	1.20	1.26
3 min	**0.80**	1.16	2.85	1.76	1.98	**0.81**	1.20	2.38	1.45	1.46	**0.85**	1.11	2.08	1.40	1.38
5 min	**1.02**	1.28	3.59	2.55	2.43	**1.02**	1.40	3.24	2.10	2.32	**0.99**	1.32	2.57	1.88	1.93

RMSE (multiplied by 10^5) of different IV estimators. RRDV and RRDV* are constructed from intraday candlestick information, which is obtained from second-by-second and half-minute observations, respectively. The choice of truncation parameters for TRV, DV and RRDV follows the instructions in Section 3.4.2, with $(C_\zeta^{\mathrm{TRV}}, C_\zeta^{\mathrm{DV}}, C_\zeta^{\mathrm{RRDV}}, \varpi) = (3, 3\sqrt{2}, 2, 1/2)$. The discretization errors of RRDV are corrected following the steps in Section 3.4.1. The DGP is the Heston model in Eq. (3.38). We simulate the additive heterogeneous Gaussian noise in Eq. (B.97), and follow the persistent noise model of Andersen et al. (2023a) to simulate the three different patterns of episodic extreme return persistence. All simulated prices are further rounded to cents.

Appendix C

Appendix to Chapter 4

C.1 Proofs

C.1.1 Proof of Proposition 4.1

Proof. As the claimed result holds for every $d = 1, 2, \ldots$, it suffices to prove the result for $d = 1$ on the interval $[0, 1]$ with $X_0 = 0$ and some threshold δ adapted to $\mathcal{F}_0$, and we shall suppress the notation of d in this proof for brevity. We start from the celebrated Dambis-Dubins-Schwarz theorem, which states that all continuous martingales are time-changed Brownian motions under the IV clock (Barndorff-Nielsen and Shiryaev, 2015), i.e., $X_t = \int_0^t \sigma_s dW_s \equiv \widetilde{W}_{V_t}$ is a standard Brownian motion under the V-time $V_t = \int_0^t \sigma_s^2 ds$. Consider the price durations $(x_i)_{1 \le i \le N_d}$ generated by Eq. (4.3), its V-time counterpart can be generated by the same algorithm under a time change:

$$\Delta_i V = \inf_{s>0} \left\{ \left| \widetilde{W}_{V_{i-1}+s} - \widetilde{W}_{V_{i-1}} \right| \ge \delta \right\}, \qquad V_i = \sum_{j=1}^{i} \Delta_j V, \tag{C.1}$$

since the stopping rule commutes with a time change, i.e., $|\widetilde{W}_{V_i} - \widetilde{W}_{V_{i-1}}| = |X_{\tau_i} - X_{\tau_{i-1}}| = \delta$. By the Brownian scaling law:

$$Z_i = \frac{\Delta_i V}{\delta^2} = \inf_{s>0} \left\{ \left| \widetilde{W}^*_{\widetilde{V}_{i-1}+s} - \widetilde{W}^*_{\widetilde{V}_{i-1}} \right| \ge 1 \right\}, \tag{C.2}$$

where $\widetilde{W}^*_{\widetilde{V}_t} = \delta^{-2} \widetilde{W}_{V_t/\delta^2}$ is again a Brownian motion that normalizes the stopping threshold to 1. By the strong Markov property of the Brownian motion, Z_i is independent of $\mathcal{F}_{i-1}$ and $\delta \in \mathcal{F}_0$.

The time homogeneity of Brownian motion implies that Z_i must have the same distribution of the first exit time of a Brownian motion B with respect to a symmetric unit interval, i.e., $\inf_{t>0}\{|B_t| \geq 1\}$, and hence (Z_i) is a sequence of i.i.d. random variables. This completes the proof.

□

C.1.2 Proof of Proposition 4.2

Proof. Similar to the proof of Proposition 4.1, we shall assume $d = 1$, $X_0 = 0$, and suppress the notation of d for brevity. We start with an analysis on the sub-σ-field $\overline{\mathcal{F}}_t$. We clearly have $\overline{\mathcal{F}}_0 = \mathcal{F}_0$, which implies that $\delta \in \overline{\mathcal{F}}_0$. Moreover, $N(t)$ is adapted to $\overline{\mathcal{F}}_t$ by construction. Since by assumption $V(t)$ is adapted to $\overline{\mathcal{F}}_t$, the counting process under the IV clock, $\widetilde{N}(V(t))$, is also adapted to $\overline{\mathcal{F}}_t$. Specifically, both $N(t)$ and $\widetilde{N}(V(t))$ are $\overline{\mathcal{F}}_t$-submartingales, which implies the following Doob-Meyer decompositions:

$$N(t) = M(t) + \Lambda(t), \qquad \widetilde{N}(V(t)) = \widetilde{M}(V(t)) + \widetilde{\Lambda}(V(t)), \tag{C.3}$$

where $M(t) \equiv \widetilde{M}(V(t))$ are $\overline{\mathcal{F}}_t$-martingales, and $\Lambda(t) \equiv \widetilde{\Lambda}(V(t))$ are the compensators for $N(t)$ and $\widetilde{N}(V(t))$, which are $\overline{\mathcal{F}}_t$-predictable strictly increasing processes with the following representations:

$$\Lambda(t) = \int_0^t \lambda_s ds, \qquad \widetilde{\Lambda}(V(t)) = \int_0^{V(t)} \widetilde{\lambda}_{V(s)} dV(s), \tag{C.4}$$

where λ_t and $\widetilde{\lambda}_{V(t)}$ are $\overline{\mathcal{F}}_t$-adapted, positive-valued, and càglàd processes known as the $\overline{\mathcal{F}}_t$-conditional intensity processes of $N(t)$ and $\widetilde{N}(V(t))$, respectively (Hautsch, 2011). Since the two integrals above are identical for all t, we have for any h:

$$\int_t^{t+h} \lambda_s ds = \int_{V(t)}^{V(t+h)} \widetilde{\lambda}_{V(s)} dV(s). \tag{C.5}$$

With the definition of conditional intensity (Definition 4.1, Hautsch, 2011), we have for almost all $t \geq 0$:

$$\begin{aligned}\lambda_t &= \lim_{h\downarrow 0} \frac{1}{h} \int_t^{t+h} \lambda_s ds = \lim_{h\downarrow 0} \frac{1}{h} \int_{V(t)}^{V(t+h)} \widetilde{\lambda}_{V(s)} dV(s) \\ &= \lim_{h\downarrow 0} \frac{V(t+h) - V(t)}{h} \lim_{h\downarrow 0} \frac{1}{V(t+h) - V(t)} \int_{V(t)}^{V(t+h)} \widetilde{\lambda}_{V(s)} dV(s) \\ &= \sigma_t^2 \widetilde{\lambda}_{V(t)},\end{aligned} \tag{C.6}$$

where we utilize the fact that σ_t^2 is a càdlàg process to deduce the first limit above, and one should verify that both sides of the above equation is adapted to $\overline{\mathcal{F}}_t$ by assumption. In particular, the equality $\lambda_t = \sigma_t^2 \widetilde{\lambda}_{V(t)}$ holds for almost all $t \in [0, 1]$ except a set with Lebesgue measure zero, which is enough to ensure the equality of the corresponding integrals.

To connect the conditional intensity process with the conditional density of the durations, we use the relationship between the conditional hazard function and the conditional intensity, see, e.g., Eq. (4.1) in Hautsch (2011). In detail, we can write λ_t and $\widetilde{\lambda}_{V(t)}$ in terms of the $\overline{\mathcal{F}}_t$-conditional hazard function of x_i and $\Delta_i V$, i.e., for all $h \in (0, x_{d,i}]$:

$$\lambda_{\tau_{i-1}+h} = \frac{f(h|\overline{\mathcal{F}}_{i-1})}{1 - F(h|\overline{\mathcal{F}}_{i-1})}, \qquad \widetilde{\lambda}_{V(\tau_{i-1}+h)} = \frac{\widetilde{f}(\Delta_i V(h)|\overline{\mathcal{F}}_{i-1})}{1 - \widetilde{F}(\Delta_i V(h)|\overline{\mathcal{F}}_{i-1})}, \tag{C.7}$$

where $\widetilde{f}(\cdot|\overline{\mathcal{F}}_{i-1})$ and $\widetilde{F}(\cdot|\overline{\mathcal{F}}_{i-1})$ are the $\overline{\mathcal{F}}_{i-1}$-conditional PDF and CDF of $\Delta_i V$, respectively. Integrating the conditional intensities over $[\tau_{i-1}, \tau_{i-1} + h]$, we find that:

$$\begin{aligned}-\ln(1 - F(h|\overline{\mathcal{F}}_{i-1})) &= \int_0^h \frac{f(s|\overline{\mathcal{F}}_{i-1})}{1 - F(s|\overline{\mathcal{F}}_{i-1})} ds \\ &= \int_0^{\Delta_i V(h)} \frac{\widetilde{f}(s|\overline{\mathcal{F}}_{i-1})}{1 - \widetilde{F}(s|\overline{\mathcal{F}}_{i-1})} ds = -\ln(1 - \widetilde{F}(\Delta_i V(h)|\overline{\mathcal{F}}_{i-1})),\end{aligned} \tag{C.8}$$

from which we deduce that $F(h|\overline{\mathcal{F}}_{i-1}) = \widetilde{F}(\Delta_i V(h)|\overline{\mathcal{F}}_{i-1})$ for all i and $h \in (0, x_{d,i}]$. Finally, it suffices to notice that, conditioning on $\overline{\mathcal{F}}_{i-1} \subset \mathcal{F}_{i-1}$, it holds that $\Delta_i V \overset{\mathcal{L}}{=} \delta^2 Z_i$ where Z_i is independent of $\overline{\mathcal{F}}_{i-1}$. Therefore, it implies that

$$F(h|\overline{\mathcal{F}}_{i-1}) = \widetilde{F}(\Delta_i V(h)|\overline{\mathcal{F}}_{i-1}) = F_Z\left(\frac{\Delta_i V}{\delta^2}\right), \tag{C.9}$$

which proves Eq. (4.9) with the inverse function of $F_Z(\cdot)$.

For Eq. (4.10), we utilize the fact that $\lambda_t = \sigma_t^2 \widetilde{\lambda}_{V(t)}$ holds for almost all t (see Eq. (C.6)). Substituting Eq. (C.7) into this, with the Jacobian transformation $\delta^{-2} f_Z(\delta^{-2}\Delta_i V(h)) = \widetilde{f}(\Delta_i V(h)|\overline{\mathcal{F}}_{i-1})$, we find that, for almost all $h \in (0, x_{d,i}]$:

$$\sigma_{\tau_{i-1}+h} = \frac{\lambda_{\tau_{i-1}+h}}{\widetilde{\lambda}_{V(\tau_{i-1}+h)}} = \frac{f(h|\overline{\mathcal{F}}_{i-1})}{\widetilde{f}(\Delta_i V(h)|\overline{\mathcal{F}}_{i-1})} = \frac{\delta^2 f(h|\overline{\mathcal{F}}_{i-1})}{f_Z(\delta^{-2}\Delta_i V(h))}. \tag{C.10}$$

Substituting $\Delta_i V(h) = \delta^2 F_Z^{-1}(F(h|\overline{\mathcal{F}}_{i-1}))$ into the above yields the desired result. This completes the proof.

□

C.1.3 Proof of Corollary 4.1

Proof. Similar to the proof of Proposition 4.1, we shall assume $d = 1$, $X_0 = 0$, and suppress the notation of d for brevity. The relation $x_i = \gamma_{i-1}^{-1}\delta^2 Z_i$ implies the following relations of the conditional PDF and CDF of x_i and Z_i:

$$F(h|\overline{\mathcal{F}}_{i-1}) = F_Z\left(\frac{h\gamma_{i-1}}{\delta^2}\right), \qquad f(h|\overline{\mathcal{F}}_{i-1}) = \frac{\gamma_{i-1}}{\delta^2} f_Z\left(\frac{h\gamma_{i-1}}{\delta^2}\right). \tag{C.11}$$

We substitute the above $F(h|\overline{\mathcal{F}}_{i-1})$ and $f(h|\overline{\mathcal{F}}_{i-1})$ into Eq. (4.10):

$$\sigma_{\tau_{i-1}+h} = \frac{\delta^2 f(h|\overline{\mathcal{F}}_{i-1})}{f_Z(G_i(h))} = \frac{\gamma_{i-1} f_Z\left(\frac{h\gamma_{i-1}}{\delta^2}\right)}{f_Z\left(F_Z^{-1}\left(F_Z\left(\frac{h\gamma_{i-1}}{\delta^2}\right)\right)\right)} = \gamma_{i-1}. \tag{C.12}$$

This completes the proof. □